– Ferrocene-Based Pyridylphosphine Ligands –
Coordination Chemistry
of Group 10, 11 and 12 Metals

Dissertation

zur
Erlangung des akademischen Grades
eines

Doktors der Naturwissenschaften
(Dr. rer. nat.)

am Fachbereich
Mathematik und Naturwissenschaften
der Universität Kassel

von

Thorsten Klemann

2010

By three methods we may learn wisdom: First, by reflection, which is the noblest; second, by imitation, which is the easiest; and third by experience, which is the bitterest.

(alleged to Confucius)

Der Mensch hat dreierlei Wege Weisheit zu erlangen: Erstens durch Nachdenken, das ist der Edelste; zweitens durch Nachahmen, das ist der Leichteste; drittens durch Erfahrung, das ist der Bitterste.

(Konfuzius zugeschrieben)

The work described in this thesis was carried out in the Institute of Chemistry, University of Kassel (Germany), since 2008 in the research group of Prof. Siemeling and in the Department of Inorganic Chemistry, Charles University Prague (Czech Republic), in 2009 and 2010 under supervision of Prof. Štěpnička.

Day of disputation: 01st of December, 2010.

1. Supervisor: Prof. Dr. Ulrich Siemeling
2. Supervisor: Prof. Dr. Petr Štěpnička

Acknowledgements

With the first words I would like to express my sincerest gratitude to my academic teacher, Prof. Ulrich Siemeling, for giving me the opportunity to work in his group, his scientific guidance and for providing the interesting topic of this thesis. Beyond that, he was marvellous for being not only the supervisor, but a supporting advisor as well.

I had the good fortune to visit for two times the Czech Republic and work under the supervision of Prof. Petr Štěpnička at Charles University in Prague. I would like to thank him sincerely for his generousness and support during this time and for the amazing opportunity to experience a different (academic) culture at its best.

In this context the DAAD (Deutscher Akademischer Austauschdienst), the Ministry of Education of the Czech Republic and the Czech Science Foundation are thanked very much indeed for their financial support of my visits to Charles University.

I would like to thank all my mater colleagues during my time in the MOC in Kassel, namely Dr. Frauke Bretthauer, Dr. Jens Hoßbach, Dr. Mario Gatterdam, Dr. Christian Färber, Dr. Christian Schirrmacher, Ulrich Glebe, Stefan Rittinghaus, Lutz Klapp, Jan Schröder, Alexander Girod, Tim Fellinger, Stella Helten, Sandra Tripp, Michael Kurlemann, Henry Memczak, Tim Koppenrath, Steffen Koppenrath, Alexander Mundstock, Tim Schulz, Dr. Pavel Turek and also the great people from the Prague group, Dr. Jan Demel, Jiří Tauchman and Jiří Schulz for creating stimulating and pleasant environments.

Furthermore I am indebted to several people, without whom I would not have been able to conclude my work:

Dr. Maurer for recording all kinds of NMR spectra.
Dr. Bruhn and A. Pilz for collecting and solving the X-ray crystal structures in Kassel, very special thanks!
Dr. Císařová for the crystallographic work in Prague.
Dr. Fürmeier for mass spectrometry.
Dr. Leibold for DFT calculations.
Jörg Ho for excellent elemental analyses.

Finally I would like to thank my family, first of all my wife Tanja and my parents, Monika und Ulrich, as well as my sister Patricia, whose mainly non-scientific, but endless support was absolutely essential to reach this goal.

Declaration

The entire body of this work is my own unless stated to the contrary and has not been submitted previously for any degree at this or any other university.

Kassel, 28th of October, 2010

(Thorsten Klemann)

Erklärung

Ich versichere, dass ich die vorliegende Dissertation selbstständig, ohne unerlaubte Hilfe angefertigt habe und keine anderen als die in der Dissertation angegebenen Hilfsmittel benutzt habe. Alle Stellen, die wörtlich oder sinngemäß aus veröffentlichten Schriften entnommen sind, wurden mit Quellenangaben kenntlich gemacht. Kein Teil dieser Arbeit ist in einem anderen Promotions- oder Habilitationsverfahren verwendet worden.

Kassel, am 28. Oktober 2010

(Thorsten Klemann)

Publications

Parts of the work described in this thesis have been published previously:

P. Štěpnička, J. Schulz, T. Klemann, U. Siemeling, I. Císařová: Synthesis, Structural Characterization, and Catalytic Evaluation of Palladium Complexes with Homologous Ferrocene-Based Pyridylphosphine Ligands, *Organometallics* **2010**, *29*, 3187.

Summary

The present thesis describes the synthesis of 1,1'-ferrocendiyl-based pyridylphosphine ligands, the exploration of their fundamental coordination chemistry and preliminary experiments with selected complexes aimed at potential applications. One main aspect is the synthesis of the bidentate ferrocene-based pyridylphosphine ligands **1**, **2** and **3** (Fig. I).

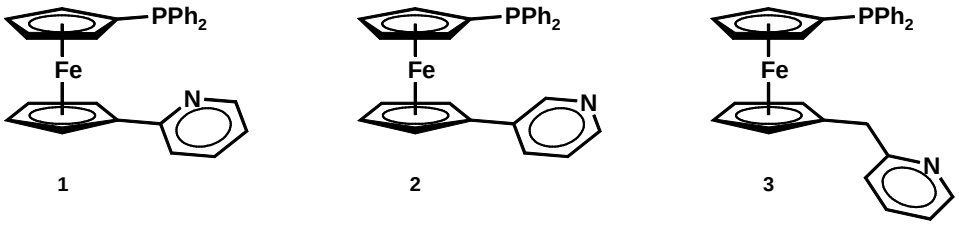

Fig. I: Bidentate 1,1'-ferrocenediyl-based pyridylphosphine ligands.

A specific feature of these ligands is the ball-bearing like flexibility of the ferrocene-based backbone. An additional flexibility element is the rotation around the C–C single bonds. Consequently, the donor atoms can realise a wide range of positions with respect to each other and are therefore able to adapt to the coordination requirements of different metal centres.

The flexibility of the ligand also plays a role in another key aspect of this work, which concerns the coordination mode, i. e. bridging vs. chelating. In addition to the flexibility, also the position of the donor atoms to each other is important. This is largely affected by the position of the pyridyl nitrogen (pyrid-2-yl vs. pyrid-3-yl) and the methylen group in **3**.

Another interesting point is the combination of a soft phosphorus donor atom with a harder nitrogen donor atom, according to the HSAB principle. This combination generates a unique binding profile, since the π-acceptor character of the *P* site is able to stabilise a metal centre in a low oxidation state, while the nitrogen σ-donor abili-

ty can make the metal more susceptible to oxidative addition reactions. A *P*,*N*-donor combination can afford hemilabile binding profiles, which would be ideal for catalysis.

Beyond 1,2-substituted ferrocene derivatives, which are quite successful in catalytic applications, 1,1'-derivatives are rather underrepresented. While a low-yield synthetic pathway to ligand **1** was already described in the literature,[1] it was possible to find a new, improved and simplified synthetic pathway. **2** and **3** were unknown prior to this work. Satisfactory results in the synthesis of **2** could be achieved by working in analogy to the new synthetic procedure for **1**. The synthesis of **3** has been handled by the group of Prof. Petr Štěpnička from Charles University, Prague, Czech Republic. The synthesis of tridentate ligands with an analogous heterodentate arrangement, was investigated briefly as a sideline of this study.

The major part of this thesis deals with the fundamental coordination chemistry towards transition metals of the groups 10, 11 and 12. Due to the well-established catalytic properties of analogous palladium complexes, the coordination chemistry towards palladium (group 10) is of particular interest. The metals zinc and cadmium (group 12) are also of substantial importance because they are redox-inert in their divalent state. This is relevant in view of electrochemical investigations concerning the utilisation of the ligands as molecular redox sensors. Also mercury and the monovalent metals silver and gold (group 11) are included because of their rich coordination chemistry. It is essential to answer questions concerning aspects of the ligands' coordination mode bearing in mind the HSAB principle.

Depending on the metal source used, on the reaction stoichiometry and, in a few cases, on the experimental conditions, the ligands **1**, **2** and **3** exhibit a variety of coordination modes. Fig. II schematically presents the coordination modes which occurred during this investigation.

The results of the coordination chemistry experiments are summarised in Tab. I. The listed metal sources were reacted with one or two equivalent(s) (eq.) of the ligands, affording the complexes **5a** to **35**. Information about the coordination modes encountered and aspects of the structural characterisation are given, too.

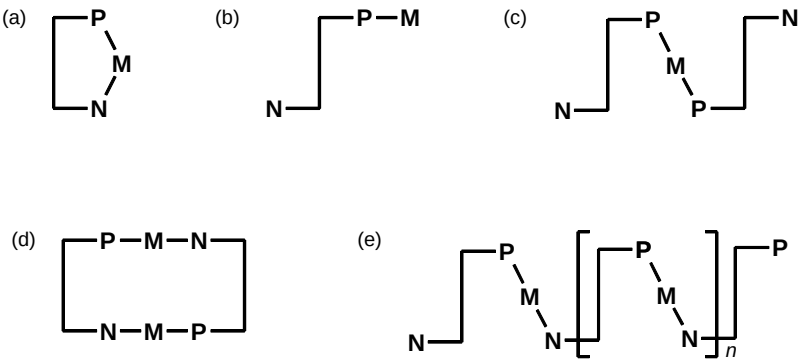

Fig. II: Observed coordination modes of **1**, **2** and **3**; *P*,*N*-chelate "C" (a), monodentate *P*-coordination "M" (b), *P*-coordinated bis(phosphine) complex "B" (c), centrosymmetric dimer "D" (d) and polymer "P" (e).

Not surprisingly reactions of group 12 metal halides with 1 eq. of **1** afforded the corresponding *P*,*N*-chelates, which have been fully characterised with three exceptions only. It was impossible to crystallise the chelate complexes **5c**, **6a** and **8a**. Interestingly, two new compounds were obtained in both cases by the crystallisation experiments, viz. the *P*-coordinated bis(phosphine) complexes **7** and **9a**. Complex **8c** crystallises not as a chelate, but as a dimeric, iodo-bridged, *P*-coordinated bis(phosphine) complex. Reactions of $HgBr_2$ with 2 eq. of the ligand gave the *P*-coordinated bis(phosphine) complex **9b**. The reaction with 2 eq. of zinc bromide only gave the 1:1 chelate **5b**.

Reactions of **2** with group 12 metal bromides gave polymers exclusively. The less predictable coordination behaviour of **3** can be ascribed to the presence of the methylene group in this ligand, which makes the ligand more flexible. Reactions of **3** with group 12 metal halides resulted in the *P*,*N*-chelates **13**, **14**, **15** and **16**. Due to poor crystallisation tendencies, the crystallisation of compound **14** was attempted also in a diffusion experiment, which surprisingly did not afford the expected chelate, but the polymer **14a**. In analogous crystallisation experiments performed with the chelates **13** and **16**, **3** turned out to act as a bridging ligand, resulting in the centrosymetric dimer **13a** and the polymer **17**. Interestingly, the molecular structure of the mercury polymer **17** exhibits a 1:2 (ligand:metal) stoichiometry with halide bridges, even though the experiment was carried out in a 1:1 stoichiometry.

In reactions with silver(I) tetrafluoroborate all three ligands coordinated the metal in a bridging manner. **1** and **3**, containing a pyrid-2-yl group, form the polymers **19** and **21**. The pyrid-3-yl containing ligand **2** forms the centrosymmetric dimer **20**.

Tab. I: Summary of the results of the coordination chemistry experiments concerning the bidentate ligands **1**, **2** and **3**.

		1		**2**		**3**	
		1 eq.	2 eq.	1 eq.	2 eq.	1 eq.	2 eq.
Zn	Cl_2	**5a** C	–	–	–	–	–
	Br_2	**5b** C	**5b** C	**10** P	–	**13** C; **13a** D[a]	**13a** D[a]
	I_2	**5c** C[b]	–	–	–	–	–
Cd	Cl_2	**6a** C[b,c]	**7** B[a,d]	–	–	–	–
	Br_2	**6b** C	–	**11** P[b]	–	**14** C[c]; **14a** P[a]	–
	I_2	**6c** C	–	–	–	**15** C; –	–
Hg	Cl_2	**8a** C[b,c]	**9a** B[a,d]	–	–	–	–
	Br_2	**8b** C	**9b** B	**12** P	–	**16** C; **17** P[a,e]	**18** B
	I_2	**8c** C[f]	–	–	–	–	–
Ag	BF_4	**19** P	–	**20** D	–	**21** P	–
Au	Cl(tht)	**22** M	–	**23** M	–	**24** M	–
	BF_4	**25** D	–	**26** X[b]	–	**27** X[b]	–
Pd	Cl_2	**28** C	**30** B	–	–	**29** C[b]	**31** B
	$Cl(L^{NC})$	**32** M[b]	–	–	–	**33** M[b]	–
	$(L^{NC})(MeCN)_2ClO_4$	**34** C	–	–	–	**35** C	–

B = *P*-coordinated, monodentate bis(phosphine) complex, C = *P*,*N*-chelate, D = centrosymmetric dimer, M = monodentate *P*-coordination, P = polymer, X = structure not clear, – = no investigations realised or investigations did not lead to clear results. [a]Only characterised by X-ray diffraction. [b]No X-ray data available. [c]Crystallisation leads to new compound with 2:1 (ligand:metal) stoichiometry. [d]Crystals obtained by a diffusion experiments with 1:1 stoichiometry. [e]**17** has a 1:2 stoichiometry, the polymer is formed via halide bridges. [f]Crystallisation leads to *P*-coordinated iodo-bridged dimer.

The gold complexes **22**, **23** und **24** obtained from the reaction of **1**, **2** and **3**, respectively with [AuCl(tht)] (tht = tetrahydrothiophene) each contain a monodentate, *P*-coordinated Ligand. Further reactions, aimed at the abstraction of the chloro ligand to induce Au-N coordination resulted in the less soluble and poorly crystalline complexes **25**, **26** and **27**. Only **25** was structurally characterised. Additional experiments aimed at the preparation of Au-Ag binuclear complexes failed.

The ligands **1** and **3** react with [$PdCl_2$(cod)] (cod = η^2:η^2-cycloocta-1,5-diene) in a *P*-coordinated monodentate and in a *P*,*N*-chelating manner, depending on the reaction stoichiometry, to form the palladium complexes **28**, **29**, **30** and **31**. Both ligands were also reacted with [Pd(μ-Cl)(L^{NC})]$_2$ (L^{NC} = [(2-dimethylamino-κN)methyl]phenyl-κC^1), leading to the *P*-coordinated bis(phosphine) complexes **32** and **33**. A similar reaction with the solvento complex [Pd(L^{NC})($MeCN)_2$][ClO_4] gave the cationic complexes **34** and **35**, in which the ligands exhibited a chelating coordination behavior.

Catalytic investigations of Suzuki-Miyaura cross-coupling reactions showed that complexes **28** and **29** and precatalyst formed *in situ* from **1** and **3** with $Pd(OAc)_2$ promote the reaction of 4-bromotoluene with phenylboronic acid efficiently. For the catalyst based on ligand **3** similar or slightly better results were obtained than for the corresponding dppf-based (dppf = 1,1'-bis(diphenylphosphino)ferrocene) catalyst. The results for the catalysts based on **1** are comparable, too, but only slightly inferior to those of the dppf benchmark. The Pd-catalysed cyanation reaction is more efficiently promoted by the defined precatalyst complexes, with dppf being a ligand superior to both pyridylphosphines.

The ligands **1**, **2** and **3** exhibited a reversible behaviour concerning the ferrocene-based redox wave in cyclovoltammetric investigations. The chlorogold(I) complexe **22**, **23** and **24** showed such a behavior, too. The coordination causes a notable shift of the formal electrode potential of about ca. 0.2 V with respect to the corresponding uncoordinated ligand.

Zusammenfassung

Die vorliegende Arbeit befasst sich mit der Synthese, der Untersuchung der fundamentalen Koordinationschemie und ersten Modellexperimenten zur Anwendungserprobung von Pyridylphosphin Liganden mit 1,1'-Ferrocendiyl-Rückgrat. Einer der Hauptaspekte ist die Synthese der zweizähnigen Liganden **1**, **2** und **3** (Abb. I).

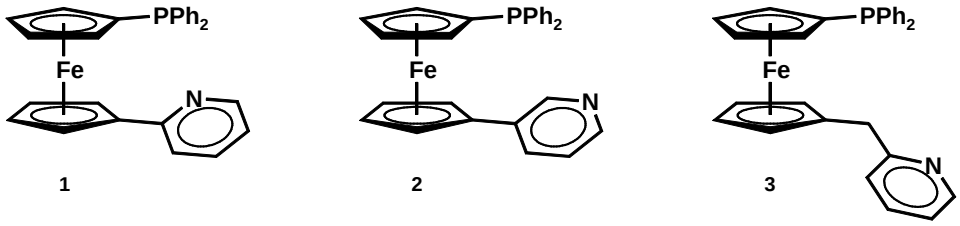

Abb. I: Zweizähnige Pyridylphosphin-Liganden mit 1,1'-Ferrocendiyl-Rückgrat.

Ein besonderes Charakteristikum dieser zweizähnigen Liganden ist die kugellagerartige Beweglichkeit des Ligand-Rückgrates. Hinzu kommen die Flexibilitätselemente der C–C-Einfachbindung mit ihrer freien Drehbarkeit. Die Donoratome können auf diese Weise viele verschiedene Positionen zueinander einnehmen und sich so den Koordinationsbedürfnissen unterschiedlichster Metallzentren anpassen.

Ein weiterer wichtiger Aspekt dieser Arbeit, bei dem die Beweglichkeit der Liganden eine Rolle spielt, ist der Koordinationsmodus der Liganden: verbrückend oder chelatisierend. Nicht nur die Flexibilität, sondern auch die Position der Donoratome zueinander ist dabei von Bedeutung. Diese wird hauptsächlich durch die Position des Pyridylstickstoffes (pyrid-2-yl vs. pyrid-3-yl) und durch die Methylengruppe in **3** bestimmt.

Ein weiterer interessanter Aspekt ist die Kombination eines, nach dem HSAB-Prinzip weichen, Phosphordonors mit einem härteren Stickstoffdonor. Diese Kombination eröffnet interessante Bindungsprofile, da der π-Akzeptorcharakter des *P*-Donors Metallzentren in niedrigen Oxidationsstufen stabilisiert, während die σ-Donorfähigkeit des *N*-Donors die Metallzentren anfälliger für oxidative Additionsreaktionen macht. Ein sol-

ches Donorprofil kann möglicherweise zu hemilabiler Koordination führen, was optimal für katalytische Zwecke wäre.

Neben Ferrocenderivaten mit 1,2-Substitution, die sehr erfolgreich in katalytischen Bereichen eingesetzt werden, sind 1,1'-Derivate in der wissenschaftlichen Literatur eher unterrepräsentiert. Die Synthese des Liganden **1** war bereits in der Literatur beschrieben,[1] allerdings mit geringen Ausbeuten. In der vorliegenden Arbeit konnte eine neue, verbesserte Syntheseroute gefunden werden. Die Liganden **2** und **3** waren gänzlich unbekannt. Durch Übertragung und Modifizierung des neuen Synthesewegs für **1** auf die Synthese von **2** konnte eine zufriedenstellende Syntheseroute gefunden werden. Die Synthese von **3** wurde vom Arbeitskreis um Prof. Petr Štěpnička an der Karls-Universität Prag, Tschechische Republik, durchgeführt. Auch die Synthese von dreizähnigen Liganden mit analogem Aufbau war von Interesse, spielte aber im Nachhinein nur eine untergeordnete Rolle.

Der Kernteil der Arbeit befasst sich mit der Auslotung der fundamentalen Koordinationschemie der Liganden mit Übergangsmetallen der Gruppen 10, 11 und 12. Aufgrund von guten katalytischen Eigenschaften, die analoge Palladiumkomplexe bisher gezeigt haben, ist die Untersuchung der Koordinationschemie gegenüber Palladium (Gruppe 10) besonders interessant. Auch Zink und Cadmium (Gruppe 12) sind für diese Arbeit substanziell, da sie über keine eigene Redoxchemie verfügen. Letzteres ist im Hinblick auf elektrochemische Untersuchungen bezüglich der Eignung der Liganden als molekulare Redoxsensoren von Bedeutung. Auch Quecksilber und die einwertigen Metalle Silber und Gold (Gruppe 11) sind aufgrund ihrer vielseitigen Koordinationschemie in die Untersuchungen einbezogen worden. Es gilt, Antworten auf Fragestellungen bezüglich des Koordinationsverhaltens der Liganden unter Berücksichtigung des HSAB-Prinzips zu klären.

Abhängig vom eingesetzten Metall, der Reaktionsstöchiometrie und, in einigen wenigen Fällen, von den experimentellen Bedingungen zeigen die Liganden **1**, **2** und **3** unterschiedlichste Koordinationsformen. Die während den Untersuchungen beobachteten sind in den schematischen Darstellungen in Abb. II gezeigt.

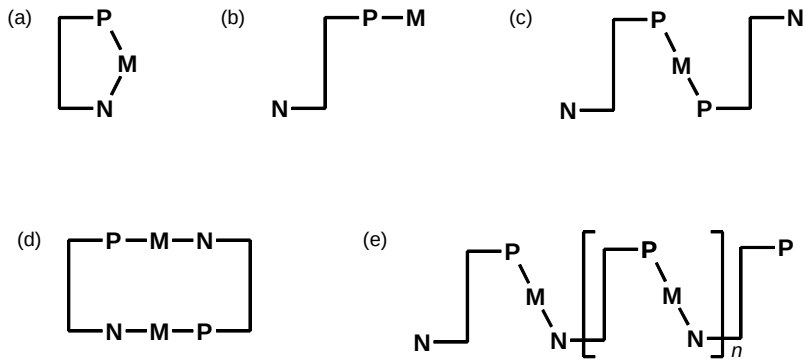

Abb. II: Beobachtete Koordinationsformen von **1**, **2** und **3**; *P*,*N*-Chelat „C“ (a), einzähnige *P*-koordination „M“ (b) , *P*-koordinierter Bis(phosphin)-Komplex „B“ (c), zentrosymmetrisches Dimer „D“ (d) und Polymer „P“ (e).

Die Ergebnisse der koordinationschemischen Experimente sind in Tab. I zusammengefasst. Die aufgelisteten Metalle wurden mit einem oder zwei Äquivalenten (eq.) des entsprechenden Liganden umgesetzt. Die Komplexverbindungen **5a** bis **35** wurden erhalten. Ebenfalls sind Informationen über die Koordinationsformen und die strukturelle Charakterisierung enthalten.

Wenig überraschend führen Reaktionen von Metallhalogeniden der Gruppe 12 mit einem Äquivalent **1** zu den entsprechenden Chelatkomplexen, die, bis auf drei Ausnahmen, umfassend charakterisiert wurden. Es gelang nicht, die Komplexe **6a**, **5c** und **8a** zu kristallisieren. Interessanterweise führten Kristallisationsexperimente in diesen beiden Fällen zu neuen Verbindungen: den einzähnig *P*-koordinierten Bis(phosphin)-Komplexen **7** und **9a**. Die Kristallisation von **8c** führte nicht zum erwarteten Chelatkomplex, sondern zu einem dimeren iodo-verbrückten *P*-koordinierten Bis(phosphin)-Komplex. In Reaktionen von $HgBr_2$ mit zwei Äquivalenten Ligand entstand der einzähnig *P*-koordinierte Bis(phosphin)-Komplex **9b**. Im Falle des Zinks konnte bei Reaktionen mit zwei Äquivalenten des Liganden lediglich der Chelatkomplex **5b** mit 1:1-Stöchiometrie isoliert werden.

Reaktionen von **2** mit Metallbromiden der Gruppe 12 ergaben ausschließlich Koordinationspolymere. Hingegen zeigt der flexiblere Ligand **3** ein ambivalentes Verhalten.

Reaktionen zwischen **3** und Metallhalogeniden der Gruppe 12 resultierten in *P*,*N*-Chelatkomplexen **13**, **14**, **15** und **16**. Da Verbindung **14** keine Tendenz zur Kristallisation zeigte, wurde eine Kristallisation mittels Diffusionsexperiment versucht. Das Ergeb-

Tab. I: Zusammenfassung der Ergebnisse der koordinationschemischen Experimente bezüglich der zweizähnigen Liganden **1**, **2** und **3**.

		1		**2**		**3**	
		1 eq.	2 eq.	1 eq.	2 eq.	1 eq.	2 eq.
Zn	Cl_2	**5a** C	–	–	–	–	–
	Br_2	**5b** C	**5b** C	**10** P	–	**13** C; **13a** D[a]	**13a** D[a]
	I_2	**5c** C[b]	–	–	–	–	–
Cd	Cl_2	**6a** C[b,c]	**7** B[a,d]	–	–	–	–
	Br_2	**6b** C	–	**11** P[b]	–	**14** C[c]; **14a** P[a]	–
	I_2	**6c** C	–	–	–	**15** C; –	–
Hg	Cl_2	**8a** C[b,c]	**9a** B[a,d]	–	–	–	–
	Br_2	**8b** C	**9b** B	**12** P	–	**16** C; **17** P[a,e]	**18** B
	I_2	**8c** C[f]	–	–	–	–	–
Ag	BF_4	**19** P	–	**20** D	–	**21** P	–
Au	Cl(tht)	**22** M	–	**23** M	–	**24** M	–
	BF_4	**25** D	–	**26** X[b]	–	**27** X[b]	–
Pd	Cl_2	**28** C	**30** B	–	–	**29** C[b]	**31** B
	$Cl(L^{NC})$	**32** M[b]	–	–	–	**33** M[b]	–
	$(L^{NC})(MeCN)_2ClO_4$	**34** C	–	–	–	**35** C	–

„B“ = *P*-koordinierter Bis(phosphin)-Komplex; „C“ = *P*,*N*-Chelat; „D“ = Zentrosymmetrisches Dimer, „M“ = einzähnige *P*-Koordination, „P“ = Polymer, „X“ = Struktur nicht geklärt, „–“ = keine Untersuchungen realisiert oder die Untersuchungen führten zu keinem klaren Ergebnis. [a]Nur durch Röntgenstruktur charakterisiert. [b]Keine Röntgenstruktur verfügbar. [c]Kristallisation führte zu einer neuen Verbindung mit 2:1-Stöchiometrie (Ligand:Metall). [d]Kristallisation erfolgte im Diffusionsexperiment mit 1:1-Stöchiometrie. [e]**17** weist 1:2-Stöchiometrie auf, die Verknüpfung erfolgt über verbrückende Bromatome. [f]Kristallisation führt zu einem *P*-koordinierten, iodverbrückten Dimer.

nis war nicht wie erwartet der Chelatkomplex, sondern überraschenderweise wurde das Polymer **14a** erhalten. Bei analogen Kristallisationsexperimenten mit den Chelatkomplexen **13** und **16** zeigte der Ligand **3** verbrückendes Koordinationsverhalten, mit dem Ergebnis des zentrosymmetrischen Dimers **13a** und des Polymers **17**. Kurioserweise zeigt die Molekülstruktur des Polymers **17** eine halogenverbrückte 1:2-Stöchiometrie (Ligand:Metall), obwohl das Experiment in 1:1-Stöchiometrie durchgeführt wurde.

Mit Silber(I)-tetrafluoroborat reagieren alle drei Liganden in einer verbrückenden Form. Die Liganden **1** und **3**, die eine Pyrid-2-yl-gruppe enthalten, bilden die Koordinationspolymere **19** und **21**. Ligand **2**, welcher eine Pyrid-3-yl-gruppe enthält, bildet das zentrosymmetrische Dimer **20**.

Die Goldkomplexe **22**, **23** und **24** wurden aus Reaktionen von **1**, **2** und **3** mit [AuCl(tht)] (tht = Tetrahydrothiophen) erhalten und sind alle einzähnig *P*-koordiniert. Weitere Reaktionen, beginnend mit dem Austausch des Chloroliganden durch ein nicht koordinierendes Tetrafluoroborat-Anion, resultieren in den kaum löslichen Komplexen **25**, **26** und **27**, die nur teilweise Kristallisationstendenzen zeigen. Nur **25** konnte mittels Röntgendiffraktometrie charakterisiert werden. Zusätzliche Experimente zur Darstellung von Au-Ag binuklearen Komplexen scheiterten.

Die Liganden **1** und **3** reagieren mit [$PdCl_2$(cod)] (cod = η^2:η^2-Cycloocta-1,5-dien) in einer *P*-koordinierenden einzähnigen und in einer *P*,*N*-chelatisierenden Weise, abhängig von der Stöchiometrie der Reaktion. Es bilden sich die Palladiumkomplexe **28, 29, 30** und **31**. Die Reaktionen beider Liganden mit [Pd(μ-Cl)(L^{NC})]$_2$ (L^{NC} = [(2-Dimethylamino-κN)methyl]phenyl-κC^1) führen zu den entsprechenden Komplexen **32** und **33**, in denen beide Liganden jeweils einzähnige *P*-Koordination zeigen. Ähnliche Reaktionen mit dem Solvens-Komplex [Pd(L^{NC})(MeCN)$_2$][ClO_4] ergeben die kationischen Komplexe **34** und **35**. Hier hingegen zeigen die Liganden chelatisierendes Koordinationsverhalten.

Katalytische Untersuchungen an der Suzuki-Miyaura Kreuz-Kupplung haben gezeigt, dass die definierten Komplexe **28** und **29** und die *in situ* hergestellten Katalysatoren

1/$Pd(OAc)_2$ und **3**/$Pd(OAc)_2$ die Reaktion von 4-Bromtoluol mit Phenylboronsäure gut unterstützen. Die Katalysatoren, die auf Ligand **3** basieren, liefern mindestens genauso gute Ergebnisse bezüglich der Ausbeute wie der analoge Komplex mit dppf (dppf = 1,1'-Bis(diphenylphosphino)ferrocen). Die Ausbeuten, die mit Katalysatoren basierend auf Ligand **1** erreicht wurden sind ebenfalls gut, allerdings ein wenig niedriger als die vom dppf-Analogon erreichten Werte. Die Pd-katalysierte Cyanierung wird von den definierten Komplexen mit dppf besser unterstützt als von beiden Ferrocen-basierten Pyridylphosphinliganden.

Die Liganden **1**, **2** und **3** zeigen in cyclovoltammetrischen Untersuchungen reversibles Verhalten bezüglich der ferrocenbasierten Redoxwelle. Die Chlorogold(I)-Komplexe **22**, **23** und **24** zeigen ebenfalls ein solches Verhalten. Durch die Koordination wird das formale Elektrodenpotential deutlich um ca. 0.2 V gegenüber den unkoordinierten Liganden verschoben.

Contents

1 Introduction

1.1 General Introduction — Motivation and Outline

Phosphinylated *N*-heterocycles, particularly pyridylphosphines, are of great importance in coordination chemistry and have found numerous applications in catalysis.[2–4] Their ligand properties can be easily tuned by changing molecular parameters like the type of the donor groups or their substituents. This explains their high popularity. Pyridylphosphines are oligodentate ligands. They have at least two coordination sites. Consequently, two different modes of coordination are possible: bridging versus chelating. A bridging ligand forms oligonuclear complexes or polymers. A chelating ligand forms usually mononuclear complexes.

The combination of a soft *P* and a hard *N* donor atom[5] makes these ligands typical hybrid ligands, which can exhibit particularly interesting binding profiles. For suitable metal-ligand combinations this can result in a hemilabile binding profile.[6–8] The term “hemilabile” was coined by Jeffrey and Rauchfuss in 1979.[9] They investigated the chemistry of phosphine-amine and phosphine-ether ligands with the expectation that these ligands would bind sufficiently strong to allow isolation of the corresponding complexes. However, the hard ligand component tended to dissociate readily, thus generating a vacant site for substrate binding.[10] This is ideal for catalysis.

Ligands are usually differentiated by the number and type of donor atoms and the length and flexibility of the bridging unit. A wide range of ligands with simple organic backbone units like alkyls and aryls is known.[2] Ligands, which contain a ferrocendiyl-

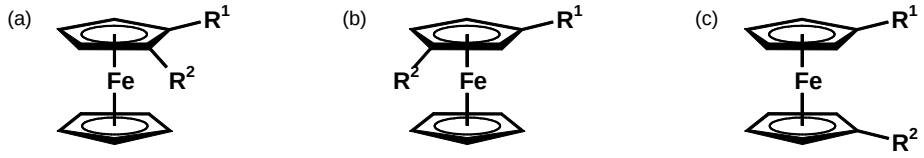

Fig. 1.1: Unsymmetrical disubstitution on ferrocene: 1,2- (a), 1,3- (b) and 1,1'-type (c).

based backbone are a special class. The ferrocene moiety can act in three general ways as a connector between two substituents or donor groups. First, ferrocene can be 1,2-disubstituted, second, 1,3-disubstituted and, third, (the more relevant) 1,1'-disubstituted (Fig. 1.1). Phosphinoferrocenes of the 1,2-type are relatively common and comprehensively documented.[11–16] Almost all of them are utilised in asymmetric catalysis because of their stereochemical characteristics. Derivatives of the 1,2-type are planar chiral, unless the two substituents are identical. Ferrocene-based *P*,*N*-ligands of this type such as [2-(diphenylphosphino)ferrocenyl]ethyldimethylamine (PPFA) are well known and widely applied.[17–19] 1,3-disubstituted ferrocenes have found usage as electrochemical sensing molecules, photoresponsive molecules and liquid-crystalline materials, for instance.[20] However, analogous systems with a 1,1'-arrangement are rare, which is surprising in view of the ubiquity and versatility of 1,1'-substituted bidentate ferrocene ligands.[21,22] The only such system that has attracted some attention is the ferrocene-based pyridylphosphine ligand 1-(diphenylphosphino)-1'-(pyrid-2-yl)-ferrocene (**1**) shown in Fig. 1.2.

While the synthesis of **1** was described already by Butler in 1992,[1] nearly no investigations concerning the coordination chemistry of this ligand have been reported to

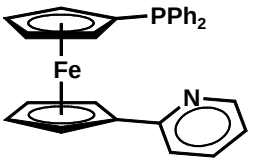

1

Fig. 1.2: 1-(Diphenylphosphino)-1'-(pyrid-2-yl)ferrocene (**1**).

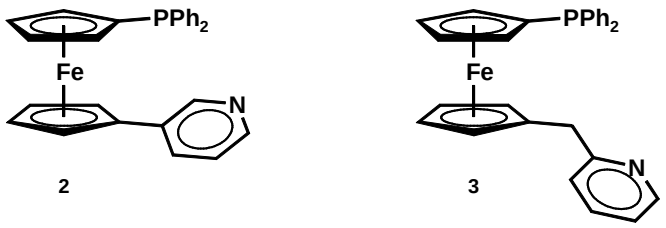

Fig. 1.3: Homologous 1,1'-ferrocene-based pyridylphosphines **2** and **3**.

date. Only Tani and coworkers utilised **1** in the synthesis of a rhodium bis(chelate) complex,[23] which later became subject of a quantum-chemical study.[24]

Systematic variations of **1** are its 3-pyridyl isomer, 1-(diphenylphosphino)-1'-(pyrid-3-yl)ferrocene (**2**) and the more flexible methylene-spaced analogue 1-(diphenylphosphino)-1'-[(pyrid-2-yl)methyl]ferrocene (**3**) displayed in Fig. 1.3.

Subtle structural differences may have a dramatic influence on the coordination mode, i. e. chelating versus bridging, and this will be a key issue of this thesis. Ligands like 2,2'-bipyridine, which contain pyrid-2-yl groups in the neighbourhood to a second donor atom, are known for chelating coordination.[25] **1** contains a pyrid-2-yl group and forms a rhodium bis(chelate) complex [Rh(cod)(**1**)],[23] although the number of atoms in the resulting chelate ring is seven, which is larger than the preferred ring sizes of five and six atoms. Ligands equipped with pyrid-3-yl groups instead mostly bind in a bridging coordination mode. For example, 3,3'-bipyridine usually forms polymeric complexes.[26] The number of atoms in a hypothetical chelate ring formed by **2** would be eight, a chelate coordination is therefore unlikely. **3** is equipped with a pyrid-2-yl group. If **3** forms a chelate, the chelate ring would contain eight atoms, like in the case of **2**. Nevertheless, both modes, bridging and chelating, might be possible for **3**, owing to the presence of the methylene spacer.

The ball-bearing like characteristics of the 1,1'-ferrocendiyl backbone allows twist angles between 0 ° (eclipsed) and 180 ° (diametrically opposed) for the substituents. Tilting of the ferrocene moiety facilitates small variations in the distance between both

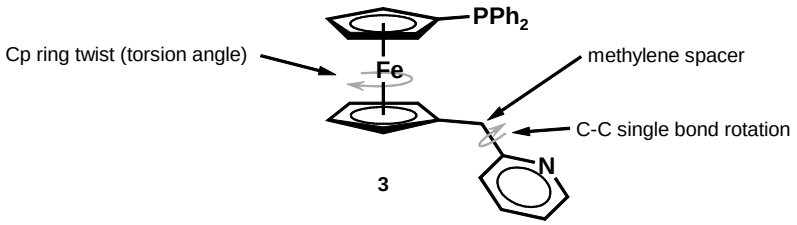

Fig. 1.4: Flexibility elements in **3**.

donor groups. Furthermore, the methylene spacer in **3** leads to additional flexibility and allows an even larger range of distances between the *N*-donor and the ligand backbone. Also the adjustment of the nitrogen donor atom in the pyridyl group can be influenced by the rotation around the C–C single bond. These factors may cause a variable, potentially hemilable, coordination behaviour of **3**, taking advantage of its flexibility. In Fig. 1.4 the relevant flexibility elements of **3** are shown.

The primary objective of the research described in this thesis is the preparation of the ligands **1** - **3** and the subsequent exploration of their fundamental coordination chemistry. In particular, the focus will be on transition metals of group 12 (zinc, cadmium, mercury), group 11 (silver, gold) and group 10 (palladium).

The coordination chemistry of the divalent group 12 metal ions is expected to be particularly simple. The coordination number is usually four, which is expressed in a typical tetrahedral coordination geometry, caused by the d^{10} electron configuration. Furthermore, Zn^{II} and Cd^{II} are redox-inert. Metal redox processes would interfere unfavourably with cyclovoltammetric experiments to explore the utilisation of the ligands as potential molecular electrochemical sensors. The monovalent group 11 metal ions of silver and gold are also d^{10} configurated. The coordination numbers of Ag^{I} and Au^{I} are usually even lower than four, which can give rise to interesting secondary metal-ligand or metal-metal interactions. Because of the high popularity and the commercial benefit of palladium complexes in catalytic processes (Nobel prize for chemistry 2010[27]), the

coordination chemistry towards Pd^{II} (group 10) is investigated, too. Again tetracoordination is expected to occur, in this case, however, in a square-planar geometry owing to the d^8 configuration.

In addition to differences concerning the coordination chemistry of the selected transition metals in terms of the HSAB principle, the resulting complexes are also expected to show up variability due to the ligands' geometric properties. Potential applications of **1** - **3** as redox-active ligands in electrochemical ion sensing will be addressed utilising redox-inert metal ions like Zn^{II} and Cd^{II}. Furthermore the application of palladium complexes in selected catalytic processes will be investigated.

1.2 Ferrocene

Ferrocene was prepared for the first time in 1951, independently by two different groups. The discovery was made by serendipity. Kealy and Pauson tried to synthesise fulvalene by the oxidative coupling of cyclopentadienyl magnesium bromide with ferric chloride.[28] The high temperature reaction of cyclopentadiene with iron observed by the group around Miller also afforded ferrocene.[29] Wilkinson[30] and Fischer[31] were awarded with the Nobel prize for chemistry in 1973 for the elucidation of the ferrocene structure. The interest in complexes of transition metals with hydrocarbons increased immediately. Historically, this may be considered as the hour of birth for organotransition metal chemistry. Since its discovery, ferrocene has become more and more remarkable. Today, ferrocene-based compounds are used in applications ranging from catalysis and material sciences to bioorganometallic chemistry.[11,32]

1.2.1 Physical and Electronic Properties

Ferrocene is an air-stable, orange crystalline solid which can be easily sublimed in vacuum or at atmospheric pressure by heating. This is due to its comparatively high vapour pressure of 2.6 hPa (100 °C). It is soluble in all common solvents, except water.

Formally, ferrocene can be considered as being composed of two cyclopentadienyl anions which bind to the central iron(II) ion in a sandwich-like manner. However, the bonding is not ionic, but predominantly covalent. The resulting uncharged complex has 18 valence electrons (VE). This noble gas electron configuration of krypton makes ferrocene exceptionally stable. Interestingly, the iron(II) centre is easily oxidised to iron(III) at low potentials (ca. 0.5 V vs. SCE[33]). The ferrocene/ferrocenium redox couple shows perfectly reversible behaviour because of the stability of the 17 VE ferrocenium cation. This can be understood by considering the molecular orbital (MO) scheme of ferrocene (Fig. 1.5), which shows that the highest occupied molecular orbital (HOMO) is essen-

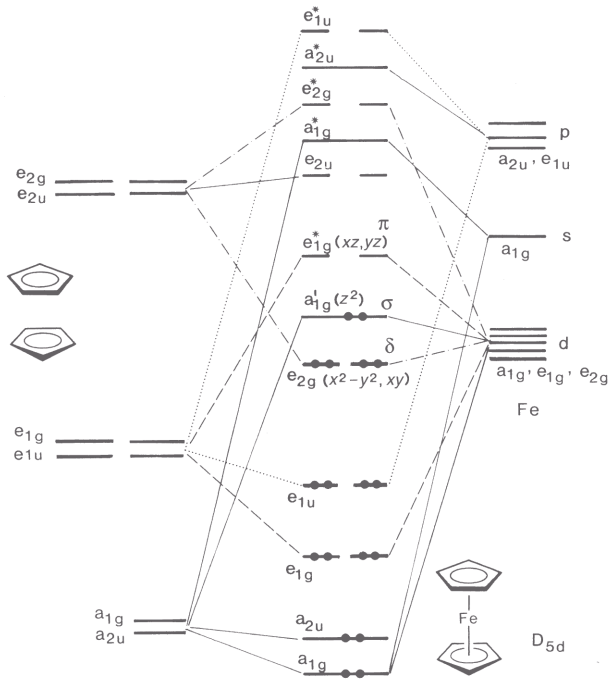

Fig. 1.5: MO scheme of ferrocene in staggered conformation.[33]

tially non-bonding. The weakly bonding character of the e_2- and the nearly non-bonding character of the a_1-symmetric orbitals is a reason for the existence of metallocenes with less than 18 valence electrons, for example manganocene (17 VE), the isoelectronic ferrocenium cation (17 VE), chromocene (16 VE) and even vanadocene (15 VE).[33] Due to their stability and reversible redox behaviour, ferrocene derivatives are well suited for electrochemical experiments like cyclic voltammetry (CV). Ferrocene is recommended by the International Union of Pure and Applied Chemistry (IUPAC) as a reference standard in such experiments.

1.2.2 Chemical Behaviour

Ferrocene undergoes reactions which are characteristic for electron-rich aromatic compounds. It is prone to electrophilic aromatic substitution. This is caused by the high electron density of the cyclopentadienyl ring systems. In comparison to benzene, ferrocene reacts $3 \cdot 10^6$ times faster in these reactions.[33] Ferrocenium instead, which is formed by the reaction of ferrocene with strongly oxidising electrophiles, is inert towards electrophilic attack. Hence, direct halogenation, nitration etc. of ferrocene is impossible.

Derivatisation of ferrocene can be also realised conveniently by metallation reactions. For example, the reaction with two equivalents of butyllithium in the presence of *N*,*N*,*N*',*N*'-tetramethylethylendiamine (TMEDA) and subsequent treatment with an electrophile[34] cleanly leads to symmetrical 1,1'-disubstitution. The preparation of 1,1'-unsymmetrical ferrocenes is less straightforward. A selective monolithiation of ferrocene by simple reaction with one equivalent of buthyllithium is not possible. Today, suitable synthetic procedures have been developed and new routes to unsymmetrical substitution are known: 1. selective transmetallation of 1,1'-bis(tri-*n*-butylstannyl)ferrocene, 2. selective lithium-halogen exchange of 1,1'-dibromoferrocene and 3. 1-phenyl-1-phospha-[1]-ferrocenophane ring opening reaction.[35] The latter two routes have been used in the work describes in this thesis (for details see Chapter 2).

1.3 *P,N*-Donors

P,*N*-ligands are heterodentate ligands, which combine a hard *N* donor site with a soft *P* donor site in one and the same ligand molecule. This combination generates a unique binding profile, since the π-acceptor character of the *P* site is able to stabilise a metal centre in a low oxidation state, while the nitrogen σ-donor ability can make the metal more susceptible to oxidative addition reactions. A survey about hard and soft donors in terms of the HSAB principle is given by Pearson[5,36] and Woodward.[37] Heteroditopic ligands are of great importance in coordination chemistry, since this combination can afford hemilabile binding profiles. Not surprisingly, they have found numerous applications in catalysis.[18,19,38] A classification of *P*,*N*-ligands has recently been developed and reviewed, featuring their catalytic applications by the type of donor groups[17] and their backbone unit.[2] Because the present work exclusively deals with pyridine type *N*-donors and phosphine type *P*-donors, other donor types will not be described here.

Generally, the pyridine donor is classified as a medium hard donor. Pyridine and ammonia split d-orbitals of metal cations energetically in a similar manner.[39] Due to its π-system and the nitrogen sp^2-lone pair, pyridine is easier to polarise than ammonia. Pyridine is a weaker ligand than ammonia; it is placed on the borderline between hard and soft according to Pearson.[40] The coordination chemistry of pyridine has been extensively investigated and reviewed.[41]

Phosphine donors are classified as soft in terms of the HSAB principle. They have π-acceptor character. Usually, the π-acidity of the phosphorus donor atom increases with the electronegativity of its substituents.

1.3.1 Pyridylphosphines

Pyridylphosphine ligands have been known since 1944.[3,42] Initially, these simple phosphine derivatives (Fig. 1.6) were only prepared in very low yields. Over the years,

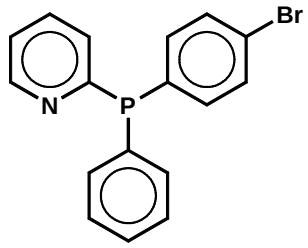

Fig. 1.6: One of the first pyridylphosphines: Phenyl-*p*-bromophenyl-2-pyridylphosphine.

the availability of such compounds increased and a wide variety of pyridylphosphine ligands are known today. Most of them have been used for palladium-catalysed reactions, as mentioned before. 1,2-Ferrocene-based ligands of this type are well known and have proved useful in this field.[11,12,43] There is still a lack of information concerning the coordination behaviour of 1,1'-ferrocene-based *P*,*N*-ligands in the literature. Chapters 3 - 5 will give detailed insight into the coordination chemistry of known 1,1'-ferrocene-based *P*,*N*-ligands towards group 12 and group 11 metals in comparison to the new ligands investigated in the present work.

1.4 Field of Potential Applications

Potential uses of ferrocene-based pyridylphosphine ligands are manifold. Within the scope of this theses, two aspects are of particular interest: The redox chemistry of ferrocene, or metallocenes in general, has been explored in detail. The utilisation of ferrocene ligands as electrochemical sensors needs no special mentioning.[44] Also the use of *P*,*N*-ligands in homogeneous catalysis is well documented.[4,17,18,38] Most of them are simple organic ligands or 1,2-substituted ferrocenes. 1,1'-unsymmetrically disubstituted ferrocenes instead, are hardly known at all in catalytic chemistry.

1.4.1 Electrochemical Sensors

A molecular redox sensor is a host molecule which has, according to its redox state, different chemical affinities to a guest molecule. Such sensors are composed of a redox-active unit and a receptor. The redox-active unit needs to show reversible electrochemical behaviour. The receptor needs to exhibit strong affinity and also selectivity for a guest molecule. Furthermore, these two functional units need to interact substantially with one another. Only if these conditions are fulfilled, the coordinated and the free species will gave rise to separate redox signals in the voltammogram. Only in this rare and special case can a redox sensor be characterised as highly effective.

The cyclic voltammogram is the result of the CV experiment. In Fig. 1.7 an ideal CV is displayed. A starting potential E is varied with constant scan rate v to a reversal potential E_λ and back to the potential E. The measurement category is the current i. The redox-behaviour of a sample can be classified as reversible if 1. the current ratio i_{pa}/i_{pc} is equal to 1, which shows that the electrogenerated species is stable (at least on the CV timescale), 2. $i_{pc} \approx \sqrt{v}$ and 3. the peak-to-peak separation between E_{pa} and

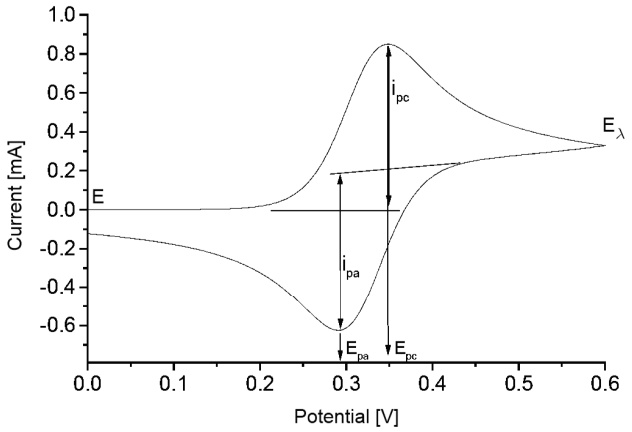

Fig. 1.7: Basic parameters for a cyclic voltammogram. E = starting potential, E_λ = reversal potental, E_{pa} = anodic peak potential, E_{pc} = cathodic peak potential, i_{pa} = anodic peak current, i_{pc} = cathodic peak current.

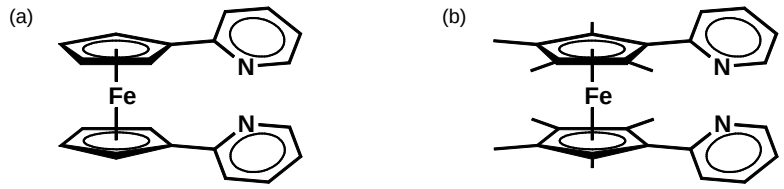

Fig. 1.8: 1,1'-Di(pyrid-2-yl)ferrocene (a) and 1,1'-di(pyrid-2-yl)octamethylferrocene (b).

E_{pc} (ΔE_p) = 59/n mV (n = number of electrons exchanged per molecule). It must be stressed, however, that, in measuring the peak-to-peak separation, a deviation of 10-20 mV from the theoretical value (especially at higher scan rates) does not compromise the criterion of reversibility.[45–47]

Two examples of pyridyl-functionalised ferrocene-based redox-sensors are displayed in Fig. 1.8.[48,49] Both ligands show high chemical affinities towards Pd^{II} and Pt^{II} compounds. Coordination-induced shifts of the half-wave potentials of ca. 120 mV were detected.[50,51] Particularly large shifts of the half-wave potential of up to ca. 400 mV were detected with the octamethylated ligand (Fig. 1.8 b) for the metal ions Zn^{II}, Cd^{II}, Ca^{II} or Mg^{II}.[52] These significant shifts characterise 1,1'-di(pyrid-2-yl)octamethylferrocene as a highly effective ferrocene-based redox sensor.

1.4.2 Catalytic Application

Lowering of the activation barrier in chemical reactions by catalysts is of great commercial importance. More than 80 % of the processes in the chemical industry are catalysed to optimise their commercial usage. Selectivity of catalysts is important if more than one product is obtained in the reaction process. If the chosen catalyst promotes only the desired reaction, impurities by side products can be avoided.[53,54]

Ferrocene-based ligands are enormously successful in catalytic applications. One of the most versatile and popular 1,1'-disubstituted chelate ligand in this context is 1,1'-

bis(diphenylphosphino)ferrocene (dppf). For example, suitable complexes of dppf are able to promote C–C, C–N and C–S bond forming reactions.[21,55]

Chiral ferrocene ligands are extremely successful in asymmetric catalysis. One of several privileged examples is the Josiphos ligand family,[43,56] certainly one of the most versatile and successful ligand families in asymmetric catalysis. Besides these famous *P*,*P*-ligands, some *P*,*N*-ligands have attracted similar attention. For example, PPFA (Fig. 1.9) proved to be very effective for a variety of catalytic asymmetric transformations.[43]

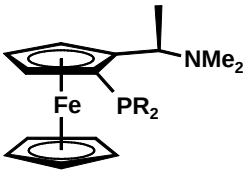

Fig. 1.9: [2-(Diphenylphosphino)ferrocenyl]ethyldimethylamine (PPFA).

2 Ferrocene-Based Pyridylphosphine Ligands

The synthesis and characterisation of bidentate and tridentate 1,1'-unsymmetrical ferrocene-based pyridylphosphine ligands is described. Spectroscopic data, results of X-ray diffraction analyses and electrochemical investigations will be discussed.

2.1 Introduction

Ferrocene ligands bearing a combination of both donor groups, viz. ferrocene-based pyridylphosphines, gave their debut in the literature in the beginning of the 1990s. 1-(Diphenylphosphino)-1'-(pyrid-2-yl)ferrocene (**1**), its 1,2-isomer and other 1-(diphenylphosphino)-1'-(N-heteroaryl)ferrocenes were reported by Butler.[1,57] Selected examples are shown in Fig. 2.1. Due to the difficulties concerning their synthesis, the interest in these systems waned away. Today, new more convenient methods for the preparation of 1,1'-unsymmetrical functionalised systems have been developed. Although the accessibility of such systems is much easier, ferrocene-based pyridylphosphine ligands are still rare.

A useful method to prepare 1,1'-unsymmetrical phosphinoferrocene is the *P*-[1]-ferrocenophane ring opening reaction with phenyllithium. Starting from 1-phenyl-1-phospha-[1]-ferrocenophane, which can be prepared by the reaction of 1,1'-dilithioferrocene with

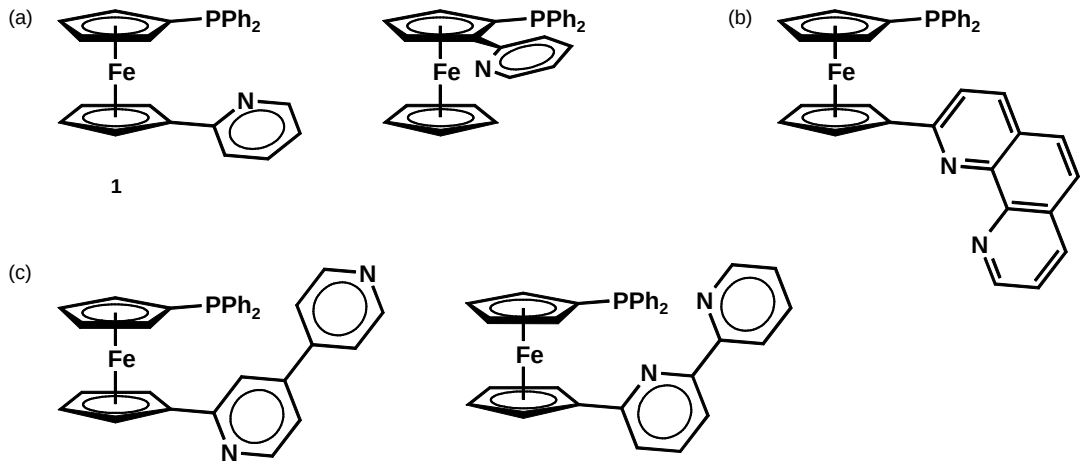

Fig. 2.1: 1-(Diphenylphosphino)-1'-(N-heteroaryl)ferrocenes; heteroaryl is pyridine (a), phenanthroline (b) and bipyridine (c).

dichlorophenylphosphine, 1-(lithio)-1'-diphenylphosphinoferrocene is afforded by the reaction with phenyllithium. This active species reacts easily with electrophiles (E) to 1,1'-unsymmetrical phosphinoferrocene derivatives (Fig. 2.2). The ferrocenophane cleavage reaction, first described by Seyferth and Withers,[58] has been utilised by Butler and Cullen for the preparation of 1,1'-bis[(alkyl/aryl)phosphino]ferrocenes.[59]

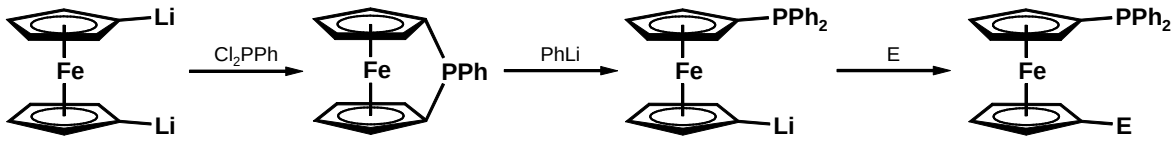

Fig. 2.2: *P*-[1]-ferrocenophane ring opening reaction.

A method with much wider scope involves the reaction of 1,1'-dilithioferrocene with two equivalents of tributylstannyl chloride leading to 1,1'-bis(tri-*n*-butylstannyl)ferrocene, which is a precursor for the preparation of a wide range of 1,1'-unsymmetrical ferrocenes (Fig. 2.3). Adeleke utilised this precursor in the early 1990s to prepare *P*,*S*-ligands based on ferrocene by selective transmetallation at low temperatures.[60]

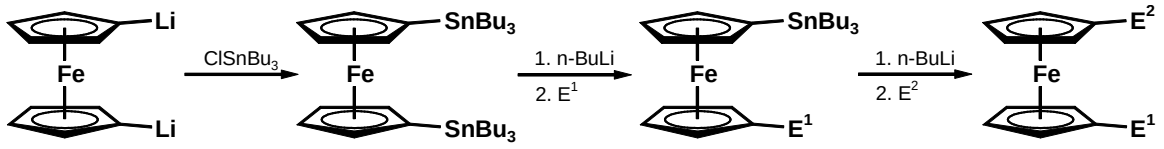

Fig. 2.3: Selective transmetallation of 1,1'-bis(tri-*n*-butylstannyl)ferrocene.

In 1994 Dong developed an elegant method to synthesise 1,1'-unsymmetrical ferrocenes.[61] He established the selective lithium halogen exchange of 1,1'-dibromoferrocene at low temperatures as shown in Fig. 2.4.[62,63] By this method a variety of unsymmetrical ferrocene derivatives have been synthesised amongst others by Butler in high yields.[64]

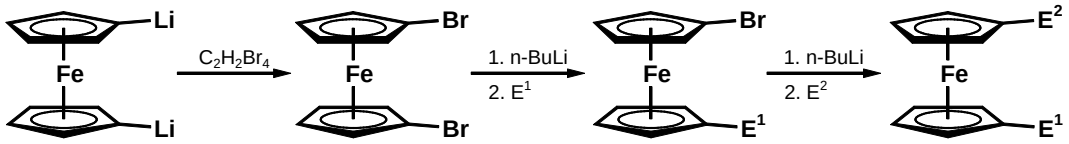

Fig. 2.4: Selective lithium halogen exchange of 1,1'-dibromoferrocene.

The focus of this work is on the ferrocene-based pyridylphosphines **1**, **2** and **3** (Chapter 1.1). While the synthesis of **1** has already been described by Butler,[1] compounds **2** and **3** are unknown so far. In his publication, Butler reported the coordination chemistry of a series of ferrocenyl- and ruthenocenylbipyridines, as mentioned before (Fig. 2.1 b, c). In conjunction with the potential structural modification of these ligands, he tried the reaction of pyrid-2-ylferrocene with butyllithium and then chlorodiphenylphosphine, which gave the ferrocene-based pyridylphospine 1-(pyrid-2-yl)-2-(diphenylphosphino)-ferrocene (Fig. 2.1 a). A different approach resulted in **1**, which was utilised independently by Tani in the synthesis of the bis-chelate complex [Rh(cod)(**1**)],[23] which later became subject of a quantum-chemical study.[24]

The synthetic procedure of **1** is described as the *in situ* preparation of 1-lithio-1'-(diphenylphosphino)ferrocene via cleavage reaction of 1-phenyl-1-phospha-[1]-ferrocenophane with phenyllithium in diethyl ether at -70 °C, followed by the treatment with

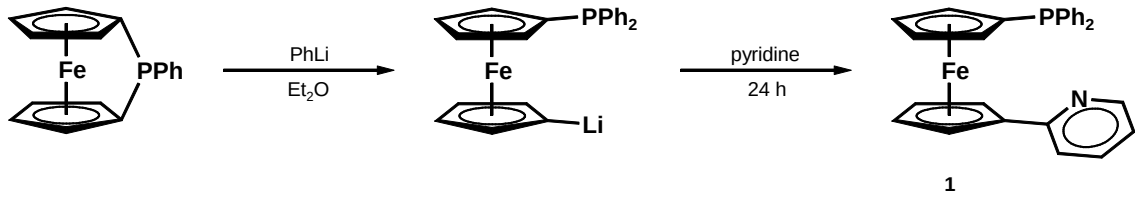

1

Fig. 2.5: Synthesis of **1** presented by Butler in 1992.

an excess of pyridine (Fig. 2.5). After hydrolysis the product was purified by column chromatography, yielding ca. 10 % of an orange oil, which solidified during drying under vacuum. Butler characterised **1** by ^{1}H NMR, MS and elemental analysis. This low-yield synthetic pathway affords the product contaminated with phosphine oxide impurities. This is probably caused by the introduction of the pyridyl group by Ziegler reaction, which involves an oxidative final step. It was therefore an aim of this work to improve the synthesis of **1**.

2.2 Bidentate Ligands (1 - 3)

Bidentate ligands contain two donor groups. They are able to form chelate complexes with a single metal centre or cyclic oligomers and polymeric chains. They can also form simple dinuclear complexes with two metal centres.

2.2.1 Synthesis and Characterisation of 1

By following Butler's published procedure for the synthesis of **1**, his unsatisfactory results could be reproduced. A moderate improvement of the yield (23 %) could be achieved by using particularly pure 1-phenyl-1-phospha-[1]-ferrocenophane, which was obtained by a literature procedure[58] with a revised, non-aqueous work-up. Instead of treatment with aqueous NH_4Cl solution the reaction mixture was filtered, evaporated

to dryness and purified by column chromatography under exclusion of moisture. The difficulties in the synthesis and handling of the ferrocenophane precursor may explain the lack of information about ferrocene-based pyridylphosphines in the literature.

As described above, there is the opportunity to prepare 1,1'-unsymmetrical ferrocenes by selective lithium-halogen exchange. Starting from 1,1'-dibromoferrocene, which is treated with one equivalent of *n*-butyllithium at low temperature and subsequently with chlorodiphenylphosphine, it is quite easy to prepare 1-bromo-1'-(diphenylphosphino)-ferrocene according to a known procedure[64] (Fig. 2.6). Purification of 1-bromo-1'-(diphenylphosphino)ferrocene by crystallisation gives brown, air-stable material in reproducible yields of about 70-80 %. Introduction of the pyridyl group by Ziegler reaction after selective lithium-halogen exchange gives **1**, but still not in acceptable yield.

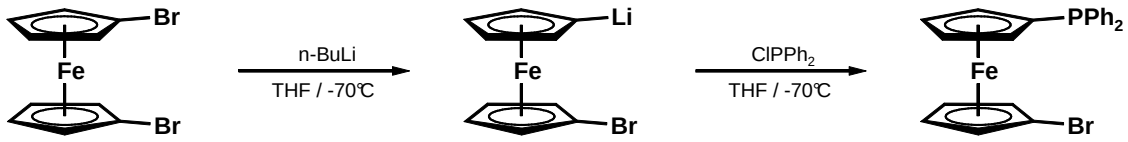

Fig. 2.6: Synthesis of 1-bromo-1'-(diphenylphosphino)ferrocene.

The classic palladium-catalysed Negishi cross-coupling reaction[65–67] turned out to be a much better method of attaching the *N*-donor site in the final step of the sequence. The addition of [$ZnCl_2$(1,4-dioxane)] after the selective lithium-halogen exchange of 1-bromo-1'-(diphenylphosphino)ferrocene leads to the active organozinc compound *in situ*. Reaction with 2-bromopyridine (Fig. 2.7) and subsequent column chromatographic work-up afforded pure **1** in satisfactory yield (48 %) as a dark orange oil, which solidified upon prolonged standing.

1 was found to be air-stable. Its solubility in polar solvents like dichloromethane is high. Crystals suitable for X-ray diffraction analysis were grown from a concentrated dichloromethane solution. The results of the structural characterisation are presented in Fig. 2.8. Structural and spectroscopic data are rather unexceptional. The signal of the pyridyl H^6 in the ^{1}H NMR and the phosphorus signal in the ^{31}P NMR spectrum

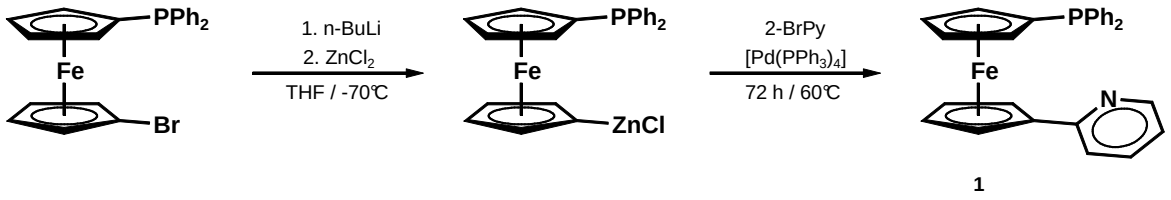

Fig. 2.7: Negishi cross-coupling reaction affording **1**.

are interesting diagnostic markers for later coordination chemistry experiments. NMR spectra of metal complexes of **1** are expected to exhibit shifted signals if the corresponding donor atom is coordinated.

Electrochemical investigations of **1** by cyclic voltammetry revealed the expected ferrocene-based oxidation plus an additional irreversible oxidation process at higher potential (Fig. 2.9 a). The ferrocene-based redox wave of **1** exhibits reversible behaviour, if the scan is reversed before the second oxidation process starts (Fig. 2.9 b). The ΔE_{P} value is 65 mV. The formal electrode potential $E^{0\prime}$ of the ferrocene-based process is anodically shifted by ca. 0.55 V with respect to decamethylferrocene (fc*). Comparison

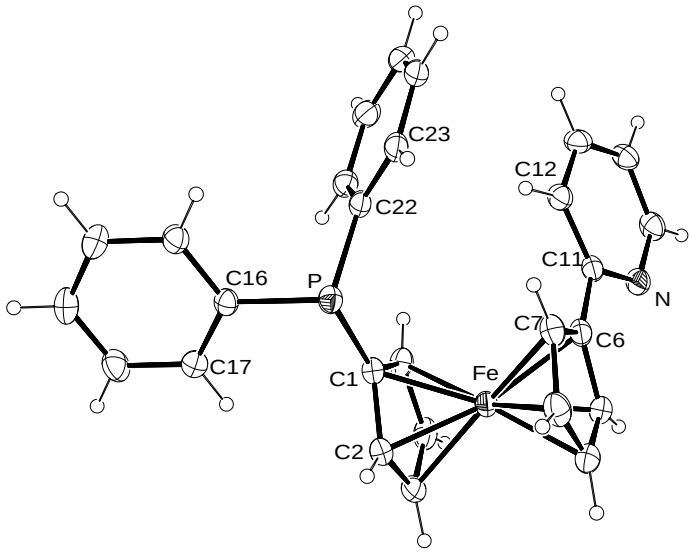

Fig. 2.8: Molecular structure of **1** in the crystal.

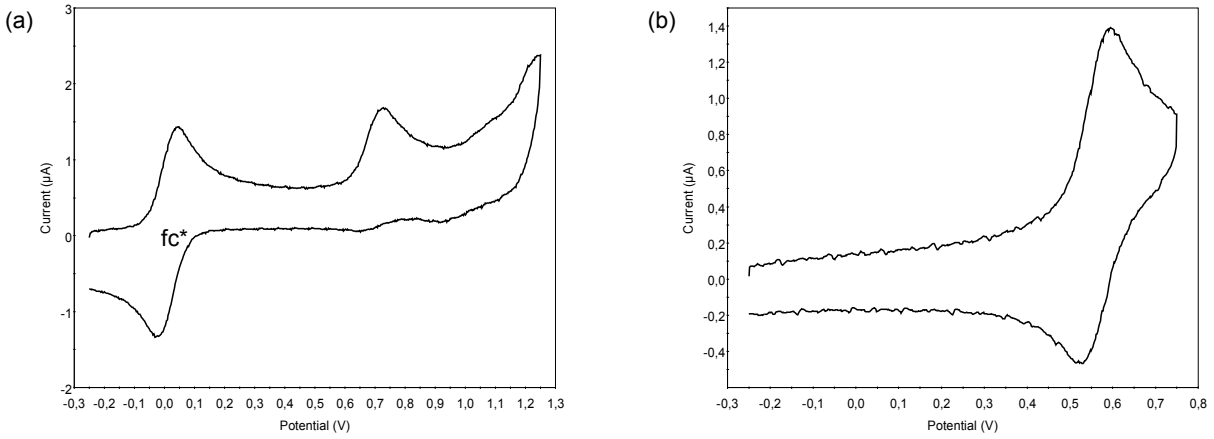

Fig. 2.9: CV of **1** (0.1 mM in DCM, 0.1 M [N^{n}Bu][PF_6], 100 mV/s), scan range from –0.25 V to +1.25 V (a) and from –0.25 V to +0.75 V (b).

with the results for simple ferrocene (0.53 V anodically shifted vs. fc*[47]) shows, that the electron-withdrawing effect of the pyridyl substituent and the weak electron releasing effect of the diphenylphosphino group in **1** almost cancel each other.

2.2.2 Synthesis and Characterisation of 2

The introduction of a pyrid-3-yl group instead of the pyrid-2-yl group by applying an analogous Negishi cross-coupling protocol with 3-bromopyridine failed. No product formation was observed and the starting materials were recovered. The nitrogen donor atom in the pyridyl group potentially coordinates to the organozinc moiety. This coordination affects the orientation of the bromo substituent, which is important for the following catalytic reaction. In the case of the pyrid-2-yl group the bromo substituent is in a position close to the chlorozinc moiety, so the transmetalation step of the catalytic cycle is unhindered. If the bromo substituent is in β-position to the nitrogen donor, the coordination could prevent the reactive parts undergoing the transmetalation step by holding them too far apart from each other.

Another option for C-C bond formation is the Suzuki cross-coupling reaction between organoboronic acids and aryl halides.[68–70] The starting point is again 1-bromo-1'-(di-

phenylphosphino)ferrocene, which contains the halide for the cross-coupling reaction. 3-Pyridyl boronic acid is commercially available, but it is rather expensive. Therefore the preparation of the synthetic equivalent 3-pyridylboroxin was attempted,[71,72] which can be directly assembled in the Suzuki reaction in a 1,4-dioxane/water solvent mixture (Fig. 2.10). Column chromatographic work-up afforded **2** in yields of up to 43 %. The dark orange oil crystallised upon prolonged standing.

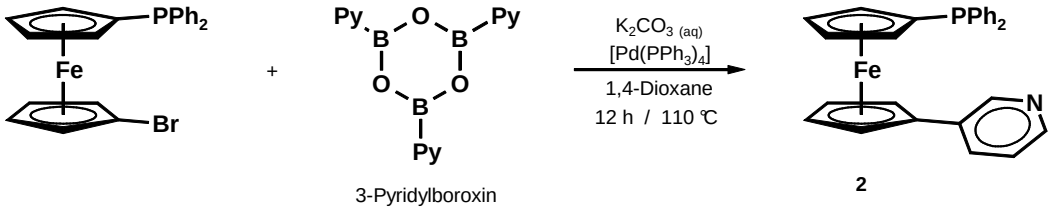

Fig. 2.10: Synthesis of **2** via Suzuki reaction with 3-pyridylboroxin.

The solubility properties of the air-stable ligand **2** are comparable to those of **1**. Structural characterisation of crystals suitable for X-ray diffraction analysis has been carried out and the result is shown in Fig. 2.11. No unusual features concerning the bond

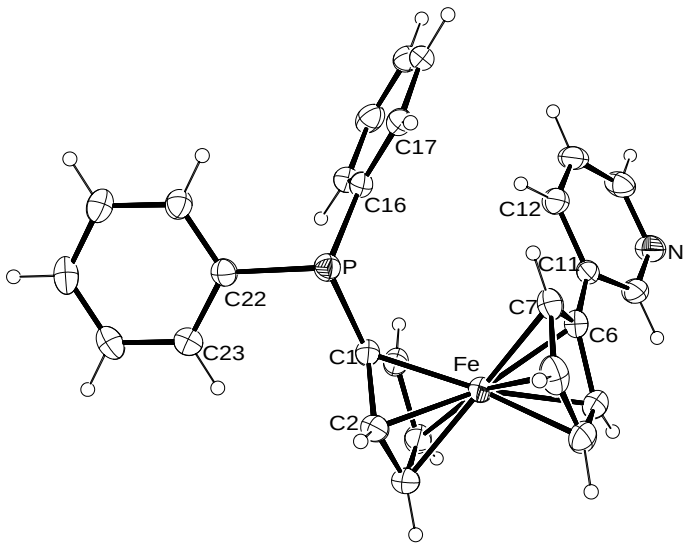

Fig. 2.11: Molecular structure of **2** in the crystal.

parameters are observed. The ^{1}H NMR spectrum shows four signals typical for a 1,1'-unsymmetrical substitution at the ferrocene unit and two characteristic low field signals of the pyridyl protons H^2 and H^6. A single signal is observed in the ^{31}P NMR spectrum at –17.7 ppm. The APCI mass spectrum shows peaks at 464 (45%) $[MO + H]^+$ (caused by reactions during the ionisation process, cf. ^{31}P NMR), 448 m/z (100%) $[M + H]^+$ and several defined fragments at lower m/z.

2 was also investigated by cyclic voltammetry. Under the same conditions its behaviour is rather comparable to that of **1**: A ferrocene-based oxidation plus an additional irreversible oxidation process at higher potential is observed. The ferrocene-based redox wave is anodically shifted by ca. 0.70 V with respect to fc* and displays reversible behaviour (ΔE_P = 64.5 mV) if the scan is reversed before the second oxidation process starts. Interestingly, the pyrid-3-yl group causes an anodic shift which is ca. 150 mV higher than that of **1** containing a pyrid-2-yl group.

2.2.3 Synthesis and Characterisation of 3

The synthesis of **3** was carried out by Jiří Schulz in the group of Prof. Petr Štěpnička at Charles University, Prague, Czech Republic.

The synthesis of **3** started also with 1-bromo-1'-(diphenylphosphino)ferrocene,[64] which was first converted into 1-lithio-1'-(diphenylphosphino)ferrocene. Without isolation, this intermediate was reacted with pyridine-2-carbaldehyde to afford 1-[(pyrid-2-yl)hydroxymethyl]-1'-(diphenylphosphino)ferrocene (Fig. 2.12 a). Also a small amount of its corresponding ketone was obtained (Fig. 2.12 b). Following an analougous literature procedure,[73] the secondary alcohol was obtained after aqueous work-up and chromatography as an ochre solid in 58 % yield,

The subsequent reduction of the hydroxyl group proved to be a challenging task since the conventional methods, utilising Me_3SiCl / NaI, $NaBH_4$ / CF_3CO_2H or $LiAlH_4$ / $AlCl_3$

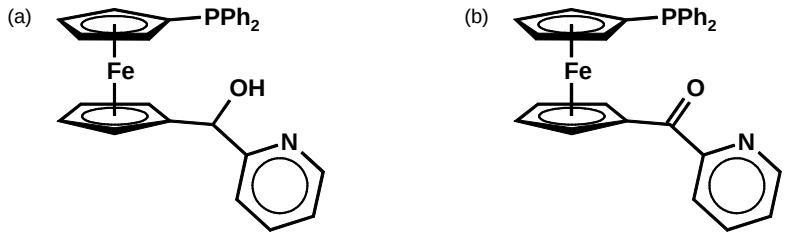

Fig. 2.12: 1-[(Pyrid-2-yl)hydroxymethyl]-1'-(diphenylphosphino)ferrocene (a) and its corresponding ketone (b).

failed.[74] In the end, the dehydroxylation was accomplished by reaction with SmI_2 / $(Me_2N)_3PO$ followed by the treatment with pivalic acid.[75] This synthetic procedure (Fig. 2.13) gave **3** in yields of up to 55 % as an amber oil, which solidified upon standing.

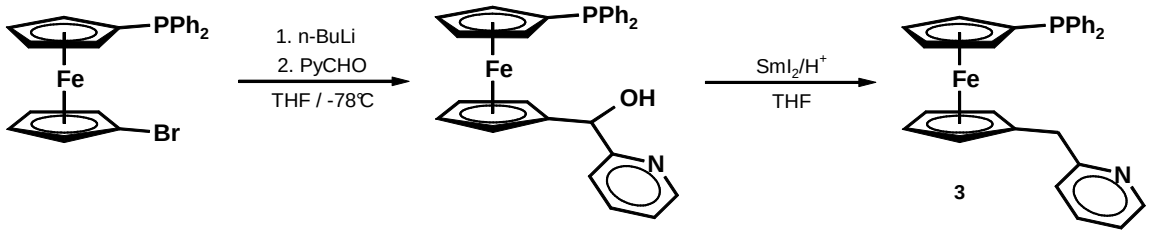

Fig. 2.13: Synthetic route to **3**.

The air-stable compound **3** is soluble in polar solvents like dichloromethane and diethyl ether. It was possible to obtain single crystals suitable for X-ray diffraction analysis. The molecular structure is shown in Fig. 2.14. Bond lengths and angles are as expected. The ^1H NMR spectrum shows four signals for the 1,1'-ferrocendiyl backbone and an additional signal for the methylene group next to the pyridyl unit between 3.63 ppm and 4.33 ppm. The signal due to the pyridyl H^6 is observed at lower field as mentioned before. The phosphorus NMR spectrum shows a single signal, whose chemical shift of –16.5 ppm is close to that of the corresponding signals found for **1** and **2**.

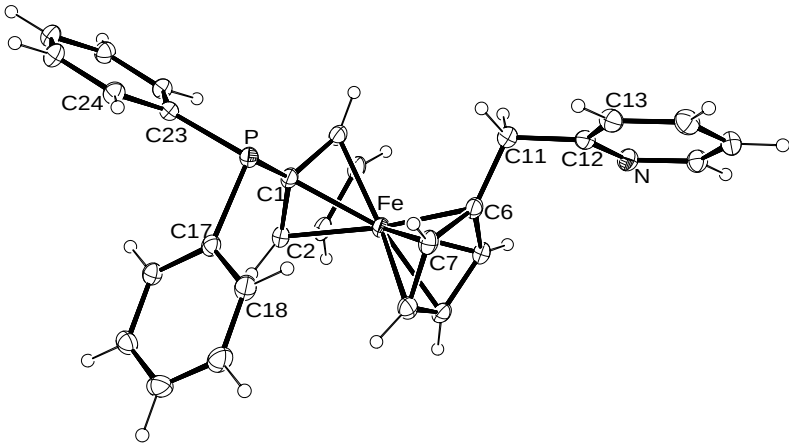

Fig. 2.14: Molecular structure of **3** in the crystal.

Similar to what was observed for **1** and **2**, cyclic voltammetry experiments with **3** resulted in a reversible oxidation wave of the ferrocene unit and an irreversible oxidation wave at higher potentials (Fig. 2.15 a). The reversible redox wave of the ferrocene unit appears 0.62 V anodically shifted with respect to fc*, if the scan is reversed before the second oxidation process starts (Fig. 2.15 b). The result is comparable with that of **1** and **2**. The ca. 70 mV higher Fe^{II}/Fe^{III} redox potential is caused by the positive inductive effect of the methylene group. The higher ΔE_P of 102 mV is probably caused by the tenfold higher concentration of **3** in the experiment.

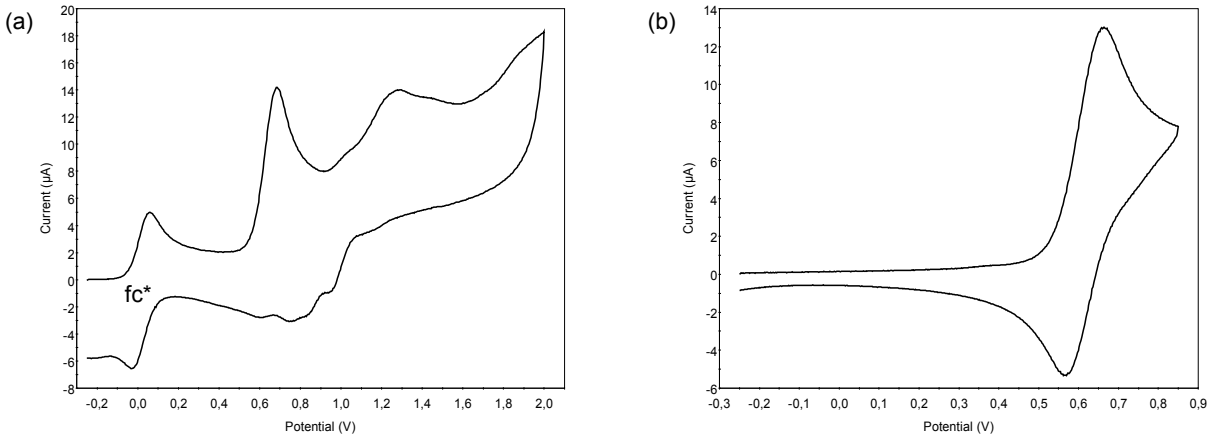

Fig. 2.15: CV of **3** (1.0 mM in DCM, 0.1 M $[N^nBu][PF_6]$, 100 mV/s), scan range from –0.25 V to +2.0 V (a) and from –0.25 V to +0.85 V (b).

2.3 Tridentate Ligands (4)

Beyond the bidentate ligands, it is an interesting question what happens if the ligand offers more than just two donor sites. There could be a “choice” for the metal centre, which donor atom is preferred. The *P*,*N*-motif can be expanded to an *N*,*P*,*N*- and a *P*,*N*,*P*-motif. Both possibilities were investigated.

2.3.1 Synthesis and Characterisation of a *N,P,N*-Ligand

The easiest way to synthesise an *N*,*P*,*N*-ligand system, which is very similar to **1**, is to start with the known bis(1’-bromoferrocenyl)phenylphosphine.[64] The Negishi coupling reaction with two equivalents of 2-bromopyridine is expected to afford the corresponding ligand (Fig. 2.16).

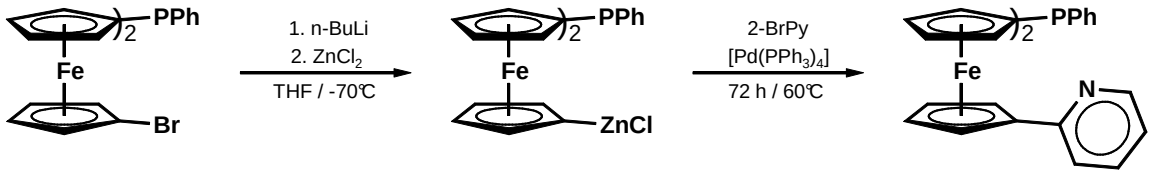

Fig. 2.16: Synthetic route to bis[1’-(pyrid-2-yl)ferrocenyl]phenylphosphine.

In my hands, it was not possible to reproduce the synthesis of bis(1’-bromoferrocenyl)-phenylphosphine Butler presented. The final ^{1}H NMR data did not correspond to those published by Butler. He obtained only one set of signals for the ferrocene unit. In our case, the NMR spectrum revealed two sets of signals belonging to the ferrocene unit, which implied inequivalence of both ferrocene units. Further reaction via the Negishi coupling gave a compound whose identity could not be established unequivocally. Only later crystallographic investigations of coordination experiments with mercury bromide revealed the nature of this ligand. It turned out that only one of the two ferrocene units is substituted with a pyridyl group. It is not clear in which step the problem occurs.

After several attempts this project was put on hold and the synthesis of an alternative *P*,*N*,*P*-ligand was considered in more detail.

2.3.2 Synthesis and Characterisation of the *P*,*N*,*P*-Ligand 4

The *P*,*N*,*P*-Ligand **4**, which contains one pyridine donor and two phosphine donor atoms, is easily synthesised by Negishi cross-coupling reaction of 2,6-dibromopyridine with two equivalents of 1-bromo-1'-(diphenylphosphino)ferrocene (Fig. 2.17). Column chromatography afforded 2,6-bis(1'-diphenylphosphinoferrocenyl)pyridine (**4**) in yields of up to 33 %.

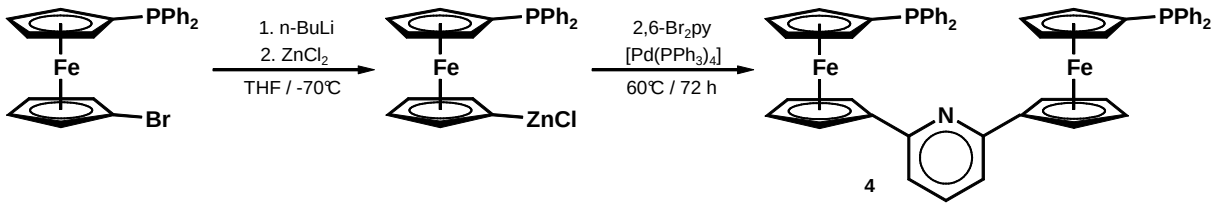

Fig. 2.17: Synthesis of 2,6-bis(1'-diphenylphosphanylferrocenyl)pyridine (**4**).

Characterisation was achieved by NMR spectroscopy, mass spectrometry and elemental analysis. Only a single signal is observed for both phosphorus atoms in the ^{31}P NMR spectrum, which demonstrates the symmetric structure of the molecule. The proton NMR spectrum shows only one set of signals belonging to both ferrocene units. The result of a single crystal X-ray diffraction study is shown in Fig. 2.18. Crystallisation in the presence of air causes oxidation of one of the phosphorus atoms. **4** shows only limited stability towards oxygen in solution.

The cyclic voltammogram of **4** shows two irreversible oxidation processes. The peak potential positions are anodically shifted with respect to fc* by 0.65 V and 1.21 V, respective.

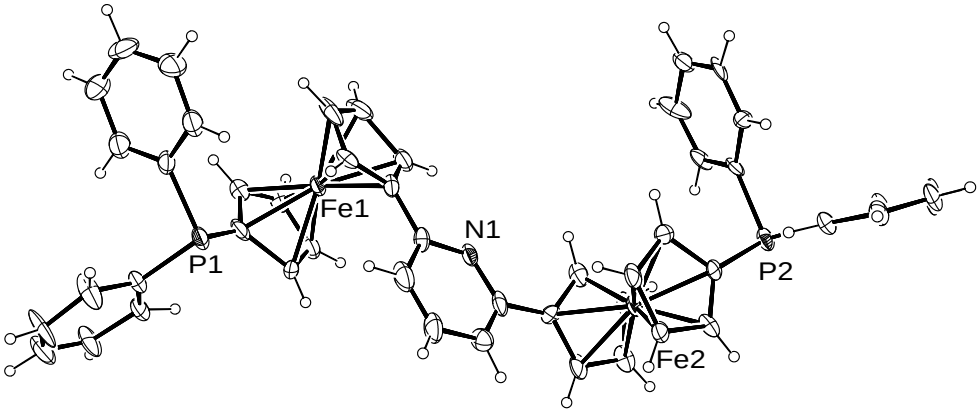

Fig. 2.18: Molecular structure of **4** in the crystal.

2.4 Summary and Conclusion

While the synthesis of the bidentate ligand **1** was already published,[1] it was possible to improve the original low yield procedure by establishing a more convenient one, whose final step is a Negishi cross-coupling instead of a Ziegler reaction in the originally reported synthesis. Key advantages are the air-stable intermediate 1-bromo-1'-(diphenylphosphino)ferrocene and higher yields. The synthesis of the new 3-pyridine isomer **2** by Suzuki cross-coupling reaction has been developed. The homologous ligand **3**, which contains a CH_2-linker between ferrocene and its pyrid-2-yl unit was synthesised via less conventional methods by the cooperation partners from the Czech Republic. Furthermore, the synthesis of analogous tridentate ligands was attempted. The synthesis of a *N*,*P*,*N*-ligand in analogy to the route to **1** met with limited success. Instead, the *P*,*N*,*P*-ligand **4** was synthesised using the Negishi methodology established in the synthesis of **1**. Structural characterisation of all ligands was possible by single crystal X-ray diffraction studies, which revealed no unexceptional features. CV measurements of **1**, **2** and **3** show a reversible ferrocene-based redox process if the scan is reversed before a second oxidation process starts at higher potentials. Probably the second oxidation process induces irreversible chemical reactions.

3 Coordination Chemistry I: Zinc, Cadmium and Mercury

This chapter describes the coordination chemistry towards the divalent group 12 metal ions Zn^{II}, Cd^{II} and Hg^{II} and discusses the synthesis and characterisation of complexes of the ligands **1**, **2** and **3**.

3.1 Introduction

The metals zinc, cadmium and mercury were chosen to explore the fundamental coordination chemistry of the ligands **1**, **2** and **3**. Aspects of the coordination behaviour in terms of the HSAB principle on the one hand and questions concerning the issue of bridging versus chelating coordination mode on the other hand were in the focus of interest. An important feature of these metals is the redox-inertness of the divalent M^{II} ions in the case of zinc and cadmium. Metal redox processes would interfere unfavourably with cyclovoltammetric experiments to explore the utilisation of the ligands as potential molecular electrochemical sensors.

It is known that pyridine and triphenylphosphine react coordinatively with group 12 metal halides. The molecular structures of simple pyridine complexes of the type $[MX_2(PyH)_2]$ (X = Cl, Br, I) of Zn^{II},[76,77] Cd^{II}[78] and Hg^{II}[79] show an approximately tetrahedral coordination geometry with two exceptions. $[CdCl_2(PyH)_2]$ and $[HgCl_2(PyH)_2]$

exhibit an octahedral coordination geometry in which each metal centre is surrounded by four halide atoms in equatorial and two pyridines in axial positions. The metal centres are bridged by both chloro ligands to form a chain of edge-sharing octahedra. Donor-metal distances are listed in Tab. 3.1.

The corresponding triphenylphosphine complexes $[MX_2(PPh_3)_2]$ with halides of zinc, cadmium and mercury have also been prepared and structurally characterised in the past.[80–82] The interligand angles of all three compounds lie between 103 °-116 °, which corresponds to an only slightly distorted tetrahedral coordination geometry. The donor-metal distance (Tab. 3.1) are considerably larger than in the pyridine compounds, which

Tab. 3.1: Selected bond lengths (pm) of $[MX_2(PyH)_2]$, $[MX_2(PPh_3)_2]$ and $[MX_2(dppf)]$ (M = Zn, Cd, Hg; X = Cl, Br, I).

	$[MX_2(PyH)_2]$	$[MX_2(PPh_3)_2]$	$[MX_2(dppf)]$
Zn–Donor[α]1 (X = Cl)	204.6	261.0	
Zn–Donor2 (X = Cl)	205.2	249.9	
Zn–Donor1 (X = Br)	203.6		
Zn–Donor2 (X = Br)	204.3		
Cd–Donor1 (X = Cl)	235	263.3	
Cd–Donor2 (X = Cl)	235	264.6	
Cd–Donor1 (X = Br)			265.4
Cd–Donor2 (X = Br)			261.8
Cd–Donor1 (X = I)		263.4	263.3
Cd–Donor2 (X = I)		265.7	265.4
Hg–Donor1 (X = Cl)	226.6	250.3	251.0
Hg–Donor2 (X = Cl)	226.6	253.2	251.6
Hg–Donor1 (X = Br)	238.2	255.0	
Hg–Donor2 (X = Br)	239.2	249.2	
Hg–Donor1 (X = I)	230.6	257.2	255.8
Hg–Donor2 (X = I)	230.6	255.6	257.2

[α]Donor = N in $[MX_2(PyH)_2]$, P in $[MX_2(PPh_3)_2]$ and $[MX_2(dppf)]$.

is expected with respect to the differences of the covalence radii of both donor atoms (P = 110 ppm, N = 70 ppm).[39] The largest difference in the donor-metal (M–N, M–P) distances was obtained in the case of zinc (ca. 50 pm). In the case of cadmium and mercury the differences have an average value of 25 pm. A single exception is detected in the $HgBr_2$ complexes. The donor-metal distances here differ only less than 15 ppm.

These facts can be understood, at least to a first approximation, by considering the HSAB principle. The medium hard Zn^{II} interacts strongly with the medium hard pyridine (comparatively short Zn–N bond), but only comparatively weakly with the soft phosphine (comparatively long Zn–P bond). The opposite is true in the case of the soft Hg^{II}, which interacts strongly with the soft phosphine (comparatively short Hg–P bond), but only weakly with pyridine (comparatively long Zn–N bond), which leads to very similar Hg-donor bond lengths despite the large difference of the covalence radii of N and P.

The ferrocene-based bis(phosphine) 1,1'-bis(diphenylphosphino)ferrocene (dppf) forms chelate complexes with several metal halides. Complexes containing group twelve metals are structurally characterised only in the case of Cd^{II} and Hg^{II}.[83–86] For both metals the typical tetrahedral coordination geometry has been found. The donor-metal distances are in line with those of the simple triphenylphosphine complexes (Tab. 3.1). Crystallographic data on zinc compounds have not been published. Only a single publication reports on physicochemical properties of [MCl_2(dppf)] (M = Co, Ni, Pd, Pt, Zn, Cd, Hg).[87] For the pyridine analogue of dppf, 1,1'-di(pyrid-2-yl)ferrocene, surprisingly no complexes with group 12 metals have been described. A zinc compound of its octamethyl analogue was reported in conjunction with the detection of divalent ions in solution.[52]

A ferrocene-based *P*,*O*-ligand (Fig. 3.1), which has its donor atoms in structurally similar positions like **1**, has been investigated in group 12 metal coordination chemistry.[88] Interestingly, for all three metals of the series, different results concerning their coordination behaviour were obtained. The molecular structure of the complex obtained with $ZnBr_2$ was identified as a *P*,*O* chelate (Fig. 3.2 a), which shows the expected tetrahedral coordination geometry (coordination number (CN) = 4). In contrast, the reac-

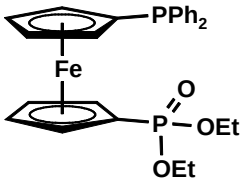

Fig. 3.1: Diethyl [1'-(diphenylphosphino)ferrocenyl]phosphonate.

tion with $HgBr_2$ afforded a symmetric bromo-bridged dimeric bis(phosphine) complex [{Hg(μ-Br)Br(L-κ^2*P*)}$_2$] (Fig. 3.2 b). Due to the short distance between the phosphoryl oxygen and the mercury atom of the neighbouring molecule (278.8 pm), the coordination geometry is better described as a distorted trigonal bipyramid (CN = 4 + 1).

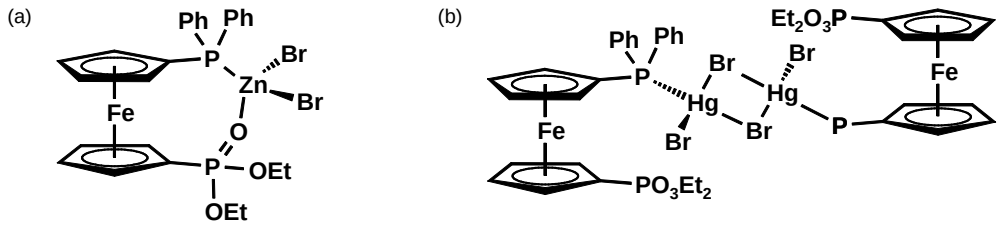

Fig. 3.2: Zinc (a) and mercury (b) complexes of the *P*,*O*-ligand shown in Fig. 3.1.

In solution an equilibrium between this bis(phosphine) species, a zinc-analogous *P*,*O*-chelate and a *P*,*O*-bridged dimer was observed. The existence of several isomers in solution (NMR spectroscopy) compared to a single molecular structure in the solid state (X-ray diffraction analysis) is a typical problem in this context and will become relevant for the work described in the present thesis.

The reaction with cadmium bromide gave a coordination polymer in which dinuclear {Cd(μ-Br)Br}$_2$ units are linked to infinite chains by symmetric pairs of the *O*,*P*-bridging phosphinophosphonate ligand (Fig 3.3). The donor set around the cadmium atoms is classified as a trigonal bipyramid rather than a square pyramid (CN = 5). The Cd–P bond length of 263.1 pm is in line with the donor-metal distance in [$CdBr_2$(dppf)].

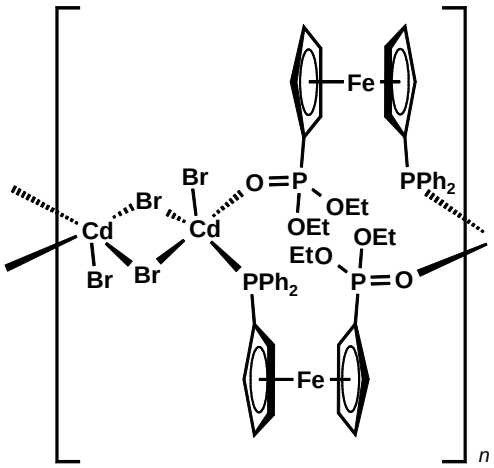

Fig. 3.3: Cadmium complex of the *P*,*O*-ligand shown in Fig. 3.1.

Related ligands, which are interesting due to their similarity with **1**, **2** and especially **3** concerning their flexibility and donor set (pyridyl and diphenylphosphino group) are the 1,1'-ferrocene-based pyridylphosphinocarboxamide ligands 1-(diphenylphosphino)-1'-*N*-[(pyrid-2-yl)-methyl]carbamoylferrocene and its pyrid-4-yl isomer (Fig. 3.4), whose coordination chemistry towards group 12 metals has been explored.[89] Only in the case of mercury and cadmium, well-defined solid products were obtained. The zinc compounds were reluctant to crystallise, presumably due to their high solubility.

The reaction of $CdBr_2 \cdot 4H_2O$ and $HgBr_2$, respectively, with the pyrid-4-yl isomer resulted in linear coordination polymers, as expected for pyrid-4-yl donors. Each metal centre is coordinated to the phosphorus and the pyridyl nitrogen donor of the neigh-

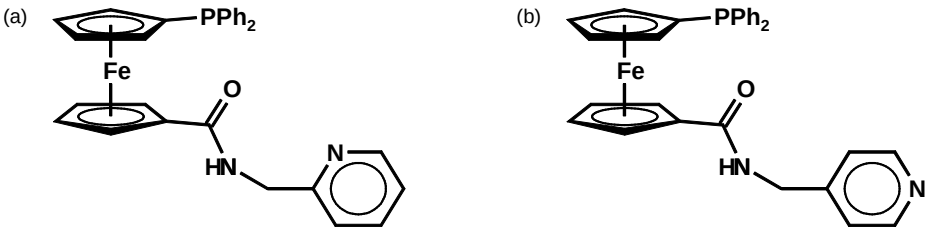

Fig. 3.4: 1,1'-Ferrocene-based pyridylphosphinocarboxamide ligands with pyrid-2-yl (a) and pyrid-4-yl (b) donors.

bouring molecule. Both molecular structures are very similar. Interestingly, the donor-metal distances (P–Hg, N–Hg) in the mercury complex are both identical (243.8 pm), while they differ markedly in the cadmium species (P–Cd 257.6 pm, N–Cd 230.1 pm). This is in accord with the HSAB principle (see page 29). The coordination tetrahedron is strongly distorted in the mercury complex. The interligand angles differ more than 20 ° from the ideal 109.5 °.[89]

The same reaction with the pyrid-2-yl isomer also afforded well-defined products. However, the molecular structures established by X-ray crystallography are rather complicated. The cadmium complex is formally a tetramer involving two types of cadmium centres with different coordination geometries and donor sets. This is a very special and relatively complicated molecular structure and is therefore not described further. It indicates that the coordination chemistry of cadmium may become more complicated than expected initially. The structure determination of the product obtained from the reaction with $HgBr_2$ revealed a centrosymmetric, doubly halide-bridged dimer commonly encountered among 1:1 phosphine mercury halide complexes. Because of the steric demand of the ligand, the coordination polyhedron (CN = 4) is severely distorted.[89]

3.2 Coordination Chemistry of 1

The synthesis of the ferrocene-based pyridylphosphine ligand **1** has been described in Chapter 2.2.1.

3.2.1 Synthesis and Characterisation of Zn Compounds

The reaction of an ethanolic solution of **1** with zinc halides ZnX_2 (X = Cl, Br, I) in a 1:1 molar ratio gave the orange to red chelate complexes [$ZnCl_2$(**1**)] (**5a**), [$ZnBr_2$(**1**)] (**5b**) and [ZnI_2(**1**)] (**5c**) as shown in Fig. 3.5. All three compounds have been found to be air-stable and show good solubility in polar solvents.

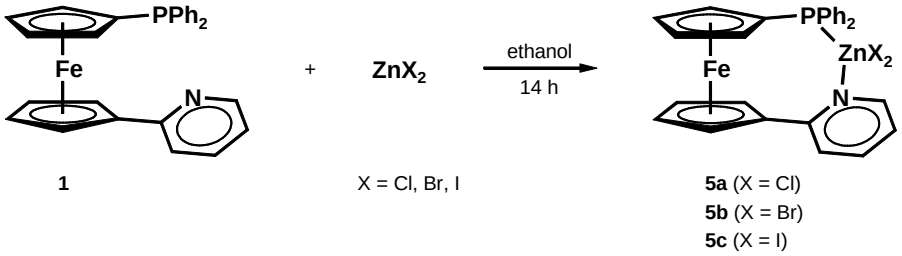

Fig. 3.5: Synthesis of Zn compounds of **1** in 1:1 stoichiometry.

One method to elucidate the binding mode in these complexes is an inspection of the shift of diagnostic signals in the ^{1}H and the ^{31}P NMR spectrum. The chemical shift of the pyridyl H^{6} and the shift of the phosphorus signal are given in Tab. 3.2. The signals of the pyridyl H^{6} in the ^{1}H NMR spectra are low-field shifted by about 1.1 ppm with respect to the free ligand. This is caused by deshielding due to the decrease of electron density in the vicinity of the pyridyl H^{6} by metal coordination to the pyridyl nitrogen atom. The phosphorus signals in the ^{31}P NMR spectra are shifted only slightly with respect to pristine **1**. While the phosphorus signals in **5a** and **5b** show the expected small low-field shift induced by the zinc coordination, the signal of **5c** was observed at slightly higher field than that of the free ligand.

Single crystal X-ray diffraction analyses gave a detailed picture of the binding mode. **5a** and **5b** each crystallise with two independent molecules in the unit cell, which differ slightly from each other. The results for molecule 1 are each shown in Fig. 3.6. For **5c** it was not possible to obtain material suitable for single crystal X-ray diffraction analysis.

Tab. 3.2: Chemical shifts of the diagnostic NMR signals of **5a**, **5b** and **5c** in ppm.

	1	**5a**	**5b**	**5c**
signal due to pyridyl H^{6} (^{1}H NMR)	8.47	9.57	9.57	9.60
phosphorus signal (^{31}P NMR)	–17.7	–14.0	–14.4	–19.2

Solvent: $CDCl_3$.

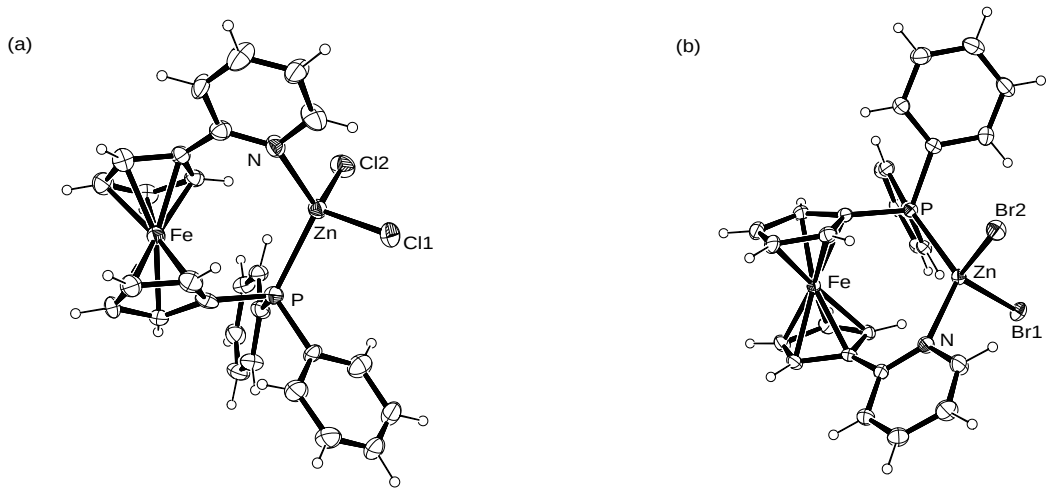

Fig. 3.6: Molecular structure of **5a** (a) and **5b** (b) in the crystal (only one of the two independent species is shown in each case).

Both structures show a distorted pseudo-tetrahedral coordination geometry as is typical for zinc. Selected parameters are listed in Tab. 3.3. The metal centre is coordinated to **1** in a chelate manner via phosphorus and nitrogen. The bite angle ∠ N-Zn-P in **5a** (120.82° molecule 1, 124.85° molecule 2) is the largest coordination angle. The differences between molecule 1 and 2 suggest a less fixed coordination geometry. Due to repulsive interactions between both halide atoms, the interhalide angle ∠ Cl1-Zn-Cl2 is also larger than the ideal tetrahedral angle of 109.5°. Accordingly, the remaining angles are smaller than 109.5°. The ferrocendiyl backbone is nearly untilted (1.39° molecule 1, 2.45° molecule 2). The flexibility of the ligand through Cp ring twist is expressed by the torsion angle τ (cf. Fig 1.4, page 4) (69.86° molecule 1, 75.01° molecule 2). The Zn–P bonds in **5a** (243.2 pm molecule 1, 245.3 pm molecule 2) are shorter than the average bond length in the simple triphenylphosphine complexes, while the Zn–N bonds (212.5 pm molecule 1, 210.4 pm molecule 2) are slightly larger than in the pyridine complexes (Tab. 3.1, page 28). Zn–Cl distances are unexceptional (ca. 223 pm).

The same tendencies were observed for both molecules in the structure of **5b**. Due to the larger atomic radius of bromine vs. chlorine, the zinc-halide bonds are considerably longer in this complex (ca. 238 pm), which allows a slighly smaller interhalide angle.

Investigations concerning the electrochemical behaviour of the ferrocene moiety in the complexes have been carried out. For all complexes the ferrocene-based redox-wave shows irreversible behaviour in the cyclic voltammogram, even if the scan is reversed before further redox processes have started at higher potentials. Probably the complexes undergo dissociation reactions, which seem to be irreversible after oxidation.

The reaction of **1** and $ZnBr_2$ was also carried out in 2:1 (ligand:metal) molar ratio. It was not possible to isolate a corresponding 2:1 complex. NMR data and X-ray diffraction analysis of the resulting crystalline product revealed the formation of the chelate **5b**.

Tab. 3.3: Selected bond lengths (pm) and bond angles (°) of **5a** and **5b**.

	5a		**5b**	
	molecule 1	molecule 2	molecule 1	molecule 2
Zn–P	243.2(2)	245.3(2)	243.48(8)	242.65(8)
Zn–N	212.5(8)	210.4(8)	211.5(3)	213.9(3)
Zn–X[a]1	224.9(3)	222.5(3)	236.99(5)	237.75(5)
Zn–X2	222.1(3)	225.6(3)	239.68(5)	240.29(5)
∠ N-Zn-X1	104.4(2)	105.7(3)	102.95(8)	106.02(8)
∠ N-Zn-X2	103.3(3)	99.6(2)	101.48(8)	103.63(7)
∠ N-Zn-P	120.3(2)	124.85(16)	125.51(8)	119.54(7)
∠ P-Zn-X1	101.82(10)	109.07(9)	109.51(2)	102.25(3)
∠ P-Zn-X2	113.77(10)	100.43(10)	102.14(3)	115.49(3)
∠ X1-Zn-X2	113.15(11)	117.67(11)	115.73(2)	109.35(2)
∠ Cp1-Cp2	1.39	2.45	1.86	1.08
∠ τ	69.86	75.01	75.41	67.16

[a]X = Cl in **5a** and Br in **5b**.

3.2.2 Synthesis and Characterisation of Cd Compounds

Reactions of **1** with CdX_2 (X = Cl, Br, I) were carried out in analogy to the zinc chemistry described in the previous chapter (Fig. 3.7). The air-stable products [$CdCl_2$(**1**)] (**6a**), [$CdBr_2$(**1**)] (**6b**) and [CdI_2(**1**)] (**6c**) are less soluble in ethanol than the zinc analogues. They are soluble in chloroform and dichloromethane.

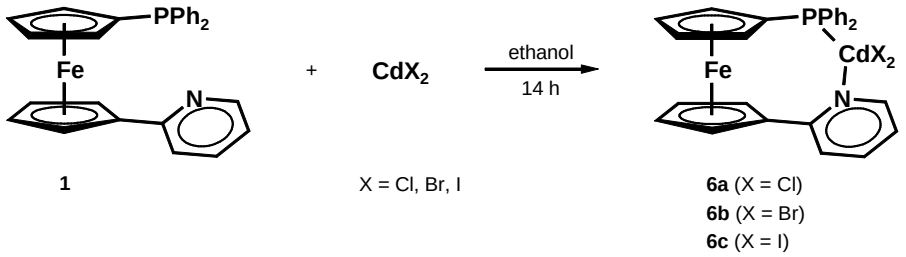

Fig. 3.7: Synthesis of Cd compounds of **1** in 1:1 stoichiometry.

The NMR results clearly indicate a chelate coordination in all three compounds. In the case of **6b** and **6c** the signal of the pyridyl H^6 is strongly shifted to lower field by almost 1 ppm compared to the corresponding signal in **1**, which confirms robust nitrogen coordination. The signal of the pyridyl H^6 in **6a** is slightly broad and only shifted by 0.52 ppm to lower field. This probably suggests a weak nitrogen coordination. Notable shifts of the phosphorus signal with respect to free **1** are detected in the ^{31}P NMR spectrum. Generally, phosphorus coordination lead to a considerable low-field shift of the ^{31}P NMR signal in the order Zn $<$ Cd $<$ Hg.[90] According to the antipodal effect of the vicinal halides in the order Cl $<$ Br $<$ I,[90] the low-field shift is expected to be in the order **6a** $>$ **6b** $>$ **6c**. **6a** does not follow this expected trend, because its low-field shift of ca. 10 ppm is less pronounced than that of **6b**. The same tendencies were also observed for cadmium halide complexes with two triphenylphosphine ligands ([$CdX_2(PPh_3)_2$]).[90] Relevant NMR data for **6a** - **6c** are collected in Tab. 3.4. In the ^{31}P NMR spectrum of **6b** cadmium satellites are observed as a pair of doublets ($J_{^{111}CdP}$ = 1708 Hz, $J_{^{113}CdP}$ = 1782 Hz).

Tab. 3.4: Chemical shifts of the diagnostic NMR signals of **6a**, **6b** and **6c** in ppm.

	1	**6a**	**6b**	**6c**
signal due to pyridyl H^6 (^{1}H NMR)	8.47	8.99	9.35	9.27
phosphorus signal (^{31}P NMR)	-17.7	-8.0	-3.6	-8.9

Solvent: $CDCl_3$.

While **6b** and **6c** could be crystallised easily, **6a** resisted crystallisation. Only diffusion experiments with a dichloromethane solution of **1** layered with a solution of $CdCl_2$ in diethyl ether afforded material suitable for single-crystal X-ray diffraction (Fig. 3.8). The obtained inversion symmetric bis(phosphine) structure reflects a 2:1 (ligand:metal) molar ratio, though the experiment was carried out in a 1:1 molar ratio. The new complex $[CdCl_2(\mathbf{1})_2]$ (**7**) was characterised by X-ray diffraction only.

Two aspects could influence the crystallisation process towards the obtained stoichiometry. First, the poor solubility of $CdCl_2$ in organic solvents could cause concentration differences at the boundary of both layers. Second, an equilibrium in solution between the chelated and the bis(phosphine) species may be responsible for this observation. In solution the equilibrium is almost entirely shifted in favour of the chelate, which can be confirmed by the low-field shifted broad signal of the pyridyl H^6 in the

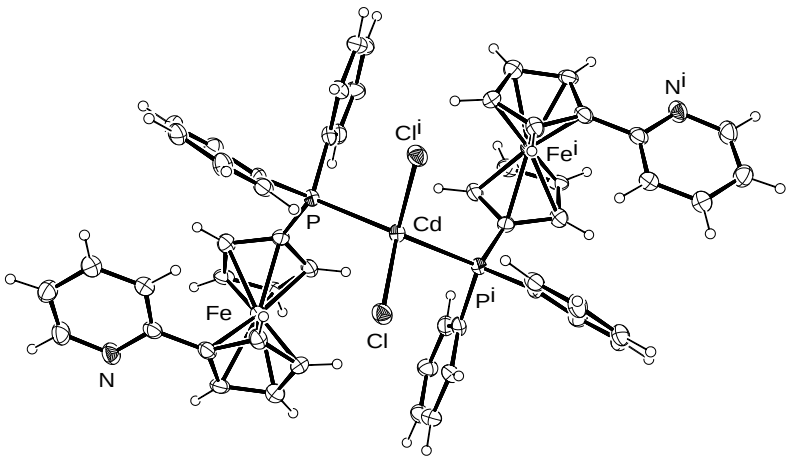

Fig. 3.8: Molecular structure of **7** in the crystal.

^{1}H NMR spectrum. However, if the bis(phosphine) species **7** is only slightly less soluble than the chelate **6a**, it crystallises first and is therefore reproduced by the equilibrium. Generating other cadmium complexes with 2:1 (ligand:metal) stoichiometry failed. Attempts with $CdBr_2 \cdot 4\,H_2O$ in ethanol gave probably a mixture of free ligand and the chelated compound. Crystallisation experiments failed with one exception, which gave the known metal chelate **6b**.

The bond angles in **7** deviate from the ideal tetrahedral angle of 109.5 °. The largest angle is ∠ P-Cd-P' (122.04 °), the smallest one in turn is the interhalide angle ∠ Cl-Cd-Cl (103.63 °). In comparison with the analogous bis(phosphine) complex $[CdCl_2(PPh_3)_2]$, this can be ascribed to the steric demand of the pyridylphosphine ligands which contain an additional bulky ferrocenediyl group. The bond lengths are similar to those of the corresponding triphenylphosphine complex (Tab. 3.5).

The molecular structure of the chelates **6b** and **6c** are shown in Fig. 3.9. **6b** crystallises in the monoclinic space group $P2_1/c$ and **6c** in the triclinic space group $P\bar{1}$. The bond

Tab. 3.5: Selected bond lengths (pm) and bond angles (°) of **7** and $[CdCl_2(PPh_3)_2]$.

	7	$[CdCl_2(PPh_3)_2]$
Cd–P1	258.0(2)	263.3
Cd–P2^a	258.0(2)	264.6
Cd–Cl1	244.8(2)	249.0
Cd–Cl2^a	244.8(2)	244.2
∠ P1-Cd-Cl1	100.55(6)	104.96
∠ P1-Cd-Cl2	114.59(5)	105.78
∠ P1-Cd-P2	122.04(8)	107.27
∠ P2-Cd-Cl1	114.59(5)	112.22
∠ P2-Cd-Cl2	100.55(6)	111.55
∠ Cl1-Cd-Cl2	103.63(9)	114.37
∠ Cp1-Cp2	2.29	
∠ τ	86.54	

^{a}P2, Cl2 = P', Cl' generated by symmetry operations in **7**.

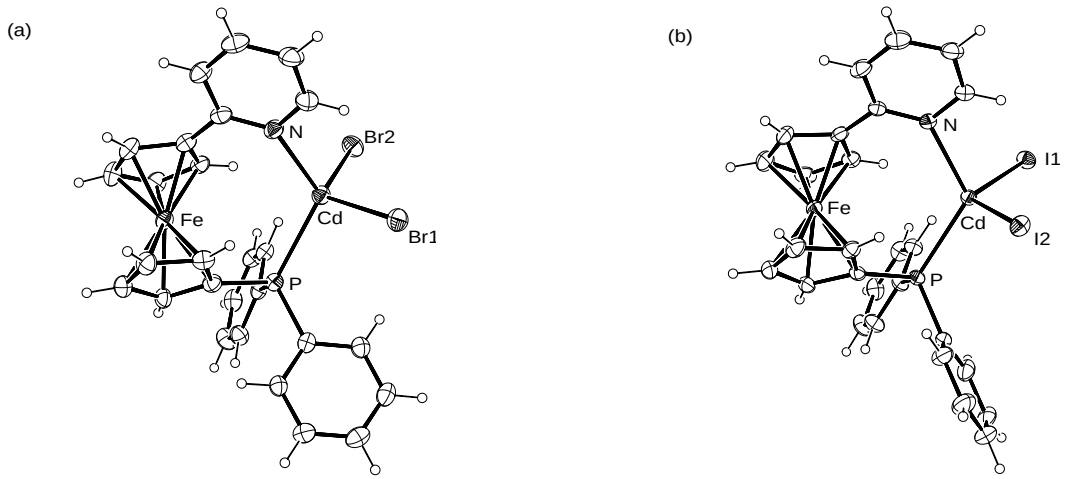

Fig. 3.9: Molecular structure of **6b** (a) and **6c** (b) in the crystal.

parameters exhibit no unusual features. The donor-metal bond lengths (Tab. 3.6) of both complexes are very similar.

Tab. 3.6: Selected bond lengths (pm) and bond angles (°) of **6b** and **6c**.

	6b	**6c**
Cd–P	261.88(12)	259.32(11)
Cd–N	234.1(4)	237.5(3)
Cd–X^{a}1	255.96(6)	273.26(4)
Cd–X2	258.00(6)	275.20(5)
∠ N-Cd-X1	103.13(9)	102.22(9)
∠ N-Cd-X2	102.19(9)	96.02(8)
∠ N-Cd-P	118.70(10)	121.60(9)
∠ P-Cd-X1	105.60(3)	115.64(3)
∠ P-Cd-X2	114.31(3)	103.49(3)
∠ X1-Cd-X2	112.58(2)	116.990(15)
∠ Cp1-Cp2	2.08	1.32
∠ τ	78.41	78.45

^{a}X = Br in **6b** and I in **6c**.

The halide-metal bonds of **6c** are longer due to the larger atomic radius of iodine vs. bromine. The bond angles in **6b** are close to the ideal tetrahedral angle of 109.5°. Only the bite angle ∠ N-Cd-P is wider by ca. 10°. In addition to packing effects, the fixed ligand geometry might be responsible for this. The coordination tetrahedron of **6c** is more distorted. With a value of only 96.02° ∠ N-Cd-I2 is the smallest angle. Probably the I2 atom is influenced by the steric demands of the adjacent phenyl ring and the pyridine ring. The distances between I2 and the nearest carbon atom of the phenyl ring is 400.6 pm. The distance between I2 and the nearest carbon atom of the pyridine ring is only 371.5 pm, which is approximately the sum of the van der Waals radii of C and I (368 pm). Tilt angle and torsion angle a very similar for both complexes.

3.2.3 Synthesis and Characterisation of Hg Compounds

The coordination behaviour of mercury has been studied in analogous reactions with **1** (Fig. 3.10). The results obtained for the reaction with $HgCl_2$ and $HgBr_2$ are very similar

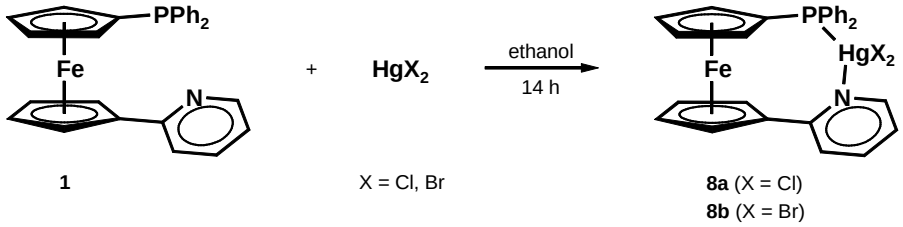

Fig. 3.10: Synthesis of Hg compounds of **1** in 1:1 stoichiometry.

to those obtained from the reactions with cadmium halides. The expected chelate complexes [$HgCl_2$(**1**)] (**8a**) and [$HgBr_2$(**1**)] (**8b**) were formed. The reaction with HgI_2 instead afforded the iodo-bridged, *P*-coordinated dimer [$\{Hg(\mu\text{-}I)I(\mathbf{1})\}_2$] (**8c**) as shown in Fig. 3.11.

single-crystal X-ray diffraction analyses failed for **8a**, because it was impossible to obtain suitable material. Diffusion experiments in a 1:1 molar ratio eventually afforded

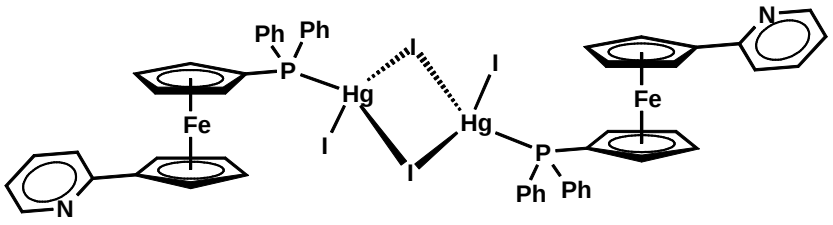

Fig. 3.11: Iodo-bridged, *P*-coordinated dimer **8c**.

crystalline material, which turned out to be the 2:1 (ligand:metal) complex $[HgCl_2(\mathbf{1})_2]$ (**9a**), described on page 43.

In the case of **8b**, single-crystal X-ray diffraction data clearly establish a distorted pseudotetrahedral chelate structure (Fig. 3.12 and Tab. 3.7). The halide-metal distances are comparable to those of **6b**. However, in accord with the HSAB principle, the Hg–P

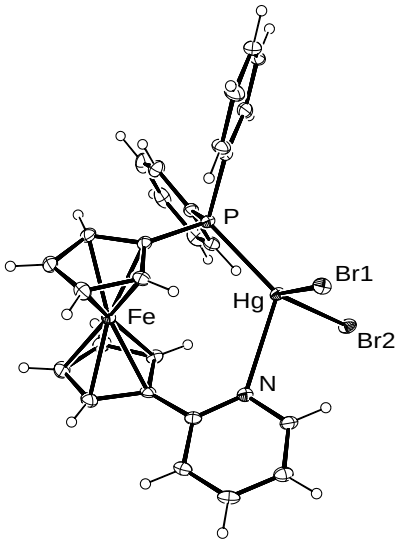

Fig. 3.12: Molecular structure of **8b** in the crystal.

Tab. 3.7: Selected bond lengths (pm) and bond angles (°) of **8b**.

Hg–P	244.62(9)
Hg–N	257.3(3)
Hg–Br1	262.91(5)
Hg–Br2	255.74(5)
∠ N-Hg-Br1	90.12(7)
∠ N-Hg-Br2	92.37(7)
∠ N-Hg-P	118.87(7)
∠ P-Hg-Br1	108.03(2)
∠ P-Hg-Br2	128.72(3)
∠ Br1-Hg-Br2	111.667(16)
∠ Cp1-Cp2	3.24
∠ τ	76.30

distance is 17 pm shorter than the Cd–P bond length in **6b**. On the other hand, the Hg–N distance is 23 pm longer than the corresponding Cd–N bond. Interestingly, in **8b** the Hg–P bond is shorter than the Hg–N bond, which indicates a very strong Hg–P bond and a very weak Hg–N bond. Due to the vicinity of the bromo ligands to the bulky phenyl groups, induced by the short Hg–P bond, the N-Hg-Br angles become particularly acute (ca. 90 °).

The molecular structure of **8c**, which was obtained by recrystallisation of the initially formed precipitate, differs from all others mentioned above (Fig. 3.13 and Tab. 3.8). One ligand molecule is coordinated via its phosphorus donor atom to one HgI_2. Two of these units form an iodo-bridged dimer containing tetracoordinate Hg^{II} centres. The pyridine nitrogen atom remains uncoordinated. Halide bridges are well known in mercury complexes (Chapter 3.1). They arise particularly in the solid state through packing effects, probably assisted by comparatively weak bonds to the nitrogen donor atom in accord with the HSAB principle. The bond angles around the Hg^{II} centres in **8c** show pseudotetrahedral coordination geometry, which is typical for the coordination number four and group 12 metals. The atoms Hg, Hg^{i}, I2 and $I2^{i}$ form a diamond, which is nearly rectangular. Three different Hg–I bond lengths are observed. The bond to the terminal I1 is the shortest (267.65 pm), the longest bond is that to the bridging $I2^{i}$ (303.12 pm).

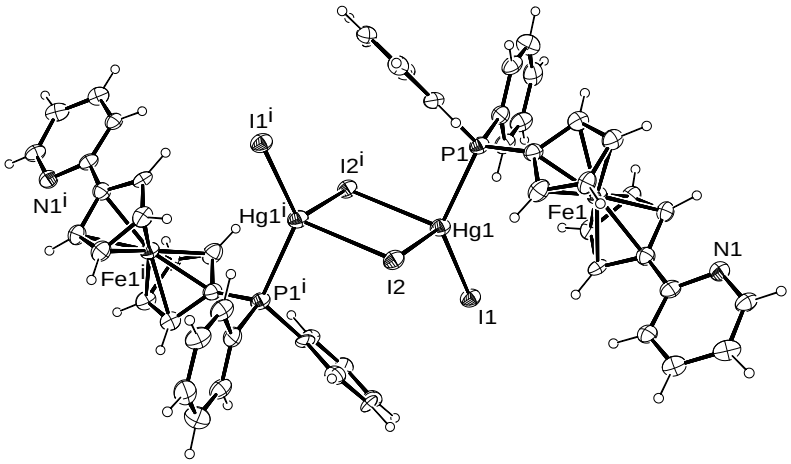

Fig. 3.13: Molecular structure of **8c** in the crystal (solvent atoms are omitted for clarity).

Tab. 3.8: Selected bond lengths (pm) and bond angles (°) of **8c**.

bond length		bond angles	
Hg–P	247.7(3)	∠ I1-Hg-I2^{i}	105.40(3)
Hg–I2^{i}	303.12(10)	∠ I2-Hg-I2^{i}	95.89(3)
Hg–I1	267.65(10)	∠ P-Hg-I2^{i}	97.99(8)
Hg–I2	287.85(11)	∠ P-Hg-I1	130.37(8)
		∠ P-Hg-I2	103.75(8)
		∠ I1-Hg-I2	116.30(3)
		∠ Hg^{i}-I2-Hg	84.11(3)
		∠ τ	146.81
		∠ Cp1-Cp2	2.80

The NMR data prove the chelate structures of **8a** and **8b** in solution. The diagnostic signals in the ^{1}H NMR as well as in the ^{31}P NMR spectrum are shifted to lower field. In the case of the coordination of mercury dichloride in **8a** this effect is most pronounced. The ^{199}Hg-P coupling constant as reflected by the mercury satellites in the ^{31}P NMR spectrum of **8a** is larger than that observed in the spectrum of **8b**. The pyridyl H^{6} is shifted downfield by nearly 0.9 ppm and the phosphorus signal is detected about 47 ppm shifted downfield with respect to the signal of the free ligand. In **8b** and **8c** these shifts are increasingly less pronounced (Tab. 3.9). The coordination-induced shift observed for the pyridyl H^{6} signal in **8c** is surprising in view of the uncoordinated nature of the pyridyl group in the crystalline compound. This indicates a highly dynamic equilibrium in solution between different isomers of **8c**, including an *N*-coordinated chelate.

The crystallisation of **8a** by diffusion experiments by layering a ligand solution with a solution of $HgCl_2$ afforded the bis(phosphine) complex [$HgCl_2$(**1**)$_2$] (**9a**), similar to the crystallisation of the cadmium analogue **6a**, which afforded **7**. As in the case of **7** an equilibrium in solution between the chelate and the bis(phosphine) complex together with the poorer solubility of the latter could be responsible for this effect. **9a** was characterised by X-ray diffraction analysis only. The reaction of $HgBr_2$ with two

Tab. 3.9: Chemical shifts of the diagnostic NMR signals of **8a**, **8b** and **8c** in ppm.

	1	**8a**	**8b**	**8c**
signal due to pyridyl H^6 (^{1}H NMR)	8.47	9.36	9.15	8.89
phosphorus signal (^{31}P NMR)	–17.7	32.2	28.5	19.7
$J_{^{199}HgP}$ in Hz (^{31}P NMR)		7470	6359	

Solvent: $CDCl_3$.

equivalents of **1** gave the analogous bis(phosphine) complex $[HgBr_2(\mathbf{1})_2]$ (**9b**), which has been fully characterised. The results of the structure determination carried out for both 2:1 (ligand:metal) complexes are displayed in Fig 3.14. Both structures show the

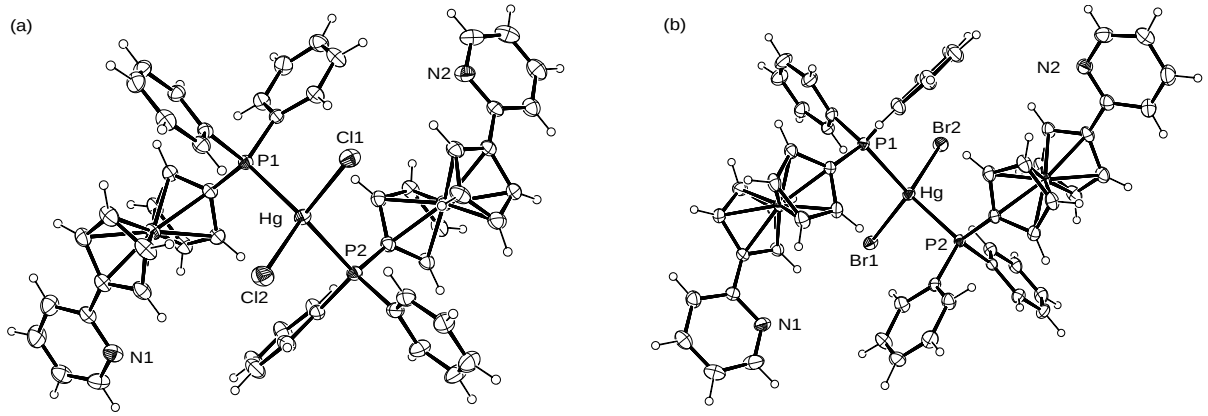

Fig. 3.14: Molecular structures of **9a** (a) and **9b** (b) in the crystal.

typical, distorted pseudotetrahedral coordination with the P2-Hg-P1 angles being the largest coordination angles (ca. 124 °) (Tab. 3.10). The other angles are unexceptional and very similar in both complexes. The Hg–P bond lengths are almost identical. Due to the larger atomic radius of bromine vs. chlorine, the halide-metal bonds of **9b** are longer than those of **9a**.

No coordination-induced shift is observed for the pyridyl H^6 atom in the ^{1}H NMR spectrum. The phosphorus signal is strongly shifted about 32.2 ppm downfield (δ = 14.5 ppm), indicating phosphorus coordination. This means that the coordination motif of **9b** is the

Tab. 3.10: Selected bond lengths (pm) and bond angles (°) of **9a** and **9b**.

	9a	**9b**
Hg–P1	249.46(6)	250.29(11)
Hg–P2	249.49(6)	249.71(12)
Hg–X[a]1	255.54(7)	268.18(6)
Hg–X2	255.46(7)	267.75(6)
∠ P2-Hg-X1	113.85(2)	102.59(3)
∠ P2-Hg-X2	100.29(2)	114.27(3)
∠ P2-Hg-P1	123.99(2)	124.28(4)
∠ P1-Hg-X1	102.29(2)	114.59(3)
∠ P1-Hg-X2	114.23(2)	98.71(3)
∠ X1-Hg-X2	100.04(3)	100.26(2)
∠ Cp1-Cp2	1.76, 2.90	3.45, 2.08
∠ τ	163.95, 152.61	149.74, 164.64

[a]X = Cl in **9a** and Br in **9b**.

same in solution and the solid state. There is no indication for an equilibrium of the type [$HgBr_2$(**1**-κP)$_2$] $\rightleftharpoons$ [$HgBr_2$(**1**-$\kappa^2 P,N$)] + **1** in solution.

3.3 Coordination Chemistry of 2

Ligand **2**, synthesised as described in Chapter 2.2.2, was investigated in the coordination chemistry towards group 12 metal ions as well. The reactions were carried out exclusively with the metal bromides in a 1:1 molar ratio, similar to the reactions described before with **1**. In each case a poorly soluble solid precipitated immediately after the addition of the metal bromide to a solution of **2**.

3.3.1 Synthesis and Characterisation of the Zn Compound

The reaction of **2** with $ZnBr_2$ in ethanol gave a yellow-brown solid, which is nearly insoluble in dichloromethane and completely insoluble in chloroform and non-polar solvents. This behaviour and the expected preference of the pyrid-3-yl group for implementing a bridging coordination mode led to the assumption that a coordination polymer had formed. The structural link-up of $[ZnBr_2(\mathbf{2})]_n$ (**10**) was identified by X-ray diffraction analysis of crystals obtained from a diffusion experiment. The result (Fig. 3.15) shows the expected polymer chain, with the metal centre coordinated by the ligand in a *P*,*N*-bridging coordination mode.

The interligand angles around the metal centre do not differ much from the ideal tetrahedral angle of 109.5 ° (Tab. 3.11). The smallest angle is ∠ N'-Zn-P (104.2 °) and the largest is the interhalide angle ∠ Br1-Zn-Br2 (119.2 °), probably caused by repulsive interactions. The structural parameters approximate those of the analogous chelate **5b** with one main exception. The N-Zn-P angle in **5b** (120.3 ° molecule 1, 124.8 ° molecule 2) is more than 15 ° larger, which is probably caused by the more fixed geometry in the chelate. The observed bond lengths are unexceptional. The difference between the donor-metal bond lengths of ca. 40 pm is caused by the different covalence radii of nitrogen (70 pm) and phosphorus (110 pm). The Zn–N' bond and the Zn–P bond are in

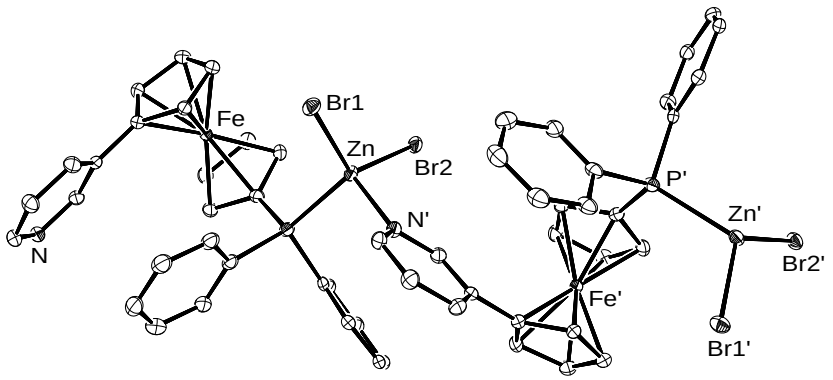

Fig. 3.15: Section of the polymer chain in the crystal structure of **10** (H atoms are omitted for clarity).

Tab. 3.11: Selected bond lengths (pm) and angles (°) of **10**.

bond lengths		bond angles	
Zn–P	246.28(14)	∠ N'-Zn-P	104.22(12)
Zn–N'	207.7(4)	∠ N'-Zn-Br1	105.01(11)
Zn–Br1	237.71(7)	∠ P-Zn-Br1	116.07(4)
Zn–Br2	238.23(7)	∠ N'-Zn-Br2	104.51(12)
		∠ P-Zn-Br2	106.18(4)
		∠ Br1-Zn-Br2	119.20(3)
		∠ Cp1-Cp2	4.21
		∠ τ	73.84

good agreement with those of the simple pyridine and triphenylphosphine complexes described in Chapter 3.1.

Because of the poor solubility of **10**, its NMR characterisation was carried out in the donor solvent dimethylsulfoxide (DMSO), which dissolves **10** by depolymerisation. In the ^{1}H NMR spectrum, two characteristic signals due to the pyridyl protons H^2 and H^6 were observed at 8.38 ppm and 8.67 ppm. Both are nearly unshifted in comparison with those of **2**, which is indicative of essentially uncoordinated pyridyl groups in solution. Two signals are observed in the ^{31}P NMR spectrum, a large one at –18.9 ppm, exhibiting almost the same chemical shift as that of the free ligand and a small one at 25.3 ppm, markedly shifted downfield. These observation are compatible with the presence of two species in the solution: uncoordinated ligand and a *P*-coordinated species. However, the shift of the phosphorus signal should be weaker in the case of a Zn-coordination than the shift observed in the ^{31}P NMR spectrum. Therefore the signal at 25.3 ppm is rather due to the corresponding *P*-oxide of **2**.

The dissolution of coordination polymers in donor solvents usually coincides with substitutional displacement of the original ligand. In this case probably the solvato complex $[ZnBr_2(DMSO)_2]$[91] has formed in the presence of an excess of the donor solvent. The

NMR data indicate that a *P*-coordinated species, probably [$ZnBr_2$(DMSO)(**2**-κP)], is present. This is contraintuitive in view of the HSAB classification of Zn^{II} as an acid borderline between hard and soft, which should prefer the pyridyl group (also borderline) instead of the soft phosphine donor.

3.3.2 Synthesis and Characterisation of the Cd Compound

From the reaction with $CdBr_2 \cdot 4\,H_2O$, an orange solid was obtained, whose solubility and NMR spectroscopic behaviour turned out to be very similar to that of **10**. 1:1 stoichiometry was confirmed by elemental analysis. A polymeric structure analogous to that of **10**, [$CdBr_2$(**2**)]$_n$ (**11**), is therefore very likely (Fig. 3.16).

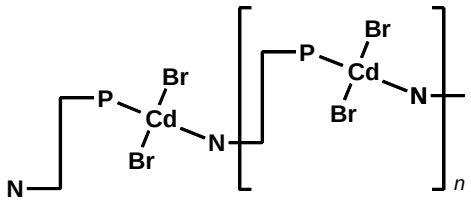

Fig. 3.16: Potential structural association in **11**.

It was not possible to grow single crystals suitable for X-ray diffraction, even by diffusion experiments. **11** showed no tendency to crystallise. Mass spectrometric investigations met with limited success. During the ionisation in ESI and MALDI mass spectrometry the polymeric framework was destroyed; only peaks of the free ligand were observed.

3.3.3 Synthesis and Characterisation of the Hg Compound

An insoluble, orange solid was also obtained from the reaction of **2** with $HgBr_2$ in a 1:1 molar ratio. In contrast to the cadmium analogue described before, it was possible to obtain crystals suitable for structural characterisation in this case. The result (Fig. 3.17)

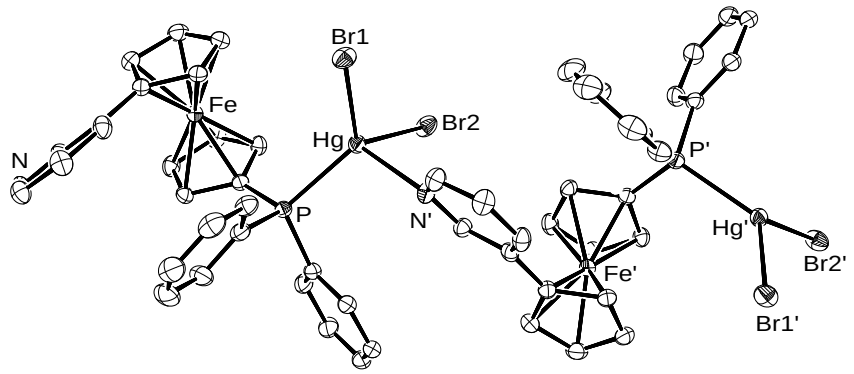

Fig. 3.17: Section of the polymer chain in the crystal structure of **12** (H atoms are omitted for clarity).

supports the preference of **2** for realising a coordination polymer in the solid state by acting as a bridging ligand. Even though **12** is a coordination polymer ($[HgBr_2(\mathbf{1})]_n$), bond lengths and bond angles (Tab. 3.12) are comparable to those of the chelate **8b** (Tab. 3.7, page 41), with the notable exception of the N-Hg-P angle, which is much larger in the chelate (118.87° in **8b** vs. 107.63° in **12**). Furthermore, the Hg–N bond length in **8b** (257.3 pm) is 14 pm larger than the Hg–N' distance in **12** (243.9 pm). Probably, the larger values in **8b** is caused by the more fixed geometry of the chelating ligand. Also the distortion of the pseudotetrahedral coordination geometry is rather

Tab. 3.12: Selected bond lengths (pm) and angles (°) of **12**.

bond lengths		bond angles	
Hg–P	244.23(10)	∠ N'-Hg-P	107.63(9)
Hg–N'	243.9(3)	∠ N'-Hg-Br1	94.97(8)
Hg–Br1	257.27(4)	∠ P-Hg-Br1	123.16(3)
Hg–Br2	258.47(4)	∠ N'-Hg1-Br2	93.37(8)
		∠ P-Hg-Br2	116.89(3)
		∠ Br1-Hg-Br2	112.81(2)
		∠ Cp1-Cp2	2.50
		∠ τ	73.86

similar. Bond length and angles are also comparable with the linear coordination polymer of the 1,1'-ferrocene-based pyriylphosphinocarboxamide ligands (Chapter 3.1).

Obviously, **12** is more stable during the mass spectrometric ionisation process. In addition to the peak due to the ligand fragment, also peaks of coordinated fragments can be observed in a MALDI mass spectrometry experiment. Interestingly, the phosphorus NMR spectrum shows only a single broadened signal at 19.3 ppm. Probably the Hg–P bond is sufficiently strong to resist dissociation in DMSO solution. According to the HSAB principle, mercury has the highest affinity to a phosphorus donor in the series of the group 12 metals. Not surprisingly, the ^{1}H NMR spectrum shows no coordination induced shift of the signals due to the pyridyl protons H^2 and H^6.

3.4 Coordination Chemistry of 3

The synthesis of **3** as described in Chapter 2.2.3 and the synthesis of the complexes **13**, **14**, **16** and **18** was carried out by Jiří Schulz during his stay as a visiting scholar at the University of Kassel.

3.4.1 Synthesis and Characterisation of Zn Compounds

The reaction of $ZnBr_2$ with **3** in a 1:1 molar ratio in ethanol and subsequent evaporation gave a yellow, air-stable solid, whose composition according to elemental analysis was [$ZnBr_2$(**3**)] (**13**). The solid was recrystallised from chloroform and the single crystals subjected to an X-ray diffraction study (Fig. 3.18 and Tab. 3.13), which revealed the anticipated chelate structure, exhibiting a distorted pseudotetrahedral coordination environment. The Zn–P bond (243.89 pm) is shorter than in the related complex [$ZnBr_2(PPh_3)_2$] (Tab. 3.1, page 28), but in line with those of the chelate **5b**, formed with ligand **1** (Tab. 3.3, page 35). Due to the higher flexibility of **3** vs. **1**, the Zn–N bond in **13** (208.7) is slightly shorter than in **5b** (211.5 pm molecule 1, 213.9 molecule 2). The bite

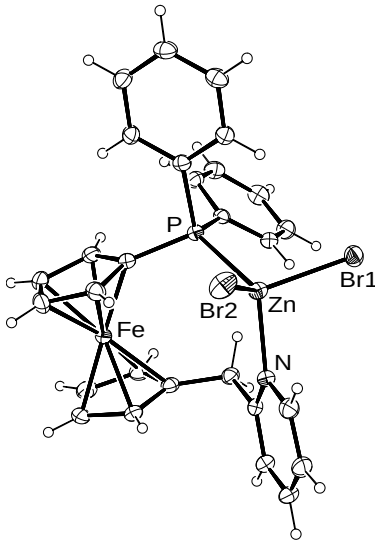

Fig. 3.18: Molecular structure of **13** in the crystal.

Tab. 3.13: Selected bond lengths (pm) and bond angles (°) of **13**.

Zn–P	243.89(9)
Zn–N	208.7(3)
Zn–Br1	240.40(5)
Zn–Br2	239.04(5)
∠ N-Zn-Br1	103.32(7)
∠ N-Zn-Br2	102.34(8)
∠ N-Zn-P	122.64(8)
∠ P-Zn-Br1	108.05(3)
∠ P-Zn-Br2	106.58(3)
∠ Br1-Zn-Br2	114.19(2)
∠ Cp1-Cp2	5.25
∠ τ	7.48

angle and the interhalide angle in **13** are similar to the corresponding average value of molecule 1 and 2 of **5b**. The 1,1'-ferrocenediyl backbone unit of the ligand is slightly tilted (5.25 °).

An NMR spectroscopic investigation revealed that the signal of the pyridyl H^6 is markedly shifted to lower field (9.66 ppm), whereas the signal in the phosphorus NMR spectrum is observed nearly unshifted at –18.1 ppm. The unshifted phosphorus signal indicates that the metal centre is probably dissociated from the phosphorus donor in solution.

Interestingly, if the isolation was carried out by storing the diluted reaction mixture for several days to obtain crystalline material directly from the ethanolic solution, a different structural result was obtained. This procedure afforded a centrosymmetric dimer containing ligand **3** in a bridging coordination mode (**13a**). Also a mixed-solvent diffusion experiment in 2:1 (ligand:metal) molar ratio (2 eq. **3** in DCM layered with 1 eq. $ZnBr_2$ in ethanol) afforded crystals of the 1:1 centrosymmetric dimer **13a**. Due to

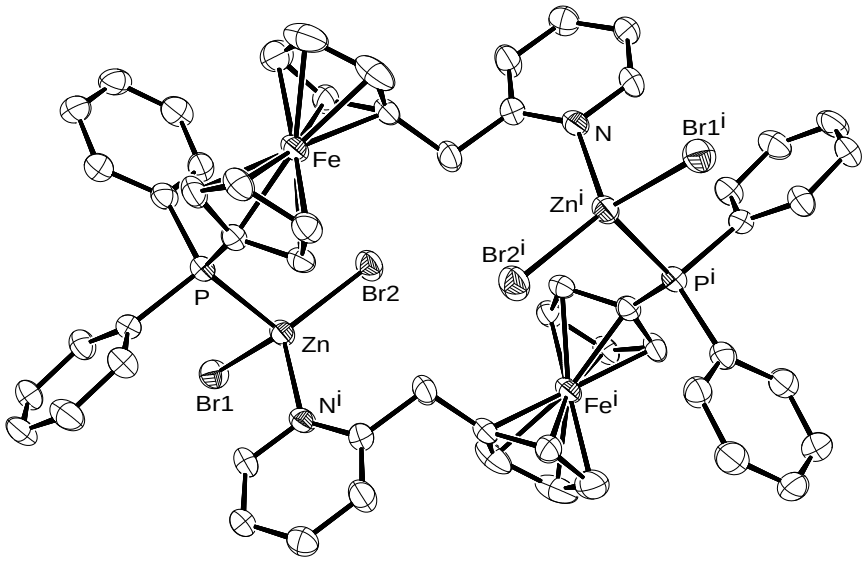

Fig. 3.19: Molecular structure of **13a** in the crystal (H and solvent atoms are omitted for clarity).

the better structural refinement, the structure obtained from the diffusion experiment is discussed (Fig. 3.19 and Tab. 3.14).

The bond lengths and angles compare well to those of the corresponding chelate **13** (Tab. 3.13) with two exceptions. The N-Zn-P angle in the corresponding chelate **13** (122.6 °) is considerably larger than in the centrosymmetric dimer **13a** (100.6 °), which

Tab. 3.14: Selected bond lengths (pm) and angles (°) of **13a**.

bond lengths		bond angles	
Zn–P	245.5(2)	∠ N^i-Zn-Br1	103.48(16)
Zn–N^i	209.7(6)	∠ N^i-Zn-Br2	121.3(2)
Zn–Br1	240.03(12)	∠ N^i-Zn-P	100.5(2)
Zn–Br2	237.90(12)	∠ P-Zn-Br1	104.85(6)
		∠ P-Zn-Br2	112.58(6)
		∠ Br1-Zn-Br2	112.31(5)
		∠ Cp1-Cp2	3.67
		∠ τ	85.47

is caused by the more rigid character in the chelate, because both coordinated donor atoms are located in a single ligand molecule. Consequently, more space is available for the coligands, which is reflected by a widening of the angle ∠ N-Zn1-Br2. Its value is 102.3 ° in the chelate and 121.3 ° in the centrosymmetric dimer.

3.4.2 Synthesis and Characterisation of Cd Compounds

The reaction of **3** with an ethanolic solution of $CdBr_2 \cdot 4\,H_2O$ in a 1:1 molar ratio gave a precipitate of the composition [$CdBr_2$(**3**)], according to elemental analysis. NMR spectroscopic investigations showed a low-field shifted signal for the pyridyl H^6. However, the phosphorus signal could not been detected.

Unfortunately, characterisation of the precipitated solid by X-ray diffraction was not possible, because crystals could not be obtained despite several attempts of simple recrystallisation from CH_2Cl_2 and $CHCl_3$ and liquid phase diffusion of non-polar solvents into a dichloromethane solution of the precipitate. Also, layering of an ethanolic solution of $CdBr_2 \cdot 4\,H_2O$ with an ethanolic solution of the ligand proved to be ineffective. Finally, crystals were obtained in a diffusion experiment using two different solvents. A solution of 0.05 mmol **3** in dichloromethane (ca. 0.5 mL) was layered first with pure ethanol and then with an ethanolic solution (ca. 0.5 mL) of 0.05 mmol $CdBr_2 \cdot 4\,H_2O$. The crystals obtained do not contain the expected chelate **14**, but the corresponding coordination polymer **14a** (Fig. 3.20).

Instead of forming complicated, halide-bridged polynuclear complexes with CN = 5 as that described in Chapter 3.1, the coordination geometry remains tetrahedral with the coordination number four. The interligand angles deviate only less than 10 ° from the ideal tetrahedral angle of 109.5 ° (Tab. 3.15). The Cd–P' bond length in **14a** (263.7 pm) is only slightly longer than the Cd–P bond length in the comparable chelate **6b** (261.9 pm), containing ligand **1**. Due to the more fixed geometry of the chelating ligand in **6b**, the N-Cd-P angle is larger (118.7 °) than that of the polymer **14a** (109.13). Consequently, the bromo ligands are forced closer to each other in the chelate, which is

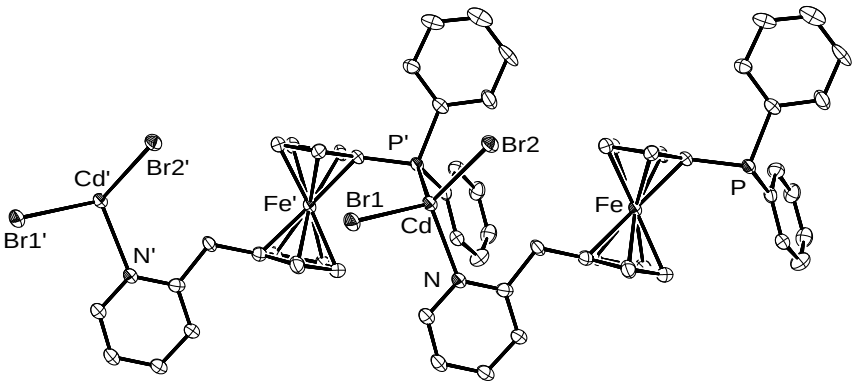

Fig. 3.20: Section of the polymer chain of **14a** in the crystal (H atoms are omitted for clarity).

expressed by the smaller interhalide angle ∠ Br1-Cd-Br2 in the chelate (112.6 °) than in the polymer (115.4 °).

The reaction of CdI_2 with **3** in a 1:1 molar ratio in ethanol afforded a yellow precipitate, whose stoichiometric composition was proved by elemental analysis. The resulting complex [CdI_2(**3**)] was identified as metal chelate **15**. It exhibits low-field shifted NMR signals due to the pyridyl H^6 (9.23 ppm) and for phosphorus (24.3 ppm) with respect to **3** (δ of pyridyl H^6 = 8.44 ppm, δ of phosphorus = –16.5 ppm). Liquid phase diffusion of

Tab. 3.15: Selected bond lengths (pm) and angles (°) of **14a**.

bond lengths		bond angles	
Cd–P'	263.7(2)	∠N-Cd-Br1	100.34(17)
Cd–N	232.3(7)	∠N-Cd-Br2	114.82(17)
Cd–Br1	255.78(10)	∠N-Cd-P'	109.13(19)
Cd–Br2	257.34(10)	∠P'-Cd-Br1	115.59(5)
		∠P'-Cd-Br2	102.02(5)
		∠Br1-Cd-Br2	115.36(4)
		∠ Cp1-Cp2	2.95
		∠ τ	146.53

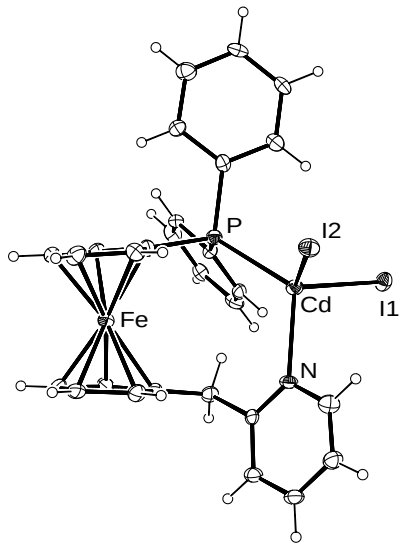

Fig. 3.21: Molecular structure of **15** in the crystal.

Tab. 3.16: Selected bond lengths (pm) and bond angles (°) of **15**.

Cd–P	260.7(2)
Cd–N	230.9(6)
Cd–I1	276.75(9)
Cd–I2	276.05(8)
∠ N-Cd-I1	102.2(2)
∠ N-Cd-I2	99.0(2)
∠ N-Cd-P	120.0(2)
∠ P-Cd-I1	108.59(5)
∠ P-Cd-I2	110.36(5)
∠ I1-Cd-I2	116.74(3)
∠ Cp1-Cp2	6.03
∠ τ	6.27

hexane into a $CHCl_3$ solution of **15** gave single crystals, which were subjected to an X-ray diffraction study (Fig. 3.21 and Tab. 3.16).

The results compare well to those obtained for the metal chelate **6c**. The Cd–P bond length, the bite angle and the interhalide angle differ only marginally. The Cd–N bond length in **15** (230.9 pm) is notably shorter than in **6c** (237.5 pm) containing the less flexible ligand. Interestingly, the ferrocene moiety in **15** exhibits a comparably strong ring tilt (∠ Cp1-Cp2 = 6.03 °). In **6c** the planes Cp1 and Cp2 are nearly parallel (∠ Cp1-Cp2 = 1.32 °).

3.4.3 Synthesis and Characterisation of Hg Compounds

The reaction of **3** with $HgBr_2$ in a 1:1 molar ratio afforded a solid of the composition [$HgBr_2$(**3**)]. Performing the reaction as a diffusion experiment in an NMR tube by layering $HgBr_2$ in ethanol with a solution of the ligand in ethanol resulted in the formation

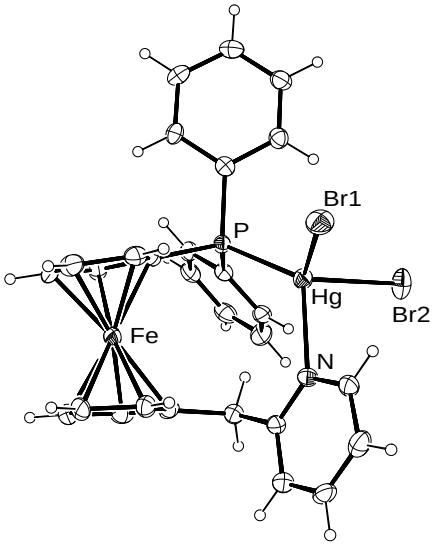

Fig. 3.22: Molecular structure of **16** in the crystal.

Tab. 3.17: Selected bond lengths (pm) and bond angles (°) of **16**.

Hg–P	244.3(2)
Hg–N	237.2(7)
Hg–Br1	261.20(13)
Hg–Br2	262.78(10)
∠ N-Hg-Br1	93.6(2)
∠ N-Hg-Br2	97.3(2)
∠ N-Hg-P	123.8(2)
∠ P-Hg-Br1	116.21(6)
∠ P-Hg-Br2	112.92(6)
∠ Br1-Hg-Br2	110.31(4)
∠ Cp1-Cp2	7.32
∠ τ	8.51

of single crystals. The result of the X-ray diffraction analysis exhibits the anticipated chelate structure of **16** (Fig. 3.22 and Tab. 3.17).

The tetrahedral coordination geometry is significantly distorted. The bite angle ∠ N-Hg-P is the largest of the coordination angles (123 °) and the N-Hg-Br1 angle is the smallest one (93.6 °). In accord with the HSAB principle the Hg–P distance is shorter than that of the analogous cadmium complex **15**. The tendencies observed in the comparison of the cadmium chelates **6c** and **15**, are paralleled in the comparison of **16** with **8b**, containing ligand **1**. The Hg–P distances are almost equal in both complexes (244.3 pm in **16**, 244.6 pm in **8b**) and the Hg–N distance in **8b** (257.3 pm) is considerably larger than that of **16** (237.2 pm), due to the more flexible pyridyl group in **16**. Also, the relatively strong ring tilt of the ferrocene moiety was observed (∠ Cp1-Cp2 = 7.32 ° in **16** and 3.24 ° in **8b**). The tendency is inverted for the bite angle ∠ N-Hg-P, which is larger in **16** (123.3 °) than in **8b** (118.9 °). Probably the larger atomic radius of mercury vs. cadmium is responsible for this.

NMR spectroscopic investigation revealed that the chelate structure of **16** remains intact in solution. The diagnostic NMR signals are shifted to lower field as expected for a metal chelate. The resonance signal of the pyridyl H^6 is observed at 9.09 ppm, which is shifted downfield by 0.65 ppm with respect to free **3**. The phosphorus signal is located at 24.4 ppm, shifted to lower field by 40.9 ppm. Due to the coupling with ^{199}Hg, mercury satellites are observed ($J_{^{199}HgP}$ = 6321 Hz).

Carrying out the diffusion experiment described above under mixed-solvent conditions gave a completely different result. Layering a dichloromethane solution of **3** with a very small amount of pure ethanol and then with one equivalent of $HgBr_2$ in ethanol afforded crystals of a bromo-bridged polymer with a 1:2 (ligand:metal) stoichiometry [$(HgBr_2)_2$(**3**)] (**17**) (Fig. 3.23), although the diffusion experiment was carried out in a 1:1 molar ratio.

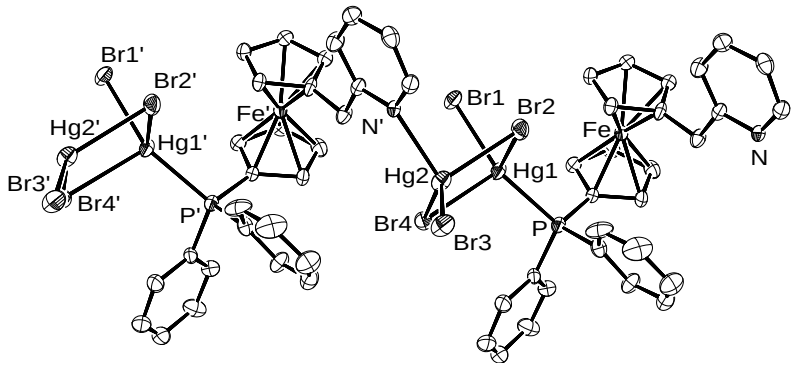

Fig. 3.23: Section of the polymer chain of **17** in the crystal (H and solvent atoms are omitted for clarity).

Halide bridges are quite common in crystal structures of mercury complexes (Chapter 3). The coordination number for each mercury atom is four. The coordination tetrahedron is extremely distorted. The largest angle ∠ P-Hg1-Br1 has a value of 147°, which deviates almost 40° from the ideal tetrahedral angle of 109.5°. This is probably caused by repulsive interactions between the halide atoms and the steric demand of the ferrocene backbone of the ligand. The sum of the angles in the diamond spanned by the bridging atoms Hg1-Br2-Hg2-Br4 is 359.86°. The most acute coordination angle is ∠ Br1-Hg1-Br2 with only 82.50° (Tab. 3.18). The Hg–Br distances cover a wide

Tab. 3.18: Selected bond lengths (pm) and angles (°) of **17**.

bond lengths		bond angles		bond angles	
Hg1–Br1	247.14(12)	∠ P-Hg1-Br1	147.82(8)	∠ Br1-Hg1-Br4	96.77(4)
Hg2–Br2	265.19(12)	∠ P-Hg1-Br2	110.52	∠ Br3-Hg2-Br4	126.49(5)
Hg2–Br3	253.19(14)	∠ P-Hg1-Br4	110.21(7)	∠ Br3-Hg2-Br2	117.81(5)
Hg2–Br4	260.02(13)	∠ N'-Hg2-Br3	99.2(2)	∠ Br4-Hg2-Br2	98.26(4)
Hg1–Br4	286.48(12)	∠ N'-Hg2-Br4	117.3(2)	∠ Br1-Hg1-Br2	82.50
Hg1–Br2	315.0	∠ N'-Hg2-Br2	93.9(2)	∠ Hg2-Br4-Hg1	93.13(4)
Hg1–P	241.9(3)				
Hg2–N'	236.9(8)	∠ Cp1-Cp2	2,93	∠ τ	73.74

range from ca. 247.1 pm - 315.0 pm. The Hg2–Br distances lies between ca. 253.2 pm and 265.2 pm, the shortest bond being that to the terminal Br3. For the phosphine coordinated Hg1 a very short bond to the terminal Br1 of only 241.9 pm is observed plus two very long ones (ca. 286.5 pm and 315.0 pm).

The "inverted" complex, where two equivalents of **3** are coordinated only to one equivalent of mercury bromide [$HgBr_2$(**3**)$_2$] (**18**), has also been prepared and characterised. Liquid phase diffusion of hexane into a chloroform solution of the complex afforded the solvate **18** · $CHCl_3$, which was structurally characterised by X-ray diffraction as the expected bis(phosphine) complex (Fig. 3.24 and Tab. 3.19), which is an analogue of **9b** containing ligand **1** instead of **3**. All bond parameters compare well with those of the bis(phosphine) complex **9b**. However, while **9b** crystallises in the monoclinic space group $P2_1/n$, **18** is orthorhombic ($Iba2$).

Tab. 3.19: Selected bond lengths (pm) and angles (°) of **18**.

bond lengths		bond angles	
Hg–P1	251.0(2)	∠ P1-Hg-Br1	99.21(5)
Hg–P2	251.2(2)	∠ P1-Hg-Br2	115.33(5)
Hg–Br1	266.15(8)	∠ P1-Hg-P2	124.01(5)
Hg–Br2	266.40(8)	∠ P2-Hg-Br1	113.23(5)
		∠ P2-Hg-Br2	100.58(5)
		∠ Br1-Hg-Br2	103.16(3)

3.5 Coordination Chemistry of 4

During the coordination experiments with mercury and zinc halides, it turned out that the resulting solids were not the expected well-defined complexes, but very likely ill-defined mixtures. It was not possible to grow crystals suitable for X-ray diffraction analysis and the NMR spectra turned out to be too complex for a meaningful analysis. For example, immediately after the addition of $ZnCl_2$ to a dichloromethane solution of the ligand, the colour changed from orange to a very dark red. Even though coordina-

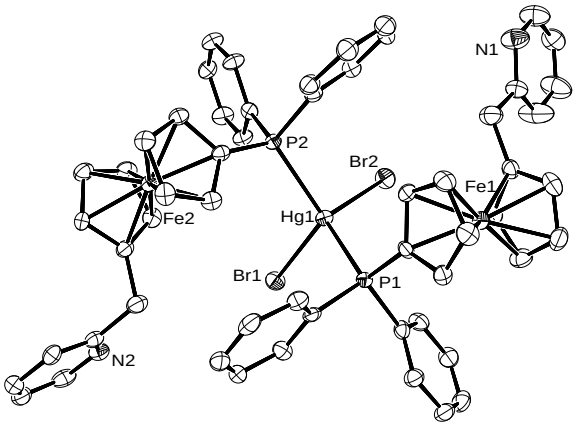

Fig. 3.24: Molecular structure of **18** in the crystal (H and solvent atoms are omitted for clarity).

tion had obviously occurred, no defined complex could be isolated. DFT calculations performed by Dr. Leibold in our group suggest that tetrahedral coordination is sterically hindered if all three donor atoms of the ligand are involved in the coordination to a single zinc atom. More detailed, and probably very time-consuming, investigations will be needed to understand the coordination behaviour of **4**. In view of the time constrictions of the present work, experiments with **4** were abandoned at this preliminary stage.

3.6 Summary and Conclusion

The ferrocene-based pyridylphosphine ligands **1** - **4** were investigated in terms of the coordination chemistry towards the group 12 metals zinc, cadmium and mercury, which are used in form of the metal halide salts of the type MX_2 (M = Zn, Cd, Hg and X = Cl, Br, I). The results of the experiments are summarised in Tab. 3.20. Depending on the ligand and the reaction stoichiometry the ligands **1, 2** and **3** react with different salts in a *P*,*N*-chelating, *P*,*N*-bridging or a *P*-coordinated monodentate coordination mode.

Tab. 3.20: Results of the coordination chemistry experiments concerning **1**, **2** and **3**.

		1		**2**		**3**	
		1 eq.	2 eq.	1 eq.	2 eq.	1 eq.	2 eq.
Zn	Cl_2	**5a** C	–	–	–	–	–
	Br_2	**5b** C	**5b** C	**10** P	–	**13** C; **13a** D[a]	**13a** D[a]
	I_2	**5c** C[b]	–	–	–	–	–
Cd	Cl_2	**6a** C[b,c]	**7** B[a,d]	–	–	–	–
	Br_2	**6b** C	–	**11** P[b]	–	**14** C[c]; **14a** P[a]	–
	I_2	**6c** C	–	–	–	**15** C; –	–
Hg	Cl_2	**8a** C[b,c]	**9a** B[a,d]	–	–	–	–
	Br_2	**8b** C	**9b** B	**12** P	–	**16** C; **17** P[a,e]	**18** B
	I_2	**8c** C[f]	–	–	–	–	–

C = *P*,*N*-chelate, P = polymer, D = centrosymmetric dimer, B = *P*-coordinated bis(phosphine) complex, – = no investigations realised or investigations did not lead to clear results. [a]Only characterised by X-ray diffraction. [b]No X-ray data available. [c]Crystallisation leads to new compound with 2:1 (ligand:metal) stoichiometry. [d] Crystals obtained by diffusion experiments with 1:1 stoichiometry. [e]**17** has a 1:2 stoichiometry, the polymer is formed via halide bridges. [f]Crystallisation leads to isomeric iodo-bridged dimer.

Reactions in a 1:1 molar ratio with **1** resulted mostly in *P*,*N*-chelated complexes, reactions with **2** led to polymeric structures. The less predictable coordination behaviour of **3** can be ascribed to the presence of the methylene group in this ligand, which makes the ligand more flexible.

Reactions with two equivalents of the ligand gave *P*-coordinated, monodentate bis-(phosphine) complexes with the ligands **1** and **3** in the case of mercury. Zinc complexes with a monodentate coordination mode were not observed; for **1** only the 1:1 chelating complex and for **3** the centrosymmetric dimer was isolated.

The coordination chemistry of **4** was not explored in detail. Preliminary experiments show low crystallisation tendencies and very complicated spectral data.

4 Coordination Chemistry II: Silver and Gold

The coordination chemistry of the ferrocene-based ligands **1** - **3** towards silver(I) and gold(I) is described. The synthesis, characterisation and electrochemical investigations concerning the potential application of **1** - **3** as molecular redox sensor are presented.

4.1 Introduction

Silver and gold have not only a cultural importance by being used as currency or for objects in arts and jewellery, they have also great importance in chemistry. Numerous applications in catalysis[92–94] and medicine[95] have been reported in the scientific literature.

Silver is classified in terms of the HSAB principle as a relatively soft acid with a versatile coordination chemistry. Oxidation states from (I) to (III) and coordination numbers from one to ten are known. However, Ag^{I} compounds with the coordination numbers three (mostly distorted trigonal planar) and four (usually distorted tetrahedral) are most common. The metal-donor distances vary from 202 pm to 246 pm for monodentate nitrogen donors and from 236 pm to 270 pm in the case of phosphorus donors.[96–98]

Even though silver shows such a diverse and well-investigated coordination chemistry, complexes with the popular structural analogue of the ferrocene-based pyridylphos-

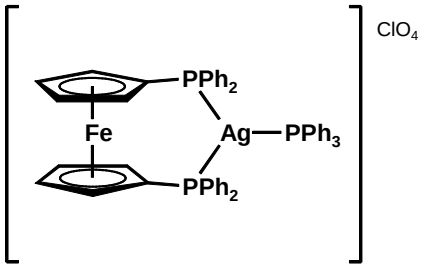

Fig. 4.1: 1,1'-[Bis(diphenylphosphino)ferrocene]-triphenylphosphine-silver(I).

phines **1**, **2** and **3**, 1,1'-bis(diphenylphosphino)ferrocene (dppf), are rare. The structure of $[Ag(dppf)_2][BF_4]$ has been reported by Long and coworkers.[99] One silver atom is coordinated by two chelating dppf molecules. The complex has a tetrahedral coordination geometry as expected for the coordination number four. The coordination tetrahedron is distorted due to the steric demand of the eight phenyl groups. The chelate bite angles are only 97.7 ° and 105.5 °. The Ag–P distances range from 255.3 pm to 266.2 pm.

A related Ag^{I} dppf complex with the coordination number three is shown in Fig. 4.1.[100] The metal centre is coordinated by one dppf molecule in a chelate manner and by one molecule of triphenylphosphine. Coordination angles are close to 120 ° (sum of angles 359.94 °) and the silver atom is in a trigonal planar coordination environment. The donor-metal bond lengths have an average of 244.5 pm, which is shorter than in the bis(dppf) complex, owing to the lower coordination number.

A search in the cambridge structural database (CSD) for silver compounds with pyridyl-substituted ferrocenes, gave just a single hit, viz. a silver complex of 1,1'-bis(pyrid-2-yl)ferrocene.[101] The silver atom is chelated by the two nitrogen donors in a quasilinear dicoordinated fashion (∠ N1-Ag-N2 = 163.1 °). The perchlorate counter ions are not connected to the metal centre. Due to the smaller atomic radius of nitrogen vs. phosphorus, the Ag–N distances (214.3 pm and 218.7 pm) are significantly shorter than those between Ag–P in the dppf complex (244.5 pm).

The chemistry of gold is dominated by the oxidation states (I) and (III), having the electron configuration [Xe] $4f^{14}$ $5d^{10}$ $6s^0$ and [Xe] $4f^{14}$ $5d^8$ $6s^0$, respectively. Compounds

of Au^{I} assume the coordination number two with a linear coordination geometry and a 14 VE configuration in most cases. Au^{I} complexes with a coordination number of three (16 VE, trigonal planar) or four (18 VE, tetrahedral) are also known, but less common,[102] since the participation of the energetically high lying $6p_y$ and $6p_z$ orbitals causes high promotion energies. The general form of gold(I) complexes is [LAuX] (L= neutral ligand; X = anionic ligand) and gold(I) exhibits a strong preference for large and soft (easily polarisable) donor ligands L.[103] Particularly stable gold(I) complexes are formed with organic *P*- or *S*-donor ligands.

Several gold complexes with the archetypal phosphinoferrocene ligand dppf are found in the literature.[104] The simplest one was prepared by the reaction of dppf with two equivalents of [AuCl(tht)]. The resulting binuclear complex $[(AuCl)_2(dppf)]$ exhibits a linear dicoordinate arrangement for both gold atoms (Fig. 4.2). Short Au–P distances

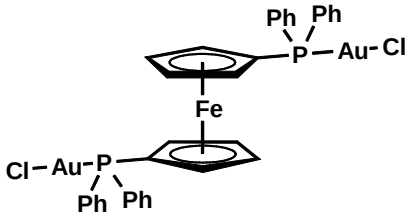

Fig. 4.2: Linear coordination geometry in $[(AuCl)_2(dppf)]$.

(222.8 pm) underline the stability of this complex. Interestingly, $[(AuCl)_2(dppf)]$ has been described to lack electrochemical activity. Either, electron transfer is very slow or this complex is indeed inert to electrochemical oxidation or reduction.[105] It seems likely that the AuCl fragments possess such a high electron withdrawing ability to make the HOMO levels of the ferrocene moiety inaccessible.[106] This Au^{I} complex appears to be the first example of an electrochemically inert ferrocene derivative. Gold complexes of pyridyl-substituted ferrocene ligands are not known.

4.2 Synthesis and Characterisation of Ag Compounds

The synthesis and characterisation of silver complexes with the ferrocene-based pyridylphosphine ligands **1** - **3** is described. This was carried out in analogy to the synthesis of an Ag^{I} compound with an imidazole-based *P*,*N*-ligand.[107]

4.2.1 Ag Complex of 1

The reaction of the ligand, dissolved in methanol, and one equivalent of solid $AgBF_4$ at room temperature yielded [Ag(**1**)][BF_4] (**19**), which was isolated by a solvent exchange to dichloromethane and following precipitation with hexane. ESI mass spectrometry and elemental analysis confirm the stoichiometry.

The signal of the pyridyl H^6 is located at 8.87 ppm in the ^{1}H NMR spectrum ($CHCl_3$), which means a low-field shift of about 0.4 ppm with respect to pristine **1**. The ^{31}P NMR spectrum shows a single signal, observed as a doublet (Ag-P coupling). Due to intermolecular dynamic processes, the signal is broadened. This is typical for ^{31}P NMR spectra of Ag-P complexes at room temperature. In low temperature NMR spectra two doublets would be observed usually, one due to the coupling with ^{107}Ag and the other one due to the coupling with ^{109}Ag.[90,108] The phosphorus signal here is located low-field shifted with respect to uncoordinated **1** (δ = –17.7 ppm) at δ = 6.8 ppm. The averaged coupling constant of the broad doublet has a value of $J_{^{107}AgP,^{109}AgP} \approx 712$ Hz.

Recrystallisation of **19** from chloroform gave material suitable for structural characterisation by X-ray diffraction analysis. Under these conditions **19** crystallises as a polymeric solvate with two molecules of $CHCl_3$ per asymmetric unit (Fig. 4.3).

Compared to known complexes (Chapter 4.1), the donor–metal distances of 237.1 pm (Ag–P) and 217.4 pm (Ag–N) are rather short. The N-Ag-P angle (164 °) deviates from a linear coordination geometry. The distortion is probably caused by weak interactions

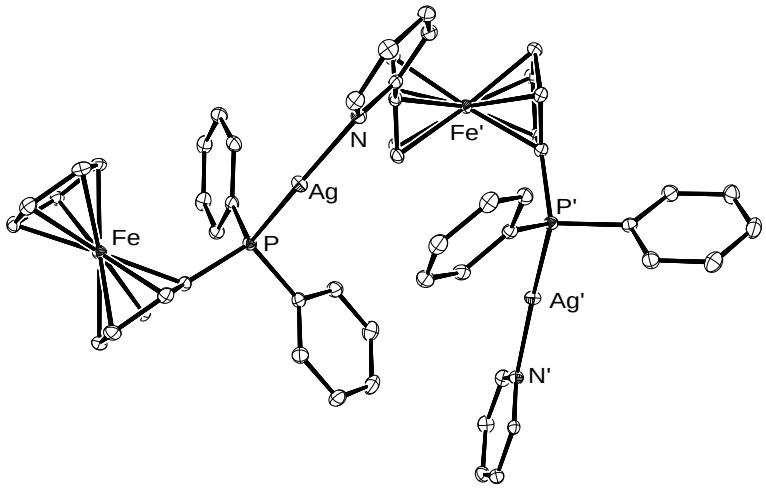

Fig. 4.3: Section of the polymer chain in the crystal structure of **19** (H, counter ion and solvent atoms are omitted for clarity).

Tab. 4.1: Selected bond lengths (pm) and bond angles (°) of **19**.

Ag–P	237.08(8)
Ag–N	217.4(3)
Ag–F4	273.7
∠ P-Ag-N	164.21(6)

between the silver atom and one flourine atom of the BF_4^- counter ion (F4 in the crystal structure), whose distance is only 273.7 pm (Tab. 4.1), which is smaller than the sum of the van der Waals radii of silver and fluorine (ca. 308 pm). Such a coordination motif (CN = 2 + 1) is frequently observed in Ag^I chemistry.[109,110]

4.2.2 Ag Complex of 2

The reaction of **2** with one equivalent of $AgBF_4$ in methanol gave an orange precipitate, which was filtered off, rinsed with methanol, washed with diethyl ether and hexane and finally dried in vacuum. The resulting complex [Ag(**2**)][BF_4] (**20**) was characterised by

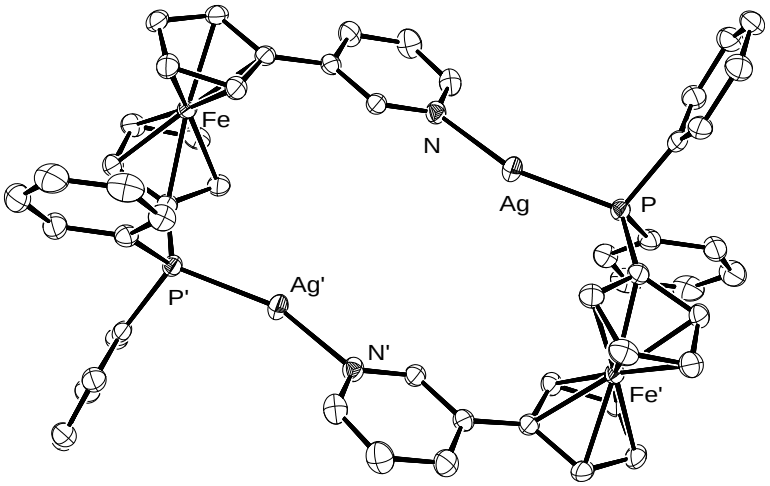

Fig. 4.4: Molecular structure of **20** in the crystal (H, counter ion and solvent atoms are omitted for clarity).

the same methods as **19** before. The elemental analysis confirms the stoichiometry. The ESI mass spectrum exhibits a peak at higher m/z than the simplest coordinated monomeric cation $[C_{27}H_{22}AgFeNP]^+$. This indicates that the product is not monomeric.

In the ^{1}H NMR spectrum ($CHCl_3$) one of the pyridyl protons next to the nitrogen atom (H^2, H^6) gives rise to a signal at 9.00 ppm, low-field shifted with respect to the free ligand **2**. The signal due to the other pyridyl proton of these is observed at 8.08 ppm, shifted in the opposite field direction. The ^{31}P NMR spectrum shows a single signal, observed broad and split into a doublet (δ = 11.1 ppm), in accord with the Ag-P coupling ($J_{^{107}AgP,^{109}AgP} \approx 691$ Hz).

Liquid phase diffusion of hexane into a chloroform solution of **20** afforded crystals suitable for X-ray diffraction analysis, which revealed a centrosymmetric dimeric molecular structure with one molecule of $CHCl_3$ per asymmetric unit (Fig. 4.4).

The metal-donor distances are very similar to those of **19** (Tab. 4.2). Again, a 2 + 1 coordination is observed. The angle ∠ P-Ag-N deviates even more from linearity, due to a stronger interaction with the anion, which is reflected by a comparatively smaller Ag–F distance of only 266.6 pm as opposed to 273.7 pm in the case of **19**.

Tab. 4.2: Selected bond lengths (pm) and bond angles (°) of **20**.

Ag–P	235.91(10)
Ag–N	217.3(3)
Ag–F4	266.6
∠ P-Ag-N	156.61(10)

4.2.3 Ag Complex of 3

The analogous reaction of **3** with $AgBF_4$ in methanol gave [Ag(**3**)][BF_4] · 0.5 C_6H_{14} (**21**), according to elemental analysis after precipitation with hexane. Single crystals were obtained from chloroform. An X-ray diffraction analysis revealed the polymeric structure of the solvate [Ag(**3**)][BF_4] · $CHCl_3$ (Fig. 4.5 and Tab. 4.3).

Bond parameters are similar to those of the the two silver complexes describes before. Not surprisingly, the strongest similarity occurs between **19** and **21**, which are both coordination polymers. The P-Ag-N angle and Ag–F4 distances are almost identical.

A *P*,*N*-coordination in solution is indicated by NMR spectroscopy ($CHCl_3$). The diagnostic pyrdiyl H^6 signal is observed at 8.77 ppm, 0.33 ppm low-field shifted in compar-

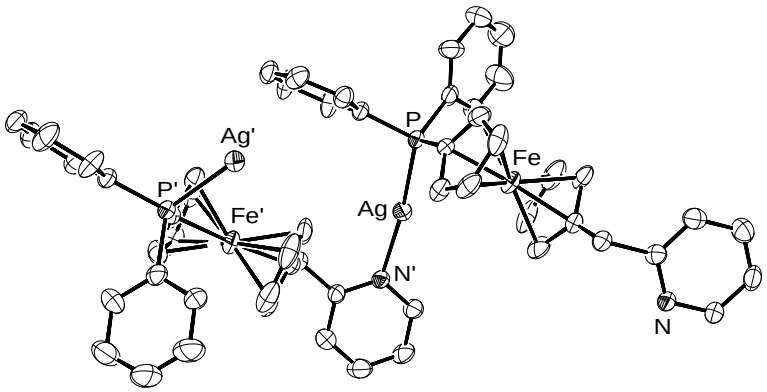

Fig. 4.5: Section of the polymer chain in the crystal structure of **21** (H, counter ion and solvent atoms are omitted for clarity).

Tab. 4.3: Selected bond lengths (pm) and bond angles (°) of **21**.

Ag–P	235.8(2)
Ag–N	216.2(6)
Ag–F4	275.2
∠ P-Ag-N	166.9(2)

ison with pristine **3**. The signal observed in the ^{31}P NMR spectrum is also broad and split into a doublet, located at 7.1 ppm. The doublet is located at a similar chemical shift than this of **19** (6.8 ppm).

4.3 Synthesis and Characterisation of Au Compounds

4.3.1 Simple Au Complexes of 1, 2 and 3

The ligands were reacted with one equivalent of [AuCl(tht)] in dichloromethane at room temperature. Precipitation with hexane, washing and drying in vacuum afforded [AuCl(**1**)] (**22**), [AuCl(**2**)] (**23**) and [AuCl(**3**)] (**24**) as orange to yellow solids, whose stoichiometry was proved by elemental analysis.

4.3.1.1 Characterisation

All three products were structurally characterised by single crystal X-ray diffraction analysis. Suitable crystals were obtained in all cases by liquid phase diffusion of diethyl ether into a chloroform or dichloromethane solution of the complexes. The results are shown in Fig. 4.6. The typical linear coordination geometry with the coordination number two was found in all cases (Chapter 4.1). The structures are very similar, which is not surprising, because the nitrogen donor remains uncoordinated.

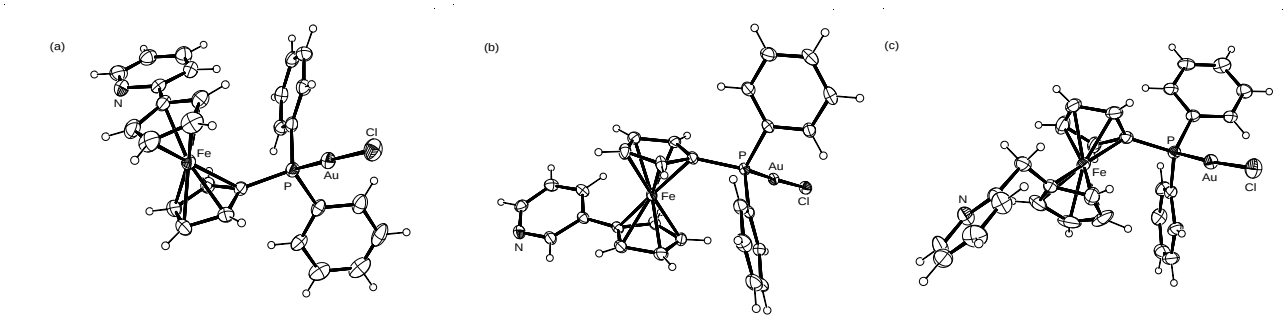

Fig. 4.6: Molecular structures of **22** (a), **23** (b) and **24** (c) in the crystal.

The Au–P and the Au–Cl distances differ only marginally (Tab. 4.4). The same is true for the angle ∠ P-Au-Cl. Close intermolecular contacts or aurophilic interactions are not observed. The Au–P and Au–Cl distances in **22**, **23** and **24** are slightly larger than in the corresponding dppf complex $[(AuCl)_2(dppf)]$. In turn the P-Au-Cl angles are smaller than in the dppf analogue.

Tab. 4.4: Selected bond lengths (pm) and bond angles (°) of **22**, **23** and **24**.

	22	**23**	**24**	$[(AuCl)_2(dppf)]$
Au–P	225.0(9)	223.66(11)	223.71(16)	222.8
Au–Cl	230.8(10)	230.55(10)	230.1(2)	228.4
∠ P-Au-Cl	176.2(4)	175.33(4)	176.75(6)	178.51

A monodentate *P*-coordination in solution is indicated by a pronounced shift of the phosphorus signal in the ^{31}P NMR spectra of **22**, **23** and **24**. The signals are located close to 28 ppm, downfield shifted by approximately 45 ppm with respect to the respective free ligand (δ = ca. –17 ppm). The ^{1}H NMR signals diagnostic for nitrogen coordination remain unshifted.

4.3.1.2 Electrochemical Investigations

22 was investigated in standard cyclic voltammetry, which revealed a ferrocene-based oxidation plus an additional irreversible oxidation process at higher potential (Fig. 4.7 a).

In view of the presumptive redox-inertness of [$(AuCl)_2$(dppf)] (Chapter 4), this complex surprisingly exhibited reversible behaviour concerning the ferrocene-based redox waves, if the scan was reversed before the start of the second oxidation process (Fig. 4.7 b). The redox potential for the ferrocene-based process of **22** has a value of E^{0}' = 0.91 V vs. decamethylferrocene (fc*) at a scan rate of 100 mV/s, which corresponds to a remarkable coordination-induced anodic shift of ca. 0.36 V with respect to pristine **1**. Compared with the well established redox sensors 1,1'-di(pyrid-2-yl)ferrocene and 1,1'-di(pyrid-2-yl)octamethylferrocene, introduced in Chapter 1.4.1, this is a respectable result.

23 and **24** were also subjected to CV. Both exhibited reversible behaviour for the ferrocene-based redox process, if the scan was reversed before the onset of a further oxidation process at higher potentials. For **23** the ΔE_P value is 61 mV. After the reference standard fc* had been added, the reversible behaviour disappeared. Hence, the half wave potential could not been referenced. In the case of **24** the formal electrode potential could be identified for the ferrocene-based redox process. It has a value of E^{0}' = 0.85 V vs. fc*. Again, this corresponds to a remarkable coordination-induced anodic shift of ca. 0.23 V with respect to the free ligand **3**.

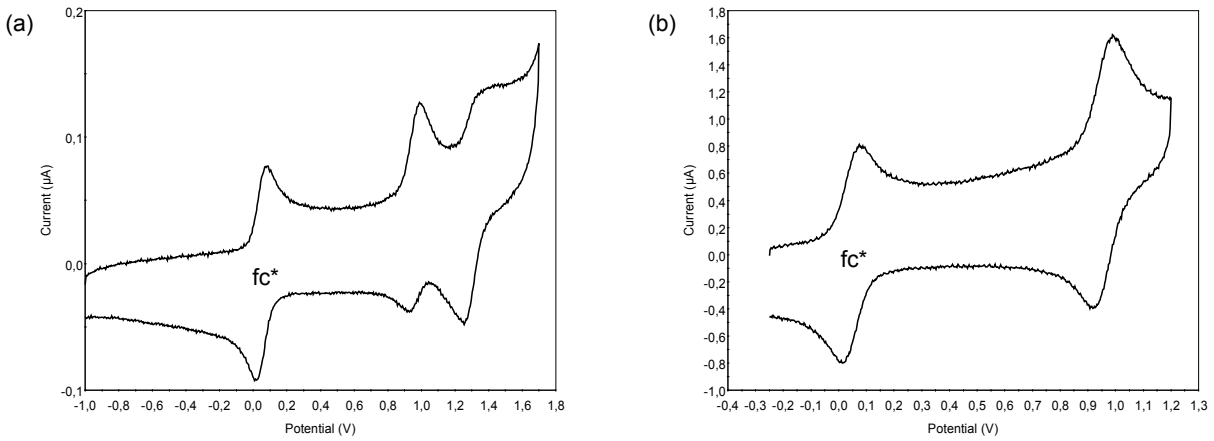

Fig. 4.7: CV of **22** (0.1 mM, DCM, 0.1 M [N^{n}Bu][PF_6], 100 mV/s), scan range from –1.0 V to +1.7 V (a) and from –0.25 V to +1.2 V (b).

4.3.2 Further experiments

The gold complexes **22**, **23** and **24** open the possibility for further reactions, because one of the ligand's donor sites stayed unoccupied and is therefore available for further coordination. Two aspects are of interest: First, the abstraction of the chloro ligand to induce Au-N coordination and, second, the preparation of bimetallic complexes.

4.3.2.1 Reaction with $AgBF_4$

Inspired by known reactions of chlorogold complexes of organic *P*,*N*-ligands,[111] the replacement of the strongly bonded chloro ligand by a weakly or even non-coordinating counter ion seemed to be feasible. **22**, **23** and **24** were each reacted with one equivalent of $AgBF_4$ in order to abstract the chloro ligand and to liberate a coordination site at the gold metal centre for nitrogen coordination, expecting a *P*,*N*-coordinated dimer or polymer (Fig. 4.8). Due to the ligand geometry and the preferred linear coordination geometry of Au^I, a chelate seemed highly improbable.

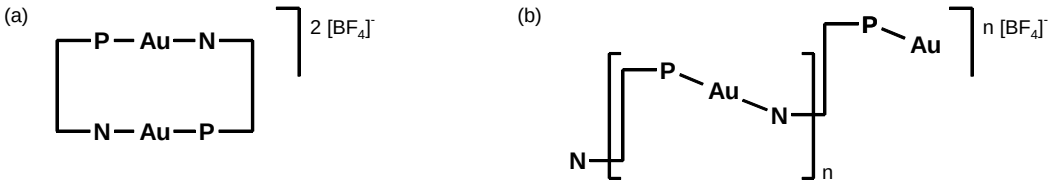

Fig. 4.8: Possible expected results from the reaction of **22**, **23** and **24** with $AgBF_4$.

The resulting complexes **25**, **26** and **27** were poorly soluble after isolation. Therefore a characterisation by NMR spectroscopic methods met with limited success. The isolated solids were used for mass spectrometry and elemental analysis. The results turned out to be in accord with the composition $[Au(L)][BF_4]$. In the case of **25**, it was possible to isolate a small amount of crystalline material suitable for structural characterisation by X-ray diffraction analysis. Full structure refinement failed, but the connectivity of the atoms could be established (Fig. 4.9).

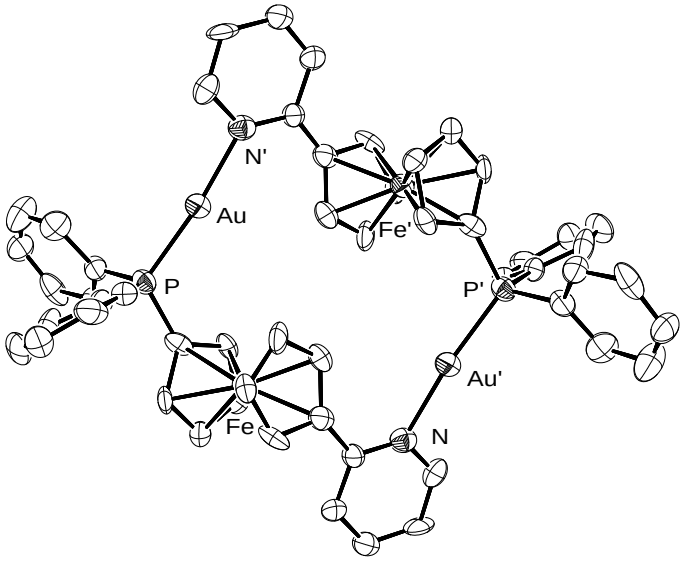

Fig. 4.9: Molecular structure of **25** in the crystal (H and counter ion atoms are omitted for clarity, remaining electron density of probably disordered solvent could not be refined).

A *P*,*N*-coordinated dimer was found. The gold atoms are in a nearly linear coordination environment (Tab. 4.5). The Au–P distance of 224.5 ppm is indistinguishable from that of the related compound [$(AuCl)_2$(dppf)] (Chapter 4.1). The Au–N' bond in **25** is about 8 pm longer than the corresponding bond in the pyridine complexes [$AuX(C_5H_5N)$] (X = Cl, I).[112] Aurophilic interactions are absent in **25**.

Tab. 4.5: Selected bond lengths (pm) and bond angles (°) of **25**.

Au–P	224.5(5)
Au–N'	214.1(2)
∠ P-Au-N'	174.0(5)

4.3.2.2 Bimetallic Complexes

As a sideline of these investigations the preparation of heterobimetallic complexes of **1** and **3** with gold and silver was attempted. An interesting aspect of such complexes are potential metallophilic interactions. Reaction of the simple chlorogold complexes **22** and **24** with $AgBF_4$ in the presence of one equivalent of a phosphine ligand (PMe_3, PCy_3, **1**) gave no crystalline material. Also, reactions of $[Au(tht)_2][BF_4]$ with two equivalents of **1** and **3**, respectively, followed by the addition of silver tetrafluoroborate, failed. Crystallisation experiments with $AgSbF_6$ as silver source instead of $AgBF_4$ failed, too.

4.4 Summary and Conclusion

The ligands **1**, **2** and **3** were examinated in coordination reactions with Au^I and Ag^I. The reactions with $AgBF_4$ in a 1:1 molar ratio gave the corresponding complexes **19**, **20** and **21**. All three ligands show a bridging coordination mode. **1** and **3**, containing a pyrid-2-yl group, form polymers , while the pyrid-3-yl containing ligand **2** forms a cyclic dimer. The complexes **22**, **23** and **24** obtained from the reactions of **1** - **3** with [AuCl(tht)] afforded monodentate, *P*-coordinated phosphine complexes. These complexes show a reversible behaviour concerning the ferrocene-based redox wave in the cyclovoltammetric investigations. Further reactions, aimed at the abstraction of the chloro ligand to induce Au-N coordination resulted in the less soluble and poorly crystalline complexes **25**, **26** and **27**. Only **25** was structurally characterised. Additional experiments aimed at the preparation of Au-Ag binuclear complexes failed.

5 Coordination Chemistry III: Palladium

This chapter deals with the coordination chemistry of ligands **1** and **3** towards palladium(II). The synthesis and characterisation of relevant complexes is described. Due to the intrinsic attractiveness of *P*,*N*-donors in catalytic applications, the utilisation of these complexes in palladium-catalysed C–C bond forming reactions is scrutinised.

5.1 Introduction

It is well known that palladium readily coordinates both, donors containing phosphorus and nitrogen.[113–115] Many organic *P*,*N*-ligands form palladium complexes, when they are reacted with the popular Pd source [$PdCl_2$(cod)] (cod = η^2:η^2-cycloocta-1,5-diene). They simply substitute the chelating diolefin ligand in this reaction. A typical example is shown in Fig. 5.1(a).[116] Concerning the palladium chemistry of ferrocene-based ligands, it is essential to address 1,1'-bis(diphenylphosphino)ferrocene (dppf). It is one of the most useful and popular 1,1'-disubstituted chelate ligands in this field of chemistry. Details of the coordination and catalytic chemistry have been comprehensively reviewed.[21,55] Dppf and the complex [$PdCl_2$(dppf)], Fig. 5.1 b, are used in the following for comparison in structural chemistry and catalytic tests, respectively.

The number of palladium complexes of ferrocene-based ligands closely related to **1** and **3** is rather small. A rare example is the square-planar *trans*-[$PdCl_2$(bipyppf)]

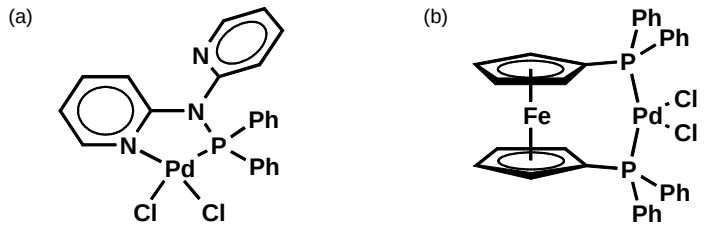

Fig. 5.1: $PdCl_2$ complexes of *P*-functionalised donors.

(bipyppf = 1-(diphenylphosphino)-1'-(2,2'-bipyridyl-6-yl)ferrocene), which is a chelate of a bipyridyl-substituded phosphinoferrocene. The structure of this complex has been established by X-ray diffraction analysis (Fig. 5.2).[117] Selected distances and angles are given in Tab. 5.3 on page 83.

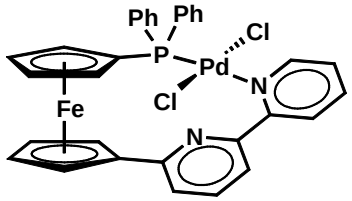

Fig. 5.2: *trans*-[$PdCl_2$(bipyppf)].

Ligands which are closely related to **1** and **3** concerning their flexibility elements and donor groups (pyridyl and diphenylphosphino group) are 1-(diphenylphosphino)-1'-N-[(pyrid-2-yl)methyl]carbamoylferrocene, Fig. 5.3 a, and its ethylene-spaced analogue 1-(diphenylphosphino)-1'-N-[2-(pyrid-2-yl)ethyl]carbamoylferrocene, Fig. 5.3(b).[118]

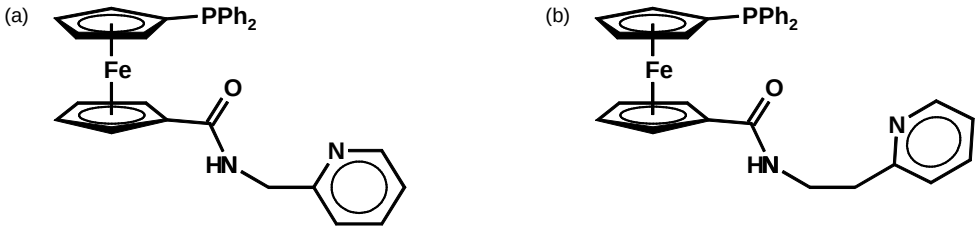

Fig. 5.3: 1,1'-Ferrocene-based pyridylphosphinocarboxamide ligands.

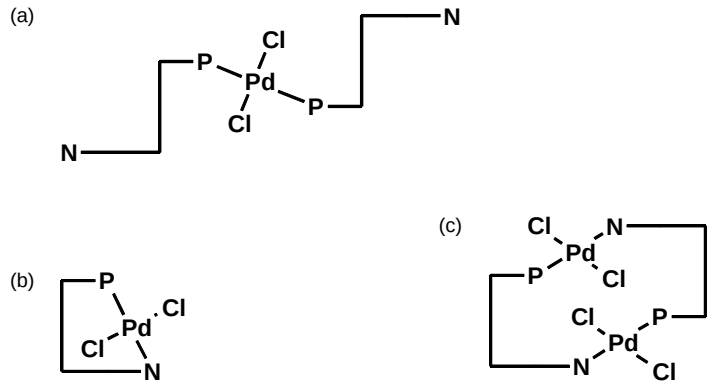

Fig. 5.4: Coordination behaviour of the pyridylphosphinocarboxamide ligands shown in Fig 5.3: monodentate bis(phosphine) complex (a), chelate (b) and centrosymmetric dimer (c).

The reaction of $[PdCl_2(cod)]$ with two equivalents of the *P*,*N*-ligand afforded a *trans*-square-planar, bis(phosphine) complex in both cases. Fig. 5.4 shows possible binding modes of both pyridylphosphinocarboxamide ligands. When the reaction was carried out in 1:1 molar ratio, both ligands showed different behaviour. On the one hand, the ligand with the shorter methylene bridge, 1-(diphenylphosphino)-1'-N-[(pyrid-2-yl)-methyl]carbamoylferrocene, forms a *trans*-chelate complex. On the other hand, the ligand with the longer ethylene bridge, 1-(diphenylphosphino)-1'-N-[2-(pyrid-2-yl)ethyl]-carbamoylferrocene, forms a centrosymmetric, dimer (Fig. 5.4 c). Similar behaviour was observed for $ZnBr_2$ complexes containing **3** (Capter 3.4.1).

Selected structural data are collected in Tab. 5.1. The coordination angles deviate less than 6 ° from the value of 90 ° for an undistorted square-planar arrangement. The Pd–N distances are close to ca. 210 pm, while the Pd–P distances are ca. 224 pm in the chelate and the dimer. This effect (small Pd–N, larger Pd–P distances) is caused by the different covalence radii of both atoms. The Pd–P bond lengths are even ca. 232 pm in the bis(phosphine) complex, due to the larger *trans* influence of the *P*-donor. Pd–Cl bond lengths (ca. 230 pm) are essentially identically in all three complexes.

Tab. 5.1: Selected bond lengths (ppm) and angles (°) of the Pd complexes of pyridylphosphinocarboxamide ligands shown in Fig 5.3.

	bis(phosphine) complex	chelate	centrosymmetric dimer
Pd–P	232.5(1)	224.3(1)	224.3(1)
Pd–N	–	212.4(2)	210.7(4)
Pd–Cl(1)	229.6(1)	229.6(1)	230.0(1)
Pd–Cl(2)	–	230.2(1)	229.8(1)
∠ N-Pd-Cl(1)	–	88.85(6)	85.8(1)
∠ N-Pd-Cl(2)	–	88.55(6)	90.0(1)
∠ P-Pd-Cl(1)	86.22(3)	92.78(3)	95.57(5)
∠ P-Pd-Cl(2)	–	89.95(3)	88.77(5)

5.2 Synthesis and Characterisation of Pd-Compounds

The synthesis of compounds **29, 31, 33** and **35** was carried out by the group members of Prof. Petr Štěpnička at Charles University, Prague. All analytical, X-ray crystallographic and catalytic data of the palladium complexes were collected in the laboratories of the cooperation partners in the Czech Republic.

5.2.1 Simple Palladium Complexes of 1 and 3

Starting from [$PdCl_2$(cod)], it was first attempted to synthesise palladium complexes of **1** and **3** in a 1:1 and 1:2 metal to ligand molar ratio. For 1:1 stoichiometry, both ligands form chelate complexes, viz. [$PdCl_2$(**1**)] (**28**) and [$PdCl_2$(**3**)] (**29**). The analogous reaction with two equivalents of **1** or **3** afforded the respective bis(phosphine) complexes *trans*-[$PdCl_2$(**1**)$_2$] (**30**) and *trans*-[$PdCl_2$(**3**)$_2$] (**31**) as shown in Fig. 5.5. The complexes were isolated as air-stable solids and characterised by spectroscopic methods and elemental analysis. Due to the poor solubility of the bis(phosphine) complexes **30** and

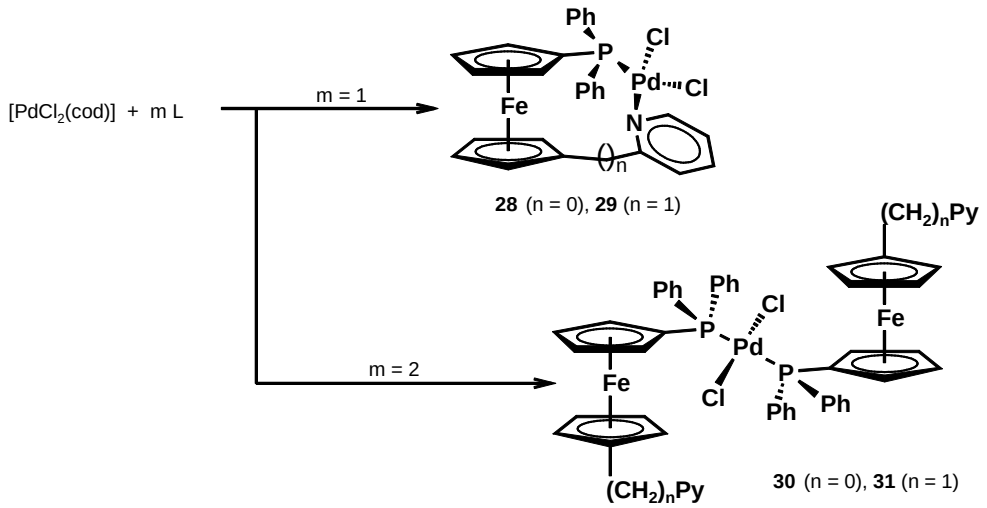

Fig. 5.5: Synthesis of simple Pd complexes **28**, **29**, **30** and **31**, (n = 0: L = **1**, n = 1: L = **3**).

31, NMR characterisation was carried out with *in situ* generated compounds. Except for **29**, the molecular structures were determinated by single crystal X-ray diffraction analysis.

The coordination of the phosphorus donor atom in both chelates is manifested by a low-field shift of the phosphorus signal in the ^{31}P NMR spectrum of 34.1 ppm for **28** and 38.7 ppm for **29** with respect to the free ligand **1** or **3** (Tab. 5.2). The signal of the pyridyl H^6 is only shifted by about 0.12 ppm to lower field in **28** and into the opposite field direction for **29**. Interestingly, the signals of the ferrocene moiety in the chelated complex **28** are markedly shifted from the usual region. They are located between 4.63 ppm and 6.64 ppm, probably influenced by ring currents of the nearby aromatic rings. This

Tab. 5.2: Chemical shifts of the diagnostic NMR signals of **28, 29, 30** and **31** in ppm.

	1	**28**	**30**	**3**	**29**	**31**
signal due to pyridyl H^6 (^{1}H NMR)	8.47	8.55	8.49	8.44	8.32	8.48
phosphorus signal (^{31}P NMR)	–17.7	16.4	16.2	–16.5	22.2	15.9

Solvent: CD_2Cl_2, except for **1** ($CDCl_3$).

is a result of the chelating coordination, which leads to conformationally locked, C_1-symmetric structures. These chiral structures make the CH groups of the ferrocene moiety diastereotopic and anisochronic. In the analogous chelate **29**, the protons of the ferrocene CH groups and the methylene protons become also diastereotopic and anisochronic. Their signals were detected between 2.32 ppm and 5.03 ppm.

In contrast, the signals of the CH groups of the ferrocene moiety of the bis(phosphine) complexes **30** and **31** are similar to those of free ligands. They were observed to be degenerate, indicating conformational flexibility and equivalence of the ligands. In both bis(phosphine) complexes the phosphorus signal was also low-field shifted with respect of the corresponding free ligand (33.9 ppm for **30** and 32.4 ppm for **31**), as shown in Table 5.2. Not surprisingly, the NMR signals due to the pyridyl H^6 of the uncoordinated pyridyl donor remained similar to those of the free ligand.

The molecular structure of **28** is shown in Fig. 5.6, as the result of the X-ray diffraction analysis. Unlike *trans*-[$PdCl_2$(bipyppf)],[117] complex **28** shows a *cis*-*P*,*N*-geometry, which apparently reflects the tighter disposition of the donor atoms. The typical square-planar coordination geometry of Pd^{II} was found. The coordination angles do not differ

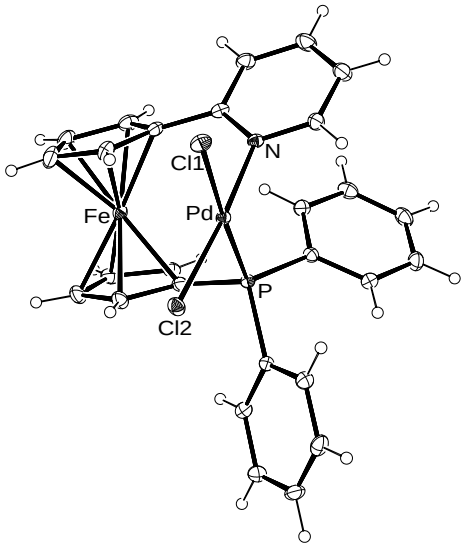

Fig. 5.6: Molecular structure of **28** in the crystal.

Tab. 5.3: Selected bond lengths (pm) and bond angles (°) of **28** and comparable complexes.

	28	$[PdCl_2(dppf)]\cdot CHCl_3$	$[PdCl_2(bipyppf)]\cdot[PdCl_2(cod)]$
Pd–P	224.42(7)	228.3(1)	223.5(1)
Pd–N^a	204.50(2)	230.1(1)	212.6(4)
Pd–Cl1	236.38(7)	234.7(1)	231.5(1)
Pd–Cl2	230.62(7)	234.8(1)	232.2(1)
∠ N^a-Pd-Cl1	88.44(7)		
∠ N^a-Pd-Cl2	175.30(6)		
∠ N^a-Pd-P	89.77(7)	99.07(5)	173.92(10)
∠ P-Pd-Cl1	177.27(2)		
∠ P-Pd-Cl2	90.67(2)		
∠ Cl1-Pd-Cl2	91.28(2)	87.80(1)	176.09(4)
∠ Cp1-Cp2	5.71		
∠ τ	17.40		

^{a}N = P2 donor atom in the compared dppf complex.

significantly from the ideal right angle (Tab. 5.3). The bond lengths, in particular the palladium-donor distances, compare well to those of the dppf analogue $[PdCl_2(dppf\text{-}\kappa^2P,P')] \cdot CHCl_3$[119] and other known bis(phosphine) complexes.[88,120–123] The differences in the Pd–Cl bond length can be accounted for by a bigger *trans* influence of the second phosphine donor instead of a nitrogen donor atom in **28**.[124] The *trans* influence can also be observed in the bipyppf analogue (Tab. 5.3), which causes a larger Pd–N bond than in the *cis* complex **28** (212.6 pm vs. 204.5 pm). The widened bite angle in the dppf complex arises from the less flexible geometry of the dppf compared with **1**, in which the position of the nitrogen donor atom becomes more flexible due to the rotation around the C–C single bond between the pyridyl group and the ferrocene moiety. The Pd–N distance is considerably shorter than in the mentioned *trans*-$[PdCl_2$(1-(2,2'-bipyrid-6-yl)-1'-diphenylphosphinoferrocene)].

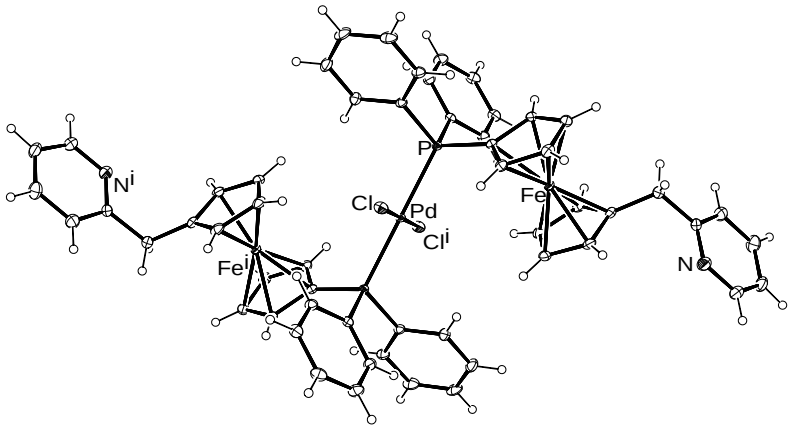

Fig. 5.7: Molecular structure of **31** in the crystal.

The molecular structures of **30** and **31**, obtained from X-ray diffraction analysis, share many common features (Fig. 5.7, 5.8 and Tab. 5.4). The symmetry of the triclinic spacegroup $P\bar{1}$ in the crystal structure of **31** causes an ideal planar coordination geometry with the Pd atoms residing on the crystallographic inversion centre. The bulky pyridylphosphinoferrocene ligands are situated in *trans* positions, while making their PC_3 moieties mutually staggered as viewed along the P–P' direction. This feature was encountered in the structurally characterised bis(phosphine) complexes mentioned before.[88, 120–123]

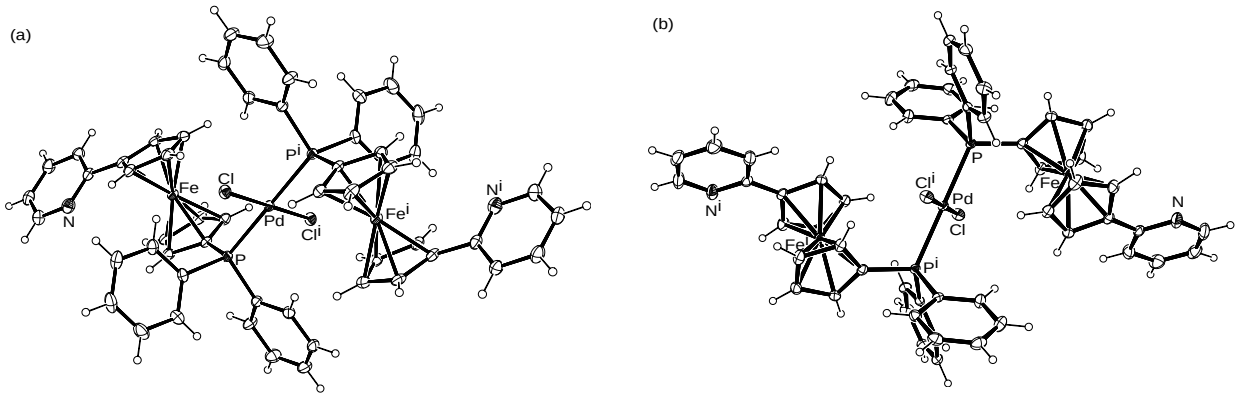

Fig. 5.8: Molecular structure of the independent molecule 1 (a) and 2 (b) of **30** in the crystal (solvate atoms have been omitted for clarity).

Tab. 5.4: Selected bond lengths (pm) and bond angles (°) of **30** and **31**.

	30·CH_2Cl_2		
	molecule 1	molecule 2	**31**
Pd–P	233.57(8)	233.94(8)	234.90(4)
Pd–Cl	229.94(7)	230.37(8)	230.41(4)
∠ P-Pd-Cl	94.36(3)	86.37(3)	88.11(2)

30 crystallises as the solvate **30** · CH_2Cl_2 with two structurally independent complex molecules per unit cell. Both independent molecules are shown in Fig. 5.8. The Pd–P and Pd–Cl distances in **31** and **30** (molecule 1 and molecule 2) are almost equal. The P-Pd-Cl angle in **31** is slightly smaller than the ideal angle for a square-planer arrangement of 90 °. While the corresponding angles in both independent molecules in the structure of **30** are different (94.4 ° molecule 1, 86.4 ° molecule 2), their average instead is close to the ideal angle value (90.4 °).

5.2.2 (L^{NC})-Palladium Complexes of 1 and 3

The reaction of [Pd(μ-Cl)(L^{NC})]$_2$ (L^{NC} = [(2-dimethylamino-κN)methyl]phenyl-κC^1) with two molar equivalents of **1** or **3** leads to the corresponding bridge-cleavage complexes [PdCl(L^{NC})(**1**)] (**32**) and [PdCl(L^{NC})(**3**)] (**33**) (Fig. 5.9).

The NMR data of **33** are in accord with the suggested structure. A single phosphorus signal at 33.1 ppm, shifted to lower field by 49.6 ppm with respect to the free ligand and an essentially unshifted pyridyl H^6 signal at 8.45 ppm (8.44 ppm in **3**) illustrate an exclusive phosphorus coordination. The coupling of the aliphatic protons of the L^{NC} ligand with phosphorus is an indication for the P–N *trans* geometry.[125–130]

However, the NMR data of **32** provide a more complicated picture. It seems that two species are present in solution, as indicated by two signals (δ = 32.7 ppm and

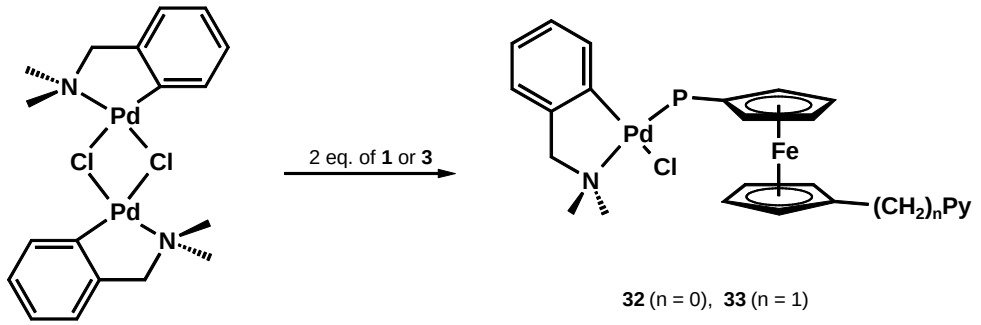

Fig. 5.9: Reaction of $[Pd(\mu\text{-}Cl)(L^{NC})]_2$ with two molar equivalents of ligands **1** and **3**.

32.9 ppm) in the ^{31}P NMR spectrum. The diagnostic pyridyl H^6 also gives rise to two signals, an essentially unshifted one at 8.45 ppm and a second one, shifted to lower field, at 8.92 ppm, which indicates pyridyl coordination. Most likely this is due to an equilibrium between the primary bridge-cleavage product **32** and a dissociated form **34a** (Fig. 5.10), which exhibits a chelate structure.

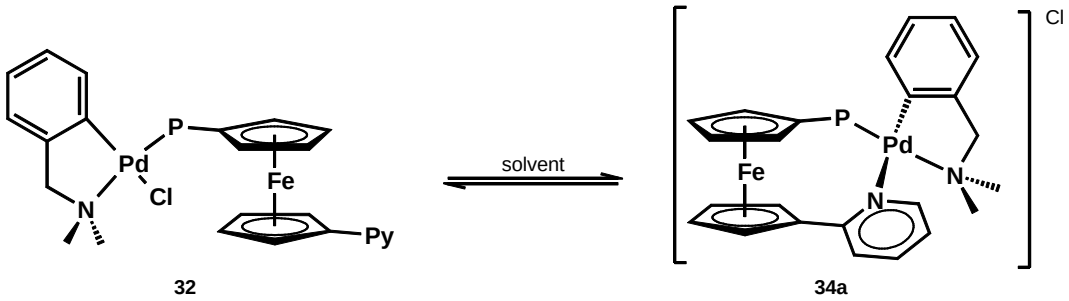

Fig. 5.10: Solvent constrained equilibrium between **32** and **34a**.

This assumption is strongly supported by NMR data concerning the signals of the ferrocene CH groups. These become diastereotopic in **34a** due to a fixed chelate geometry, which is in accord with eight well separated signals observed for them. Moreover, the involvement of a dissociation process is in line with the observation that the NMR spectra recorded in CD_3CN as a donor solvent suggested an additional species to be present. The strong solvent dependence of the equilibrium occurs probably due to the better stabilisation of the cationic complex by polar solvents, which is in accord with

a shift of the equilibrium in favour of the neutral complex **32**, observed if the NMR is measured in non-polar C_6D_6.

A similar reaction of both ligands with the solvato complex $[Pd(L^{NC})(MeCN)_2][ClO_4]$ in a 1:1 molar ratio afforded the cationic complexes $[Pd(L^{NC})(\mathbf{1})][ClO_4]$ (**34**) and $[Pd(L^{NC})(\mathbf{3})][ClO_4]$ (**35**), displayed in Fig. 5.11.

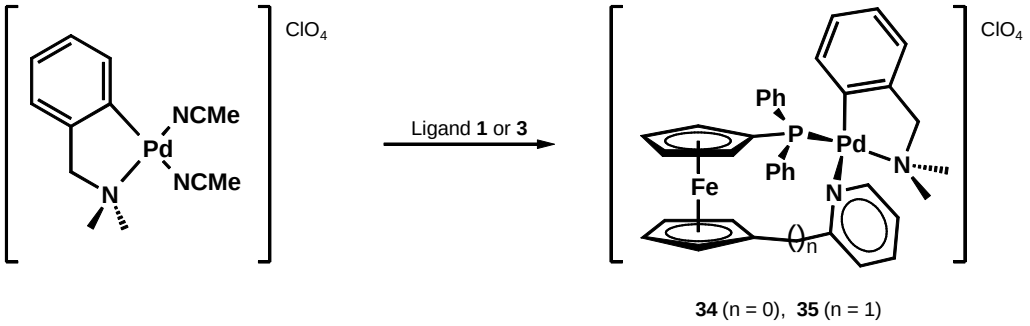

Fig. 5.11: Reaction of **1** and **3** with $[Pd(L^{NC})(MeCN)_2][ClO_4]$.

NMR characterisation of the products indicated a *cis*-chelating coordination of both ligands. The constrained geometry makes several protons of the compound, especially the ferrocene CH groups, diastereotopic. The behaviour is comparable with that of the simple Pd chelate complexes **28** and **29**. The shifts of the pyridyl H^6 signal (δ = 8.98 ppm vs. 8.47 ppm in free **1**) and the phosphorus signal (δ = 32.6 ppm vs. –17.7 ppm in free **1**) are consistent with the *P,N*-coordination. The phosphorus signal of **35** is also shifted (δ = 34.3 ppm), whereas the pyridyl H^6 signal is located at slightly higher field (δ = 8.38 ppm vs. 8.44 ppm in free **3**), an effect already known from **29**. The ESI mass spectra showed only the respective cation $[Pd(L^{NC})(L)]^+$ (L = **1**, **3**). The presence of the perchlorate counter ion was proven by IR spectroscopy, elemental analysis verified the stoichiometry.

The results of the structural characterisation of **34** and **35** are shown in Fig. 5.12. Both coordination environments of the metal centres are distorted square-planar. The donor-metal distances of **34** and **35** are in accord with those of related complexes.[125–130] The bite angle of L^{NC} ($\angle$ N2-Pd-C29) in **34** and **35** is the most acute coordination angle and

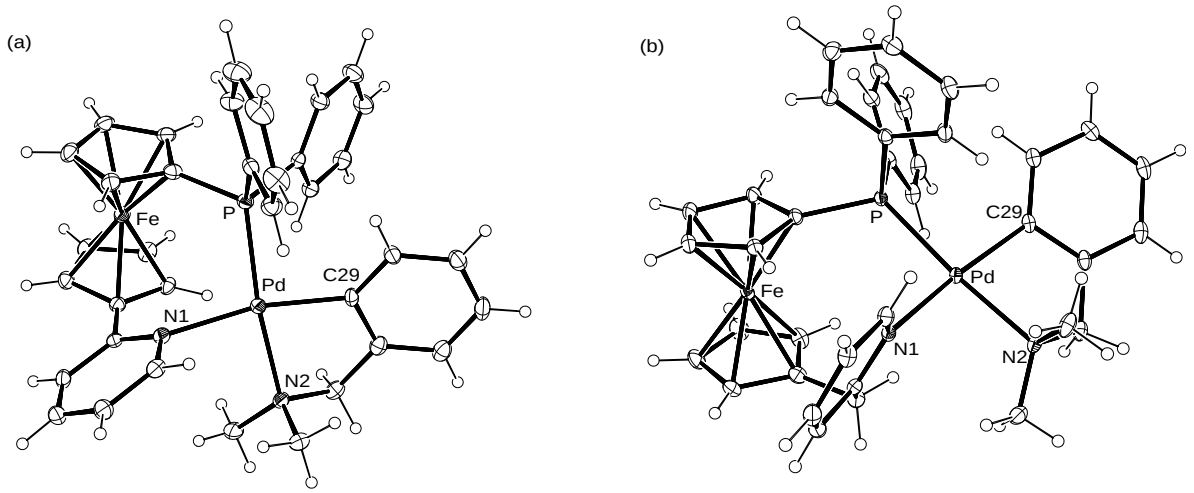

Fig. 5.12: Molecular structures of **34** (a) and **35** (b) in the crystal (counterion and solvent molecules have been omitted for clarity).

very similar in both compounds (Tab. 5.5). The bite angles of the ferrocene ligands (∠ P-Pd-N) differ considerably from each other. The higher flexibility of **3**, induced by the

Tab. 5.5: Selectet distances (pm) and angles (°) of **34** and **35**.

	34	**35**
Pd–P	225.71(9)	224.91(7)
Pd–N1	217.4(3)	214.2(2)
Pd–N2	216.6(3)	213.8(2)
Pd–C29	201.3(3)	203.2(2)
∠ P-Pd-N1	99.13(8)	91.90(6)
∠ P-Pd-C29	91.8(1)	94.41(8)
∠ N1-Pd-N2	89.2(1)	91.07(7)
∠ N2-Pd-C29	81.5(1)	81.93(9)
∠ Cp1-Cp2	3.05	2.91
∠ τ	57.67	39.92

methylene group, allows a closer approach to the ideal right angle (91.9 °), while the constrained geometry of **1** requires a more obtuse bite angle (99.1 °).

5.3 Catalytic Evaluation

The catalytic properties of palladium complexes of **1** and **3** were evaluated in Pd-catalysed C–C bond forming reactions, namely in Suzuki-Miyaura arylation[68,131,132] and cyanation[133,134] of 4-bromotoluene as a deactivated model substrate. The experiments were performed simultaneously with both donors. The very successful ferrocene ligand dppf[32] was used for comparison. Complexes of the type $[PdCl_2(L)]$ (L = **1**, **3**, dppf) were used as well-defined precatalyst and compared to precatalysts generated *in situ* from palladium(II) acetate and the appropriate ligand.

The Suzuki-Miyaura cross-coupling reaction of 4-bromotoluene with phenylboronic acid (Fig. 5.13) was carried out in 1,4-dioxane at 80 °C using 0.5 or 0.25 mol% palladium catalyst. Potassium carbonate was used as base. The obtained results showed that the defined catalyst as well as the *in situ* generated complexes boost the coupling reaction efficiently at 0.5 mol% Pd loading (Tab. 5.6). At 80 °C the reaction proceeded with similar conversions, regardless of the nature of the ligand. Raising the reaction temperature up to 100 °C, better conversions and discrimination by the ligand is achieved. The conversions increased for $[PdCl_2(L)]$ in the order of the ligands dppf $\approx$ **1** $<$ **3**. The *in situ* generated catalyst ($Pd(OAc)_2$/L) showed similar trends with a higher activity in general. Both reactivity trends can be attributed to changed electronic properties and the ease of reduction of the metal source to a catalytically active species.[135]

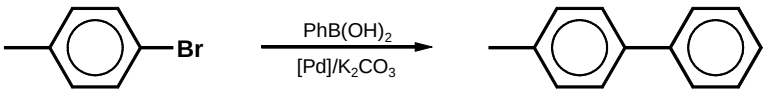

Fig. 5.13: Suzuki-Miyaura cross-coupling reaction of 4-bromotoluene.

Tab. 5.6: Catalytic results for Suzuki cross-coupling reaction at 0.5 mol% palladium loading.

	yield of 4-methylbiphenyl (%)[a]								
	$[PdCl_2(L)]$[b] at 80 °C			$[PdCl_2(L)]$[b] at 100 °C			$Pd(OAc)_2/L$[c] at 100 °C		
time (h)	dppf	**1**	**3**	dppf	**1**	**3**	dppf	**1**	**3**
2	36	35	35	37	42	52	82	89	90
4	41	39	41	42	46	57	93	94	97
6	44	42	44	50	51	61	96	96	99
8	45	47	47	56	55	64	97	96	100
12	50	51	51	65	61	71	99	97	100
24	63	59	60	84	75	85	100	98	100

[a] The reactions were performed with 0.5 mol% of palladium using 2.0 mmol of 4-bromotoluene, 2.2 mmol of phenylboronic acid and 4.4 mmol of K_2CO_3 in dry dioxane (10 mL). [b] Defined precatalyst. [c] *In situ* generated catalyst.

Benzonitriles, the products of palladium-catalysed cyanation of aryl halides, are versatile synthetic intermediates and therefore important commodity chemicals. The cyanation reaction remains still less explored. The reaction with a CN^- source, a base and a catalyst (sometimes an additional cocatalyst like a zinc salt is necessary) proceeds satisfactorily mostly only under harsh temperature conditions. The cyanation test reaction, Fig. 5.14, of the deactivated substrate 4-bromotoluene with potassium hexacyanoferrate(II), Na_2CO_3 and 0.5 mol% catalyst in *N*,*N*-dimethylformamide (DMF) or *N*-methyl-2-pyrrolidone (NMP) was performed at 130 °C for 16 h (Tab. 5.7). The overall conversions in NMP were high, but the reaction was accompanied by undesired reductive dehalogenation of the substrate to give toluene (Tab. 5.7 in parentheses). Both

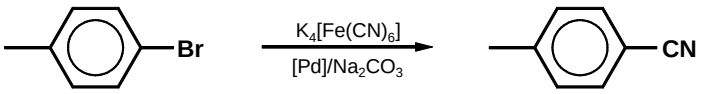

Fig. 5.14: Palladium-catalysed cyanation reaction of 4-bromotoluene.

Tab. 5.7: Catalytic results for the palladium-catalysed cyanation reaction of 4-bromotoluene.

	conversion to 4-cyanotoluene (%)[a,b]	
catalyst	NMP	DMF
$[PdCl_2(dppf)]$	93(7)	100(n.d.)
$[PdCl_2(\mathbf{1})]$ (**28**)	92(8)	100(n.d.)
$[PdCl_2(\mathbf{3})]$ (**29**)	87(9)	100(n.d.)
$Pd(AcO)_2$/dppf	92(8)	91(9)
$Pd(AcO)_2$/**1**	64(22)	90(6)
$Pd(AcO)_2$/**3**	71(20)	90(6)

[a] Conditions: 4-bromotoluene (2.0 mmol), $K_4[Fe(CN)_6]$ (0.5 mmol), Na_2CO_3 (2.0 mmol) and 0.5 mol% of a Pd catalyst in dry solvent (3 mL) at 130 °C for 16 h. Conversions were determined by integration of ^{1}H NMR signals. [b] NMR yield of toluene is given in parentheses; n.d. = toluene not detected.

dppf catalysts, $[PdCl_2(dppf)]$ and *in situ* generated $Pd(OAc)_2$/dppf, performed similarly and with the best conversions. For the catalysts based on ligands **1** and **3** the defined complexes gave better results than the mixtures. Changing the solvent to DMF, the reaction proceeded with complete conversions for all three defined catalysts. The catalyst mixtures are only slightly inferior with conversions of about 90 %.

5.4 Summary and Conclusion

The ferrocene-based pyridylphosphine ligands **1** and **3** were examined with respect to their coordination chemistry towards palladium(II). The ligands react with dichloro-(cod)palladium(II) in a *P*-coordinated monodentate and in a *P*,*N*-chelating manner, depending on the reaction stoichiometry, to form the simple Pd complexes **28, 29, 30** and **31**.

Both ligands were also reacted with $[Pd(\mu\text{-}Cl)(L^{NC})]_2$ (L^{NC} = [(2-dimethylamino-κN)methyl]phenyl-κC^1), leading to the corresponding complexes **32** and **33**. Similar reactions with the preformed solvato complex $[Pd(L^{NC})(MeCN)_2][ClO_4]$ gaves the cationic complexes **34** and **35**. The reaction behaviour of **1** and **3** in these reactions compared well to that observed in the reactions with $[PdCl_2(cod)]$. The resulting compounds were fully characterised by standard methods. **28**, **30**, **31**, **34** and **35** were analysed by single crystal X-ray diffraction. Structural differences can be attributed mainly to the presence of the methylene group in ligand **3**, which makes this ligand more flexible than **1**.

Catalytic investigations of Suzuki-Miyaura cross-coupling reactions showed that complexes **28** and **29** and precatalyst formed *in situ* from **1** and **3** with $Pd(OAc)_2$ promote the reaction of 4-bromotoluene with phenylboronic acid efficiently. The catalyst based on ligand **3** works similar to or slightly better than the corresponding dppf-based catalyst. The results for the **1**-based catalysts are comparable, too, but only slightly inferior to those of the dppf benchmark. The Pd-catalysed cyanation reaction is more efficiently promoted by the defined precatalyst complexes with dppf being a ligand superior to both pyridylphosphines.

6 Experimental

6.1 General Techniques and Methods

All preparations involving air-sensitive compounds were carried out under an atmosphere of dry nitrogen (N50) using standard Schlenk techniques or a conventional glove box (Argon N50). Solvents and reagents were appropriately dried and purified by conventional methods and stored under inert gas atmosphere.

Safety note

Caution! *Although I have not encountered any problems it should be noted that perchlorate salts of metal complexes with organic ligands are potentially explosive**!** Only small quantities of these materials should be prepared and they should be handled with the necessary respect and caution*.

NMR Spectroscopy

NMR spectra were recorded on different spectrometers: 1. *Varian Unity INOVA (500 MHz)*, 2. *Varian Unity INOVA (400 MHz)* 3. *Varian NMR System (500 MHz)* and 4. *Varian 400-MR (400 MHz)*. ^{13}C and ^{31}P NMR data were collected by proton decoupled methods. Chemical shifts δ are given in ppm and are referenced to the shift of the residual protioimpurities of the solvents used relative to trimethylsilane (TMS) for ^{1}H and to the solvent signal for ^{13}C.[136, 137] In the case of ^{31}P NMR samples in $CDCl_3$ were indirectly referenced to triphenyl phosphane (δ = -6 ppm, relative to 85% phosphoric

acid in D_2O[138]). Samples in DMSO-d6 were also indirectly referenced (85% phosphoric acid in DMSO$-d_6$ δ = 0 ppm). Coupling constants were given as absolute value in Hz. Data were analysed by the computer programs Mest-ReC and Spinworks.

Mass spectrometry

ESI and APCI Mass spectra were recorded on a Bruker Esquire 3000 spectrometer (ESI) and a quadrupole ion-trap spectrometer (ESI and APCI) *Finnigan LCQ DECA* (ThermoQuest, San José, USA).

HR-ESI Mass spectra were recorded on a *micrOTOF* spectrometer (Bruker Daltonics, Bremen, Germany).

MALDI Mass spectra were recorded on a *BiFlex IV* (Bruker Daltonics, Bremen, Germany) spectrometer equipped with an N_2-Laser with a wavelength of 337 nm and 3 ns pulse duration. DCTB (2-[(2E)-3-(4-tert-butylphenyl)-2-methylprop-2-enyliden]malononitril) was used as matrix. Mass calibration was performed immediately prior to the measurements using polystyrole standard (Ag-Adduct).

Elemental Analysis

Analysis were carried out by the microanalytical laboratories of the Institute of Thermal Energy Management at the University of Kassel and the department of Chemistry, Charles University, Prague.

Crystal Structure Analysis

X-ray crystallographic data collection was performed using a *Stoe & Cie "IPDS II"* diffractometer with an Eu doped BaFCl area detector and a *Nonius KappaCCD* diffractometer. Graphite-monochromatised Mo$K_{\bar{\alpha}}$ radiation (λ_0 = 0.71073 Å) was used in each case. The datasets were corrected for Lorentz and polarisation effects. A numerical absorption correction was applied. The program SHELXS-97[139] was used for structure solution by direct methods. Refinement was carried out using the program SHELXL-97[139] by full-matrix least-squares against F^2. All non H atoms were refined

anisotropically. H atoms were included to the model at calculated positions according to the riding model. Graphics were generated with the program ORTEP-3 win,[140] showing the displacement elipsoides enclosing the 30 % probability level.

Electrochemistry

Electrochemistry was performed in a home-built cylindrical single-compartment cell with Ag pseudo-reference electrode and Pt working and auxiliary electrodes. The electroactive species was investigated in 0.1 mM or 1.0 mM solution in CH_2Cl_2 (99.9% Extra Dry, Acros Organics) with 0.1 M $[N^nBu_4][PF_6]$ as supporting electrolyte at a scan rate of 100 mV/s at room temperature and under nitrogen atmosphere. The supporting electrolyte was recrystalised three times from dry ethanol before use. Decametylferrocene (fc*) was used as internal standard. An appropriate amount of decamethylferrocene was added after the scans had been recorded. Electrochemical data were acquired with a computer-controlled Princeton Applied potentiostat model Versa Stat II utilising the Princeton PowerSuite (vers. 2.58) software package.

Chromatography

For column chromatography (CC) silica gel 60 M 0.04-0.063 mm / 230-400 mesh ASTM for CC (Chery-Nagel GmbH & Co. KG) or neutral alumina 0.05-0.2 mm (ICN Alumina N - Super I) were used. Thin layer chromatography (TLC) was performed on standard aluminium sheets with silica gel 60 F_{254} (Merck KGaA). Detection was carried out by fluorescence quenching at 254 nm and 366 nm.

6.2 Synthetic Details

All non-indexed compounds were either present in our workgroup or commercially available and used as received.

6.2.1 Starting Materials

Following compounds were synthesised by literature procedures:

1,1'-(Ferrocediyl)phenylphosphane[58]
(Note: Work-up procedure was changed: The reaction mixture was filtered through celite and evaporated under vacuum. Subsequent CC using neutral alumina under inert conditions with dry hexane and subsequent with dry diethyl ether afforded pure product.)
1,1'-Dibromoferrocene[141]
1,1'-Dilithioferrocene[141]
1-Bromo-1'-diphenylphosphinoferrocene[64]
1-Lithio-1'-diphenylphosphinoferrocene[59]
3-Pyridylboroxin[72]
Chloro(tetrahydrothiophene)gold(I)[142]
Bis(1'-bromoferrocenyl)phenylphosphane[64]
Chloro(η^2:η^2-cycloocta-1,5-diene)palladium(II)[143]
Di-μ-chloro-bis[(2-dimethylamino-κN)methyl]phenyl-κC^1dipalladium(II) (L^{NC})[144]
Bis(acetonitrile-κN)[(2-dimethylamino-κN)methyl]phenyl-κC^1palladium(II) perchlorate[125]

6.2.2 Experimental Procedures

6.2.2.1 Ligand Synthesis

1-(Pyrid-2-yl)-1'-diphenylphosphinoferrocene (**1**)
A solution of 1.6 M n-buthyllithium in hexane (12.0 mmol, 7.5 mL) was slowly added at –70 °C to a solution of 1-bromo-1'-diphenylphosphinoferrocene of (11 mmol, 5.0 g) in THF (40 mL) via syringe. After 45 min of stirring at –70 °C [$ZnCl_2$(1,4-dioxane)] (11 mmol, 2.5 g) was introduced in one portion and stirring was continued at room

temperature for 3 h. A solution of [$Pd(PPh_3)_4$] (1 mol%, 0.11 mmol, 127 mg) and 2-bromopyridine (11 mmol, 1.1 mL) in THF (5 mL) was added. The resulting mixture was warmed to 60 °C and stirred for 72 h. The reaction mixture was evaporated using a rotary evaporator and the residue was dissolved in dichloromethane (DCM) (20 mL). The solution was washed with water (2 x 20 mL), dried with Na_2SO_4 and evaporated to dryness. The residue was purified by CC using neutral alumina first with hexane to remove non-polar side products and subsequently with DCM to elute the product. Subsequent evaporation gave **1** as a dark orange oil, which crystallised upon standing. **Yield**: 2.39 g (48 %). **Crystallisation**: Crystals suitable for single-crystal X-ray diffraction analysis were obtained from a highly concentrated DCM solution by slow evaporation in the air. **^{1}H NMR** ($CDCl_3$): 3.96 (m, 2H, Fc), 4.21 (m, 2H, Fc), 4.27 (m, 2H, Fc), 4.83 (m, 2H, Fc), 7.04 (m, 1H, Py), 7.27 (m, 1H, Py), 7.29-7.38 (m, 10H, Ph), 7.51 (m, 1H, Py), 8.47 (m, 1H, Py). **^{13}C NMR** ($CDCl_3$): 68.41 (s), 71.41 (s), 73.10 (d, J_{PC} = 4 Hz), 74.34 (d, J_{PC} = 14 Hz), 76.95 (d, J_{PC} = 7 Hz), 84.59 (s), 120.48 (s), 120.79 (s), 128.29 (d, J_{PC} = 7 Hz), 128.64 (s), 133.64 (d, J_{PC} = 20 Hz), 136.05 (s), 139.14 (d, J_{PC} = 10 Hz), 149.41 (s), 158.67 (s). **^{31}P NMR** ($CDCl_3$): –17.7 (s). **MS/APCI(+)** (m/z (%)): 464 (40) $[MO + H]^+$, 448 (100) $[M + H]^+$, 263 (29) $[C_{15}H_{12}FeN]^+$.

1-(Pyrid-3-yl)-1'-diphenylphosphinoferrocene (**2**)

In a Schlenk-tube 1-bromo-1'-diphenylphosphinoferrocene (4 mmol, 1.8 g) was dissolved in 1,4-dioxane (25 mL). 3-Pyridylboroxin (2 mmol, 0.63 g), K_2CO_3 (20 mmol, 2.8 g) dissolved in water (10 mL) (c(K_2CO_3): 2.0 mol/L) and solid [$Pd(PPh_3)_4$] (2.5 mol%, 0.1 mmol, 115 mg) were added successively. The reaction mixture was heated up to 120 °C (bath temp.) and stirred for 14 h. The organic layer was separated and evaporated using a rotary evaporator. The residue was dissolved in DCM (20 mL). The solution was washed with water (2 x 20 mL) and the aqueous layer extracted with DCM (2 x 10 mL). The combined organic phases were dried with Na_2SO_4 and filtered. Neutral alumina (5 g) was added and volatile compounds were removed. This material subjected to CC with neutral alumina, eluting first with petroleum ether 40 °C - 60 °C (PE) / diethyl ether 5:1 to remove non-polar side products and subsequently with chloroform.

Evaporation gave **2** as an orange oil, which solidified upon standing. **Yield**: 0,76 g (43 %). **Crystallisation**: Slow evaporation of a highly concentrated DCM solution in the air gave crystals suitable for single-crystal X-ray diffraction analysis. **^{1}H NMR** ($CDCl_3$): 3.96 (m, 2H, Fc), 4.22 (m, 2H, Fc), 4.26 (m, 2H, Fc), 4.56 (m, 2H, Fc), 7.15 (m, 1H, Py), 7.30-7.36 (m, 10H, Ph), 7.58 (m, 1H, Py), 8.40 (m, 1H, Py), 8.61 (m, 1H, Py). **^{1}H NMR** ($DMSO-d_6$): 3.88 (s, 2H, Fc), 4.22 (s, 2H, Fc), 4.27 (s, 2H, Fc), 4.78 (s, 2H, Fc), 7.27 (m, 1H, Py), 7.30-7.37 (m, 10H, Ph), 7.59 (m, 1H, Py), 8.40 (m, 1H, Py), 8.61 (m, 1H, Py). **^{13}C NMR** ($CDCl_3$): 67.67 (d, J_{PC} = 1 Hz), 70.94 (d, J_{PC} = 1 Hz), 73.08 (d, J_{PC} = 4 Hz), 74.52 (d, J_{PC} = 15 Hz), 82.56 (s), 123.38 (s), 128.33 (d, J_{PC} = 7 Hz), 128.73 (s), 133.37 (s), 133.59 (d, J_{PC} = 20 Hz), 134.82 (s), 138.96 (d, J_{PC} = 10 Hz), 147.33 (s), 147.56 (s). **^{31}P NMR** ($CDCl_3$): –17.8 (s). **^{31}P NMR** ($DMSO-d_6$): –18.8 (s). **MS/APCI(+)** (m/z (%)): 464 (45) $[MO + H]^+$, 448 (100) $[M + H]^+$, 370 (21) $[C_{21}H_{17}FeNP]^+$, 263 (15) $[C_{15}H_{12}FeN]^+$. **Elemental analysis** (%) calculated for $C_{27}H_{22}FeNP$ (477.3): C 72.50, H 4.96, N 3.13. Found: C 73.34, H 4.94, N 3.23.

1-[(pyrid-2-yl)methyl]-1'-(diphenylphosphino)ferrocene (**3**)

The synthesis of **3** was carried out by Jiří Schulz in the group of Prof. Petr Štěpnička at Charles University, Prague, Czech Republic.

Precursor: A stirred solution of 1-bromo-1'-diphenylphosphinoferrocene (10 mmol, 4.49 g) in THF (50 mL) was treated with a 2.5 M solution of n-butyllithium in hexane (10 mmol, 4.0 mL) at ca. –78 °C (dry ice/ethanol bath). After 15 min neat pyridine-2-carboxaldehyde (12 mmol, 1.29 g) was added and the resulting mixture was stirred at –78 °C for 15 min and then at room temperature for 90 min. The reaction mixture was quenched by addition of water and extracted with DCM after 30 min. The extract was washed successively with saturated aqueous $NaHCO_3$ and NaCl solutions, dried with $MgSO_4$, filtered and evaporated under vacuum. The residue was purified by CC on silica gel using an ethyl acetate:hexane mixture 1:5 (v/v) to elute first a yellow band containing (diphenylphosphino)ferrocene (1.04 g, 28 %) and then a minor red band containing the corresponding ketone (cf. Fig 2.12, page 22) (burgundy red solid; 27 mg,

ca. 0.6 %). Then, the mobile phase was changed to ethyl acetate:hexane 1:1 (v/v) to elute the alcohol 1-[(pyrid-2-yl)hydroxymethyl]-1'-(diphenylphosphino)ferrocene, which was isolated as an ochre solid following evaporation. **Yield**: 2.78 g (58 %). **^{1}H NMR** ($CDCl_3$): 4.01 (td, J = 2.4, 1.3 Hz, 1H, Fc), 4.04 (td, J = 2.4, 1.3 Hz, 1H, Fc), 4.10 (m, 2H, Fc), 4.14 (m, 1H, Fc), 4.20 (dt, J = 2.5, 1.3 Hz, 1H, Fc), 4.21 (br s, 1H, CHO*H*), 4.40 (td, J = 2.4, 1.2 Hz, 1H, Fc), 4.41 (td, J = 2.4, 1.2 Hz, 1H, Fc), 5.36 (s, 1H, C*H*OH), 7.16 (ddd, J_{HH} = 7.5, 4.9, 1.2 Hz, 1H, Py), 7.26 (dm, $J_{HH} \approx$ 8 Hz, 1H, Py), 7.28-7.41 (m, 10H, Ph), 7.63 (td, J_{HH} = 7.7, 1.7 Hz, 1H, Py), 8.51 (ddd, J_{HH} = 4.9, 1.8, 1.0 Hz, 1H, Py). **^{13}C NMR** ($CDCl_3$): 66.79 (s), 68.32 (s), 69.37 (s), 69.33 (s), 71.21 (s, *C*HOH), 71.65 (d, $J_{PC} \approx$ 5 Hz), 71.68 (d, $J_{PC} \approx$ 5 Hz), 73.39 (d, J_{PC} = 13 Hz), 73.62 (d, J_{PC} = 15 Hz), 76.22 (d, J_{PC} = 6 Hz), 92.89 (s), 120.79 (s), 122.49 (s), 128.14 (d, J_{PC} = 6 Hz), 128.49 (s), 128.58 (s), 133.48 (vt, J' = 20 Hz), 136.76 (s), 138.77 (d, J_{PC} = 9 Hz), 138.95 (d, J_{PC} = 9 Hz), 147.90 (s), 161.02 (s). **^{31}P NMR** ($CDCl_3$): –16.3 (s). **Elemental analysis** (%) calculated for $C_{18}H_{24}FeNOP$ (477.3): C 70.45, H 5.07, N 2.94. Found: C 70.27, H 5.18, N 2.84.

Ligand: Commercial SmI_2 solution (10 mmol, 100 mL of 0.1 M in THF) was added to a stirred mixture of 1-[(pyrid-2-yl)hydroxymethyl]-1'-(diphenylphosphino)ferrocene (4 mmol, 1.91 g), $(Me_2N)_3PO$ (HMPA; 40 mmol, 7.0 mL) and 10 mL dry THF during 10 min, yielding a dark brown mixture. After stirring for 5 min, a solution of pivalic acid (5.0 mmol, 514 mg in 5 mL THF) was added, causing the color of the reaction mixture to turn back to the initial orange-yellow. The mixture was stirred for another 15 min, diluted with diethyl ether and saturated aqueous NaCl. The organic layer was separated, and the aqueous layer was extracted with diethyl ether, adding little hexane to facilitate phase separation. The combined organic layers were washed with saturated aqueous NaCl, dried with $MgSO_4$, filtered and evaporated. The residue was passed through a short silica gel column eluting with ethyl acetate:hexane (1:1 v/v) to remove some polar by-products and inorganic residuals. The first yelloworange band was collected and evaporated to afford crude product, which was immediately purified by chromatography on an alumina column using diethyl ether:hexane (4:1 v/v) as the eluent. Evapora-

tion of the first yellow band followed by careful evaporation and drying under vacuum (80 °C/0.1 Torr) gave **3** as a dark orange-brown oil, which slowly crystallised when stored at 4 °C. **Yield**: 1.02 g (55 %). **Crystallisation**: Crystals suitable for single-crystal X-ray diffraction analysis were grown by recrystallisation from diethyl ether. **^{1}H NMR** (CD_2Cl_2): 3.63 (s, 2H, CH_2Py), 3.97 (m, 2H, Fc), 4.05 (m, 2H, Fc), 4.07 (m, 2H, Fc), 4.33 (m, 2H, Fc), 7.02 (m, 1H, Py), 7.06 (m, 1H, Py), 7.28-7.40 (m, 10H, Ph), 7.54 (m, 1H, Py), 8.44 (m, 1H, Py). **^{13}C NMR** (CD_2Cl_2): 38.65 (s), 69.36 (s), 70.31 (s), 72.18 (d, J_{PC} = 4 Hz), 73.96 (d, J_{PC} = 15 Hz), 76.34 (d, J_{PC} = 6 Hz), 87.50 (s), 121.44 (s), 122.73 (s), 128.48 (d, J_{PC} = 7 Hz), 128.80 (s), 133.86 (d, J_{PC} = 20 Hz), 136.50 (s), 139.92 (d, J_{PC} = 9 Hz), 149.43 (s), 161.44 (s). **^{31}P NMR** (CD_2Cl_2): –16.5 (s). **MS/ESI(+)** (m/z): 462 $[M + H]^+$, 484 $[M + Na]^+$. **HR-ESI**: m/z calculated for $C_{28}H_{24}FeNP$ $[M^+]$ 461.0996. Found: 461.1000.

2,6-Bis(1'-diphenylphosphinoferrocenyl)pyridine (**4**)

1-Bromo-1'-diphenylphosphinoferrocene (6.4 mmol, 2.89 g) was dissolved in THF (40 mL) and the solution cooled to –70 °C. 1.6 M n-buthyllithium in hexane (6.5 mmol, 4.1 mL) was added by syringe. The mixture was stirred at this temperature for 0.5 h. Solid [$ZnCl_2$(1,4-dioxane)] (7.1 mmol, 1.58 g) was added. After 0.5 h the mixture was allowed to warm to room temperature and stirred further for a 2.5 h. Subsequently 2,6-dibromopyridine (3.1 mmol, 0.73 g) and [$Pd(PPh_3)_4$] (2 mol% per coupling, 0.12 mmol, 133 mg) were added. The resulting mixture was warmed to 60 °C and stirred for 72 h. A small amount of silica gel was added and the reaction mixture was evaporated using a rotary evaporator to afford a pourable solid, which was subjected to CC on silica gel, eluting first with PE / diethyl ether 10:1 to remove non-polar side products and then with DCM (+0.5% of triethylamine) to elute the product. Subsequent evaporation gave **4** · 0.25 CH_2Cl_2 as an orange foamy solid. **Yield**: 0.824 g (33 %). **Crystallisation**: Material suitable for single-crystal X-ray diffraction analysis was obtained in a NMR tube by layering a highly concentrated DCM solution with a small amount of pure DCM and then with hexane under inert gas atmosphere to avoid oxidation. **^{1}H NMR** ($CDCl_3$): 3.94 (s, 4H, Fc), 4.17 (s, 4H, Fc), 4.26 (s, 4H, Fc), 4.88 (s, 4H, Fc), 7.01 (m, 2H, Py),

7.30-7.38 (m, 21H, Ph + Py). **^{13}C NMR** ($CDCl_3$): 68.50 (s), 71.20 (d, J_{PC} = 1 Hz), 73.23 (d, J_{PC} = 4 Hz), 74.28 (d, J_{PC} = 15 Hz), 76.72 (d, J_{PC} = 7 Hz), 85.19 (s), 117.04 (s), 128.28 (d, J_{PC} = 7 Hz), 128.61 (s), 133.63 (d, J_{PC} = 20 Hz), 135.93 (s), 139.15 (d, J_{PC} = 10 Hz), 157.60 (s). **^{31}P NMR** ($CDCl_3$): –17.7 (s). **MS/MALDI(+)** (m/z (%)): 815 (100) $[M]^+$. **Elemental analysis** (%) calculated for $C_{49}H_{39}Fe_2NP_2 \cdot 0.25\,CH_2Cl_2$ (836.7): C 70.70, H 4.76, N 1.67. Found: C 70.85, H 4.78, N 1.64.

6.2.2.2 Group 12 Metal Complexes

General Procedure

Solid metal halide MX_2 (M = Zn, Cd, Hg and X = Cl, Br, I) (0.1 mmol) was added to a solution of one (0.1 mmol) or two equivalents (0.2 mmol) of the ligand in ethanol (10 mL). The mixture was stirred at room temperature for 14 h in a 50 mL Schlenk flask. If precipitation of the product occurred, the solvent volume was reduced in vacuum to less than half. If no precipitation occurred the solvent was removed in vacuum, the residue was dissolved in DCM and hexane was added to precipitate the product. In either case the suspension was filtered and the solid residue was washed with diethyl ether (2 mL) and subsequently with hexane (5 mL). Finally, drying under reduced pressure afforded the respective product. Diffusion Experiments to obtain crystals directly from the reaction were carried out usually in an NMR tube with 0.05 mmol substance in 0.5 mL of respective solvent. Potential deviations are given in the detailed description.

[$ZnCl_2$(1)] (**5a**)

Reactants: **1** (0.1 mmol, 44.7 mg), $ZnCl_2$ (0.1 mmol, 13.6 mg). **Work-up**: The solvent was evaporated in vacuum and the residue dissolved in DCM (2 mL). **5a** was precipitated with hexane (25 mL). **Yield**: 55 mg (95 %). **Crystallisation**: Crystals suitable for single-crystal X-ray diffraction analysis were obtained by layering a DCM solution of **1** with a solution of $ZnCl_2$ in diethyl ether. **^{1}H NMR** ($CDCl_3$): 4.30 (m, 4H, Fc), 4.58 (m, 2H, Fc), 5.19 (m, 2H, Fc), 7.42 (m, 8H, Ph + Py), 7.76 (m, 5H, Ph + Py), 9.57 (m, 1H, Py). **^{13}C NMR** ($CDCl_3$): 71.41 (s), 71.59 (s), 73.39 (d, J_{PC} = 6 Hz), 75.63 (d, J_{PC} = 10 Hz),

84.34 (s), 123.10 (s), 125.22 (s), 128.98 (d, J_{PC} = 10 Hz), 131.22 (s), 133.79 (d, J_{PC} = 13 Hz), 139.32 (s), 152.78 (s), 158.46 (s). **^{31}P NMR** ($CDCl_3$): –14.0 (s). **MS/ESI(+)** (m/z (%)): 605 (10) $[M + Na]^+$, 546 (20) $[M - Cl]^+$, 510 (35) $[C_{27}H_{22}FeNPZn]^+$, 464 (30) $[C_{27}H_{22}FeNPO]^+$, 448 (100) $[C_{27}H_{22}FeNP]^+$. **Elemental analysis** (%) calculated for $C_{27}H_{22}Cl_2FeNPZn$ (583.6): C 55.57, H 3.80, N 2.40. Found: C 56.27, H 3.84, N 2.57.

$[ZnBr_2(1)]$ (**5b**)

Reactants: **1** (0.1 mmol, 44.7 mg), $ZnBr_2$ (0.1 mmol, 22.5 mg). **Work-up**: The solvent was evaporated in vacuum and the residue dissolved in DCM (2 mL). **5a** · 0.25 C_6H_{14} was obtained by adding hexane (15 mL), filtering off, washing and drying in vacuum. **Yield**: 41 mg (61 %). **Crystallisation**: Single-crystals suitable for X-ray diffraction analysis were obtained analogue to the procedure for **5a**. **^{1}H NMR** ($CDCl_3$): 4.23 (m, 2H, Fc), 4.54 (m, 2H, Fc), 4.60 (m, 2H, Fc), 5.02 (m, 2H, Fc), 7.43 (m, 8H, Ph + Py), 7.78 (m, 5H, Ph + Py), 9.57 (m, 1H, Py). **^{13}C NMR** ($CDCl_3$): 71.32 (s), 71.40 (s), 73.69 (br d, $J_{PC} \approx$ 5 Hz), 75.97 (d, J_{PC} = 12 Hz), 84.75 (s), 123.12 (s), 125.10 (s), 128.96 (d, J_{PC} = 10 Hz), 131.22 (s), 133.82 (d, J_{PC} = 12 Hz), 139.29 (s), 153.46 (s), 157.93 (s). **^{31}P NMR** ($CDCl_3$): –14.4 (s). **MS/ESI(+)** (m/z (%)): 592 (15) $[M - Br]^+$, 510 (15) $[C_{27}H_{22}FeNPZn]^+$, 464 (22) $[C_{27}H_{22}FeNPO]^+$, 448 (100) $[C_{27}H_{22}FeNP]^+$. **Elemental analysis** (%) calculated for $C_{27}H_{22}Br_2FeNPZn$ · 0.25 C_6H_{14}(694.0): C 49.32, H 3.70, N 2.02. Found: C 49.73, H 3.73, N 2.16.

$[ZnI_2(1)]$ (**5c**)

Reactants: **1** (0.1 mmol 44.7 mg), ZnI_2 (0.1 mmol, 31.9 mg). **Work-up**: The solvent volume was reduced to more than half. The product was precipitated by the addition of hexane (10 mL). **Yield**: Yield: 49 mg (65 %). **^{1}H NMR** ($CDCl_3$): 4.18 (m, 2H, Fc), 4.60 (m, 2H, Fc), 4.69 (m, 2H, Fc), 4.94 (m, 2H, Fc), 7.38 (m, 1H, Py), 7.41-7.52 (m, 7H, Ph + Py), 7.74-7.83 (m, 5H, Ph + Py), 9.60 (m, 1H, Py). **^{13}C NMR** ($CDCl_3$): 70.95 (s), 71.34 (s), 73.79 (d, J_{PC} = 10 Hz), 76.14 (d, J_{PC} = 12 Hz), 77.36 (s), 84.88 (s), 122.87 (s), 124.67 (s), 128.91 (d, J_{PC} = 10 Hz), 130.60 (d, J_{PC} = 39 Hz), 131.18

(s), 134.01 (d, J_{PC} = 11 Hz), 139.26 (s), 153.95 (s), 157.45 (s). **^{31}P NMR** ($CDCl_3$): –19.2 (s). **MS/ESI(+)** (m/z (%)): 767 (7) $[M]^+$, 510 (33) $[C_{27}H_{22}FeNPZn]^+$, 447 (100) $[C_{27}H_{22}FeNP]^+$. **Elemental analysis** (%) calculated for $C_{27}H_{22}FeI_2NPZn$ (766.5): C 42.31, H 2.89, N 1.83. Found: C 42.29, H 3.12, N 1.80.

[$CdCl_2$(1)] (**6a**)

Reactants: **1** (0.1 mmol, 44.7 mg), $CdCl_2$ (0.1 mmol, 18.3 mg). **Work-up**: The formed precipitate was filtered off, washed and dried. **Yield**: 14 mg (22 %). **^{1}H NMR** ($CDCl_3$): 4.12 (s, 2H, Fc), 4.27 (s, 2H, Fc), 4.43 (s, 2H, Fc), 5.04 (s, 2H, Fc), 7.25 (m, 1H, Py), 7.37 (m, 1H, Py), 7.41 (m, 6H, Ph), 7.59 (m, 4H, Ph), 7.65 (m, 1H, Py), 8.99 (br s, 1H, Py). **^{13}C NMR** ($CDCl_3$): 68.28 (s), 71.56 (s), 73.23 (d, J_{PC} = 6 Hz), 75.15 (d, J_{PC} = 13 Hz), 77.36 (s), 84.73 (s), 122.82 (s), 128.93 (s), 129.18 (d, J_{PC} = 10 Hz), 130.03 (s), 131.22 (s), 133.77 (d, J_{PC} = 14 Hz), 138.69 (s), 152.03 (s), 158.26 (s), 167.90 (s). **^{31}P NMR** ($CDCl_3$): –8.0 (br s). **Elemental analysis** (%) calculated for $C_{27}H_{22}CdCl_2FeNP$ (630.6): C 51.43, H 3.52, N 2.22. Found: C 52.44, H 3.52, N 2.33.

[$CdBr_2$(1)] (**6b**)

Reactants: **1** (0.1 mmol, 44.7 mg), $CdBr_2 \cdot 4\,H_2O$ (0.1 mmol, 34.4 mg). **Work-up**: The yellow-orange precipitate was filtered off, washed and dried. **Yield**: 43 mg (60 %). **Crystallisation**: Single-crystals suitable for X-ray diffraction analysis were obtained by slow evaporation of a DCM solution of the crude product. **^{1}H NMR** ($CDCl_3$): 4.21 (m, 2H, Fc), 4.27 (m, 2H, Fc), 4.60 (m, 2H, Fc), 5.19 (m, 2H, Fc), 7.38 (m, 1H, Py), 7.44-7.52 (m, 7H, Ph + Py), 7.72 (m, 1H, Py), 7.75 (m, 4H, Ph), 9.35 (m, 1H, Py). **^{13}C NMR** ($CDCl_3$): 71.05 (s), 71.44 (s), 73.44 (d, J_{PC} = 7 Hz), 75.62 (d, J_{PC} = 13 Hz), 77.36 (s), 85.06 (s), 123.19 (s), 124.48 (s), 129.22 (d, J_{PC} = 10 Hz), 129.42 (s), 131.58 (d, J_{PC} = 2 Hz), 133.80 (d, J_{PC} = 13 Hz), 139.12 (s), 152.87 (s), 157.88 (s). **^{31}P NMR** ($CDCl_3$): –3.6 ($J_{^{111}CdP}$ = 1708 Hz, $J_{^{113}CdP}$ = 1782 Hz). **MS/MALDI(+)** (m/z (%)): 639 (21) $[M - Br]^+$, 446 (100) $[C_{27}H_{22}FeNP]^+$. **Elemental analysis** (%) calculated for $C_{27}H_{22}Br_2CdFeNP$ (719.5): C 45.07, H 3.08, N 1.95. Found: C 45.32, H 3.00, N 2.07.

[CdI_2(1)] (**6c**)

Reactants: **1** (0.1 mmol, 44.7 mg), CdI_2 (0.1 mmol, 36.6 mg). **Work-up**: The solvent volume was reduced in vacuum. The addition of hexane (10 mL) gave **6c** · 0.5 C_6H_{14}. **Yield**: 25 mg (34 %). **Crystallisation**: Single-crystals suitable for X-ray diffraction analysis were obtained by layering a $CDCl_3$ solution of **6c** with hexane. **^{1}H NMR** ($CDCl_3$): 4.21 (m, 2H, Fc), 4.34 (m, 2H, Fc), 4.57 (m, 2H, Fc), 5.06 (m, 2H, Fc), 7.34-7.40 (m, 2H, Py), 7.43-7.52 (m, 6H, Ph), 7.67-7.74 (m, 5H, Ph + Py), 9.27 (m, 1H, Py). **^{13}C NMR** ($CDCl_3$): 70.66 (s), 71.31 (s), 73.55 (d, J_{PC} = 6 Hz), 75.76 (d, J_{PC} = 12 Hz), 77.40 (s), 85.42 (s), 122.88 (s), 123.94 (s), 129.07 (d, J_{PC} = 10 Hz), 131.21 (d, J_{PC} = 44 Hz), 131.23 (s), 133.90 (d, J_{PC} = 13 Hz), 134.18(s), 138.67 (s), 153.08 (s), 157.56 (s). **^{31}P NMR** ($CDCl_3$): –8.9 (bs). **MS/ESI(+)** (m/z (%)): 838 (3) $[M + Na]^+$, 688 (15) $[M – I]^+$, 464 (34) $[C_{27}H_{22}FeNPO]^+$, 448 (100) $[C_{27}H_{22}FeNP]^+$. **Elemental analysis** (%) calculated for $C_{27}H_{22}CdFeI_2NP$ · 0.5 C_6H_{14} (856.6): C 42.07 , H 3.41, N 1.64. Found: C 42.63, H 2.98, N 1.73.

[$CdCl_2$(1)$_2$] (**7**)

Reactants: **1** (0.1 mmol, 44.7 mg), $CdCl_2$ (0.1 mmol, 18.3 mg). **Crystallisation**: Single-crystals suitable for X-ray diffraction analysis were obtained analogue to the procedure in **5a**.

[$HgCl_2$(1)] (**8a**)

Reactants: **1** (0.1 mmol, 44.7 mg), $HgCl_2$ (0.1 mmol, 27.1 mg). **Work-up**: The solvent volume was reduced in vacuum. The precipitate was filtered off, washed and dried in vacuum. **Yield**: 61 mg (84 %). **^{1}H NMR** ($CDCl_3$): 4.25 (s, 2H, Fc), 4.32 (s, 2H, Fc), 4.60 (s, 2H, Fc), 5.19 (s, 2H, Fc), 7.30 (m, 1H, Py), 7.36 (m, 1H, Py), 7.56 (m, 6H, Ph), 7.64 (m, 1H, Py), 7.80 (m, 4H, Ph), 9.36 (m, 1H, Py). **^{13}C NMR** ($CDCl_3$): 71.44 (s), 71.47 (s), 74.08 (d, J_{PC} = 9 Hz), 75.53 (d, J_{PC} = 14 Hz), 77.36 (s), 86.36 (s), 122.91 (s), 123.25 (s), 127.75 (d, J_{PC} = 52 Hz), 129.70 (d, J_{PC} = 11 Hz), 132.69 (d, J_{PC} = 3 Hz), 133.61 (d, J_{PC} = 13 Hz), 137.72 (s), 152.21 (s), 156.97 (s). **^{31}P NMR** ($CDCl_3$): 32.2 ($J_{^{199}HgP}$ = 7470 Hz). **MS/ESI(+)** (m/z (%)): 684 (100) $[M – Cl]^+$, 447 (35) $[C_{27}H_{22}FeNP]^+$.

Elemental analysis (%) calculated for $C_{27}H_{22}Cl_2FeHgNP$ (718.8): C 45.12, H 3.08, N 1.95. Found: C 45.28, H 3.15, N 1.94.

[$HgBr_2$(1)] (**8b**)

Reactants: **1** (0.1 mmol, 44.7 mg), $HgBr_2$ (0.1 mmol, 36.0 mg). **Work-up**: The formed precipitate was filtered off, washed and dried in vacuum. **Yield**: 67 mg (83 %). **Crystallisation**: Layering a solution of **8b** in DCM with a small amount of pure DCM and then with diethyl ether gave single-crystals suitable for X-ray diffraction analysis. **^{1}H NMR** ($CDCl_3$): 4.33 (m, 2H, Fc), 4.38 (m, 2H, Fc), 4.57 (m, 2H, Fc), 5.11 (m, 2H, Fc), 7.24 (m, 1H, Py), 7.30 (m, 1H, Py), 7.52-7.62 (m, 7H, Ph + Py), 7.77 (m, 4H, Ph), 9.15 (m, 1H, Py). **^{13}C NMR** ($CDCl_3$): 70.75 (s), 71.62 (s), 74.47 (d, J_{PC} = 9 Hz), 75.52 (d, J_{PC} = 13 Hz), 86.46 (s), 122.46 (s), 122.54 (s), 129.58 (d, J_{PC} = 9 Hz), 132.49 (d, J_{PC} = 2 Hz), 133.64 (d, J_{PC} = 13 Hz), 137.35 (s), 152.04 (s), 156.84 (s). **^{31}P NMR** ($CDCl_3$): 28.5 ($J_{^{199}HgP}$ = 6359 Hz). **MS/MALDI(+)** (m/z (%)): 728 (80) $[M - Br]^+$, 447 (100) $[C_{27}H_{22}FeNP]^+$. **Elemental analysis** (%) calculated for $C_{27}H_{22}Br_2FeHgNP$ (807.7): C 40.15, H 2.75, N 1.73. Found: C 40.21, H 2.58, N 1.84.

[HgI_2(1)] (**8c**)

Reactants: **1** (0.1 mmol, 44.7 mg), HgI_2 (0.1 mmol, 45.4 mg). **Work-up**: The addition of hexane (10 mL) completed the precipitation. The product was filtered and washed. Subsequent drying under reduced pressure gave **8c** · 0.25 C_6H_{14}. **Yield**: 72 mg (80 %). **Crystallisation**: Single-crystals suitable for X-ray diffraction analysis were obtained from a $CHCl_3$ solution. **^{1}H NMR** ($CDCl_3$): 4.23 (m, 2H, Fc), 4.37 (m, 2H, Fc), 4.44 (m, 2H, Fc), 4.98 (m, 2H, Fc), 7.18 (m, 1H, Py), 7.24 (m, 1H, Py), 7.45-7.55 (m, 6H, Ph), 7.57 (m, 1H, Py), 7.66 (m, 4H, Ph), 8.89 (m, 1H, Py). **^{13}C NMR** ($CDCl_3$): 70.03 (s), 70.30 (s), 71.71 (s), 74.44 (d, J_{PC} = 8 Hz), 75.43 (d, J_{PC} = 13 Hz), 86.39 (s), 121.57 (s), 122.12 (s), 129.5 (d, J_{PC} = 12 Hz), 131.95 (s), 133.68 (d, J_{PC} = 12 Hz), 136.93 (s), 151.72 (s), 156.85 (s). **^{31}P NMR** ($CDCl_3$): 19.74 (br s). **MS/ESI(+)** (m/z (%)): 776 (33) $[M - I]^+$, 448 (100) $[C_{27}H_{22}FeNP]^+$. **Elemental analysis** (%) calculated for $C_{27}H_{22}FeHgI_2NP$ · 0.25 C_6H_{14} (923.2): C 37.08, H 2.78, N 1.52. Found: C 37.65, H

2.61, N 1.62.

[$HgCl_2(1)_2$] (**9a**)

Reactants: **1** (0.1 mmol, 44.7 mg), $HgCl_2$ (0.1 mmol, 27.1 mg). **Crystallisation**: Single-crystals suitable for X-ray diffraction analysis were obtained analogue to the procedure for **5a**.

[$HgBr_2(1)_2$] (**9b**)

Reactants: **1** (0.2 mmol, 89.4 mg), $HgBr_2$ (0.1 mmol, 36.0 mg). **Work-up**: The precipitate was filtered off, washed with ethanol and dried in vacuum. **Yield**: 107 mg (85 %). **Crystallisation**: Layering of a DCM solution of **9b** with a small amount pure DCM and then with diethyl ether gave crystals suitable for X-ray diffraction analysis. **^{1}H NMR** ($CDCl_3$): 4.12 (m, 4H, Fc), 4.19 (m, 4H, Fc), 4.36 (m, 4H, Fc), 4.86 (m, 4H, Fc), 7.05 (m, 2H, Py), 7.15 (m, 2H, Py), 7.36 (m, 8H, Ph + Py), 7.43-7.51 (m, 8H, Ph), 7.35-7.45 (m, 6H, Ph + Py), 7.61 (m, 8H, Ph), 8.48 (m, 2H, Py). **^{13}C NMR** ($CDCl_3$): 69.19 (s), 70.42 (s), 72.94 (s), 74.76 (s), 77.39 (s), 85.41 (s), 120.85 (s), 121.13 (s), 128.99 (s), 131.27 (s), 133.71 (s), 136.29 (s), 149.55 (s), 157.74 (s). **^{31}P NMR** ($CDCl_3$): 14.5 (s). **MS/ESI(+)** (m/z (%)): 448 (100) $[C_{27}H_{22}FeNP]^+$, 728 (19) $[C_{27}H_{22}FeNPHgBr]^+$, 1175 (4) $[M - Br]^+$, 1254 (3) $[M]^+$. **Elemental analysis** (%) calculated for $C_{54}H_{44}Br_2Fe_2HgN_2P_2$ (1254.9): C 51.68, H 3.53, N 2.23. Found: C 51.32, H 3.49, N 2.05.

[$ZnBr_2(2)]_n$ (**10**)

Reactants: **2** (0.1 mmol, 44.7 mg), $ZnBr_2$ (0.1 mmol, 22.5 mg). **Work-up**: After the addition of solid $ZnBr_2$, immediately a yellow-brown solid precipitated. The reaction mixture was stirred for a further 6 h. The solvent volume was reduced in vacuum. Filtration, an ethanol wash and drying under reduced pressure gave **10** as a yellow solid. **Yield**: 42 mg (53 %). **Crystallisation**: Crystals suitable for X-ray diffraction analysis were obtained by layering a DCM solution (0.5 mL) of **2** (0.05 mmol) with a small amount pure ethanol and then with an ethanolic solution (0.5 mL) of $ZnBr_2$ (0.05 mmol)

in an NMR tube. **^{1}H NMR** (DMSO$-$d$_6$): 3.88 (s, 2H, Fc), 4.22 (s, 2H, Fc), 4.28 (s, 2H, Fc), 4.77 (s, 2H, Fc), 7.31 (m, 5H, Ph + Py), 7.34 (m, 6H, Ph), 7.79 (m, 1H, Py), 8.38 (m, 1H, Py), 8.67 (m, 1H, Py). **^{13}C NMR** (DMSO$-$d$_6$): 67.52 (s), 70.55 (s), 72.83 (d, J_{PC} = 4 Hz), 74.02 (d, J_{PC} = 15 Hz), 76.42 (d, J_{PC} = 8 Hz), 81.98 (s), 123.62 (s), 128.34 (d, J_{PC} = 7 Hz), 128.68 (s), 133.04 (d, J_{PC} = 20 Hz), 133.41 (s), 134.40 (s), 138.53 (d, J_{PC} = 10 Hz), 146.78 (s), 146.87 (s). **^{31}P NMR** (DMSO$-$d$_6$): –18.9 (s), 25.3 (s). **MS/MALDI(+)** (m/z (%)): 447 (100) $[C_{27}H_{22}FeNP]^+$.

[CdBr$_2$(2)]$_n$ (**11**)

Reactants: **2** (0.1 mmol, 44.7 mg), $CdBr_2 \cdot 4\,H_2O$ (0.1 mmol, 34.4 mg). **Work-up**: After the addition of $CdBr_2 \cdot 4\,H_2O$, immediately an orange solid precipitated. Over-night stirring, filtration, ethanol wash and drying under reduced pressure gave **11** as a yellow solid. **Yield**: 30 mg (38 %). **^{1}H NMR** (DMSO$-$d$_6$): 3.89 (s, 2H, Fc), 4.22 (s, 2H, Fc), 4.28 (s, 2H, Fc), 4.77 (s, 2H, Fc), 7.29 (m, 5H, Ph + Py), 7.34 (m, 6H, Ph), 7.78 (m, 1H, Py), 8.38 (m, 1H, Py), 8.67 (s, 1H, Py). **^{13}C NMR** (DMSO$-$d$_6$): 67.46 (s), 70.51 (s), 72.80 (d, J_{PC} = 4 Hz), 73.98 (d, J_{PC} = 15 Hz), 76.38 (d, J_{PC} = 8 Hz), 82.03 (s), 123.49 (s), 128.31 (d, J_{PC} = 7 Hz), 128.65 (s), 132.92 (s), 133.18 (d, J_{PC} = 20 Hz), 134.25 (s), 138.49 (s), 146.89 (s), 146.94 (s). **^{31}P NMR** (DMSO$-$d$_6$): –18.8 (s), 25.3 (s). **MS/MALDI(+)** (m/z (%)): 447 (100) $[C_{27}H_{22}FeNP]^+$. **Elemental analysis** (%) calculated for $(C_{27}H_{22}Br_2CdFeNP)_n$ (719.5, n = 1): C 45.07, H 3.08, N 1.95. Found: C 44.77, H 3.02, N 1.88.

[HgBr$_2$(2)]$_n$ (**12**)

Reactants: **2** (0.1 mmol, 44.7 mg) and $HgBr_2$ (0.1 mmol, 36.0 mg). **Work-up**: Immediately after the addition of $HgBr_2$ an orange solid precipitated. Over-night stirring, filtration, ethanol wash and drying under reduced pressure gave **12** as a yellow solid. **Yield**: 55 mg (68 %). **Crystallisation**: Layering a DCM solution (0.5 mL) of **2** (0.05 mmol) with a small amount pure DCM and then with an ethanolic (0.5 mL) solution of $HgBr_2$ (0.05 mmol) gave crystals suitable for X-ray diffraction analysis. **^{1}H NMR** (DMSO$-$d$_6$): 4.41-4.46 (m, 6H, Fc), 4.85 (s, 2H, Fc), 7.53 (m, 5H, Ph + Py), 7.61 (m, 7H, Ph +

Py), 8.36 (m, 1H, Py), 8.57 (m, 1H, Py). **^{13}C NMR** (DMSO$-$d$_6$): 68.11 (s), 71.56 (s), 73.55 (d, J_{PC} = 13 Hz), 74.65 (d, J_{PC} = 7 Hz), 83.48 (s), 123.53 (s), 129.35 (d, J_{PC} = 11 Hz), 130.76 (d, J_{PC} = 10 Hz), 132.28 (s), 133.01 (d, J_{PC} = 13 Hz), 133.15 (s), 146.85 (s), 147.37 (s). **^{31}P NMR** (DMSO$-$d$_6$): 19.3 (br s). **MS/MALDI(+)** (m/z (%)): 808 (8) $[C_{27}H_{22}Br_2FeHgNP]^+$, 728 (29) $[C_{27}H_{22}BrFeHgNP]^+$, 447 (100) $[C_{27}H_{22}FeNP]^+$. **Elemental analysis** (%) calculated for $(C_{27}H_{22}Br_2FeHgNP)_n$ (807.7, n = 1): C 40.15, H 2.75, N 1.73. Found: C 40.15, H 2.72, N 1.79.

[ZnBr$_2$(3)] (**13**)

Reactants: **3** (0.05 mmol, 23.1 mg), ZnBr$_2$ (0.05 mmol, 11.3 mg). **Work-up**: A Solution of ZnBr$_2$ in ethanol (5 mL) was mixed with solution of the ligand in ethanol (5 mL) and stirred for 0.5 h. The solvent was removed under reduced pressure. The residue was dissolved in DCM (1 mL) and dropped into hexane to afford **13** $\cdot$ 0.25 CH_2Cl_2. **Yield**: 30 mg (90 %). **Crystallisation**: Liquid phase diffusion of hexane into a chloroform solution (0.7 mL) of **13** gave crystals suitable for X-ray diffraction analysis. **^{1}H NMR** ($CDCl_3$): 3.85 (br s, 2H), 4.01 (s, 2H), 4.37-4.59 (br m, 6H), (Fc + CH_2Py); 7.39 (m, 5H, Ph + Py), 7.45 (m, 2H, Ph), 7.52 (m, 1H, Py), 7.55-7.82 (br m, 4H, Ph), 7.96 (m, 1H, Py), 9.66 (m, 1H, Py). **^{13}C NMR** ($CDCl_3$): 37.45 (s), 68.96 (s), 69.83 (s), 72.92 (s), 74.24 (s), 77.36 (s), 87.01 (s), 123.58 (s), 127.19 (s), 128.85 (d, J_{PC} = 10 Hz), 130.16 (d, J_{PC} = 40 Hz), 131.06 (s), 133.91 (d, J_{PC} = 12 Hz), 140.56 (s), 150.96 (s), 159.96 (s). **^{31}P NMR** ($CDCl_3$): –18.1 (s). **MS/ESI(+)** (m/z (%)): 524 (100) $[C_{28}H_{24}FeNPZn]^+$. **Elemental analysis** (%) calculated for $C_{28}H_{24}Br_2FeZnNP \cdot 0.25\,CH_2Cl_2$ (707.7): C 47.94, H 3.49, N 1.98. Found: C 47.59, H 3.58, N 1.92.

[ZnBr$_2$(3)]$_n$ (**13a**)

Reactants: **3** (0.1 mmol, 46.1 mg), ZnBr$_2$ (0.1 mmol, 22.5 mg). **Work-up**: The solvent volume was reduced in vacuum to half. To obtain crystals directly from the reaction mixture, it was stored several 72 h. The obtained crystalline material was filtered and dried in vacuum. **Yield**: 42 mg (61 %). **Crystallisation**: The product was suitable for characterisation by X-ray diffraction analysis.

[$CdBr_2$(3)] (**14**)

Reactants: **3** (0.05 mmol, 23.1 mg), $CdBr_2 \cdot 4\,H_2O$ (0.05 mmol, 17.2 mg). **Work-up**: A solution of $CdBr_2 \cdot 4\,H_2O$ was mixed with a solution of the ligand in ethanol (both 10 mL) and stirred for 1 h. The resulting precipitate was isolated by suction, washed with ethanol and dried in vacuum. **Yield**: 34 mg (94 %). **^{1}H NMR** ($CDCl_3$): 3.96 (m, 2H), 4.00 (m, 2H), 4.29 (m, 2H), 4.48 (m, 2H), 4.52 (m, 2H), (Fc + CH_2Py); 7.35 (m, 1H, Py), 7.39 - 7.53 (m, 7H, Ph + Py), 7.62 (m, 4H, Ph), 7.92 (m, 1H, Py), 9.45 (m, 1H, Py). **^{13}C NMR** ($CDCl_3$): 38.35 (s), 68.64 (s), 70.31 (s), 72.93 (d, J_{PC} = 7 Hz), 74.51 (d, J_{PC} = 12 Hz), 77.39 (s), 87.12 (s), 123.61 (s), 126.38 (s), 129.16 (d, J_{PC} = 10 Hz), 131.33 (s), 133.71 (d, J_{PC} = 14 Hz), 140.26 (s), 150.77 (s), 160.50 (s). **^{31}P NMR** ($CDCl_3$): It was not possible to detect the phosphorus signal. **Elemental analysis** (%) calculated for $C_{28}H_{24}Br_2CdFeNP$ (733.5): C 45.85, H 3.30, N 1.91. Found: C 45.68, H 3.27, N 1.85.

[$CdBr_2$(3)]$_n$ (**14a**)

Reactants: **3** (0.05 mmol, 23.1 mg), $CdBr_2 \cdot 4\,H_2O$ (0.05 mmol, 17.2 mg). **Crystallisation**: Crystals were obtained by layering a solution of **3** (0.05 mmol) in DCM (0.5 mL) with pure ethanol and than with an ethanolic solution (0.5 mL) of $CdBr_2 \cdot 4\,H_2O$ (0.05 mmol).

[CdI_2(3)] (**15**)

Reactants: **3** (0.1 mmol, 46.1 mg), $HgBr_2$ (0.1 mmol, 36.0 mg). **Work-up**: The synthesis was performed in analogy to that of **14**. **Yield**: 37.3 mg (90 %). **Crystallisation**: Liquid phase diffusion of hexane into a chloroform solution (0.7 mL) of **15** gave crystals suitable for X-ray diffraction analysis. **^{1}H NMR** ($CDCl_3$): 4.04 (s, 2H), 4.07 (s, 2H), 4.17 (s, 2H), 4.39 (s, 2H), 4.55 (s, 2H), (Fc + CH_2Py); 7.22 (m, 1H, Py), 7.35 (m, 1H, Py), 7.50 (m, 6H, Ph), 7.73 (m, 5H, Ph + Py), 9.23 (m, 1H, Py). **^{13}C NMR** ($CDCl_3$): 37.63 (s), 69.25 (s), 70.64 (s), 73.69 (d, J_{PC} = 8 Hz), 74.65 (d, J_{PC} = 12 Hz), 77.39 (s), 88.49 (s), 122.90 (s), 125.11 (s), 129.48 (d, J_{PC} = 12 Hz), 132.27 (s), 133.56 (d, J_{PC} = 13 Hz), 138.45 (s), 150.16 (s), 159.88 (s). **^{31}P NMR** ($CDCl_3$): 24.3 (s). **Elemental analysis**

(%) calculated for $C_{28}H_{24}CdFeI_2NP$ (827.5): C 40.64, H 2.92, N 1.69. Found: C 40.40, H 2.93, N 1.68.

[$HgBr_2$(3)] (**16**)

Reactants: **3** (0.05 mmol, 23.1 mg), $HgBr_2$ (0.05 mmol, 18.0 mg). **Work-up**: A solution of $HgBr_2$ was mixed with a solution of **3** in ethanol (both 10 mL) and stirred for 1 h. The resulting precipitate was isolated by suction, washed with ethanol and dried in vacuum. **Yield**: 37 mg (91 %). **Crystallisation**: Crystallisation was performed by layering $HgBr_2$ (0.01 mmol) in ethanol (0.1 mL) with the ligand (0.01 mmol) in ethanol (0.1 mL). **^{1}H NMR** ($CDCl_3$): 4.07 (s, 4H), 4.10 (s, 2H), 4.12 (s, 2H), 4.55 (s, 2H), (Fc + CH_2Py); 7.19 (m, 1H, Py), 7.30 (m, 1H, Py), 7.51 (m, 6H, Ph), 7.69-7.72 (m, 5H, Ph + Py), 9.09 (m, 1H, Py). **^{13}C NMR** ($CDCl_3$): 37.65 (s), 69.84 (s), 70.69 (s), 73.84 (d, J_{PC} = 9 Hz), 74.61 (d, J_{PC} = 13 Hz), 77.39 (s), 88.38 (s), 122.73 (s), 124.82 (s), 128.83 (d, J_{PC} = 51 Hz), 129.50 (d, J_{PC} = 12 Hz), 132.31 (d, J_{PC} = 3 Hz), 133.55 (d, J_{PC} = 13 Hz), 138.29 (s), 149.93 (s), 159.92 (s). **^{31}P NMR** ($CDCl_3$): 24.4 ($J_{^{199}HgP}$ = 6321 Hz). **MS/ESI(+)** (m/z (%)): 742 (76) $[C_{28}H_{24}BrFeHgNP]^+$, 462 (100) $[C_{28}H_{24}FeNP]^+$. **Elemental analysis** (%) calculated for $C_{28}H_{24}Br_2FeHgNP$ (821.7): C 40.93, H 2.94, N 1.71. Found: C 40.93, H 2.94, N 1.69.

[($HgBr_2$)$_2$(3)]$_n$ (**17**)

Reactants: **3** (0.1 mmol, 46.1 mg), $HgBr_2$ (0.1 mmol, 36.0 mg). **Crystallisation**: Crystals were obtained in analogy to the procedure for **14a**.

[$HgBr_2$(3)$_2$] (**18**)

Reactants: **3** (0.2 mmol, 92.3 mg), $HgBr_2$ (0.1 mmol, 36.0 mg). **Work-up**: Immediately after the addition of the metal salt a yellow solid precipitated. The Reaction mixture was stirred 14 h. The precipitate was filtered, washed with ethanol (10 mL) and diethyl ether (20 mL) and dried in a stream of nitrogen and under vacuum. **Yield**: 71.1 mg (55 %). **Crystallisation**: Layering a solution of **9b** in chloroform (0.7 mL) with hexane

gave single-crystals suitable for X-ray diffraction analysis. **^{1}H NMR** ($CDCl_3$): 3.48 (s, 4H, CH_2Py), 3.92 (s, 4H, Fc), 4.06 (s, 4H, Fc), 4.19 (s, 4H, Fc), 4.30 (s, 4H, Fc), 7.04 (m, 4H, Py), 7.36 (m, 8H, Ph), 7.44 (m, 4H, Ph), 7.51 (m, 2H, Py), 7.66 (m, 8H, Ph), 8.44 (s, 2H, Py). **^{13}C NMR** ($CDCl_3$): 37.98 (s), 70.53 (s), 70.99 (s), 73.31 (s), 74.44 (s), 77.36 (s), 88.12 (s), 121.34 (s), 122.99 (s), 128.93 (s), 131.23 (s), 133.75 (s), 136.67 (s), 148.92 (s), 160.79 (s). **^{31}P NMR** ($CDCl_3$): 15.4 (s). **MS/APCI(+)** (m/z (%)): 1283 (3) $[M]^+$, 1202 (5) $[M - Br]^+$, 741 (46) $[C_{28}H_{24}BrFeHgNP]^+$, 462 (100) $[C_{28}H_{24}FeNP]^+$. **Elemental analysis** (%) calculated for $C_{56}H_{48}Br_2Fe_2HgN_2P_2$ (1283.0): C 52.42, H 3.77, N 2.18. Found: C 52.68, H 3.25, N 2.19.

6.2.2.3 Gold and Silver Complexes

[Ag(1)][BF_4] (**19**)

1 (0.1 mmol, 44.7 mg) was dissolved in methanol (4 mL). Solid $AgBF_4$ (0.1 mmol, 19.5 mg) was added. The reaction mixture was stirred in the dark at room temperature for 5 h. The solvent was removed in vacuum. The residue was dissolved in DCM (2 mL). A tan yellow product was recovered by the addition of hexane (15 mL). Filtration and washing with diethyl ether and hexane (both 3 mL) gave **19**, which was finally dried in vacuum. **Yield**: 54.8 mg (85 %). **Crystallisation**: Recrystallisation from a highly concentrated $CHCl_3$ solution gave suitable crystals for characterisation by X-ray diffraction analysis. **^{1}H NMR** ($CDCl_3$): 4.16 (s, 2H, Fc), 4.34 (s, 2H, Fc), 4.55 (s, 2H, Fc), 4.90 (s, 2H, Fc), 7.37 (m, 1H, Py), 7.47 (m, 7H, Ph + Py), 7.61 (m, 4H, Ph), 7.75 (m, 1H, Py), 8.87 (s, 1H, Py). **^{13}C NMR** ($CDCl_3$): Due to the poor solubility ^{13}C NMR characterisation met with limited success, despite prolonged recording. **^{31}P NMR** ($CDCl_3$): 6.8 (br d, $J_{^{107}AgP,^{109}AgP} \approx 712$ Hz). **MS/ESI(+)** (m/z (%)): 556 (100) $[C_{27}H_{22}AgFeNP]^+$. **MS/ESI(-)** (m/z (%)): 87 (100) $[BF_4]^-$. **Elemental analysis** (%) calculated for $C_{27}H_{22}AgBF_4FeNP$ (641.9): C 50.52, H 3.45, N 2.18. Found: C 50.50, H 3.66, N 2.17.

[Ag(2)][BF_4] (**20**)

2 (0.1 mmol, 44.7 mg) was dissolved in methanol (4 mL). Solid $AgBF_4$ (0.1 mmol, 19.5

mg) was added. After 14 h of stirring in the dark at room temperature, an orange solid precipitated, which was filtered, rinsed with methanol (1 mL), washed with small amounts of diethyl ether and hexane and dried in vacuum. **Yield**: 41.9 mg (65 %). **Crystallisation**: Single-crystals suitable for X-ray diffraction analysis were obtained by layering a chloroform solution (0.7 mL) with a small amount of chloroform and then with hexane. **^{1}H NMR** ($CDCl_3$): 4.05 (s, 2H, Fc), 4.17 (s, 2H, Fc), 4.75 (s, 2H, Fc), 4.87 (s, 2H, Fc), 7.43 (m, 6H, Ph), 7.60 (m, 4H, Ph), 7.66 (s, 1H, Py), 7.92 (s, 1H, Py), 8.08 (s, 1H, Py), 9.00 (br s, 1H, Py). **^{13}C NMR** ($CDCl_3$): Due to the poor solubility ^{13}C NMR characterisation met with limited success, despite prolonged recording. **^{31}P NMR** ($CDCl_3$): 11.1 (br d, $J_{^{107}AgP,^{109}AgP} \approx 691$ Hz). **MS/ESI(+)** (m/z (%)): 556 (100) $[C_{27}H_{22}AgFeNP]^+$, 697 (40) $[C_{37}H_{30}AgFeN_2P]^+$. **MS/ESI(-)** (m/z (%)): 87 (100) $[BF_4]^-$. **Elemental analysis** (%) calculated for $C_{54}H_{44}Ag_2B_2F_8Fe_2N_2P_2$ (1283.9): C 50.52, H 3.45, N 2.18. Found: C 50.49, H 3.46, N 2.30.

[Ag(3)][BF_4] (**21**)

Solid $AgBF_4$ (0.1 mmol, 19.5 mg) and **3** (0.1 mmol, 46.2 mg) were dissolved in methanol (5 mL) and stirred in the dark for 3 h. Then hexane (10 mL) was added and the precipitate was collected by suction and washing. Drying in vacuum gave **21** $\cdot$ 0.5 C_6H_{14}. **Yield**: 58.0 mg (89 %). **Crystallisation**: Single-crystals suitable for X-ray diffraction analysis were obtained by layering a chloroform solution (0.7 mL) with a small amount of chloroform and then with hexane. **^{1}H NMR** ($CDCl_3$): 3.93 (s, 2H), 4.06 (s, 2H), 4.13 (s, 2H), 4.23 (s, 2H), 4.54 (s, 2H), (Fc + CH_2Py); 7.30 (m, 1H, Py), 7.39-7.44 (m, 7H, Ph + Py), 7.50 (m, 4H, Ph), 7.79 (m, 1H, Py), 8.77 (s, 1H, Py). **^{13}C NMR** ($CDCl_3$): Due to the poor solubility ^{13}C NMR characterisation met with limited success, despite prolonged recording. **^{31}P NMR** ($CDCl_3$): 7.1 (br d, $J_{^{107}AgP,^{109}AgP} \approx 702$ Hz). **MS/ESI(+)** (m/z (%)): 558 (100) $[C_{28}H_{24}AgFeNP]^+$, 461 (45) $[C_{28}H_{24}FeNP]^+$. **Elemental analysis** (%) calculated for $C_{28}H_{24}AgBF_4FeNP \cdot 0.5\,C_6H_{14}$(698.1): C 53.34, H 4.33, N 2.01. Found: C 53.38, H 4.25, N 2.25.

[AuCl(1)] (**22**)

1 (0.1 mmol, 44.7 mg) was added to a solution of [AuCl(tht)] (0.1 mmol, 32.06 mg) in DCM (5 mL). The mixture was stirred at room temperature for 3 h. The solvent volume was reduced to half. Hexane (25 mL) was added to precipitate the product. The solid residue was filtered off, washed with diethyl ether and hexane (both 2 mL) and dried under reduced pressure. **Yield**: 26.0 mg (38 %). **Crystallisation**: Crystalline material was obtained by recrystallisation from diethyl ether. **^{1}H NMR** ($CDCl_3$): 4.18 (s, 2H, Fc), 4.35 (s, 2H, Fc), 4.44 (s, 2H, Fc), 5.00 (s, 2H, Fc), 7.09 (m, 1H, Py), 7.39 (m, 1H, Py), 7.44 (m, 4H, Ph), 7.49 (m, 1H, Py), 7.57 (m, 6H, Ph), 8.48 (m, 1H, Py). **^{13}C NMR** ($CDCl_3$): 69.25 (s), 70.05 (d, J_{PC} = 74 Hz), 72.28 (s), 74.78 (d, J_{PC} = 9 Hz), 74.95 (d, J_{PC} = 14 Hz), 85.71 (s), 120.80 (s), 121.45 (s), 129.70 (d, J_{PC} = 12 Hz), 130.64 (s), 131.19 (s), 131.81 (d, J_{PC} = 64 Hz), 133.71 (d, J_{PC} = 14 Hz), 136.79 (s), 149.46 (s), 157.10 (s). **^{31}P NMR** ($CDCl_3$): 27.6 (s). **MS/APCI(+)** (m/z (%)): 679 (5) $[M]^+$, 644 (100) $[M - Cl]^+$. **Elemental analysis** (%) calculated for $C_{27}H_{22}AuClFeNP$ (679.7): C 47.71, H 3.26, N 2.06. Found: C 47.52, H 3.25, N 2.09.

[AuCl(2)] (**23**)

2 (0.1 mmol, 44.7 mg) was added to a solution of [AuCl(tht)] (0.1 mmol, 32.0 mg) in DCM (5 mL). The mixture was stirred at room temperature for 6 h. Hexane (25 mL) was added to precipitate the product. The solid residue was filtered off, washed with diethyl ether and hexane (both 2 mL) and dried under reduced pressure. **Yield**: 33.4 mg (49 %). **Crystallisation**: Single-crystals were obtained by layering a chloroform solution (0.7 mL) of **23** with diethyl ether. **^{1}H NMR** ($CDCl_3$): 4.20 (s, 2H, Fc), 4.42 (s, 2H, Fc), 4.44 (s, 2H, Fc), 4.71 (s, 2H, Fc), 7.20 (s, 1H, Py), 7.44 (m, 4H, Ph), 7.49-7.58 (m, 6H, Ph), 7.65 (m, 1H, Py), 8.42 (s, 1H, Ph), 8.54 (s, 1H, Py). **^{13}C NMR** ($CDCl_3$): 68.34 (s), 70.37 (d, J_{PC} = 73 Hz), 72.03 (s), 74.78 (d, J_{PC} = 9 Hz), 75.06 (d, J_{PC} = 14 Hz), 83.76 (s), 123.77 (s), 129.13 (d, J_{PC} = 12 Hz), 129.31 (d, J_{PC} = 12 Hz), 130.50 (s), 131.02 (s), 131.93 (d, J_{PC} = 3 Hz), 133.59 (s), 133.68 (d, J_{PC} = 14 Hz), 147.29 (s), 147.87 (s). **^{31}P NMR** ($CDCl_3$): 28.26 (s). **MS/ESI(+)** (m/z (%)): 644 (100) $[M - Cl]^+$. **Elemental analysis** (%) calculated for $C_{27}H_{22}AuClFeNP$ (679.7): C 47.71, H 3.26, N

2.06. Found: C 47.43, H 3.27, N 2.15.

[AuCl(3)] (**24**)

3 (0.1 mmol, 46.1 mg) was added to a solution of [AuCl(tht)] (0.1 mmol, 32.0 mg) in DCM (5 mL). The mixture was stirred at room temperature for 6 h. Hexane (25 mL) was added to precipitate the product. The solid residue was filtered off, washed with diethyl ether and hexane (both 2 mL) and dried under reduced pressure. **Yield**: 33.4 mg (49 %). **Crystallisation**: Single-crystals were obtained by layering a DCM solution (0.7 mL) of **24** with hexane. **^{1}H NMR** ($CDCl_3$): 3.67 (s, 2H, Fc), 4.11 (m, 2H, Fc), 4.27 (m, 4H, CH_2Py + Fc), 4.51 (m, 2H, Fc), 7.10 (m, 2H, Py), 7.41-7.52 (m, 6H, Ph), 7.54-7.62 (m, 5H, Ph + Py), 8.47 (m, 1H, Py). **^{13}C NMR** ($CDCl_3$): 38.01 (s), 68.91 (d, J_{PC} = 74 Hz), 70.02 (s), 71.01 (s), 73.54 (d, J_{PC} = 9 Hz), 74.19 (d, J_{PC} = 14 Hz), 88.23 (s), 121.36 (s), 122.78 (s), 128.95 (d, J_{PC} = 12 Hz), 130.98 (d, J_{PC} = 63 Hz), 131.62 (d, J_{PC} = 3 Hz), 133.47 (d, J_{PC} = 14 Hz), 136.58 (s), 149.01 (s), 160.27 (s). **^{31}P NMR** ($CDCl_3$): 29.2(s). **MS/ESI(+)** (m/z (%)): 695 (15) $[M]^+$, 658 (100) $[M - Cl]^+$. **Elemental analysis** (%) calculated for $C_{28}H_{24}AuClFeNP$ (693.7): C 48.48, H 3.49, N 2.02. Found: C 48.39, H 3.53, N 1.84.

$[Au(1)]_2[BF_4]_2$ (**25**)

1 (0.1 mmol, 44.7 mg) was added to a solution of [AuCl(tht)] (0.1 mmol, 32.0 mg) in DCM (5 mL). The mixture was stirred for 1.5 h at room temperature in the dark. Solid $AgBF_4$ (0.11 mmol, 21.34 mg) was added. The mixture was stirred at room temperature for 14 h. DCM (10 mL) was added to dissolve potentially precipitated product. The mixture was filtered and the filter cake was washed with DCM (5 mL). The filtrate was evaporated in vacuum and mixed with 10 mL diethyl ether to precipitate the product as an orange micro-crystalline powder. The product was filtered, washed with diethyl ether (2 mL) and dried in vacuum. **Yield**: 28.3 mg (39 %). **Crystallisation**: Crystalline material was obtained from a hot cloroform solution. **NMR**: Due to the poor solubility NMR characterisation met with limited success. **MS/ESI(+)** (m/z (%)): 1091 (85) $[M - Au]^+$, 644 (100) $[C_{27}H_{22}AuFeNP]^+$. **Elemental analysis** (%) calculated for

$C_{54}H_{44}Au_2B_2F_8Fe_2N_2P_2$ (1462.1): C 44.36, H 3.03, N 1.92. Found: C 44.76, H 3.07, N 2.01.

[Au(2)]$_n$[BF$_4$]$_n$ (**26**)

2 (0.1 mmol, 44.7 mg) was added to a solution of [AuCl(tht)] (0.1 mmol, 32.0 mg) in DCM (5 mL). The mixture was stirred for 3 h at room temperature in the dark. Solid $AgBF_4$ (0.11 mmol, 21.34 mg) and DCM (5 mL) were added . The mixture was stirred at room temperature for 14 h. The mixture was filtered and the filter cake was washed with DCM (5 mL). The filtrate was concentrated in vacuum and mixed with hexane (10 mL) to precipitate the product. Filtration, washing with diethyl ether (2 mL)and hexane (2 mL) and drying in vacuum afforded **26** · 0.5 CH_2Cl_2. **Yield**: 54.8 mg (75 %). **NMR**: Due to the poor solubility NMR characterisation met with limited success. **Elemental analysis** (%) calculated for $(C_{27}H_{22}AuBF_4FeNP)_n \cdot 0.5n\,CH_2Cl_2$ (773.5, n = 1): C 42.07, H 3.00, N 1.81. Found: C 42.84, H 2.98, N 1.94. **MS/ESI(+)** (m/z (%)): 644 (100) $[C_{27}H_{22}AuFeNP]^+$.

[Au(3)]$_n$[BF$_4$]$_n$ (**27**)

3 (0.1 mmol, 46.1 mg) was added to a solution of [AuCl(tht)] (0.1 mmol, 32.0 mg) in DCM (5 mL). The mixture was stirred for 1.5 h at room temperature. Solid $AgBF_4$ (0.11 mmol, 21.34 mg) in THF (1 mL) was added and stirred for 1 h. Then precipitate was filtered. The filter cake was washed with DCM (5 mL). The filtrate was highly concentrated in vacuum and mixed with hexane (10 mL) to precipitate the product. **27** · 2 CH_2Cl_2 was filtered, washed with diethyl ether (2 mL) and hexane (2 mL) and dried in vacuum. **Yield**: 8.7 mg (27 %). **NMR**: Due to the poor solubility NMR characterisation met with limited success. **Elemental analysis** (%) calculated for $(C_{28}H_{24}AuBF_4FeNP)_n \cdot 2n\,CH_2Cl_2$ (915.0, n = 1): C 39.38, H 3.08, N 1.53 . Found: C 40.34, H 3.26, N 1.61.

6.2.2.4 Palladium Complexes

The synthesis of compounds **29, 31, 33, 35** was carried out by the group members of Prof. Petr Štěpnička at Charles University, Prague. All analytical, X-ray crystallographic and catalytic data of the palladium complexes were collected in the laboratories of the cooperation partners in the Czech Republic.

[$PdCl_2$(1)] (**28**)
[$PdCl_2$(cod)] (0.1 mmol, 28.5 mg) and **1** (0.1 mmol, 44.5 mg) were mixed with DCM (2 mL). The mixture was stirred at room temperature for 3 h, during which the product separated as an orange solid. Pentane (2 mL) was added and the product was filtered off, washed with diethyl ether and pentane and dried under vacuum to give **28** · 0.2 CH_2Cl_2 as an orange solid. **Yield**: 60 mg (96 %). **Crystallisation**: Single crystals were obtained from a solution of DCM layered with ethanol. **^{1}H NMR** (CD_2Cl_2): 4.63 (dq, J = 1.2, 1.2 Hz, 1H, Fc), 4.76 (dt, J = 1.3, 2.6 Hz, 1H, Fc), 4.77 (dt, J = 1.3, 2.6 Hz, 1H, Fc), 4.85 (dt, J = 1.3, 2.6 Hz, 1H, Fc), 4.89 (m, 2H, Fc), 5.81 (m, 1H, Fc), 6.64 (dq, J = 1.3, 1.3 Hz, 1H, Fc), 6.67 (ddd, J = 7.5, 5.9, 1,6 Hz, 1H, Py), 6.95-7.75 (m, 12H, Ph + Py), 8.55 (dm, J = 5.9 Hz, 1H, Py). **^{13}C NMR** (CD_2Cl_2): 64.84 (d, J_{PC} = 61 Hz), 70.47 (s), 73.25 (s), 73.83 (d, J_{PC} = 3 Hz), 73.96 (d, J_{PC} = 6 Hz), 74.46 (s), 75.01 (d, J_{PC} = 11 Hz), 79.07 (d, J_{PC} = 21 Hz), 91.06 (d, J_{PC} = 2 Hz), 123.69 (s), 128.26 (d, J_{PC} = 12 Hz), 128.81 (s), 128.83 (d, J_{PC} = 10 Hz), 128.28 (s), 129.44 (d, J_{PC} = 59 Hz), 130.49 (d, J_{PC} = 9 Hz), 130.94 (d, J_{PC} = 9 Hz), 131.55 (d, J_{PC} = 3 Hz), 134.44 (d, J_{PC} = 10 Hz), 137.68 (s), 153.92 (s), 157.51 (s). **^{31}P NMR** (CD_2Cl_2): 16.4 (s). **MS/ESI(+)** (m/z): 587 $[M - Cl]^+$, 552 $[M - Cl - HCl]^+$. **Elemental analysis** (%) calculated for $C_{27}H_{22}Cl_2FeNPPd$ · 0.2 CH_2Cl_2 (641.6): C 50.92, H 3.52, N 2.18. Found: C 51.06, H 3.48, N 2.18.

[$PdCl_2$(3)] (**29**)
A solution of **3** (0.2 mmol, 93 mg) and [$PdCl_2$(cod)] (0.2 mmol, 57 mg) in DCM (5 mL) was stirred at room temperature for 1.5 h and then filtered through a PTFE syringe

filter (0.45 μm pore size). The filtrate was diluted with DCM (5 mL), layered with diethyl ether (8 mL) and the mixture was allowed to crystallise at room temperature for several days. The separated product was filtered off, washed with pentane and dried under vacuum. Evaporation of the mother liquor followed by crystallisation (DCM (3 mL) + diethyl ether:pentane 1:1 (8 mL) and isolation as above afforded a second crop of the product. **Combined yield** of **29** · 0.5 CH_2Cl_2: 120 mg (88 %). **^{1}H NMR** (CD_2Cl_2): 2.32 (br s, 1H, Fc), 3.64 (br s, 1H, Fc), 4.04 (dt, J = 2.6, 1.3 Hz, 1H, Fc), 4.08 (d, $^2J_{HH}$ = 14.8 Hz, 1H, CH_2Py), 4.24 (dt, J = 1.4, 2.6 Hz, 1H, Fc), 4.27-4.31 (m, 2H, Fc), 4.36 (br m, 1H, Fc), 5.03 (dt, J = 2.4, 1.4 Hz, 1H, Fc), 5.42 (d, $^2J_{HH}$ = 14.8 Hz, 1H, CH_2Py), 7.10 (ddd, $J \approx$ 7.3, 5.7, 1.5 Hz, 1H, Py), 7.38-7.82 (partly broad m, 11H, Ph + Py), 7.87 (td, J = 7.7, 1.6 Hz, 1H, Py), 8.32 (d of unresolved t, J = 5.9 Hz, 1H, Py). **^{13}C NMR** (CD_2Cl_2): 39.14 (s), 69.31 (d, J_{PC} = 61 Hz), 69.31 (s), 70.01 (s), 70.03 (s), 72.22 (d, J_{PC} = 7 Hz), 73.30 (d, J_{PC} = 12 Hz), 74.41 (d, J_{PC} = 8 Hz), 74.87 (br s), 75.66 (d, J_{PC} = 8 Hz), 87.35 (s), 123.70 (s), 127.64 (s), 128.09 (d, J_{PC} = 12 Hz), 129.46 (d, J_{PC} = 49 Hz), 129.48 (11), 129.67 (d, J_{PC} = 64 Hz), 131.42 (d, J_{PC} = 3 Hz), 132.01 (d, J_{PC} = 2 Hz), 134.03 (br d, $J_{PC} \approx$ 11 Hz), 134.21 (br d, $J_{PC} \approx$ 9 Hz), 139.29 (s), 151.96 (d, $J \approx$ 1 Hz), 163.39 (s). **^{31}P NMR** (CD_2Cl_2): 22.2 (s). **MS/ESI(+)** (m/z): 602 $[M - Cl]^+$, 566 $[M - Cl - HCl]^+$. **MS/ESI(-)** (m/z): 674 $[M + Cl]^-$ **Elemental analysis** (%) calculated for $C_{28}H_{24}Cl_2FeNPPd$ · 0.5 CH_2Cl_2 (681.1): C 50.16, H 3.79, N 1.78. Found: C 50.26, H 3.70, N 2.06.

[$PdCl_2(1)_2$] (**30**)

[$PdCl_2$(cod)] (0.1 mmol, 28.5 mg) and **1** (0.21 mmol, 89.5 mg) were mixed with DCM (2 mL). The resulting mixture was stirred at room temperature for 3 h to give red precipitate. Pentane (2 mL) was added to ensure complete precipitation. The separated solid was filtered off, washed successively with diethyl ether and pentane and dried under vacuum to afford **30** · 0.2 CH_2Cl_2 as a red solid. **Yield**: 101 mg, 94 %. **Crystallisation**: Crystalline material resulted when the initially separated product was dissolved by addition of more DCM. The resulting solution was layered with diethyl ether and allowed to crystallise by liquid-phase diffusion. Because the isolated (crystallised) complex is

only poorly soluble in DCM, the NMR spectra were recorded for *in situ* generated **30**. The NMR spectra indicated that **30** is formed cleanly, the liberated cycloocta-1,5-diene and a tiny amount of **28** being the only side products. **^{1}H NMR** (CD_2Cl_2): 4.18 (vt, $J' \approx$ 1.9 Hz, 2H, Fc), 4.53 (br m, 2H, Fc), 4.84 (vt, $J' \approx$ 1.9 Hz, 2H, Fc), 5.10 (vt, $J' \approx$ 1.9 Hz, 2H, Fc), 7.10 (ddd, J = 7.4, 4.9, 1.1 Hz, 1H, Py), 7.36-7.50 (m, 7H, Ph + Py), 7.57 (td, J = 7.8, 2.0 Hz, 1H, Py), 7.62-7.69 (m, 4H, Ph), 8.49 (ddd, J = 4.9, 1.8, 0.9 Hz, 1H, Py). **^{13}C NMR** (CD_2Cl_2): 69.30 (s), 74.78 (apparent t, J' = 27 Hz), 73.44 (s), 74.89 (apparent t, J' = 4 Hz), 76.41 (apparent t, J' = 5 Hz), 85.96 (s), 120.79 (s), 121.38 (s), 128.12 (apparent t, J' = 5 Hz), 130.71 (s), 131.72 (apparent t, J' = 25 Hz), 134.58 (apparent t, J' = 5 Hz), 136.38 (s), 149.83 (s), 158.31 (s). **^{31}P NMR** (CD_2Cl_2): 16.2 (s). **MS/ESI(+)** (m/z): 1035 $[M - Cl]^+$, 802 $[M - 2Cl - FeC_5H_4C_5H_4N]^+$, 589 $[M - Cl - \mathbf{1}]^+$. **Elemental analysis** (%) calculated for $C_{54}H_{44}Cl_2Fe_2N_2P_2Pd \cdot 0.2\,CH_2Cl_2$ (1088.8): C 59.78, H 4.11, N 2.57. Found: C 59.50, H 4.13, N 2.52.

$[PdCl_2(3)_2]$ (**31**)

3 (0.2 mmol, 93 mg) and $[PdCl_2(cod)]$ (0.1 mmol, 28.5 mg) were dissolved in DCM (4 mL) to give a deep red solution, which was stirred for 1 h and then filtered through a 0.45 µm PTFE syringe filter. The filtrate was diluted with DCM (1 mL) and layered with diethyl ether (ca. 10 mL). The mixture was left crystallising by liquid-phase diffusion over several days. The separated product was filtered off, washed with pentane and dried under vacuum. Yield of **31** $\cdot$ 0.2 CH_2Cl_2: 87 mg (78 %), well-developed ruby red crystals. The NMR spectra were recorded on a solution of *in situ* generated compound due to its limited solubility. **^{1}H NMR** (CD_2Cl_2): 3.81 (br s, 2H, CH_2Py, Fc), 4.32 (vt, J' = 1.8 Hz, 2H, Fc), 4.36 (unresolved vt, 2H, Fc), 4.51 (br m, 4H, Fc), 7.03-7.11 (m, 2H, Py), 7.31-7.69 (m, 11H, Ph + Py), 8.48 (br d, J = 3.1 Hz, Py). **^{13}C NMR** (CD_2Cl_2): 38.42 (s), 70.55 (s), 71.00 (s), 72.92 (apparent t, J' = 4 Hz), 75.91 (apparent t, J' = 5 Hz), 87.51 (s), 121.20 (s), 122.60 (s), 127.68 (apparent t, J' = 4 Hz), 130.18 (s), 131.41 (apparent t, J' = 25 Hz), 134.15 (apparent t, J' = 6 Hz), 136.38 (s), 149.05 (s), 160.81 (s). **^{31}P NMR** (CD_2Cl_2): 15.9 (s). **MS/ESI(+)** (m/z): 1064 $[M - Cl]^+$, 816 $[M - 2Cl - C_5H_4CH_2N]^+$, 602 $[PdCl(\mathbf{3})]^+$. **Elemental analysis** (%) calculated for

$C_{56}H_{48}Cl_2Fe_2N_2P_2Pd \cdot 0.2\,CH_2Cl_2$ (1116.9): C 60.43, H 4.37, N 2.51. Found: C 60.54, H 4.37, N 2.40.

[PdCl(L^{NC})(1)] (**32**)

[Pd(μ-Cl)(L^{NC})]$_2$ (0.05 mmol, 27.5 mg) and **1** (0.1 mmol, 44.5 mg) were dissolved in DCM (2 mL). The resulting solution was stirred for 2 h and then evaporated to dryness. The residue was washed successively with diethyl ether:pentane (1:1 v/v) and pentane and dried under vacuum to give **32** as an orange solid. **Yield**: 67 mg (87 %). (The compound retains traces of DCM, analysing as **32** $\cdot$ 0.5 CH_2Cl_2). Selected data of **32** **^{1}H NMR** (CD_2Cl_2): 3.93 (d, J = 3.4 Hz, 2H, CH_2Py), 4.09 (m, 2H, Fc), 4.15 (d, J = 2.2 Hz, 2H, NCH_2), 4.36 (m, 2H, Fc), 4.90 (vt, J' = 1.9 Hz, 2H, Fc), 5.07 (vt, J' = 1.9 Hz, 2H, Fc), 8.45 (d of unresolved m, J = 4.2 Hz, 1H, Py). Selected data of **34a** **^{1}H NMR** (CD_2Cl_2): 3.79 (d, J = 14.2 Hz, 1H, CH_2Py), 3.98 (d, J = 14.2 Hz, 1H, CH_2Py), 4.05 (m, 1H, Fc), 4.05 (dd, J = 13.4, ca. 2.5 Hz, 1H, NCH_2), 4.21 (dd, J = 13.4, 2.1 Hz, 1H, NCH2), 4.31 (m, 1H, Fc), 4.36 (m, 1H, Fc), 4.48 (m, 1H, Fc), 4.98 (d of vt, J' = 1.3, 2.6 Hz, 1H, Fc), 5.00 (d of vt, J' = 1.3, 2.6 Hz, 1H, Fc), 5.63 (d of vt, J' = 2.6, 1.3 Hz, 1H, Fc), 6.23 (d of vt, J' = 2.6, 1.3 Hz, 1H, Fc), 8.92 (dd, J = 5.6, 1.1 Hz, 1H, Py). **^{31}P NMR** (CD_2Cl_2): 32.7 (s), 32.9 (s). **MS/ESI(+)** (m/z): 687 [M – Cl]$^+$. **Elemental analysis** (%) calculated for $C_{36}H_{34}ClFeN_2PPd \cdot 0.5\,CH_2Cl_2$ (765.8): C 57.24, H 4.61, N 3.66. Found: C 57.27, H 4.67, N 3.53.

[PdCl(L^{NC})(3)] (**33**)

[Pd(μ-Cl)(L^{NC})]$_2$ (0.05 mmol, 27.5 mg) and **1** (0.1 mmol, 46.5 mg) were dissolved in DCM (3 mL). The solution was stirred for 1 h, filtered (0.45 μm PTFE filter) and evaporated to dryness. The solid residue was washed with diethyl ether and pentane and dried under vacuum to afford **33** as an orange solid. **Yield**: 62 mg (84 %). **^{1}H NMR** (CD_2Cl_2): 2.80 (d, $^4J_{PH}$ = 2.7 Hz, 3H, NMe_2), 3.85 (s, 2H, CH_2Py), 4.11 (d, $^4J_{PH}$ = 2.3 Hz, 2H, NCH_2), 4.33 (br s, 4H, Fc), 4.41 (vt, J' = 1.8 Hz, 2H, Fc), 4.52 (vt, J' = 1.8 Hz, 2H, Fc), 6.31 (ddd, J = 7.7, 6.3, 1.2 Hz, 1H, C_6H_4), 6.39 (td, J = 7.7, ca. 1.3H, 1H, C_6H_4), 6.83 (td, J = 7.3, 1.2 Hz, 1H, C_6H_4), 7.02 (dd, J = 7.4, 1.5 Hz, 1H, C_6H_4),

7.06-7.12 (m, 2H, Py), 7.32-7.62 (m, 11H, Ph + Py), 8.45 (ddd, J = 4.9, 1.8, 0.8 Hz, 1H, Py). **^{13}C NMR** (CD_2Cl_2): 38.68 (s, *C*H_2Py), 50.28 (d, J_{PC} = 2 Hz), 70.99 (s), 71.38 (s), 73.22 (d, J_{PC} = 7 Hz), 73.48 (d, J_{PC} = 59 Hz), 73.86 (d, J_{PC} = 4 Hz), 76.21 (d, J_{PC} = 10 Hz), 88.17 (s), 121.53 (s), 122.80 (s), 122.84 (s), 124.00 (s), 125.04 (d, J_{PC} = 6 Hz), 128.12 (d, J_{PC} = 10 Hz), 130.80 (d, J_{PC} = 2 Hz), 132.55 (d, J_{PC} = 49 Hz), 134.74 (d, J_{PC} = 12 Hz), 136.60 (s), 138.79 (d, J_{PC} = 10 Hz), 149.07 (d, J_{PC} = 2 Hz), 149.43 (s), 152.66 (s), 161.25 (s). **^{31}P NMR** (CD_2Cl_2): 33.1 (s). **MS/ESI(+)** (m/z): 701 $[M - Cl]^+$. **Elemental analysis** (%) calculated for $C_{37}H_{36}ClFeN_2PPd$ (737.3): C 60.27, H 4.92, N 3.80. Found: C 61.10, H 5.15, N 3.48.

[Pd(L^{NC})(1)][CLO_4] (**34**)

[Pd(L^{NC})(MeCN)$_2$][ClO_4] (0.1 mmol, 42 mg) and **1** (0.1 mmol, 44.5 mg) were dissolved in DCM (2 mL) and the mixture was stirred for 2 h. Pentane (2 mL) was added to complete precipitation of the product. The separated solid was filtered off, washed with diethyl ether and pentane and dried under vacuum to give **34** as an orange solid. **Yield**: 67 mg (85 %). **Crystallisation**: Crystalline material resulted when the initially precipitated **35** was dissolved by adding more DCM and the solution allowed to crystallise by liquid-phase diffusion of diethyl ether. **^{1}H NMR** (CD_2Cl_2): 2.03 (d, $^4J_{PH}$ = 3.4 Hz, 3H, NMe), 2.55 (d, $^4J_{PH}$ = 1.8 Hz, 3H, NMe), 3.02 (m, 1H, Fc), 3.61 (dd, $^2J_{HH}$ = 13.4, $^4J_{PH}$ = 3.7 Hz, 1H, NCH_2), 3.72 (m, 1H, Fc), 4.30 (m, 1H, Fc), 4.59 (tdd, J = 2.6, 1.2, 0.4 Hz, 1H, Fc), 4.71 (m, 1H, Fc), 4.82 (d, $^2J_{HH}$ = 13.4 Hz, 1H, NCH_2), 4.90-4.93 (m, 2H, Fc), 6.37-6.46 (m, 2H, C_6H_4), 6.84 (m, 1H, Fc; partly obscured by the neighboring signal), ca. 6.84-6.90 (m, 1H, C_6H_4), 7.07 (d of unresolved m, $J \approx$ 7.4 Hz, 1H, C_6H_4), 7.24-7.69 (m, 9H of Ph + Py), 7.69 (ddd, J = 8.1, 1.4, 0.7 Hz, 1H, Py), 7.89 (ddd, J = 8.1, 7.6, 1.7 Hz, 1H, Py), 7.99-8.06 (m, 2H, Ph), 8.98 (ddd, J = 5.5, 1.6, 0.7 Hz, 1H, Py). **^{13}C NMR** (CD_2Cl_2): 49.39 (d, J_{PC} = 2 Hz), 49.41 (d, J_{PC} = 2 Hz), 70.65 (s), 71.75 (d, J_{PC} = 7 Hz), 72.54 (d, J_{PC} = 60 Hz), 72.63 (s), 73.15 (d, J_{PC} = 3 Hz), 74.24 (s), 76.07 (d, J_{PC} = 8 Hz), 76.17 (d, J_{PC} = 8 Hz), 77.42 (d, J_{PC} = 4 Hz), 78.68 (d, J_{PC} = 12 Hz), 81.37 (s), 123.38 (s), 123.68 (s), 125.09 (s), 125.28 (s), 126.13 (d, J_{PC} = 6 Hz), 128.08 (d, J_{PC} = 46 Hz), 128.65 (br d, $J_{PC} \approx$ 12 Hz), 129.97 (d, J_{PC} = 11 Hz), 130.36 (d, J_{PC} = 56 Hz), 130.90 (d, J_{PC} = 2 Hz), 131.42 (d, J_{PC} = 2 Hz), 136.11 (d, J_{PC} = 14 Hz), 139.80 (d, J_{PC} = 12

Hz), 140.02 (s), 147.56 (d, J_{PC} = 2 Hz), 148.49 (d, J_{PC} = 2 Hz), 150.13 (s), 161.04 (s). **^{31}P NMR** (CD_2Cl_2): 32.6 (s). **MS/ESI(+)** (m/z): 687 [Pd(L^{NC})(**1**)]$^+$. **Elemental analysis** (%) calculated for $C_{36}H_{34}ClFeN_2O_4PPd$ (787.3): C 54.92, H 4.35, N 3.56. Found: C 54.76, H 4.25, N 3.49

[Pd(L^{NC})(3)][CLO_4] (**35**)

[Pd(L^{NC})(MeCN)$_2$][ClO_4] (0.1 mmol, 42 mg) and **3** (0.1 mmol, 44.5 mg) were dissolved in DCM (3 mL). The solution was stirred for 1 h and filtered (0.45 μm PTFE filter). The filtrate was diluted with DCM (3 mL) and overlayered with diethyl ether (12 mL). Crystallisation at room temperature for several days afforded crystalline product, which was filtered off, washed with diethyl ether and dried under vacuum. **Yield**: 74 mg (92 %), rusty brown crystals. **^{1}H NMR** (CD_2Cl_2): 2.25 (d, $^4J_{PH}$ = 3.3 Hz, 3H, NMe), 2.54 (d, $^4J_{PH}$ = 2.1 Hz, 3H, NMe), 2.80 (br s, 1H, CH of Fc), 3.84 (br s, 1H, CH of Fc), 3.98 (dd, $^2J_{HH}$ = 13.4, $^4J_{PH}$ = 3.2 Hz, 1H, NCH_2), 3.98 (dt, J' = 2.7, 1.3 Hz, 1H, Fc), 4.25 (dt, J' = 1.3, 2.4 Hz, 1H, Fc), 4.28 (dt, J = 1.3, 2.6 Hz, 1H, Fc), 4.33 (d, $^2J_{HH}$ = 14.3 Hz, 1H, CH_2Py), 4.37 (m, 1H, Fc), 4.48 (m, 1H, Fc), 4.48 (br d, $^2J_{HH}$ = 13.4 Hz, 1H, NCH_2), 4.63 (dt, J' = 2.4, 1.3 Hz, 1H, Fc), 5.03 (d, $^2J_{HH}$ = 14.3 Hz, 1H, CH_2Py), 6.35-6.43 (m, 2H, C_6H_4), 6.85-6.92 (m, 1H, C_6H_4), 7.06-7.10 (m, 1H, C_6H_4), 7.27-7.63 (m, 9H, Ph + Py), 7.69 (dt, J = 7.9, 1.1 Hz, 1H, Py), 7.77-7.84 (m, 2H, Ph), 8.03 (td, J = 7.8, 1.7 Hz, H^4 of Py), 8.38 (ddd, J = 5.5, 1.6, 0.6 Hz, 1H, Py). **^{13}C NMR** (CD_2Cl_2): 39.28 (s), 50.71 (d, J_{PC} = 2 Hz), 50.32 (d, J_{PC} = 2 Hz), 70.01 (s), 70.32 (s), 70.48 (s), 72.27 (s), 72.46 (d, J_{PC} = 7 Hz), 72.83 (d, J_{PC} = 59 Hz), 72.86 (d, J_{Pc} = 3 Hz), 73.37 (d, J_{Pc} = 10 Hz), 74.62 (d, J_{Pc} = 7 Hz), 75.45 (d, J_{Pc} = 10 Hz), 85.96 (s), 123.51 (s), 125.07 (s), 125.30 (s), 125.69 (d, J_{Pc} = 5 Hz), 127.81 (s), 128.45 (d, J_{Pc} = 12 Hz), 129.48 (d, J_{Pc} = 11 Hz), 130.18 (d, J_{Pc} = 48 Hz), 130.57 (d, J_{Pc} = 56 Hz), 131.50 (d, J_{Pc} = 2 Hz), 131.97 (d, J_{Pc} = 2 Hz), 134.35 (d, J_{Pc} = 12 Hz), 134.88 (d, J_{Pc} = 12 Hz), 139.79 (d, J_{Pc} = 12 Hz), 140.02 (s), 148.32 (d, J_{Pc} = 2 Hz), 148.53 (d, J_{Pc} = 2 Hz), 150.18 (s), 160.98 (s). **^{31}P NMR** (CD_2Cl_2): 34.3 (s). **MS/ESI(+)** (m/z): 701 [Pd(L^{NC})(**3**)]$^+$. **Elemental analysis** (%) calculated for $C_{37}H_{36}ClFeN_2O_4PPd$ (801.3): C 55.45, H 4.53, N 3.50. Found: C 55.15, H 4.63, N 3.38.

7 References

[1] I. R. Butler, *Organometallics* **1992**, *11*, 74.

[2] S. Maggini, *Coord. Chem. Rev.* **2009**, *253*, 1793.

[3] G. R. Newkome, *Chem. Rev.* **1993**, *93*, 2067.

[4] G. Chelucci, G. Orrù, G. A. Pinna, *Tetrahedron* **2003**, *59*, 9471.

[5] R. G. Pearson, *J. Am. Chem. Soc.* **1963**, *85*, 3533.

[6] A. Bader, E. Lindner, *Coord. Chem. Rev.* **1991**, *108*, 27.

[7] P. Braunstein, F. Naud, *Angew. Chem. Int. Ed.* **2001**, *40*, 680.

[8] K.-J. Wei, J. Ni, Y. Liu, *Inorg. Chem.* **2010**, *49*, 1834.

[9] J. C. Jeffrey, T. B. Rauchfuss, *Inorg. Chem.* **1979**, *18*, 2658.

[10] T. B. Rauchfuss, F. T. Patino, D. M. Roundhill, *Inorg. Chem.* **1975**, *4*, 652.

[11] A. Togni, T. Hayashi, Eds., *Ferrocenes: Homogeneous Catalysis, Organic Synthesis, Materials Science*, 1. ed., VCH, Weinheim, **1995**.

[12] A. Togni, N. Bieler, U. Burckhardt, C. Köllner, G. Pioda, R. Schneider, *Pure Appl. Chem.* **1999**, *71*, 1531.

[13] T. J. Colacot, *Chem. Rev.* **2003**, *103*, 3101.

[14] L.-X. Dai, T. Tu, S.-L. You, W.-P. Deng, X.-L. Hou, *Acc. Chem. Res.* **2003**, *36*, 659.

[15] P. Barbaro, C. Bianchini, G. Giambastiani, S. L. Parisel, *Coord. Chem. Rev.* **2004**, *248*, 2131.

[16] C. J. Richards, A. J. Locke, *Tetrahedron: Asymmetry* **1998**, *9*, 2377.

[17] P. J. Guiry, C. P. Saunders, *Adv. Synth. Catal.* **2004**, *346*, 497.

[18] P. Espinet, K. Soulantica, *Coord. Chem. Rev.* **1999**, *293*, 499.

[19] F. Speiser, P. Braunstein, L. Saussine, *Acc. Chem. Res.* **2005**, *38*, 784.

[20] P. Štěpnička, M. Lamač in *Ferrocenes: Ligands, Materials and Biomolecules*, Ed.: P. Štěpnička, 1. ed., Wiley, Chichester, Ch. 7, **2008**.

[21] K. S. Gan, T. S. A. Hor in *Ferrocenes: Homogeneous Catalysis, Organic Synthesis, Materials Science*, Eds.: A. Togni, T. Hayashi, 1. ed., VCH, Weinheim, Ch. 1, **1995**.

[22] U. Siemeling, T.-C. Auch, *Chem. Soc. Rev.* **2005**, *34*, 584.

[23] T. Yoshida, K. Tani, T. Yamagata, Y. Tatsuno, T. Saito, *J. Chem. Soc. Chem. Commun.* 292 **1990**.

[24] Y. Zhang, J. C. Lewis, R. G. Bergman, J. A. Ellman, E. Oldfield, *Organometallics* **2006**, *25*, 3515.

[25] W. W. Brandt, F. P. Dwyer, E. C. Gyarfas, *Chem. Rev.* **1954**, *54*, 959.

[26] G. F. Cavichiolia, D. P. Martina, A. J. Ursinia, R. L. LaDuca, *J. Mol. Struct.* **2008**, *881*, 107.

[27] R. F. Heck, E.-I. Negishi, A. Suzuki, The Nobel Prize in Chemistry “for palladium-catalysed cross couplings in organic synthesis”, **2010**.

[28] T. J. Kealy, P. L. Pausen, *Nature* **1951**, *168*, 1039.

[29] S. A. Miller, J. A. Tebboth, J. F. Tremaine, *J. Chem. Soc.* 632 **1952**.

[30] G. Wilkinson, M. Rosenblum, M. C. Whiting, R. B. Woodward, *J. Am. Chem. Soc.* **1952**, *74*, 2125.

[31] E. O. Fischer, W. Pfab, *Z. Naturforsch. B* **1952**, *7*, 377.

[32] P. Štěpnička, Ed., *Ferrocenes: Ligands, Materials and Biomolecules*, 1. ed., Wiley, Chichester, **2008**.

[33] C. Elschenbroich, A. Salzer, *Organometallchemie*, 6. ed., B. G. Teubner, Stuttgart, **2008**.

[34] M. D. Rausch, D. J. Ciapenelli, *J. Organomet. Chem.* **1967**, *10*, 127.

[35] R. C. J. Atkinson, V. C. Gibson, N. J. Long, *Chem. Soc. Rev.* **2004**, *33*, 313.

[36] R. G. Pearson, J. Songstad, *J. Am. Chem. Soc.* **1967**, *89*, 1827.

[37] S. Woodward, *Tetrahedron* **2002**, *58*, 1017.

[38] P. Braunstein, *J. Organometal. Chem.* **2004**, *689*, 3953.

[39] A. F. Hollemann, E. Wiberg, N. Wiberg, *Lehrbuch der anorganischen Chemie*, 102. ed., Walter de Gruyter, Berlin, New York, **2007**.

[40] J. E. Huheey, E. A. Keiter, R. L. Keiter, *Anorganische Chemie - Prinzipien von Struktur und Reaktivität*, Walter de Gruyter, Berlin, New York, **2003**.

[41] J. Reedijk, *Comprehensive Coordination Chemistry*, 1. ed., Pergamon Press, **1987**.

[42] W. C. Davies, F. K. Mann, *J. Chem. Soc.* 276 **1944**.

[43] H.-U. Blaser, W. Chen, F. Camponovo, A. Togni in *Ferrocenes: Ligands, Materials and Biomolecules*, Ed.: P. Štěpnička, 1. ed., Wiley, Chichester, Ch. 6, **2008**.

[44] S. R. Bayly, P. D. Beer, G. Z. Chen in *Ferrocenes: Ligands, Materials and Biomolecules*, Ed.: P. Štěpnička, 1. ed., Wiley, Chichester, Ch. 8, **2008**.

[45] B. Speiser, *Chem. Unserer Zeit* **1981**, *15*, 62.

[46] J. Heinze, *Angew. Chem.* **1984**, *96*, 823.

[47] P. Zanello, *Inorganic Electrochemistry. Theory, Practice and Application*, The Royal Society of Chemistry, Cambridge, **2003**.

[48] U. Siemeling, U. Vorfeld, B. Neumann, H.-G. Stammler, *Chem. Ber.* **1995**, *128*, 481.

[49] K. Schlögl, M. Fried, *Monatsh. Chem.* **1963**, *94*, 537.

[50] J. G. P. Delis, P. W. N. M. van Leeuwen, K. Vrieze, N. Veldman, A. L. Spek, J. Fraanje, K. Goubitz, *J. Organomet. Chem.* **1996**, *514*, 125.

[51] B. Neumann, U. Siemeling, H.-G. Stammler, U. Vorfeld, J. G. P. Delis, P. W. N. M. van Leeuwen, K. Vrieze, J. Fraanje, K. Goubitz, F. F. de Biani, P. Zanello, *J. Chem. Soc. Dalton Trans.* 4705 **1997**.

[52] U. Siemeling, B. Neumann, H.-G. Stammler, A. Salmon, *Z. Anorg. Allg. Chem.* **2002**, *628*, 2315.

[53] F. Schüth, *Chem. Unserer Zeit* **2006**, *40*, 92.

[54] M. Röper, *Chem. Unserer Zeit* **2006**, *40*, 126.

[55] S. W. Chien, T. S. A. Hor in *Ferrocenes: Ligands, Materials and Biomolecules*, Ed.: P. Štěpnička, 1. ed., Wiley, Chichester, Ch. 2, **2008**.

[56] H.-U. Blaser, W. Brieden, B. Pugin, F. Spindler, M. Studer, A. Togni, *Top. Catal.*

2002, *19*, 3.

[57] I. R. Butler, *Polyhedron* **1992**, *11*, 3117.

[58] D. Seyferth, H. P. Withers(Jr), *Organometallics* **1982**, *1*, 1275.

[59] I. R. Butler, W. R. Cullen, T.-J. Kim, S. J. Rettig, J. Trotter, *Organometallics* **1985**, *4*, 972.

[60] J. A. Adeleke, Y.-W. Chen, L.-K. Liu, *Organometallics* **1992**, *11*, 2543.

[61] L.-L. Lai, T.-Y. Dong, *J. Chem. Soc. Chem. Commun.* 2347 **1994**.

[62] T.-Y. Dong, P.-H. Ho, C.-K. Chang, *J. Chin. Chem. Soc.* **2000**, *47-3*, 421.

[63] T.-Y. Dong, C.-K. Chang, *J. Chin. Chem. Soc.* **1998**, *45*, 577.

[64] I. R. Butler, R. L. Davies, *Synthesis* 1350 **1996**.

[65] J. J. Li, *Name Reactions*, 3. ed., Springer, **2006**.

[66] E. Erdik, *Tetrahedron* **1992**, *48*, 9577.

[67] E.-I. Negishi, *Acc. Chem. Res.* **1982**, *15*, 340.

[68] N. Miyaura, A. Suzuki, *Chem. Rev.* **1995**, *95*, 2457.

[69] A. Suzuki, *J. Chem. Soc. Chem. Commun.* 4759 **2005**.

[70] A. Suzuki, *Proc. Jpn. Acad.,Ser. B* **2004**, *80*, 359.

[71] D. Cai, R. D. Larsen, P. J. Reider, *Tetrahedron Lett.* **2002**, *43*, 4285.

[72] W. Li, D. P. Nelson, M. S. Jensen, R. S. Hoerrner, D. Cai, R. D. Larsen, P. J. Reider, *J. Org. Chem.* **2002**, *67*, 5394.

[73] R. J. Kloetzing, A. Krasovskiy, P. Knochel, *Chem. Eur. J.* **2007**, *13*, 215.

[74] R. C. Larock, *Comprehensive Organic Transformations, A Guide to Functional Groups Preparations*, 2. ed., Wiley-VCH, New York, **1999**.

[75] R. Gleiter, D. B. Werz, *Organometallics* **2005**, *24*, 4316.

[76] W. L. Steffen, G. J. Palenik, *Acta Cryst.* **1976**, *B32*, 298.

[77] C. A. Grapperhaus, T. Tuntulani, J. H. Reibenspies, M. Y. Darensbourg, *Inorg. Chem.* **1998**, *37*, 4052.

[78] H. Paulus, *Z. Anorg. Allg. Chem.* **1969**, *369*, 38.

[79] A. J. Canty, C. L. Raston, B. W. Skelton, A. H. White, *J. Chem. Soc. Dalton Trans.* 15 **1982**.

[80] S. Vongtragool, B. Gorshunov, M. Dressel, J. Krzystek, D. M. Eichhorn, J. Telser, *Inorg. Chem.* **2003**, *42*, 1788.

[81] A. F. Cameron, K. P. Forrest, G. Ferguson, *J. Chem. Soc. (A)* 1286 **1971**.

[82] T. S. Lobana, M. K. Sandhu, M. R. Snow, E. R. T. Tiekink, *Acta Cryst.* **1988**, *C44*, 179.

[83] Y.-Y. Niu, Y.-L. Song, S.-X. Liu, X.-Q. Xin, *Private communication to Cambridge Structural Database* **2002** (CSD refcode CADCEQ).

[84] J. McGinley, V. McKee, C. J. McKenzie, *Private communication to Cambridge Structural Database* **1998** (CSD refcode NIDWIG).

[85] Z.-X. Huang, X.-L. Wang, S.-X. Liu, *Private communication to Cambridge Structural Database* **2002** (CSD refcode TAFNOE).

[86] X.-L. Wang, Z.-X. Huang, S.-X. Liu, *Private communication to Cambridge Structural Database* **2001** (CSD refcode XOKSOF).

[87] B. Corain, B. Longato, G. Favero, D. Ajó, G. Pilloni, U. Russo, F. R. Kreissl, *Inorg.*

Chim. Acta **1989**, *157*, 259.

[88] P. Štěpnička, I. Císařová, R. Gyepes, *Eur. J. Inorg. Chem.* 926 **2006**.

[89] J. Kühnert, I. Císarová, M. Lamač, P. Štěpnička, *J. Chem. Soc. Dalton Trans.* 2454 **2008**.

[90] S. Berger, S. Braun, H.-O. Kalinowski, *NMR-Spektroskopie von Nichtmetallen - ^{31}P-NMR-Spektroskopie*, 1. ed., Georg Thieme Verlag, Stuttgart, **1993**.

[91] R. A. Edwards, O. P. Gladkikh, M. Nieuwenhuyzen, C. J. Wilkins, *Z. Kritallogr.* **1999**, *214*, 111.

[92] A. S. K. Hashmi, *Angew. Chem. Int. Ed.* **2008**, *47*, 6754.

[93] A. S. K. Hashmi, M. Rudolph, *Chem. Soc. Rev.* **2008**, *37*, 1766.

[94] A. S. K. Hashmi, *Angew. Chem. Int. Ed.* **2010**, *49*, 5232.

[95] I. Ott, *Coord. Chem. Rev.* **2009**, *253*, 1670.

[96] C. E. Holloway, M. Melnik, W. A. Nevin, W. Liu, *J. Coord. Chem.* **1995**, *35*, 85.

[97] S. M. Cortez, R. G. Raptis, *Coord. Chem. Rev.* **1997**, *162*, 495.

[98] S. M. Cortez, R. G. Raptis, *Coord. Chem. Rev.* **1998**, *169*, 363.

[99] N. J. Long, J. Martin, G. Opromolla, A. J. P. White, D. J. Williams, P. Zanello, *J. Chem. Soc. Dalton Trans.* 1981 **1999**.

[100] M. C. Gimeno, P. G. Jones, A. Laguna, C. Sarroca, *J. Chem. Soc. Dalton Trans.* 1473 **1995**.

[101] K. Tani, T. Mihana, T. Yamagata, T. Saito, *Private communication to Cambridge Structural Database* **1991** (CSD refcode SOXNUO).

[102] M. C. Gimeno, A. Laguna, *Chem. Rev.* **1997**, *97*, 511.

[103] H. Schmidbaur, *Chem. Soc. Rev.* **1995**, *24*, 391.

[104] M. C. Gimeno, A. Laguna, C. Sarroca, *Inorg. Chem.* **1993**, *32*, 5926.

[105] A. Houlton, R. Roberts, J. Silver, R. Parish, *J. Organomet. Chem.* **1991**, *418*, 269.

[106] P. Zanello in *Ferrocenes: Homogeneous Catalysis, Organic Synthesis, Materials Science*, Eds.: A. Togni, T. Hayashi, 1. ed., VCH, Weinheim, Ch. 7, **1995**.

[107] M. A. Jalil, T. Yamada, S. Fujinami, T. Honjo, H. Nishikawa, *Polyhedron* **2001**, *20*, 627.

[108] E. C. Alyea, J. Malito, J. H. Nelson, *Inorg. Chem.* **1987**, *26*, 4294.

[109] M.-X. Li, K.-K. Cheung, A. Mayr, *J. Solid State Chem.* **2000**, *152*, 247.

[110] B. Djordjevic, O. Schuster, H. Schmidbaur, *Z. Naturforsch. B* **2006**, *61*, 6.

[111] R. J. Bowen, J. Coates, E. M. Coyanis, D. Defayay, M. A. Fernandes, M. Layh, R. M. Moutloali, *Inorg. Chim. Acta* **2009**, *362*, 3172.

[112] H.-N. Adams, W. Hiller, J. Strähle, *Z. Anorg. Allg. Chem.* **1982**, *485*, 81.

[113] F. R. Hartley, *The Chemistry of Platinum and Palladium*, Applied Science, London, **1973**.

[114] C. J. Barnard, M. J. H. Russel in *Comprehensive Coordination Chemistry*, Eds.: G. Wilkinson, R. D. Gillard, J. A. McCleverty, Pergamon Press, Oxford, Vol. 5, Ch. 51, **1987**.

[115] A. T. Hutton, C. P. Morley in *Comprehensive Coordination Chemistry*, Eds.: G. Wilkinson, R. D. Gillard, J. A. McCleverty, Pergamon Press, Oxford, Vol. 5, Ch. 51.9, **1987**.

[116] T. Schareina, R. Kempe, *Angew. Chem. Int. Ed.* **2002**, *41*, 1521.

[117] I. R. Butler, M. Kalaji, L. Nehrlich, M. Hursthouse, A. I. Karaulov, K. M. A. Malik, *J. Chem. Soc. Chem. Commun.* 459 **1995**.

[118] J. Kühnert, M. Dusek, J. Demel, H. Lang, P. Štěpnička, *J. Chem. Soc. Dalton Trans.* 2802 **2007**.

[119] T. Hayashi, M. Konishi, Y. Kobori, M. Kumada, T. Higuchi, K. Hirotsuf, *J. Am. Chem. Soc.* **1984**, *106*, 158.

[120] V. C. Gibson, N. J. Long, A. J. P. White, C. K. Williams, D. J. Williams, M. Fontani, P. Zanello, *J. Chem. Soc. Dalton Trans.* 3280 **2002**.

[121] P. Štěpnička, I. Císařová, *Collect. Czech. Chem. Commun.* **2006**, *71*, 215.

[122] M. B. Hursthouse, D. E. Hibbs, I. R. Butler, *Private communication to Cambridge Structural Database* **2003** (CSD refcode GATGAF).

[123] M. B. Hursthouse, S. J. Coles, I. R. Butler, *Private communication to Cambridge Structural Database* **2003** (CSD refcode EKAQUC).

[124] T. G. Appleton, H. C. Clark, L. E. Manzer, *Coord. Chem. Rev.* **1973**, *10*, 335.

[125] P. Štěpnička, *Inorg. Chem. Commun.* **2004**, *7*, 423.

[126] J.-F. Ma, Y. Yamamoto, *Inorg. Chim. Acta* **2000**, *299*, 164.

[127] P. Štěpnička, I. Císařová, *Organometallics* **2003**, *22*, 1728.

[128] P. Štěpnička, M. Lamač, I. Císařová, *Polyhedron* **2004**, *23*, 921.

[129] P. Štěpnička, I. Císařová, *Inorg. Chem.* **2006**, *45*, 8785.

[130] P. Štěpnička, M. Krupa, M. Lamač, I. Císařová, *J. Organomet. Chem.* **2009**, *694*, 2987.

[131] A. de Meijere, F. Diederich in *Metal-Catalyzed Cross-Coupling Reactions*, 2. ed., Wiley-VCH, Weinheim, Ch. 2, **2004**.

[132] A. Suzuki, *J. Organomet. Chem.* **1999**, *576*, 147.

[133] M. Sundermeier, A. Zapf, M. Beller, *Eur. J. Inorg. Chem.* 3513 **2003**.

[134] G. P. Ellis, T. M. Romney-Alexander, *Chem. Rev.* **1987**, *87*, 779.

[135] D. Astruc, *Inorg. Chem.* **2007**, *46*, 1884.

[136] H. E. Gottlieb, V. Kotlyar, A. Nudelman, *J. Org. Chem.* **1997**, *62*, 7512.

[137] G. R. Fulmer, A. J. M. Miller, N. H. Sherden, H. E. Gottlieb, A. Nudelman, B. M. Stoltz, J. E. Bercaw, K. I. Goldberg, *Organometallics* **2010**, *29*, 2176.

[138] M. Hesse, H. Meier, B. Zeeh, *Spektroskopische Methoden in der organischen Chemie*, 7. ed., Georg Thieme Verlag, Stuttgart, **2005**.

[139] G. M. Sheldrick, *Acta Cryst.* **2008**, *A64*, 112.

[140] L. J. Farrugia, *J. Appl. Cryst* **1997**, *30*, 565.

[141] A. Shafir, M. P. Power, G. D. Whitener, J. Arnold, *Organometallics* **2000**, *19*, 3978.

[142] R. Uson, A. Laguna, M. Laguna, *Inorg. Synth.* **1989**, *26*, 85.

[143] D. Drew, J. R. Doyle, *Inorg. Synth.* **1972**, *13*, 47.

[144] A. C. Cope, E. C. Friedrich, *J. Am. Chem. Soc.* **1968**, *90*, 909.

Appendix

Contents

Abbreviations

Ac	acetyl
APCI	atmosphere pressure chemical ionisation
br	broadened
bipyppf	1-diphenylphosphino-1'(2,2'-bipyrid-6-yl)ferrocene-κ^2*P*,*N*
Bu	buthyl
ca.	circa
CC	column chromatography
cf.	confer, Latin
Cg	centroids of the Cp rings
Cp	cyclopentadienyl ring plane
CN	coordination number
CSD	cambridge structural database
cod	η^2:η^2-cycloocta-1,5-diene
CV	cyclic voltammetry (cyclic voltammogram respectively)
d	doublet
DCM	dichloromethane
DCTB	2-[(2E)-3-(4-tert-butylphenyl)-2-methylprop-2-enyliden]malononitril
DMF	*N*,*N*-dimethylformamide
DMSO	dimethylsulfoxide
dppf	1,1'-bis(diphenylphosphino)ferrocene
E	electrophile
E	potentail
E_λ	reversal potentail
ESI	electrospray ionisation
eq.	equivalent(s)
etc.	ed cetera, Latin
Fc	1,1'-ferrocenediyl
fc	ferrocene
fc*	decamethylferrocene
Fig.	Figure
h	hour(s)
HMPA	$(Me_2N)_3PO$
HOMO	highest occupied molecular orbital
HR-ESI	high resolution electrospray ionisation
HSAB	hard and soft acids and bases
i	current
i. e.	id est, Latin
IR	infra red
IUPAC	International Union of Pure and Applied Chemistry
J	coupling constant

L	ligand
L^{NC}	[(2-dimethylamino-κN)methyl]phenyl-κC^1
m	multiplet
MALDI	matrix assisted laser desorption ionisation
Me	methyl
min	minute(s)
MO	molecular orbital
MS	mass spectrometry
NMP	*N*-methyl-2-pyrrolidone
NMR	nuclear magnetic resonance
PE	petroleum ether 40 °C - 60 °C
Ph	phenyl
PPFA	[2-(diphenylphosphino)ferrocenyl]ethyldimethylamine
PTFE	polytetrafluorethylene
Py	pyridyl (C_5H_4N)
py	pyriddiyl (C_5H_3N)
s	singlet
SCE	saturated calomel electrode
t	triplet
τ	torsion angle of ferrocene (C1-Cg1-Cg2-C6)
Tab.	Table
THF	tetrahydrofurane
tht	tetrahydrothiphene
TLC	thin layer chromatography
TMEDA	*N*,*N*,*N*',*N*'-tetramethylethylendiamine
TMS	trimethylsilane
υ	scan rate
VE	valence electrons
viz.	videlicet, Latin
vs.	versus
vt	virtual triplet

List of Figures

List of Tables

List of numbered Compounds

1 1-(Pyrid-2-yl)-1'-diphenylphosphinoferrocene

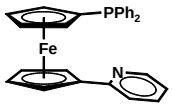

$C_{27}H_{22}FeNP$ M = 447.2891 g/mol

2 1-(Pyrid-3-yl)-1'-diphenylphosphinoferrocene

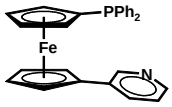

$C_{27}H_{22}FeNP$ M = 447.2891 g/mol

3 1-[(Pyrid-2-yl)methyl]-1'-diphenylphosphinoferrocene

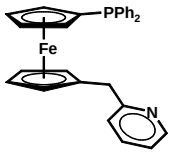

$C_{28}H_{24}FeNP$ M = 461.3260 g/mol

4 2,6-Bis(1'-diphenylphosphinoferroceneyl)pyridine

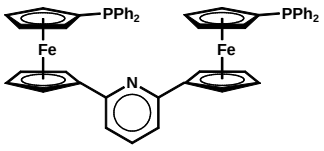

$C_{49}H_{39}Fe_2NP_2$ M = 815.4969 g/mol

5a [$ZnCl_2$(1-(Pyrid-2-yl-κN)-1'-(diphenylphosphino-κP)ferrocene)]

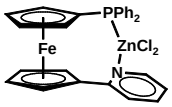

$C_{27}H_{22}Cl_2FeNPZn$ M = 583.5851 g/mol

5b [$ZnBr_2$(1-(Pyrid-2-yl-κN)-1'-(diphenylphosphino-κP)ferrocene)]

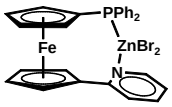

$C_{27}H_{22}Br_2FeNPZn$ M = 672.4871 g/mol

5c [ZnI_2(1-(Pyrid-2-yl-κN)-1'-(diphenylphosphino-κP)ferrocene)]

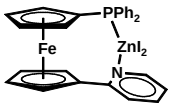

$C_{27}H_{22}FeI_2NPZn$ M = 766.4791 g/mol

6a [$CdCl_2$(1-(Pyrid-2-yl-κN)-1'-(diphenylphosphino-κP)ferrocene)]

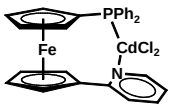

$C_{27}H_{22}CdCl_2FeNP$ M = 630.6051 g/mol

6b [$CdBr_2$(1-(Pyrid-2-yl-κN)-1'-(diphenylphosphino-κP)ferrocene)]

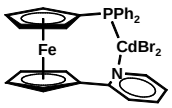

$C_{27}H_{22}Br_2CdFeNP$ M = 719.5071 g/mol

6c [CdI_2(1-(Pyrid-2-yl-κN)-1'-(diphenylphosphino-κP)ferrocene)]

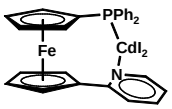

$C_{27}H_{22}CdFeI_2NP$ M = 813.4991 g/mol

7 [$CdCl_2$(1-(Pyrid-2-yl)-1'-(diphenylphosphino-κP)ferrocene)$_2$]

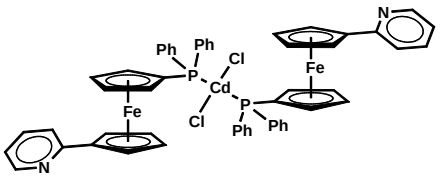

$C_{54}H_{44}CdCl_2FeNP$ M = 977.0768 g/mol

8a [$HgCl_2$(1-(Pyrid-2-yl-κN)-1'-(diphenylphosphino-κP)ferrocene)]

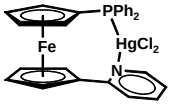

$C_{27}H_{22}Cl_2FeHgNP$ M = 718.7951 g/mol

8b [$HgBr_2$(1-(Pyrid-2-yl-κN)-1'-(diphenylphosphino-κP)ferrocene)]

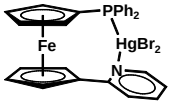

$C_{27}H_{22}Br_2FeHgNP$ M = 807.6971 g/mol

8c [HgI_2(1-(Pyrid-2-yl)-1'-(diphenylphosphino-κP)ferrocene)]$_2$

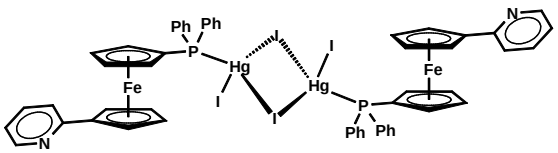

$C_{27}H_{22}FeHgI_2NP$ M = 901.6891 g/mol

9a [$HgCl_2$(1-(Pyrid-2-yl)-1'-(diphenylphosphino-κP)ferrocene)$_2$]

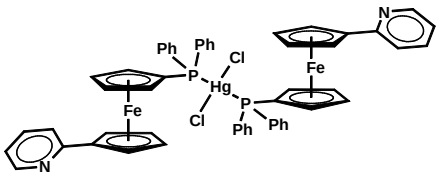

$C_{54}H_{44}Cl_2Fe_2HgN_2P_2$ M = 1166.0943 g/mol

9b [$HgBr_2$(1-(Pyrid-2-yl)-1'-(diphenylphosphino-κP)ferrocene)$_2$]

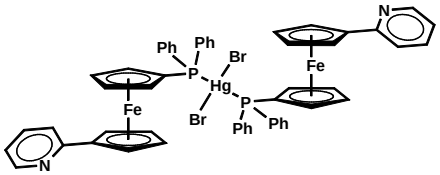

$C_{54}H_{44}Br_2Fe_2HgN_2P_2$ M = 1254.9963 g/mol

10 [$ZnBr_2$(1-(Pyrid-3-yl-κN)-1'-(diphenylphosphino-κP)ferrocene)]$_n$

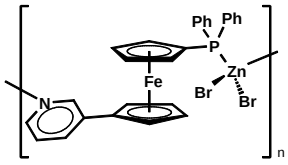

$(C_{27}H_{22}Br_2FeNPZn)_n$ M = 672.4871 g/mol (n = 1)

11 [$CdBr_2$(1-(Pyrid-3-yl-κN)-1'-(diphenylphosphino-κP)ferrocene)]$_n$

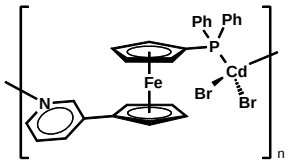

$(C_{27}H_{22}Br_2CdFeNP)_n$ M = 719.5071 g/mol (n = 1)

12 [$HgBr_2$(1-(Pyrid-3-yl-κN)-1'-(diphenylphosphino-κP)ferrocene)]$_n$

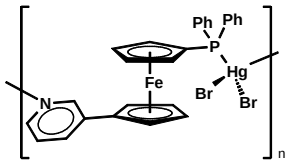

$(C_{27}H_{22}Br_2FeHgNP)_n$ M = 807.6971 g/mol (n = 1)

13 [$ZnBr_2$(1-[(Pyrid-2-yl-κN)methyl]-1'-(diphenylphosphino-κP)ferrocene)]

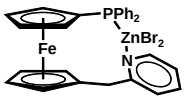

$C_{28}H_{24}Br_2FeNPZn$ M = 686.5140 g/mol

13a [$ZnBr_2$(1-[(Pyrid-2-yl-κN)methyl]-1'-(diphenylphosphino-κP)ferrocene)]$_2$

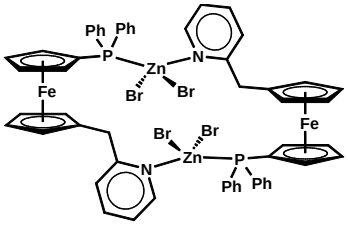

$C_{56}H_{48}Br_4Fe_2N_2P_2Zn_2$ M = 1373.0280 g/mol

14 [$CdBr_2$(1-[(Pyrid-2-yl-κN)methyl]-1'-(diphenylphosphino-κP)ferrocene)]

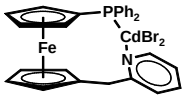

$C_{28}H_{24}Br_2CdFeNP$ M = 733.5340 g/mol

14a [$CdBr_2$(1-[(Pyrid-2-yl-κN)methyl]-1'-(diphenylphosphino-κP)ferrocene)] $_n$

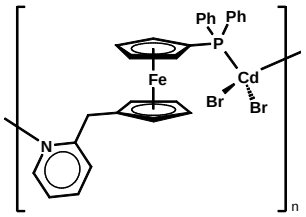

$(C_{28}H_{24}Br_2CdFeNP)_n$ M = 733.5340 g/mol (n = 1)

15 [CdI_2(1-[(Pyrid-2-yl-κN)methyl]-1'-(diphenylphosphino-κP)ferrocene)]

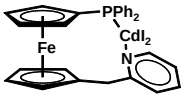

$C_{28}H_{24}CdFeI_2NP$ M = 827.5260 g/mol

16 [$HgBr_2$(1-[(Pyrid-2-yl-κN)methyl]-1'-(diphenylphosphino-κP)ferrocene)]

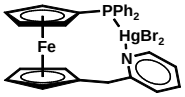

$C_{28}H_{24}Br_2FeHgNP$ M = 821.7240 g/mol

17 [$(HgBr_2)_2$(1-[(Pyrid-2-yl-κN)methyl]-1'-(diphenylphosphino-κP)ferrocene)]$_n$

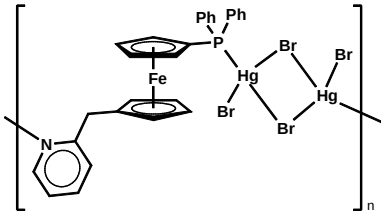

$(C_{28}H_{24}Br_4FeHg_2NP)_n$ M = 1182.1220 g/mol (n = 1)

18 [$HgBr_2$(1-[(Pyrid-2-yl)methyl]-1'-(diphenylphosphino-κP)ferrocene)$_2$]

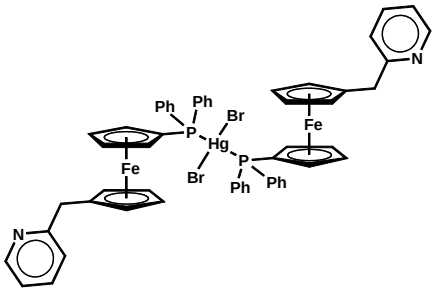

$C_{56}H_{48}Br_2Fe_2HgN_2P_2$ M = 1283.0500 g/mol

19 [Ag(1-(Pyrid-2-yl-κN)-1'-(diphenylphosphino-κP)ferrocene)]$_n$[BF_4]$_n$

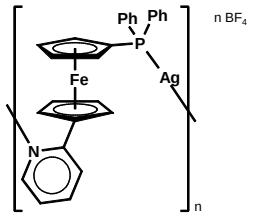

$(C_{27}H_{22}AgBF_4FeNP)_n$ M = 641.9783 g/mol (n = 1)

20 [Ag(1-(Pyrid-3-yl-κN)-1'-(diphenylphosphino-κP)ferrocene)]$_2$[BF_4]$_2$

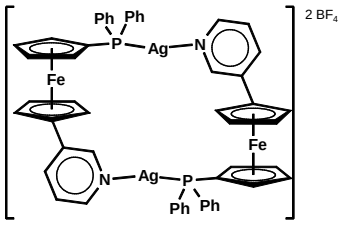

$C_{54}H_{44}Ag_2B_2F_8Fe_2N_2P_2$ M = 1238.9475 g/mol

21 [Ag(1-[(Pyrid-2-yl-κN)methyl]-1'-(diphenylphosphino-κP)ferrocene)]$_n$[BF_4]$_n$

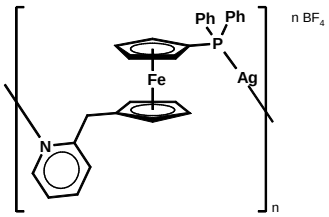

$(C_{28}H_{24}AgBF_4FeNP)_n$ M = 656.0006 g/mol (n = 1)

22 [AuCl(1-(Pyrid-2-yl)-1'-(diphenylphosphino-κP)ferrocene)]

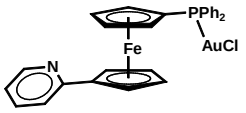

$C_{27}H_{22}FeNPAuCl$ M = 679.7091 g/mol

23 [AuCl(1-(Pyrid-3-yl)-1'-(diphenylphosphino-κP)ferrocene)]

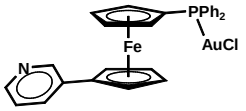

$C_{27}H_{22}FeNPAuCl$ M = 679.7091 g/mol

24 [AuCl(1-[(Pyrid-2-yl)methyl]-1'-(diphenylphosphino-κP)ferrocene)]

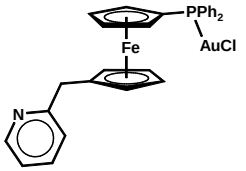

$C_{28}H_{24}FeNPAuCl$ M = 693.7455 g/mol

25 [Au_2(1-(Pyrid-2-yl-κN)-1'-(diphenylphosphino-κP)ferrocene)$_2$][BF_4]$_2$

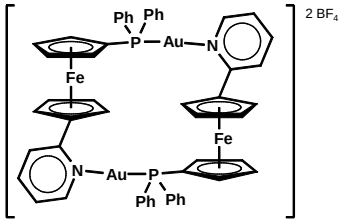

$C_{54}H_{44}Fe_2N_2P_2Au_2B_2F_8$ M = 1462.1405 g/mol

26 [Au(1-(Pyrid-3-yl)-1'-(diphenylphosphino)ferrocene)]$_n$[BF_4]$_n$

27 [Au(1-[(Pyrid-2-yl)methyl]-1'-(diphenylphosphino)ferrocene]$_n$[BF_4]$_n$

28 [$PdCl_2$(1-(Pyrid-2-yl-κN)-1'-(diphenylphosphino-κP)]

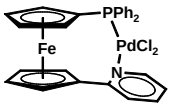

$C_{27}H_{22}Cl_2FeNPPd$ M = 624.6251 g/mol

29 [$PdCl_2$(1-[(Pyrid-2-yl-κN)methyl]-1'-(diphenylphosphino-κP)]

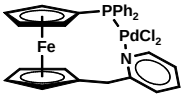

$C_{28}H_{24}Cl_2FeNPPd$ M = 638.6520 g/mol

30 [$PdCl_2$(1-(Pyrid-2-yl)-1'-(diphenylphosphino-$\kappa P)_2$]

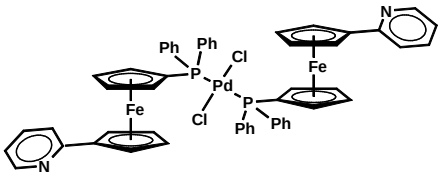

$C_{54}H_{44}Cl_2Fe_2N_2P_2Pd$ M = 1071.9243 g/mol

31 [$PdCl_2$(1-[(Pyrid-2-yl)methyl]-1'-(diphenylphosphino-$\kappa P)_2$]

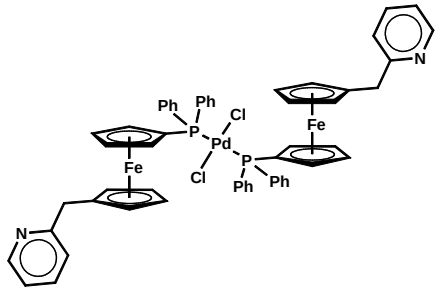

$C_{56}H_{48}Cl_2Fe_2N_2P_2Pd$ M = 1099.9780 g/mol

32 [PdCl(2-[(Dimethylamino-κN)methyl]phenyl-κC^1)(1-(pyrid-2-yl)-1'-(diphenylphosphino-κP))]

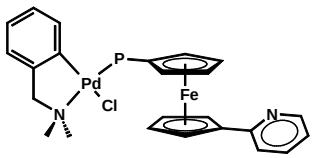

$C_{36}H_{34}ClFeN_2PPd$ M = 723.3731 g/mol

33 [PdCl(2-[(Dimethylamino-κN)methyl]phenyl-κC^1)(1-[(pyrid-2-yl)methyl]-1'-(diphenylphosphino-κP)]

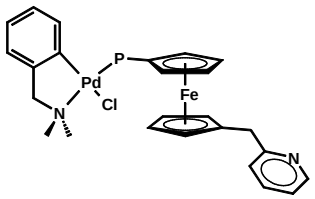

$C_{37}H_{36}ClFeN_2PPd$ M = 737.4000 g/mol

34 [Pd(2-[(Dimethylamino-κN)methyl]phenyl-κC^1)(1-(pyrid-2-yl-κN)-1'-(diphenylphosphino-κP))][ClO_4]

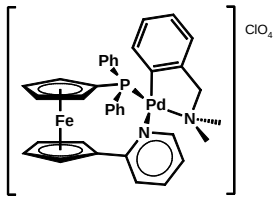

$C_{36}H_{34}ClFeN_2O_4PPd$ M = 787.3707 g/mol

34a [(Pd(2-[(Dimethylamino-κN)methyl]phenyl-κC^1)(1-(pyrid-2-yl-κN)-1'-(diphenylphosphino-κP))][Cl]

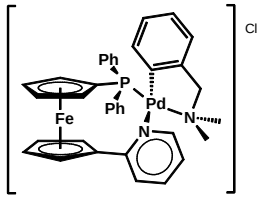

$C_{36}H_{34}ClFeN_2PPd$ M = 723.3731 g/mol

35 [Pd(2-[(Dimethylamino-κN)methyl]phenyl-κC^1)(1-[(pyrid-2-yl-κN)methyl]-1'-(diphenylphosphino-κP)][ClO_4]

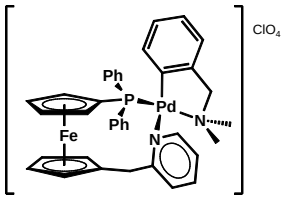

$C_{37}H_{36}ClFeN_2O_4PPd$ M = 801.3976 g/mol

List of X-ray Data

X-ray Data of 1

Table 1. Crystal data and structure refinement for i0540a.

Code	i0540a	
Empirical formula	$C_{27}H_{22}FeNP$	
Formula weight	447.28	
Temperature	173(2) K	
Wavelength	0.71073 Å	
crystal system	Triclinic	
spacegoup	$P\bar{1}$	
Unit cell dimensions	a = 10.1437(9) Å	α = 72.013(6)°
	b = 11.0401(9) Å	β = 85.964(7)°
	c = 10.9432(9) Å	γ = 66.324(6)°
Volume	1065.47(16) $Å^3$	
Z	2	
Density (calculated)	1.394 g/cm^3	
Absorption coefficient	0.797 mm^{-1}	
F(000)	464	
Crystal size	0.49 mm × 0.39 mm × 0.24 mm	
θ-range for data collection	1.96 → 25.22°	
Index ranges	-12→ h →12, -13→ k →13, -13→ l →13	
Reflections collected	9178	
Independent reflections	3636 [R_{int} = 0.0340]	
Reflections observed	3430	
Absorption correction	Integration	
Max. and min. transmission	0.8225 and 0.7162	
Refinement method	full-matrix least-squares against F^2	
Data / restraints / parameters	3636 / 0 / 271	
Goodness-of-fit on F^2	1.088	
Final R indices [$I > 2\sigma(I)$]	R_1 = 0.0264, wR_2 = 0.0732	
R indices (all data)	R_1 = 0.0278, wR_2 = 0.0739	
Largest diff. peak and hole	0.311 and -0.357 $e/Å^3$	

Table 2. Atomic coordinates ($\cdot 10^4$) and equivalent isotropic displacement parameters ($A^2 \cdot 10^3$) for i0540a. U_{eq} is defined as one third of the trace of the orthogonalized U_{ij}tensor.

	x	y	z	U_{eq}
C(1)	678(2)	2320(2)	9675(1)	32(1)
C(2)	1691(2)	2407(2)	10467(2)	38(1)
C(3)	3027(2)	1242(2)	10570(2)	44(1)
C(4)	2863(2)	441(2)	9844(2)	43(1)
C(5)	1421(2)	1097(2)	9288(2)	36(1)
C(6)	2583(2)	2893(2)	6713(1)	32(1)
C(7)	1673(2)	4106(2)	7056(2)	36(1)
C(8)	2508(2)	4344(2)	7877(2)	45(1)
C(9)	3920(2)	3284(2)	8055(2)	46(1)
C(10)	3974(2)	2383(2)	7349(2)	37(1)
C(11)	2223(2)	2334(2)	5786(1)	30(1)
C(12)	795(2)	2719(2)	5375(2)	36(1)
C(13)	527(2)	2249(2)	4431(2)	40(1)
C(14)	1685(2)	1394(2)	3918(2)	42(1)
C(15)	3064(2)	1028(2)	4392(2)	41(1)
C(16)	-2092(2)	2810(2)	10638(1)	30(1)
C(17)	-1400(2)	1791(2)	11776(2)	39(1)
C(18)	-2182(2)	1330(2)	12773(2)	48(1)
C(19)	-3676(2)	1879(2)	12650(2)	49(1)
C(20)	-4383(2)	2880(2)	11509(2)	47(1)
C(21)	-3602(2)	3344(2)	10518(2)	37(1)
C(22)	-1870(2)	3452(2)	7947(1)	32(1)
C(23)	-2504(2)	4652(2)	6903(2)	38(1)
C(24)	-3120(2)	4600(2)	5833(2)	48(1)
C(25)	-3090(2)	3359(2)	5783(2)	51(1)
C(26)	-2471(2)	2159(2)	6817(2)	47(1)
C(27)	-1880(2)	2204(2)	7900(2)	37(1)
N	3352(2)	1486(1)	5305(1)	37(1)
P	-1161(1)	3632(1)	9352(1)	31(1)
Fe	2428(1)	2436(1)	8681(1)	30(1)

X-ray Data of 2

Table 1. Crystal data and structure refinement for i0653.

Code	i0653	
Empirical formula	$C_{27}H_{24}FeNP$	
Formula weight	449.29	
Temperature	173(2) K	
Wavelength	0.71073 Å	
crystal system	Triclinic	
spacegroup	$P\bar{1}$	
Unit cell dimensions	a = 10.1847(12) Å	α = 72.890(9)°
	b = 11.0585(12) Å	β = 85.100(10)°
	c = 10.9491(13) Å	γ = 65.974(8)°
Volume	1075.6(2) $Å^3$	
Z	2	
Density (calculated)	1.387 g/cm^3	
Absorption coefficient	0.789 mm^{-1}	
F(000)	468	
Crystal size	0.25 × 0.21 × 0.02 mm	
θ-range for data collection	1.95 → 24.99°	
Index ranges	-12→ h →10, -12→ k →12, -12→ l →13	
Reflections collected	7001	
Independent reflections	3555 [R_{int} = 0.0534]	
Reflections observed	2598	
Absorption correction	Integration	
Max. and min. transmission	0.9589 and 0.5543	

Refinement method	full-matrix least-squares against F^2
Data / restraints / parameters	3555 / 0 / 271
Goodness-of-fit on F^2	0.714
Final R indices [$I > 2\sigma(I)$]	R_1 = 0.0484, wR_2 = 0.1234
R indices (all data)	R_1 = 0.0676, wR_2 = 0.1351
Largest diff. peak and hole	0.554 and -0.616 e/Å^3

Table 2. Atomic coordinates ($\cdot$ 10^4) and equivalent isotropic displacement parameters ($A^2 \cdot 10^3$) for i0540a. U_{eq} is defined as one third of the trace of the orthogonalized U_{ij}tensor.

	x	y	z	U_{eq}
C(1)	574(4)	2323(4)	9652(3)	37(1)
C(2)	1597(4)	2408(4)	10432(3)	42(1)
C(3)	2922(4)	1222(5)	10526(4)	49(1)
C(4)	2750(4)	422(4)	9797(4)	47(1)
C(5)	1304(4)	1101(4)	9245(3)	40(1)
C(6)	2552(4)	2798(4)	6680(3)	39(1)
C(7)	1670(4)	4041(4)	7025(3)	42(1)
C(8)	2513(5)	4252(5)	7852(4)	54(1)
C(9)	3903(5)	3163(5)	8031(4)	54(1)
C(10)	3944(4)	2261(5)	7320(4)	47(1)
C(11)	2175(3)	2257(4)	5748(3)	35(1)
C(12)	749(4)	2635(4)	5353(3)	43(1)
C(13)	482(4)	2164(5)	4410(4)	49(1)
C(14)	1636(4)	1299(5)	3877(4)	50(1)
C(15)	3252(4)	1379(4)	5142(3)	45(1)
C(16)	-1938(3)	3495(4)	7915(3)	37(1)
C(17)	-2520(4)	4692(4)	6891(3)	42(1)
C(18)	-3125(4)	4662(5)	5799(4)	51(1)
C(19)	-3144(4)	3448(6)	5724(4)	53(1)
C(20)	-2576(4)	2238(5)	6736(4)	50(1)
C(21)	-1992(4)	2274(4)	7839(3)	40(1)
C(22)	-2223(4)	2849(4)	10602(3)	35(1)
C(23)	-1562(4)	1886(4)	11755(4)	44(1)
C(24)	-2371(5)	1426(5)	12722(4)	53(1)
C(25)	-3860(5)	1917(5)	12557(4)	54(1)
C(26)	-4534(4)	2872(5)	11415(4)	50(1)
C(27)	-3716(4)	3333(4)	10450(4)	42(1)
N(1)	3016(3)	889(4)	4225(3)	53(1)
P(1)	-1254(1)	3654(1)	9345(1)	37(1)
Fe(1)	2354(1)	2395(1)	8648(1)	36(1)

X-ray Data of 3

Table 1. Crystal data and structure refinement for i0697a.

Code	i0697a	
Empirical formula	$C_{28}H_{24}FeNP$	
Formula weight	461.30	
Temperature	100(2) K	
Wavelength	0.71073 A	
Crystal system	Triclinic	
Space group	$P\bar{1}$	
Unit cell dimensions	a = 8.4956(11) Å	α = 67.813(9) °
	b = 10.9419(13) Å	β = 75.752(9) °
	c = 13.4071(15) Å	γ = 84.294(10) °

Volume	1118.5(2) Å^3
Z	2
Density (calculated)	1.370 g/cm^3
Absorption coefficient	0.761 mm^{-1}
F(000)	480
Crystal size	0.57 $\times$ 0.40 $\times$ 0.15 mm
θ-range for data collection	1.68 $\rightarrow$ 25.00 $^\circ$
Index ranges	-8$\rightarrow h \rightarrow$10, -13$\rightarrow k \rightarrow$13, -15$\rightarrow l \rightarrow$15
Reflections collected	8622
Independent reflections	3867 [R_{int} = 0.0501]
Reflections observed	3663
Absorption correction	Integration
Max. and min. transmission	0.8761 and 0.7248
Refinement method	Full-matrix least-squares on F^2
Data / restraints / parameters	3867 / 0 / 280
Goodness-of-fit on F^2	1.056
Final R indices [$I > 2\sigma(I)$]	R_1 = 0.0323, wR_2 = 0.0892
R indices (all data)	R_1 = 0.0336, wR_2 = 0.0900
Largest diff. peak and hole	0.383 and -0.445 e/Å^3

Table 2. Atomic coordinates ($\cdot$ 10^4) and equivalent isotropic displacement parameters ($A^2 \cdot 10^3$) for i0697a. U_{eq} is defined as one third of the trace of the orthogonalized U_{ij}tensor.

	x	y	z	U_{eq}
C(1)	1481(2)	2903(2)	2602(1)	25(1)
C(2)	3077(2)	3098(2)	1879(1)	26(1)
C(3)	3663(2)	4350(2)	1739(1)	29(1)
C(4)	2440(2)	4941(2)	2362(2)	30(1)
C(5)	1098(2)	4052(2)	2897(2)	28(1)
C(6)	2781(2)	2888(2)	5029(1)	26(1)
C(7)	2839(2)	1635(2)	4902(1)	29(1)
C(8)	4371(2)	1504(2)	4217(1)	31(1)
C(9)	5284(2)	2671(2)	3927(2)	30(1)
C(10)	4313(2)	3520(2)	4427(1)	28(1)
C(11)	1378(2)	3449(2)	5666(2)	31(1)
C(12)	1611(2)	3315(2)	6792(1)	26(1)
C(13)	761(2)	2383(2)	7768(2)	31(1)
C(14)	985(2)	2321(2)	8778(2)	35(1)
C(15)	2062(2)	3197(2)	8786(2)	33(1)
C(16)	2863(2)	4093(2)	7775(2)	31(1)
C(17)	1576(2)	244(2)	2764(1)	25(1)
C(18)	2144(2)	-755(2)	3618(2)	33(1)
C(19)	3275(3)	Y-1689(2)	3387(2)	40(1)
C(20)	3829(2)	-1633(2)	2305(2)	39(1)
C(22)	2140(2)	283(2)	1677(2)	28(1)
C(23)	-1019(2)	1935(2)	2039(1)	24(1)
C(24)	-2040(2)	974(2)	2071(2)	29(1)
C(25)	-3010(2)	1272(2)	1305(2)	32(1)
C(26)	-2992(2)	2539(2)	501(2)	32(1)
C(27)	-2016(2)	3505(2)	478(2)	30(1)
C(28)	-1038(2)	3210(2)	1239(1)	27(1)
N(1)	2664(2)	4163(2)	6792(1)	29(1)
P(1)	150(1)	1483(1)	3123(1)	24(1)
Fe(1)	3149(1)	3150(1)	3389(1)	23(1)
C(21)	3262(2)	-656(2)	1450(2)	33(1)

X-ray Data of 4

Table 1. Crystal data and structure refinement for i0724.

Code	i0724	
Empirical formula	$C_{49}H_{39}Fe_2NP_2$	
Formula weight	815.45	
Temperature	193(2) K	
Wavelength	0.71073 Å	
crystal system	Triclinic	
spacegroup	$P\bar{1}$	
Unit cell dimensions	a = 8.635(2) Å	α = 102.60(2)°
	b = 12.721(3) Å	β = 91.03(2)°
	c = 18.684(5) Å	γ = 95.93(2)°
Volume	1990.4(9) Å^3	
Z	2	
Density (calculated)	1.361 g/cm^3	
Absorption coefficient	0.845 mm^{-1}	
F(000)	844	
Crystal size	0.250 mm × 0.130 mm × 0.020 mm	
θ-range for data collection	1.65 → 25.00°	
Index ranges	-10→ h →10, -13→ k →15, -22→ l →22	
Reflections collected	12726	
Independent reflections	6591 [R_{int} = 0.2092]	
Reflections observed	1956	
Absorption correction	Integration	
Max. and min. transmission	0.9688 and 0.8064	
Refinement method	full-matrix least-squares against F^2	
Data / restraints / parameters	6591 / 0 / 482	
Goodness-of-fit on F^2	0.861	
Final R indices [$I > 2\sigma(I)$]	R_1 = 0.1169, wR_2 = 0.2847	
R indices (all data)	R_1 = 0.2343, wR_2 = 0.3740	
Largest diff. peak and hole	1.059 and -2.106 e/Å^3	

Table 2. Atomic coordinates (· 10^4) and equivalent isotropic displacement parameters (A^2 · 10^3) for i0540a. U_{eq} is defined as one third of the trace of the orthogonalized U_{ij}tensor.

	x	y	z	U_{eq}
C(1)	3070(20)	7879(14)	9329(8)	51(5)
C(2)	1596(19)	7679(15)	8790(9)	57(6)
C(3)	2040(20)	8116(14)	8189(9)	50(5)
C(4)	3600(20)	8585(15)	8265(9)	55(5)
C(5)	4170(20)	8432(13)	8937(8)	43(4)
C(6)	2682(19)	5441(11)	7790(8)	36(4)
C(7)	3300(20)	5907(19)	7255(10)	76(8)
C(8)	5020(20)	6397(17)	7507(10)	65(6)
C(9)	5120(30)	5940(20)	8195(9)	87(9)
C(10)	3720(20)	5483(15)	8349(11)	58(6)
C(11)	1020(19)	4991(11)	7753(7)	34(4)
C(12)	240(30)	4693(18)	8352(10)	74(7)
C(13)	-1300(30)	4271(16)	8312(10)	63(6)
C(14)	-2050(20)	4240(14)	7597(8)	46(4)
C(15)	-1320(20)	4410(12)	7049(8)	46(5)
C(16)	-2091(17)	4319(11)	6286(8)	32(3)
C(17)	-3690(20)	4226(14)	6113(10)	63(6)
C(18)	-3970(20)	4052(11)	5360(9)	44(4)
C(19)	-2560(20)	4056(12)	5081(9)	44(4)
C(20)	-1350(20)	4286(13)	5624(8)	46(4)
C(21)	-2529(17)	1373(10)	4866(8)	30(3)

C(22)	-1163(18)	1671(12)	5397(8)	34(3)
C(23)	-1900(20)	1754(11)	6089(9)	45(4)
C(24)	-3520(20)	1555(13)	6006(9)	49(5)
C(25)	-3850(20)	1375(11)	5229(7)	33(4)
C(26)	5311(19)	7546(13)	10295(8)	43(4)
C(27)	5920(20)	6500(15)	10140(9)	57(5)
C(28)	7500(30)	6480(20)	10209(11)	72(6)
C(29)	8450(20)	7420(20)	10494(11)	68(6)
C(30)	7890(20)	8470(20)	10652(11)	76(7)
C(31)	6250(20)	8431(15)	10583(9)	58(5)
C(32)	2680(20)	8718(14)	10799(8)	46(4)
C(33)	2830(30)	8656(15)	11558(9)	73(7)
C(34)	2380(30)	9500(19)	12108(9)	92(9)
C(35)	1910(30)	10453(19)	11879(10)	79(7)
C(36)	1730(30)	10485(14)	11144(9)	68(6)
C(37)	2030(20)	9473(15)	10608(9)	56(5)
C(38)	-2401(17)	-239(12)	3576(7)	32(3)
C(39)	-2600(30)	-699(15)	2807(10)	69(6)
C(40)	-2780(30)	-1903(12)	2614(11)	65(6)
C(41)	-2770(20)	-2518(18)	3071(12)	76(7)
C(42)	-2640(20)	-2113(14)	3874(10)	59(6)
C(43)	-2420(20)	-884(13)	4036(10)	49(5)
C(44)	-127(18)	1603(12)	3808(7)	38(4)
C(45)	967(17)	855(12)	3893(8)	36(4)
C(46)	2490(20)	1151(12)	3880(8)	48(5)
C(47)	3080(20)	2135(16)	3882(9)	57(5)
C(48)	2040(30)	2958(17)	3776(10)	67(6)
C(49)	430(20)	2603(11)	3774(9)	43(4)
N(1)	202(16)	4871(10)	7094(6)	39(3)
P(1)	3134(5)	7465(4)	10142(2)	50(1)
P(2)	-2269(5)	1239(3)	3849(2)	40(1)
Fe(1)	3465(3)	6994(2)	8272(1)	41(1)
Fe(2)	-2673(3)	2860(2)	5587(1)	36(1)

X-ray Data of 5a

Table 1. Crystal data and structure refinement for i0531.

Code	i0531	
Empirical formula	$C_{27}H_{22}Cl_2FeNPZn$	
Formula weight	583.55	
Temperature	203(2) K	
Wavelength	0.71073 Å	
crystal system	Monoclinic	
spacegroup	$P2_1/c$	
Unit cell dimensions	a = 19.2132(16) Å	α = 90°
	b = 9.1831(6) Å	β = 101.679(7)°
	c = 28.737(3) Å	γ = 90°
Volume	4965.3(7) Å^3	
Z	8	
Density (calculated)	1.561 g/cm^3	
Absorption coefficient	1.846 mm^{-1}	
F(000)	2368	
θ-range for data collection	1.62 $\rightarrow$ 25.00°	
Index ranges	-21$\rightarrow h \rightarrow$22, -10$\rightarrow k \rightarrow$7, -25$\rightarrow l \rightarrow$34	
Reflections collected	9793	
Independent reflections	5901 [R_{int} = 0.0825]	
Reflections observed	2875	
Absorption correction	Integration	

Refinement method	full-matrix least-squares against F^2
Data / restraints / parameters	5901 / 0 / 595
Goodness-of-fit on F^2	0.772
Final R indices [$I > 2\sigma(I)$]	R_1 = 0.0506, wR_2 = 0.1039
R indices (all data)	R_1 = 0.1090, wR_2 = 0.1163
Largest diff. peak and hole	0.587 and -0.370 $e/$Å^3

Table 2. Atomic coordinates ($\cdot$ 10^4) and equivalent isotropic displacement parameters ($A^2 \cdot 10^3$) for i0531. U_{eq} is defined as one third of the trace of the orthogonalized U_{ij}tensor.

	x	y	z	U_{eq}
C(1)	2950(5)	4940(11)	6767(4)	41(3)
C(2)	2236(5)	5221(11)	6825(4)	44(3)
C(3)	2172(6)	6771(11)	6859(4)	46(3)
C(4)	2836(6)	7411(12)	6840(4)	52(4)
C(5)	3308(6)	6277(12)	6782(4)	50(3)
C(6)	2824(5)	6496(10)	5605(4)	36(3)
C(7)	2418(5)	5146(11)	5593(4)	38(3)
C(8)	1729(5)	5543(13)	5648(4)	48(3)
C(9)	1690(5)	7038(13)	5694(4)	52(3)
C(10)	2380(5)	7652(11)	5681(4)	44(3)
C(11)	3570(5)	6617(12)	5552(4)	44(3)
C(12)	3762(5)	7891(11)	5351(5)	52(4)
C(13)	4449(6)	7984(13)	5260(5)	64(4)
C(14)	4895(6)	6861(14)	5353(5)	71(4)
C(15)	4696(6)	5615(12)	5561(5)	61(4)
C(16)	3826(5)	2504(13)	7166(4)	42(3)
C(17)	4034(6)	3341(16)	7585(4)	65(4)
C(18)	4437(7)	2748(17)	7994(5)	73(5)
C(19)	4611(6)	1343(16)	8007(5)	61(4)
C(20)	4442(7)	493(15)	7623(6)	67(4)
C(21)	4040(6)	1095(14)	7194(5)	59(4)
C(22)	2491(5)	2020(12)	6522(4)	42(3)
C(23)	2235(5)	1527(11)	6924(4)	47(3)
C(24)	1605(6)	747(13)	6855(5)	55(4)
C(25)	1254(6)	414(12)	6419(5)	55(4)
C(26)	1505(6)	880(11)	6021(4)	45(3)
C(27)	2140(5)	1634(11)	6086(4)	40(3)
C(28)	1930(5)	3820(10)	3263(4)	37(3)
C(29)	2624(5)	4117(11)	3156(4)	42(3)
C(30)	2632(5)	5602(11)	3024(3)	38(3)
C(31)	1980(7)	6237(12)	3050(4)	65(4)
C(32)	1535(5)	5164(11)	3200(4)	39(3)
C(33)	2193(5)	6136(10)	4328(4)	35(3)
C(34)	2549(5)	4790(10)	4399(4)	36(3)
C(35)	3220(5)	4962(10)	4288(4)	40(3)
C(36)	3290(5)	6403(11)	4142(4)	45(3)
C(37)	2630(5)	7166(11)	4145(4)	44(3)
C(38)	1450(5)	6475(10)	4385(4)	37(3)
C(39)	1285(5)	7851(10)	4504(4)	39(3)
C(40)	611(6)	8106(12)	4596(4)	51(4)
C(41)	158(6)	7038(12)	4613(5)	57(4)
C(42)	341(5)	5639(12)	4478(4)	49(3)
C(43)	1108(5)	1056(11)	3122(4)	38(3)
C(44)	775(5)	-65(12)	3290(4)	46(3)
C(45)	411(6)	-1088(13)	2986(5)	58(4)
C(46)	338(6)	-937(12)	2501(5)	56(4)
C(47)	639(5)	265(14)	2319(4)	53(4)
C(48)	1026(5)	1247(11)	2624(4)	39(3)
C(49)	2481(5)	1204(10)	3710(4)	37(3)
C(50)	2725(5)	434(11)	3346(4)	47(3)
C(51)	3399(6)	-256(11)	3470(4)	49(3)

C(52)	3800(5)	-182(12)	3913(4)	50(3)
C(53)	3554(6)	562(12)	4272(5)	51(4)
C(54)	2884(5)	1201(11)	4163(4)	45(3)
N(1)	4027(4)	5477(9)	5662(3)	45(3)
N(2)	982(4)	5321(9)	4367(3)	41(3)
Cl(1)	5066(1)	2952(3)	6380(1)	53(1)
Cl(2)	3582(2)	1946(3)	5380(1)	60(1)
Cl(3)	1359(1)	1864(3)	4819(1)	51(1)
Cl(4)	-115(1)	2867(3)	3756(1)	55(1)
Fe(1)	2465(1)	6224(2)	6230(1)	39(1)
Fe(2)	2443(1)	5402(1)	3699(1)	34(1)
Zn(1)	3951(1)	3427(1)	5991(1)	38(1)
Zn(2)	1017(1)	3135(1)	4153(1)	36(1)
P(1)	3284(1)	3191(3)	6622(1)	39(1)
P(2)	1661(1)	2248(3)	3554(1)	35(1)

X-ray Data of 5b

Table 1. Crystal data and structure refinement for i0544.

Code	i0544	
Empirical formula	$C_{27}H_{22}Br_2FeNPZn$	
Formula weight	672.47	
Temperature	173(2) K	
Wavelength	0.71073 Å	
crystal system	Monoclinic	
spacegroup	$P2_1$	
Unit cell dimensions	a = 14.6245(6) Å	α = 90°
	b = 9.2633(4) Å	β = 102.744(3)°
	c = 19.3704(7) Å	γ = 90°
Volume	2559.49(18) Å^3	
Z	4	
Density (calculated)	1.745 g/cm^3	
Absorption coefficient	4.705 mm^{-1}	
F(000)	1328	
Crystal size	0.33 mm × 0.23 mm × 0.16 mm	
θ-range for data collection	1.43 → 25.19°	
Index ranges	-17→ h →17, -11→ k →11, -22→ l →23	
Reflections collected	16734	
Independent reflections	8771 [R_{int} = 0.0449]	
Reflections observed	8329	
Absorption correction	Integration	
Max. and min. transmission	0.4668 and 0.3410	
Refinement method	full-matrix least-squares against F^2	
Data / restraints / parameters	8771 / 1 / 596	
Goodness-of-fit on F^2	0.990	
Final R indices [$I > 2\sigma(I)$]	R_1 = 0.0210, wR_2 = 0.0512	
R indices (all data)	R_1 = 0.0225, wR_2 = 0.0516	
Absolute structure parameter	0.00	
Extinction coefficient	0.00070(15)	
Largest diff. peak and hole	0.340 and -0.362 e/Å^3	

Table 2. Atomic coordinates (· 10^4) and equivalent isotropic displacement parameters (A^2 · 10^3) for i0544. U_{eq} is defined as one third of the trace of the orthogonalized U_{ij}tensor.

	x	y	z	U_{eq}

C(1)	-3521(2)	8108(3)	7810(2)	26(1)
C(2)	-3704(2)	6772(4)	7428(2)	27(1)
C(3)	-3449(3)	6949(4)	6765(2)	33(1)
C(4)	-3119(3)	8391(4)	6724(2)	34(1)
C(5)	-3160(2)	9110(4)	7365(2)	31(1)
C(6)	-3723(2)	8420(3)	8505(2)	26(1)
C(7)	-3985(2)	9817(4)	8654(2)	34(1)
C(8)	-4216(3)	10122(4)	9295(2)	42(1)
C(9)	-4206(3)	9008(5)	9768(2)	49(1)
C(10)	-3935(3)	7657(4)	9604(2)	44(1)
C(11)	-1512(2)	5685(3)	8081(2)	27(1)
C(12)	-1339(2)	6988(4)	8497(2)	32(1)
C(13)	-996(2)	8055(4)	8082(2)	36(1)
C(14)	-956(2)	7437(4)	7419(2)	37(1)
C(15)	-1274(2)	5976(4)	7408(2)	32(1)
C(16)	-1329(2)	2931(3)	8849(2)	29(1)
C(17)	-1692(3)	1773(4)	9172(2)	39(1)
C(18)	-1097(3)	761(4)	9560(2)	45(1)
C(19)	-132(3)	887(4)	9638(2)	46(1)
C(20)	229(3)	2036(5)	9324(2)	45(1)
C(21)	-364(3)	3057(4)	8935(2)	36(1)
C(22)	-2552(2)	3192(3)	7489(2)	27(1)
C(23)	-3499(2)	3157(3)	7144(2)	30(1)
C(24)	-3765(3)	2484(4)	6488(2)	33(1)
C(25)	-3112(3)	1832(4)	6175(2)	37(1)
C(26)	-2178(3)	1822(4)	6526(2)	35(1)
C(27)	-1894(2)	2490(4)	7176(2)	32(1)
C(28)	3675(2)	272(4)	7119(2)	28(1)
C(29)	3710(2)	1517(4)	7570(2)	29(1)
C(30)	3607(3)	1027(4)	8247(2)	35(1)
C(31)	3518(3)	-504(4)	8226(2)	37(1)
C(32)	3567(2)	-983(4)	7537(2)	35(1)
C(33)	3828(2)	250(4)	6388(2)	28(1)
C(34)	4286(3)	-943(4)	6181(2)	41(1)
C(35)	4506(3)	-978(5)	5525(2)	47(1)
C(36)	4267(3)	190(5)	5080(2)	43(1)
C(37)	3796(2)	1329(4)	5300(2)	33(1)
C(38)	1408(2)	1754(4)	7033(2)	28(1)
C(39)	1331(2)	1384(4)	7743(2)	33(1)
C(40)	1231(2)	-145(4)	7772(2)	38(1)
C(41)	1247(3)	-717(4)	7088(2)	39(1)
C(42)	1359(2)	441(4)	6639(2)	35(1)
C(43)	607(2)	4222(4)	6196(2)	33(1)
C(44)	572(3)	5679(4)	5994(2)	41(1)
C(45)	-241(3)	6276(5)	5600(2)	50(1)
C(46)	-1027(3)	5424(5)	5389(2)	51(1)
C(47)	-1000(3)	3972(6)	5561(2)	56(1)
C(48)	-184(3)	3371(5)	5970(2)	43(1)
C(49)	1901(2)	4631(3)	7522(2)	28(1)
C(50)	2803(2)	5008(4)	7877(2)	32(1)
C(51)	2953(3)	5799(4)	8498(2)	37(1)
C(52)	2201(3)	6238(4)	8774(2)	40(1)
C(53)	1295(3)	5908(4)	8420(2)	39(1)
C(54)	1140(2)	5095(4)	7802(2)	36(1)
N(1)	-3669(2)	7342(3)	8986(2)	31(1)
N(2)	3572(2)	1380(3)	5944(1)	28(1)
P(1)	-2158(1)	4183(1)	8318(1)	25(1)
P(2)	1693(1)	3507(1)	6729(1)	26(1)
Fe(7)	2464(1)	418(1)	7481(1)	27(1)
Fe(8)	-2307(1)	7328(1)	7574(1)	25(1)
Zn(1)	-3254(1)	5156(1)	8979(1)	26(1)
Zn(2)	2912(1)	3400(1)	6060(1)	25(1)
Br(1)	-4704(1)	3918(1)	8651(1)	36(1)
Br(2)	-2419(1)	4833(1)	10180(1)	39(1)
Br(3)	2079(1)	4077(1)	4892(1)	36(1)

Br(4)	4194(1)	5002(1)	6441(1)	35(1)

X-ray Data of 6b

Table 1. Crystal data and structure refinement for i0501.

Code	i0501	
Empirical formula	$C_{27}H_{22}Br_2CdFeNP$	
Formula weight	719.50	
Temperature	203(2) K	
Wavelength	0.71073 Å	
crystal system	Monoclinic	
spacegroup	$P2_1/c$	
Unit cell dimensions	a = 14.8184(13) Å	α = 90°
	b = 9.3495(6) Å	β = 91.972(7)°
	c = 18.8737(17) Å	γ = 90°
Volume	2613.3(4) Å^3	
Z	4	
Density (calculated)	1.829 g/cm^3	
Absorption coefficient	4.504 mm^{-1}	
F(000)	1400	
Crystal size	0.32 mm × 0.20 mm × 0.02 mm	
θ-range for data collection	1.37 → 25.00°	
Index ranges	-17→ h →17, -11→ k →11, -22→ l →22	
Reflections collected	16395	
Independent reflections	4593 [R_{int} = 0.0789]	
Reflections observed	3022	
Absorption correction	Integration	
Max. and min. transmission	0.9124 and 0.3289	
Refinement method	full-matrix least-squares against F^2	
Data / restraints / parameters	4593 / 0 / 298	
Goodness-of-fit on F^2	0.779	
Final R indices [$I > 2\sigma(I)$]	R_1 = 0.0310, wR_2 = 0.0601	
R indices (all data)	R_1 = 0.0550, wR_2 = 0.0632	
Largest diff. peak and hole	0.728 and -0.450 e/Å^3	

Table 2. Atomic coordinates (· 10^4) and equivalent isotropic displacement parameters (A^2 · 10^3) for i0501. U_{eq} is defined as one third of the trace of the orthogonalized U_{ij}tensor.

	x	y	z	U_{eq}
C(1)	6736(3)	1948(5)	251(2)	43(1)
C(2)	6381(3)	2980(5)	747(3)	50(1)
C(3)	5659(3)	2341(6)	1097(3)	54(1)
C(4)	5545(3)	935(6)	830(3)	49(1)
C(5)	6196(3)	690(5)	317(2)	40(1)
C(6)	7581(3)	-464(5)	1640(2)	39(1)
C(7)	6961(3)	-46(5)	2156(2)	40(1)
C(8)	7139(3)	1388(5)	2346(2)	48(1)
C(9)	7860(3)	1873(5)	1952(3)	49(1)
C(10)	8151(3)	756(5)	1498(2)	41(1)
C(11)	7465(3)	2198(5)	-244(2)	41(1)
C(12)	7617(3)	3583(5)	-498(3)	48(1)
C(13)	8275(3)	3812(6)	-979(3)	57(1)
C(14)	8776(4)	2667(6)	-1222(3)	56(1)
C(15)	8597(3)	1349(6)	-946(3)	52(1)

C(16)	6534(3)	-2970(5)	1267(2)	36(1)
C(17)	5893(3)	-3076(5)	719(3)	41(1)
C(18)	5060(3)	-3690(5)	824(3)	46(1)
C(19)	4856(3)	-4200(5)	1491(3)	51(1)
C(20)	5493(3)	-4114(6)	2042(3)	54(1)
C(21)	6328(3)	-3514(5)	1937(3)	47(1)
C(22)	8458(3)	-3211(5)	1599(2)	38(1)
C(23)	8703(3)	-2957(5)	2310(2)	41(1)
C(24)	9346(3)	-3808(6)	2655(3)	49(1)
C(25)	9726(3)	-4925(6)	2308(3)	52(1)
C(26)	9493(3)	-5209(5)	1607(3)	52(1)
C(27)	8861(3)	-4349(5)	1248(3)	45(1)
N(1)	7964(2)	1071(4)	-468(2)	42(1)
P(1)	7618(1)	-2097(1)	1129(1)	36(1)
Fe(1)	6826(1)	1206(1)	1278(1)	37(1)
Br(1)	9635(1)	-2066(1)	-324(1)	55(1)
Br(2)	6914(1)	-2450(1)	-1130(1)	52(1)
Cd(1)	7985(1)	-1359(1)	-168(1)	40(1)

X-ray Data of 6c

Table 1. Crystal data and structure refinement for i0731.

Code	i0731	
Empirical formula	$C_{27}H_{22}CdFeI_2NP$	
Formula weight	813.48	
Temperature	193(2) K	
Wavelength	0.71073 Å	
crystal system	Triclinic	
spacegroup	$P\bar{1}$	
Unit cell dimensions	a = 10.4638(10) Å	α = 72.904(6)°
	b = 10.5429(8) Å	β = 69.694(7)°
	c = 14.1699(11) Å	γ = 70.125(7)°
Volume	1351.0(2) Å^3	
Z	2	
Density (calculated)	2.000 g/cm^3	
Absorption coefficient	3.684 mm^{-1}	
F(000)	772	
Crystal size	0.36 mm × 0.19 mm × 0.04 mm	
θ-range for data collection	1.56 → 25.00°	
Index ranges	-12→ h →12, -12→ k →12, -16→ l →15	
Reflections collected	8799	
Independent reflections	4481 [R_{int} = 0.0464]	
Reflections observed	3978	
Absorption correction	Integration	
Max. and min. transmission	0.8511 and 0.2744	
Refinement method	full-matrix least-squares against F^2	
Data / restraints / parameters	4481 / 0 / 299	
Goodness-of-fit on F^2	1.111	
Final R indices [$I > 2\sigma(I)$]	R_1 = 0.0282, wR_2 = 0.0758	
R indices (all data)	R_1 = 0.0324, wR_2 = 0.0835	
Extinction coefficient	0.0041(4)	
Largest diff. peak and hole	0.793 and -0.845 e/Å^3	

Table 2. Atomic coordinates (· 10^4) and equivalent isotropic displacement parameters (A^2 · 10^3) for i0731. U_{eq} is defined as one third of the trace of the orthogonalized U_{ij}tensor.

	x	y	z	U_{eq}
C(1)	6107(4)	7162(4)	1238(3)	31(1)
C(2)	4692(4)	7543(5)	1132(3)	41(1)
C(3)	4453(5)	6395(5)	977(4)	43(1)
C(4)	5687(5)	5282(5)	989(4)	43(1)
C(5)	6712(4)	5743(4)	1152(3)	35(1)
C(6)	5416(4)	4699(4)	3651(3)	36(1)
C(7)	4923(4)	6126(5)	3756(3)	38(1)
C(8)	3539(5)	6665(5)	3633(3)	47(1)
C(9)	3145(5)	5610(6)	3466(4)	54(1)
C(10)	4296(5)	4394(5)	3477(4)	45(1)
C(11)	6765(4)	3727(4)	3766(3)	33(1)
C(12)	6915(5)	2314(5)	4009(4)	45(1)
C(13)	8142(6)	1401(5)	4186(4)	52(1)
C(14)	9223(5)	1897(5)	4157(4)	48(1)
C(15)	9030(5)	3316(5)	3897(4)	41(1)
C(16)	5555(4)	9526(4)	2092(3)	34(1)
C(17)	5271(4)	9609(4)	3106(3)	38(1)
C(18)	4180(5)	10652(5)	3512(4)	45(1)
C(19)	3366(5)	11638(5)	2917(4)	47(1)
C(20)	3669(5)	11583(5)	1889(5)	52(1)
C(21)	4745(5)	10539(5)	1479(4)	44(1)
C(22)	7975(4)	8927(4)	333(3)	34(1)
C(23)	8734(5)	8136(5)	-410(4)	47(1)
C(24)	9549(6)	8663(7)	-1356(4)	66(2)
C(25)	9596(6)	10012(7)	-1557(5)	67(2)
C(26)	8869(5)	10808(5)	-823(5)	61(2)
C(27)	8059(5)	10264(5)	128(5)	50(1)
N(1)	7850(3)	4213(3)	3668(3)	34(1)
P(1)	6959(1)	8121(1)	1565(1)	29(1)
Fe(1)	4934(1)	5965(1)	2347(1)	32(1)
Cd(1)	8408(1)	6330(1)	2768(1)	29(1)
I(1)	8628(1)	7283(1)	4287(1)	41(1)
I(2)	10892(1)	5202(1)	1428(1)	40(1)

X-ray Data of 7

Table 1. Crystal data and structure refinement for i0609a.

Code	i0609a	
Empirical formula	$C_{54}H_{44}CdCl_2Fe_2N_2P_2$	
Formula weight	1077.85	
Temperature	173(2) K	
Wavelength	0.71073 Å	
crystal system	Orthorhombic	
spacegroup	$Fdd2$	
Unit cell dimensions	a = 49.456(5) Å	α = 90°
	b = 22.4070(14) Å	β = 90°
	c = 8.2534(7) Å	γ = 90°
Volume	9146.0(13) Å^3	
Z	8	
Density (calculated)	1.566 g/cm^3	
Absorption coefficient	1.314 mm^{-1}	
F(000)	4368	
Crystal size	0.43 mm × 0.04 mm × 0.03 mm	
θ-range for data collection	1.65 → 24.99°	
Index ranges	-58→ h →58, -24→ k →24, -9→ l →9	
Reflections collected	14627	
Independent reflections	3764 [R_{int} = 0.0896]	

Reflections observed	2968
Absorption correction	Integration
Max. and min. transmission	0.9679 and 0.6208
Refinement method	full-matrix least-squares against F^2
Data / restraints / parameters	3764 / 1 / 285
Goodness-of-fit on F^2	0.919
Final R indices [$I > 2\sigma(I)$]	R_1 = 0.0408, wR_2 = 0.0759
R indices (all data)	R_1 = 0.0568, wR_2 = 0.0797
Absolute structure parameter	0.01(3)
Largest diff. peak and hole	0.470 and -0.950 $e/$Å^3

Table 2. Atomic coordinates ($\cdot$ 10^4) and equivalent isotropic displacement parameters ($A^2 \cdot 10^3$) for i0609a. U_{eq} is defined as one third of the trace of the orthogonalized U_{ij}tensor.

	x	y	z	U_{eq}
C(1)	1096(1)	-465(3)	1267(8)	38(2)
C(2)	831(1)	-536(3)	579(7)	39(2)
C(3)	692(1)	-992(3)	1410(8)	43(2)
C(4)	867(1)	-1220(3)	2617(9)	43(2)
C(5)	1115(1)	-915(3)	2545(8)	39(2)
C(6)	555(1)	393(3)	3213(7)	34(2)
C(7)	477(1)	-65(3)	4335(7)	38(2)
C(8)	699(1)	-179(3)	5361(9)	45(2)
C(9)	914(1)	192(3)	4920(7)	39(2)
C(10)	830(1)	551(3)	3604(7)	38(2)
C(11)	1305(1)	-30(4)	862(7)	38(2)
C(12)	1249(1)	455(3)	-167(8)	43(2)
C(13)	1449(1)	865(4)	-493(8)	48(2)
C(14)	1705(1)	782(4)	179(10)	51(2)
C(15)	1740(1)	295(4)	1166(9)	50(2)
C(16)	134(1)	1270(3)	2691(8)	33(1)
C(17)	4(1)	1702(3)	1770(7)	38(2)
C(18)	-166(1)	2114(3)	2478(9)	45(2)
C(19)	-213(1)	2096(4)	4149(9)	45(2)
C(20)	-85(1)	1667(3)	5088(10)	44(2)
C(21)	83(1)	1263(4)	4393(8)	41(2)
C(22)	537(1)	1118(3)	269(8)	29(1)
C(23)	693(1)	1601(3)	804(8)	37(2)
C(24)	832(1)	1954(3)	-302(8)	42(2)
C(25)	815(1)	1833(3)	-1972(9)	43(2)
C(26)	665(1)	1356(3)	-2494(8)	43(2)
C(27)	528(1)	991(3)	-1400(7)	39(2)
N(1)	1552(1)	-118(3)	1528(7)	45(2)
P(1)	332(1)	692(1)	1684(2)	31(1)
Cl(1)	215(1)	-715(1)	-1664(2)	43(1)
Fe(1)	803(1)	-326(1)	2992(1)	33(1)
Cd(1)	0	0	170(1)	33(1)

X-ray Data of 8b

Table 1. Crystal data and structure refinement for i0507a.

Code	i0507a
Empirical formula	$C_{27}H_{22}Br_2FeHgNP$
Formula weight	807.69
Temperature	100(2) K

Wavelength	0.71073 Å	
crystal system	Triclinic	
spacegroup	$P\bar{1}$	
Unit cell dimensions	a = 10.1471(10) Å	α = 104.921(8)°
	b = 10.3258(10) Å	β = 92.316(8)°
	c = 13.6179(13) Å	γ = 110.214(8)°
Volume	1280.6(2) Å^3	
Z	2	
Density (calculated)	2.095 g/cm^3	
Absorption coefficient	9.752 mm^{-1}	
F(000)	764	
Crystal size	0.18 mm × 0.16 mm × 0.05 mm	
θ-range for data collection	1.56 → 25.00°	
Index ranges	-12→ h →11, -12→ k →12, -16→ l →16	
Reflections collected	9514	
Independent reflections	4485 [R_{int} = 0.0411]	
Reflections observed	4156	
Absorption correction	Integration	
Max. and min. transmission	0.5998 and 0.2161	
Refinement method	full-matrix least-squares against F^2	
Data / restraints / parameters	4485 / 0 / 298	
Goodness-of-fit on F^2	1.002	
Final R indices [$I > 2\sigma(I)$]	R_1 = 0.0224, wR_2 = 0.0529	
R indices (all data)	R_1 = 0.0249, wR_2 = 0.0536	
Largest diff. peak and hole	1.628 and -1.305 e/Å^3	

Table 2. Atomic coordinates (· 10^4) and equivalent isotropic displacement parameters (A^2 · 10^3) for i0507a. U_{eq} is defined as one third of the trace of the orthogonalized U_{ij}tensor.

	x	y	z	U_{eq}
C(1)	-2609(4)	1202(4)	3776(3)	20(1)
C(2)	-2932(5)	-227(4)	3898(3)	24(1)
C(3)	-1626(5)	-422(4)	4059(3)	27(1)
C(4)	-493(5)	863(4)	4046(3)	28(1)
C(5)	-1072(4)	1870(4)	3870(3)	23(1)
C(6)	-1175(4)	455(4)	1364(3)	20(1)
C(7)	-2702(4)	-132(4)	1237(3)	22(1)
C(8)	-3124(5)	-1542(4)	1384(3)	30(1)
C(9)	-1891(5)	-1818(4)	1611(3)	31(1)
C(10)	-685(5)	-597(4)	1599(3)	27(1)
C(11)	-262(4)	1865(4)	1247(3)	20(1)
C(12)	1112(4)	2072(4)	1010(3)	25(1)
C(13)	1915(4)	3355(4)	812(3)	28(1)
C(14)	1327(4)	4390(4)	843(3)	26(1)
C(15)	-34(4)	4119(4)	1099(3)	26(1)
C(16)	-4079(4)	3048(4)	4694(3)	21(1)
C(17)	-2884(5)	3870(4)	5439(3)	28(1)
C(18)	-3033(6)	4670(5)	6404(3)	37(1)
C(19)	-4360(6)	4660(5)	6612(3)	35(1)
C(20)	-5542(5)	3867(4)	5867(4)	34(1)
C(21)	-5413(4)	3068(4)	4899(3)	26(1)
C(22)	-5473(4)	553(4)	2882(3)	22(1)
C(23)	-5963(4)	241(4)	1838(3)	24(1)
C(24)	-7189(5)	-953(4)	1374(3)	31(1)
C(25)	-7956(5)	-1802(4)	1955(4)	36(1)
C(26)	-7499(5)	-1474(4)	3007(4)	35(1)
C(27)	-6264(5)	-307(4)	3465(3)	29(1)
N	-822(3)	2902(3)	1323(2)	22(1)
P	-3800(1)	2016(1)	3468(1)	18(1)
Fe	-1857(1)	6(1)	2683(1)	19(1)
Br(1)	-799(1)	5905(1)	3491(1)	24(1)

Br(2)	-3938(1)	3837(1)	806(1)	27(1)
Hg	-2731(1)	3476(1)	2344(1)	19(1)

X-ray Data of 8c

Table 1. Crystal data and structure refinement for i0800.

Code	i0800	
Empirical formula	$C_{56}H_{46}Cl_6Fe_2Hg_2I_4N_2P_2$	
Formula weight	2042.07	
Temperature	100(2) K	
Wavelength	0.71073 Å	
crystal system	Triclinic	
spacegroup	$P\bar{1}$	
Unit cell dimensions	a = 9.5405(11) Å	α = 79.405(11)°
	b = 9.8309(13) Å	β = 86.852(10)°
	c = 16.591(2) Å	γ = 89.624(10)°
Volume	1527.2(3) Å^3	
Z	1	
Density (calculated)	2.220 g/cm^3	
Absorption coefficient	7.851 mm^{-1}	
F(000)	952	
Crystal size	0.11 mm × 0.11 mm × 0.01 mm	
θ-range for data collection	1.25 → 25.00°	
Index ranges	-10→ h →11, -11→ k →11, -19→ l →19	
Reflections collected	10365	
Independent reflections	5303 [R_{int} = 0.0879]	
Reflections observed	3609	
Absorption correction	Integration	
Max. and min. transmission	0.9181 and 0.4544	
Refinement method	full-matrix least-squares against F^2	
Data / restraints / parameters	5303 / 0 / 335	
Goodness-of-fit on F^2	0.931	
Final R indices [$I > 2\sigma(I)$]	R_1 = 0.0538, wR_2 = 0.1220	
R indices (all data)	R_1 = 0.0832, wR_2 = 0.1345	
Extinction coefficient	0.0026(3)	
Largest diff. peak and hole	1.149 and -1.866 e/Å^3	

Table 2. Atomic coordinates (· 10^4) and equivalent isotropic displacement parameters (A^2 · 10^3) for i0800. U_{eq} is defined as one third of the trace of the orthogonalized U_{ij}tensor.

	x	y	z	U_{eq}
C(1)	10464(13)	1964(12)	3040(8)	41(3)
C(2)	9356(15)	1160(14)	3513(10)	54(3)
C(3)	9138(14)	-23(12)	3186(8)	42(3)
C(4)	10069(14)	3(13)	2489(9)	46(3)
C(5)	10905(14)	1232(12)	2409(8)	43(3)
C(6)	6849(13)	1624(13)	1934(8)	41(3)
C(7)	7879(14)	1733(13)	1265(8)	43(3)
C(8)	8617(14)	3005(13)	1190(9)	46(3)
C(9)	8063(14)	3679(12)	1832(8)	44(3)
C(10)	6958(12)	2834(12)	2296(8)	39(3)
C(11)	5788(13)	492(13)	2221(8)	42(3)
C(12)	4820(12)	530(13)	2862(8)	39(3)
C(13)	3828(14)	-496(13)	3061(9)	47(3)

C(14)	3835(14)	-1546(14)	2581(9)	51(3)
C(15)	4873(13)	-1530(13)	1969(9)	46(3)
C(16)	11959(14)	4510(14)	2308(8)	46(3)
C(17)	11237(15)	5721(13)	1917(10)	51(3)
C(18)	11807(15)	6424(14)	1192(10)	56(4)
C(19)	13061(17)	6019(16)	831(10)	62(4)
C(20)	13782(17)	4879(14)	1213(10)	59(4)
C(21)	13214(14)	4108(13)	1957(9)	48(3)
C(22)	12590(11)	2950(12)	3949(8)	37(3)
C(23)	13767(14)	3817(14)	3950(8)	48(3)
C(24)	14816(12)	3399(13)	4479(8)	42(3)
C(25)	14726(13)	2109(13)	5012(8)	43(3)
C(26)	13585(15)	1248(15)	5015(9)	51(3)
C(27)	12496(12)	1688(12)	4478(8)	39(3)
C(28)	12813(15)	1705(16)	-250(9)	56(4)
N(1)	5858(11)	-533(10)	1755(7)	44(2)
P(1)	11176(3)	3523(3)	3267(2)	40(1)
Fe(1)	8842(2)	1745(2)	2329(1)	40(1)
I(1)	7228(1)	6374(1)	3245(1)	47(1)
I(2)	8737(1)	3147(1)	5498(1)	44(1)
Hg(1)	9346(1)	4840(1)	3909(1)	44(1)
Cl(1)	12501(5)	3484(4)	-571(3)	77(1)
Cl(2)	14154(5)	1460(5)	465(3)	75(1)
Cl(3)	11251(5)	880(5)	220(3)	85(1)

X-ray Data of 9a

Table 1. Crystal data and structure refinement for i0528.

Code	i0528	
Empirical formula	$C_{54}H_{44}Cl_2Fe_2HgN_2P_2$	
Formula weight	1166.04	
Temperature	203(2) K	
Wavelength	0.71073 Å	
crystal system	Monoclinic	
spacegroup	$P2_1/n$	
Unit cell dimensions	a = 17.1944(5) Å	α = 90°
	b = 15.4843(5) Å	β = 92.045(2)°
	c = 17.6894(5) Å	γ = 90°
Volume	4706.7(2) Å^3	
Z	4	
Density (calculated)	1.646 g/cm^3	
Absorption coefficient	4.083 mm^{-1}	
F(000)	2312	
Crystal size	0.60 mm × 0.45 mm × 0.13 mm	
θ-range for data collection	1.62 → 25.73°	
Index ranges	-20→ h →20, -18→ k →18, -21→ l →21	
Reflections collected	63890	
Independent reflections	8920 [R_{int} = 0.0814]	
Reflections observed	7954	
Absorption correction	Integration	
Max. and min. transmission	0.3889 and 0.0689	
Refinement method	full-matrix least-squares against F^2	
Data / restraints / parameters	8920 / 0 / 568	
Goodness-of-fit on F^2	1.024	
Final R indices [$I > 2\sigma(I)$]	R_1 = 0.0276, wR_2 = 0.0702	
R indices (all data)	R_1 = 0.0318, wR_2 = 0.0720	
Largest diff. peak and hole	0.864 and -2.387 e/Å^3	

Table 2. Atomic coordinates ($\cdot 10^4$) and equivalent isotropic displacement parameters ($A^2 \cdot 10^3$) for i0528. U_{eq} is defined as one third of the trace of the orthogonalized U_{ij}tensor.

	x	y	z	U_{eq}
C(1)	2736(1)	9636(2)	-1452(2)	31(1)
C(2)	2600(2)	10322(2)	-1997(2)	36(1)
C(3)	3113(2)	10192(2)	-2601(2)	41(1)
C(4)	3561(2)	9439(2)	-2447(2)	43(1)
C(5)	3331(2)	9091(2)	-1746(2)	37(1)
C(6)	2166(2)	8472(2)	-3474(2)	39(1)
C(7)	1590(2)	9135(2)	-3382(2)	43(1)
C(8)	1206(2)	8973(2)	-2696(2)	49(1)
C(9)	1534(2)	8221(2)	-2362(2)	49(1)
C(10)	2128(2)	7905(2)	-2831(2)	43(1)
C(11)	2705(2)	8389(2)	-4101(2)	40(1)
C(12)	2656(2)	8941(2)	-4720(2)	57(1)
C(13)	3154(2)	8809(2)	-5316(2)	64(1)
C(14)	3692(2)	8155(2)	-5260(2)	57(1)
C(15)	3710(2)	7652(2)	-4626(2)	55(1)
C(16)	2579(1)	10319(2)	68(1)	31(1)
C(17)	2923(2)	11076(2)	-179(2)	43(1)
C(18)	3096(2)	11742(2)	335(2)	52(1)
C(19)	2918(2)	11658(2)	1082(2)	53(1)
C(20)	2603(2)	10895(2)	1338(2)	54(1)
C(21)	2432(2)	10224(2)	837(2)	42(1)
C(22)	1223(1)	9662(2)	-765(1)	32(1)
C(23)	962(2)	10491(2)	-967(2)	38(1)
C(24)	178(2)	10635(2)	-1141(2)	48(1)
C(25)	-347(2)	9959(2)	-1118(2)	50(1)
C(26)	-102(2)	9140(2)	-904(2)	46(1)
C(27)	684(2)	8982(2)	-725(2)	38(1)
C(28)	4457(2)	7999(2)	732(2)	34(1)
C(29)	4337(2)	8908(2)	864(2)	38(1)
C(30)	4980(2)	9216(2)	1315(2)	44(1)
C(31)	5500(2)	8517(2)	1466(2)	45(1)
C(32)	5185(2)	7759(2)	1104(2)	40(1)
C(33)	4160(2)	8694(2)	2902(2)	38(1)
C(34)	4609(2)	7910(2)	2965(2)	45(1)
C(35)	4179(2)	7241(2)	2588(2)	48(1)
C(36)	3464(2)	7602(2)	2293(2)	46(1)
C(37)	3454(2)	8495(2)	2486(2)	41(1)
C(38)	4362(2)	9547(2)	3231(2)	39(1)
C(39)	4994(2)	9660(2)	3732(2)	48(1)
C(40)	5117(2)	10463(2)	4060(2)	60(1)
C(41)	4610(2)	11133(2)	3881(2)	63(1)
C(42)	3999(2)	10965(2)	3368(2)	60(1)
C(43)	3788(2)	6264(2)	619(2)	38(1)
C(44)	3122(2)	5993(2)	988(2)	42(1)
C(45)	3131(2)	5230(2)	1407(2)	52(1)
C(46)	3803(2)	4726(2)	1441(2)	62(1)
C(47)	4448(2)	4974(2)	1060(2)	64(1)
C(48)	4455(2)	5741(2)	649(2)	52(1)
C(49)	4233(2)	7216(2)	-734(2)	36(1)
C(50)	3877(2)	6684(2)	-1290(2)	46(1)
C(51)	4161(2)	6673(3)	-2015(2)	62(1)
C(52)	4783(2)	7196(3)	-2202(2)	66(1)
C(53)	5133(2)	7720(3)	-1663(2)	60(1)
C(54)	4865(2)	7727(2)	-929(2)	47(1)
Cl(1)	1695(1)	8068(1)	1181(1)	46(1)
Cl(2)	1768(1)	6776(1)	-719(1)	54(1)
Fe(1)	2383(1)	9145(1)	-2486(1)	33(1)
Fe(2)	4415(1)	8229(1)	1856(1)	34(1)
Hg(1)	2482(1)	7998(1)	-16(1)	34(1)
N(1)	3236(2)	7744(2)	-4044(2)	48(1)

N(2)	3864(2)	10198(2)	3043(2)	51(1)
P(1)	2255(1)	9457(1)	-579(1)	29(1)
P(2)	3795(1)	7331(1)	183(1)	32(1)

X-ray Data of 9b

Table 1. Crystal data and structure refinement for i0634.

Code	i0634	
Empirical formula	$C_{54}H_{44}Br_2Fe_2HgN_2P_2$	
Formula weight	1254.96	
Temperature	173(2) K	
Wavelength	0.71073 Å	
crystal system	Monoclinic	
spacegroup	$P2_1/n$	
Unit cell dimensions	a = 17.4068(8) Å	α = 90°
	b = 15.5806(5) Å	β = 92.161(4)°
	c = 17.5380(8) Å	γ = 90°
Volume	4753.1(3) Å^3	
Z	4	
Density (calculated)	1.754 g/cm^3	
Absorption coefficient	5.612 mm^{-1}	
F(000)	2456	
Crystal size	0.42 mm × 0.283 mm × 0.17 mm	
θ-range for data collection	1.62 → 25.00°	
Index ranges	-20→ h →20, -18→ k →17, -20→ l →20	
Reflections collected	30291	
Independent reflections	8305 [R_{int} = 0.0776]	
Reflections observed	7436	
Absorption correction	Integration	
Max. and min. transmission	0.7179 and 0.3150	
Refinement method	full-matrix least-squares against F^2	
Data / restraints / parameters	8305 / 0 / 569	
Goodness-of-fit on F^2	1.085	
Final R indices [$I > 2\sigma(I)$]	R_1 = 0.0474, wR_2 = 0.1142	
R indices (all data)	R_1 = 0.0513, wR_2 = 0.1165	
Extinction coefficient	0.00075(10)	
Largest diff. peak and hole	4.258 and -2.843 e/Å^3	

Table 2. Atomic coordinates (· 10^4) and equivalent isotropic displacement parameters (A^2 · 10^3) for i0634. U_{eq} is defined as one third of the trace of the orthogonalized U_{ij}tensor.

	x	y	z	U_{eq}
C(1)	9469(3)	2001(3)	5772(3)	29(1)
C(2)	10201(3)	2237(4)	6144(3)	35(1)
C(3)	10521(3)	1495(4)	6491(3)	40(1)
C(4)	10006(3)	795(4)	6357(3)	40(1)
C(5)	9361(3)	1101(4)	5910(3)	36(1)
C(6)	9213(3)	1298(4)	7964(3)	33(1)
C(7)	9691(3)	2066(4)	8030(3)	38(1)
C(8)	9271(3)	2752(4)	7670(3)	42(1)
C(9)	8548(3)	2431(4)	7377(3)	40(1)
C(10)	8514(3)	1538(4)	7558(3)	34(1)
C(11)	9394(3)	441(4)	8271(3)	35(1)
C(12)	10023(3)	299(4)	8765(3)	45(1)

C(13)	10134(4)	-518(5)	9077(3)	52(2)
C(14)	9621(4)	-1164(5)	8870(4)	55(2)
C(15)	9015(4)	-967(5)	8359(4)	57(2)
C(16)	8790(3)	3718(4)	5665(3)	36(1)
C(17)	9448(3)	4251(4)	5676(4)	47(1)
C(18)	9440(4)	5024(5)	6074(4)	58(2)
C(19)	8801(4)	5267(4)	6469(4)	57(2)
C(20)	8142(3)	4758(4)	6440(3)	46(1)
C(21)	8140(3)	3985(4)	6029(3)	37(1)
C(22)	9228(3)	2769(4)	4294(3)	32(1)
C(23)	9838(3)	2254(4)	4088(3)	42(1)
C(24)	10098(3)	2269(5)	3349(3)	52(2)
C(25)	9750(4)	2814(5)	2809(3)	58(2)
C(26)	9146(3)	3344(5)	3020(3)	55(2)
C(27)	8875(3)	3321(4)	3753(3)	42(1)
C(28)	7743(2)	378(3)	3566(2)	28(1)
C(29)	8315(3)	943(4)	3271(3)	35(1)
C(30)	8549(3)	611(4)	2560(3)	40(1)
C(31)	8119(3)	-153(4)	2407(3)	39(1)
C(32)	7624(3)	-309(3)	3015(3)	33(1)
C(33)	7144(3)	1522(4)	1529(3)	36(1)
C(34)	6590(3)	855(4)	1627(3)	40(1)
C(35)	6208(3)	1000(4)	2320(3)	43(1)
C(36)	6521(3)	1757(4)	2663(3)	43(1)
C(37)	7094(3)	2087(4)	2184(3)	37(1)
C(38)	7673(3)	1620(4)	904(3)	37(1)
C(39)	7630(3)	1084(5)	264(3)	47(1)
C(40)	8110(4)	1226(5)	-328(3)	57(2)
C(41)	8647(4)	1892(4)	-269(4)	53(2)
C(42)	8657(4)	2368(4)	378(3)	50(1)
C(43)	6258(2)	337(3)	4270(2)	28(1)
C(44)	6000(3)	-480(4)	4040(3)	36(1)
C(45)	5222(3)	-613(4)	3861(3)	42(1)
C(46)	4696(3)	56(4)	3904(3)	43(1)
C(47)	4949(3)	858(4)	4139(3)	39(1)
C(48)	5727(3)	1007(4)	4331(3)	34(1)
C(49)	7602(2)	-337(4)	5087(3)	30(1)
C(50)	7981(3)	-1062(4)	4823(3)	39(1)
C(51)	8157(3)	-1746(4)	5321(4)	46(1)
C(52)	7957(3)	-1710(4)	6073(3)	46(1)
C(53)	7596(4)	-985(4)	6343(3)	49(1)
C(54)	7423(3)	-301(4)	5855(3)	40(1)
N(36)	8880(3)	-183(3)	8068(3)	47(1)
N(54)	8192(3)	2265(3)	968(3)	43(1)
P(1)	8806(1)	2655(1)	5230(1)	28(1)
P(2)	7279(1)	535(1)	4459(1)	26(1)
Fe(1)	9462(1)	1777(1)	6911(1)	30(1)
Fe(2)	7377(1)	860(1)	2530(1)	30(1)
Br(1)	6710(1)	1875(1)	6329(1)	38(1)
Br(2)	6772(1)	3265(1)	4338(1)	45(1)
Hg(1)	7510(1)	1971(1)	5055(1)	30(1)

X-ray Data of 10

Table 1. Crystal data and structure refinement for i0818.

Code	i0818
Empirical formula	$C_{27}H_{22}Br_2FeNPZn$
Formula weight	672.47
Temperature	173(2) K

Wavelength	0.71073 Å	
crystal system	Monoclinic	
spacegroup	$P2_1/c$	
Unit cell dimensions	a = 15.3284(10) Å	α = 90°
	b = 9.0578(6) Å	β = 96.220(5)°
	c = 18.4976(10) Å	γ = 90°
Volume	2553.1(3) Å^3	
Z	4	
Density (calculated)	1.749 g/cm^3	
Absorption coefficient	4.716 mm^{-1}	
F(000)	1328	
Crystal size	0.13 mm × 0.12 mm × 0.09 mm	
θ-range for data collection	1.34 → 25.00°	
Index ranges	-18→ h →18, -10→ k →10, -21→ l →21	
Reflections collected	16069	
Independent reflections	4461 [R_{int} = 0.0776]	
Reflections observed	3378	
Absorption correction	Integration	
Max. and min. transmission	0.6663 and 0.5464	
Refinement method	full-matrix least-squares against F^2	
Data / restraints / parameters	4461 / 0 / 298	
Goodness-of-fit on F^2	0.930	
Final R indices [$I > 2\sigma(I)$]	R_1 = 0.0408, wR_2 = 0.0861	
R indices (all data)	R_1 = 0.0595, wR_2 = 0.0915	
Largest diff. peak and hole	2.014 and -0.747 e/Å^3	

Table 2. Atomic coordinates (· 10^4) and equivalent isotropic displacement parameters (A^2 · 10^3) for i0818. U_{eq} is defined as one third of the trace of the orthogonalized U_{ij} tensor.

	x	y	z	U_{eq}
C(1)	6518(3)	3105(5)	1737(3)	23(1)
C(2)	6360(3)	2789(5)	2476(3)	26(1)
C(3)	5646(3)	3682(6)	2647(3)	30(1)
C(4)	5351(3)	4552(6)	2021(3)	31(1)
C(5)	5880(3)	4205(5)	1458(3)	27(1)
C(6)	7728(3)	5575(5)	3084(3)	24(1)
C(7)	6960(3)	6392(5)	3218(3)	29(1)
C(8)	6677(4)	7204(5)	2570(3)	32(1)
C(9)	7257(3)	6875(5)	2036(3)	30(1)
C(10)	7902(3)	5870(5)	2350(3)	24(1)
C(11)	8266(3)	4614(5)	3618(3)	22(1)
C(12)	9182(3)	4716(5)	3706(3)	29(1)
C(13)	9661(3)	3825(6)	4221(3)	31(1)
C(14)	9224(3)	2859(6)	4638(3)	27(1)
C(15)	7874(3)	3632(5)	4057(3)	26(1)
C(16)	8177(3)	1614(5)	1879(3)	27(1)
C(17)	8983(3)	2371(6)	1954(3)	32(1)
C(18)	9625(4)	1979(6)	2504(3)	40(1)
C(19)	9479(4)	872(6)	2983(3)	41(1)
C(20)	8683(4)	94(7)	2909(4)	47(2)
C(21)	8044(4)	474(6)	2355(3)	33(1)
C(22)	6739(3)	536(5)	866(3)	23(1)
C(23)	7206(3)	-476(5)	486(3)	28(1)
C(24)	6788(4)	-1743(5)	174(3)	31(1)
C(25)	5917(4)	-2010(6)	256(3)	36(1)
C(26)	5453(4)	-1022(5)	650(3)	31(1)
C(27)	5867(3)	244(6)	950(3)	30(1)
N(1)	8335(3)	2767(4)	4558(2)	26(1)
P(1)	7293(1)	2239(1)	1205(1)	24(1)
Fe(1)	6656(1)	4984(1)	2357(1)	21(1)
Zn(1)	7675(1)	3708(1)	165(1)	24(1)

Br(1)	8679(1)	5680(1)	444(1)	32(1)
Br(2)	6330(1)	4184(1)	-570(1)	28(1)

X-ray Data of 12

Table 1. Crystal data and structure refinement for i0626.

Code	i0626	
Empirical formula	$C_{27}H_{22}Br_2FeHgNP$	
Formula weight	807.69	
Temperature	173(2) K	
Wavelength	0.71073 Å	
crystal system	Monoclinic	
spacegroup	$P2_1/c$	
Unit cell dimensions	a = 16.0531 Å	α = 90°
	b = 8.9781(4) Å	β = 105.934(4)°
	c = 19.1000(11) Å	γ = 90°
Volume	2647.0(2) Å^3	
Z	4	
Density (calculated)	2.027 g/cm^3	
Absorption coefficient	9.436 mm^{-1}	
F(000)	1528	
Crystal size	0.60 mm × 0.45 mm × 0.09 mm	
θ-range for data collection	1.32 → 25.23°	
Index ranges	-19→ h →17, -10→ k →10, -22→ l →22	
Reflections collected	16588	
Independent reflections	4720 [R_{int} = 0.0518]	
Reflections observed	4423	
Absorption correction	Integration	
Max. and min. transmission	0.3925 and 0.0502	
Refinement method	full-matrix least-squares against F^2	
Data / restraints / parameters	4720 / 0 / 299	
Goodness-of-fit on F^2	1.167	
Final R indices [$I > 2\sigma(I)$]	R_1 = 0.0261, wR_2 = 0.0723	
R indices (all data)	R_1 = 0.0285, wR_2 = 0.0734	
Extinction coefficient	0.00250(16)	
Largest diff. peak and hole	0.933 and -0.731 e/Å^3	

Table 2. Atomic coordinates (· 10^4) and equivalent isotropic displacement parameters (A^2 · 10^3) for i0626. U_{eq} is defined as one third of the trace of the orthogonalized U_{ij}tensor.

	x	y	z	U_{eq}
C(1)	1483(2)	2106(4)	-1282(2)	31(1)
C(2)	835(2)	1015(5)	-1230(2)	35(1)
C(3)	350(3)	657(5)	-1948(3)	43(1)
C(4)	684(3)	1484(5)	-2448(3)	41(1)
C(5)	1378(2)	2387(5)	-2047(2)	35(1)
C(6)	2737(2)	-403(4)	-2097(2)	34(1)
C(7)	2868(3)	-679(4)	-1334(2)	37(1)
C(8)	2216(3)	-1701(5)	-1254(3)	42(1)
C(9)	1691(3)	-2073(5)	-1965(3)	45(1)
C(10)	2008(3)	-1272(4)	-2481(3)	40(1)
C(11)	3268(2)	599(4)	-2426(2)	34(1)
C(12)	4139(2)	867(5)	-2087(2)	40(1)
C(13)	4604(2)	1808(6)	-2420(3)	45(1)

C(14)	4190(2)	2469(5)	-3077(2)	41(1)
C(15)	2902(3)	1314(4)	-3079(2)	34(1)
C(16)	3166(3)	3605(4)	-767(3)	37(1)
C(17)	3975(2)	3006(5)	-426(3)	42(1)
C(18)	4705(3)	3532(6)	-613(4)	55(1)
C(19)	4626(3)	4606(6)	-1131(4)	63(2)
C(20)	3825(3)	5211(6)	-1472(4)	64(2)
C(21)	3091(3)	4718(5)	-1290(3)	50(1)
C(22)	1665(2)	4639(4)	-327(2)	33(1)
C(23)	2110(3)	5594(5)	228(2)	37(1)
C(24)	1688(3)	6830(5)	412(3)	41(1)
C(25)	832(3)	7126(5)	37(3)	45(1)
C(26)	397(3)	6193(5)	-509(3)	47(1)
C(27)	805(3)	4937(5)	-698(2)	41(1)
Fe(1)	1642(1)	182(1)	-1796(1)	31(1)
N(1)	3347(2)	2227(4)	-3406(2)	36(1)
P(1)	2212(1)	2965(1)	-514(1)	30(1)
Hg(1)	2549(1)	1318(1)	545(1)	33(1)
Br(1)	3680(1)	-782(1)	733(1)	47(1)
Br(2)	1301(1)	720(1)	1114(1)	47(1)

X-ray Data of 13

Table 1. Crystal data and structure refinement for i772.

Code	i772	
Empirical formula	$C_{28}H_{24}Br_2FeNPZn$	
Formula weight	686.49	
Temperature	218(2) K	
Wavelength	0.71073 Å	
crystal system	Monoclinic	
spacegroup	$P2_1/n$	
Unit cell dimensions	a = 9.2769(5) Å	α = 90°
	b = 18.5543(9) Å	β = 93.655(4)°
	c = 15.1266(8) Å	γ = 90°
Volume	2559.49(18) Å^3	
Z	4	
Density (calculated)	1.745 g/cm^3	
Absorption coefficient	4.705 mm^{-1}	
F(000)	1328	
Crystal size	0.33 mm × 0.23 mm × 0.04 mm	
θ-range for data collection	1.74 → 25.00°	
Index ranges	-11→ h →9, -22→ k →22, -17→ l →17	
Reflections collected	14373	
Independent reflections	4562 [R_{int} = 0.0445]	
Reflections observed	3659	
Absorption correction	Integration	
Max. and min. transmission	0.7870 and 0.2810	
Refinement method	full-matrix least-squares against F^2	
Data / restraints / parameters	4562 / 0 / 307	
Goodness-of-fit on F^2	0.981	
Final R indices [$I > 2\sigma(I)$]	R_1 = 0.0296, wR_2 = 0.0685	
R indices (all data)	R_1 = 0.0419, wR_2 = 0.0714	
Largest diff. peak and hole	0.999 and -0.646 e/Å^3	

Table 2. Atomic coordinates (· 10^4) and equivalent isotropic displacement parameters (A^2 · 10^3) for i772. U_{eq} is defined as one third of the trace of the orthogonalized U_{ij}tensor.

	x	y	z	U_{eq}
C(1)	-21(3)	1337(2)	3508(2)	30(1)
C(2)	-147(4)	925(2)	4315(2)	37(1)
C(3)	836(4)	1226(2)	4976(2)	48(1)
C(4)	1553(4)	1817(2)	4605(3)	48(1)
C(5)	1040(4)	1890(2)	3698(2)	39(1)
C(6)	2774(3)	287(2)	2913(2)	31(1)
C(7)	2471(4)	-159(2)	3651(2)	41(1)
C(8)	3272(4)	106(2)	4413(2)	45(1)
C(9)	4073(4)	720(2)	4166(2)	43(1)
C(10)	3767(3)	830(2)	3235(2)	35(1)
C(11)	2230(4)	167(2)	1966(2)	33(1)
C(12)	2998(3)	628(2)	1314(2)	31(1)
C(13)	4366(4)	436(2)	1086(2)	39(1)
C(14)	5081(4)	858(2)	498(2)	46(1)
C(15)	4404(4)	1465(2)	154(2)	46(1)
C(16)	3055(4)	1641(2)	421(2)	41(1)
C(17)	-2584(3)	1880(2)	2606(2)	28(1)
C(18)	-3057(4)	2031(2)	3448(2)	33(1)
C(19)	-4282(4)	2448(2)	3534(2)	40(1)
C(20)	-5038(4)	2720(2)	2787(3)	42(1)
C(21)	-4562(4)	2587(2)	1953(3)	41(1)
C(22)	-3335(4)	2166(2)	1862(2)	34(1)
C(23)	-1891(3)	385(2)	2418(2)	28(1)
C(24)	-2848(3)	171(2)	3049(2)	32(1)
C(25)	-3451(4)	-515(2)	3018(2)	39(1)
C(26)	-3117(4)	-992(2)	2361(3)	42(1)
C(27)	-2199(4)	-778(2)	1716(2)	40(1)
C(28)	-1606(3)	-97(2)	1735(2)	32(1)
N(1)	2340(3)	1227(2)	992(2)	32(1)
P(1)	-1058(1)	1275(1)	2464(1)	26(1)
Fe(1)	1918(1)	890(1)	3911(1)	30(1)
Zn(1)	266(1)	1608(1)	1183(1)	32(1)
Br(1)	-1114(1)	1216(1)	-128(1)	43(1)
Br(2)	630(1)	2882(1)	1267(1)	55(1)

X-ray Data of 13a

Table 1. Crystal data and structure refinement for i0682.

Code	i0682	
Empirical formula	$C_{58}H_{52}Br_4Cl_4Fe_2N_2P_2Zn_2$	
Formula weight	1542.84	
Temperature	173(2) K	
Wavelength	0.71073 Å	
crystal system	Monoclinic	
spacegroup	$P2_1/n$	
Unit cell dimensions	a = 12.0066(9) Å	α = 90°
	b = 14.5539(7) Å	β = 108.865(6)°
	c = 18.3142(14) Å	γ = 90°
Volume	3028.4(4) Å^3	
Z	2	
Density (calculated)	1.692 g/cm^3	
Absorption coefficient	4.159 mm^{-1}	
F(000)	1528	
Crystal size	0.24 mm × 0.20 mm × 0.05 mm	
θ-range for data collection	1.80 → 25.00°	
Index ranges	-14→ h →14, -17→ k →16, -21→ l →21	
Reflections collected	19330	

Independent reflections	5342 [R_{int} = 0.1594]
Reflections observed	3458
Absorption correction	Integration
Max. and min. transmission	0.8180 and 0.5191
Refinement method	full-matrix least-squares against F^2
Data / restraints / parameters	5342 / 0 / 334
Goodness-of-fit on F^2	0.940
Final R indices [$I > 2\sigma(I)$]	R_1 = 0.0663, wR_2 = 0.1610
R indices (all data)	R_1 = 0.0983, wR_2 = 0.1777
Largest diff. peak and hole	1.307 and -0.889 $e/$Å^3

Table 2. Atomic coordinates ($\cdot$ 10^4) and equivalent isotropic displacement parameters ($A^2 \cdot 10^3$) for i0682. U_{eq} is defined as one third of the trace of the orthogonalized U_{ij}tensor.

	x	y	z	U_{eq}
C(1)	7552(6)	3232(5)	4979(4)	44(2)
C(2)	7368(7)	4020(5)	5397(4)	46(2)
C(3)	8006(7)	3896(6)	6194(4)	52(2)
C(4)	8618(7)	3036(6)	6277(4)	53(2)
C(5)	8354(7)	2630(6)	5534(4)	52(2)
C(6)	5163(7)	3011(5)	5847(4)	48(2)
C(7)	5958(8)	2711(9)	6565(5)	79(3)
C(8)	6424(8)	1856(9)	6452(8)	89(4)
C(9)	5956(9)	1614(7)	5675(8)	83(3)
C(10)	5174(7)	2310(5)	5301(5)	52(2)
C(11)	4461(7)	3890(6)	5673(5)	56(2)
C(12)	3447(7)	3868(5)	5995(4)	48(2)
C(13)	2622(7)	3197(7)	5801(5)	61(2)
C(14)	1675(7)	3168(6)	6085(5)	59(2)
C(15)	1616(7)	3844(5)	6597(5)	53(2)
C(16)	2485(7)	4516(6)	6791(5)	55(2)
C(17)	8392(6)	3235(5)	3699(4)	45(2)
C(18)	9373(7)	3720(6)	4183(5)	55(2)
C(19)	10341(8)	3882(7)	3943(6)	68(2)
C(20)	10332(8)	3599(7)	3221(6)	69(3)
C(21)	9398(8)	3127(6)	2756(5)	62(2)
C(22)	8396(7)	2951(6)	2972(4)	52(2)
C(23)	6571(7)	1935(5)	3729(4)	49(2)
C(24)	7393(8)	1205(6)	3859(5)	59(2)
C(25)	6992(10)	304(6)	3746(6)	73(3)
C(26)	5785(11)	106(6)	3490(6)	73(3)
C(27)	4979(9)	838(6)	3349(5)	66(2)
C(28)	5383(7)	1738(6)	3473(5)	52(2)
C(29)	1072(16)	1091(14)	3935(10)	150(7)
N(1)	3387(5)	4541(4)	6498(3)	46(1)
P(1)	7050(2)	3117(1)	3955(1)	43(1)
Fe(1)	6842(1)	2836(1)	5799(1)	48(1)
Zn(1)	5620(1)	4250(1)	3206(1)	47(1)
Br(1)	5513(1)	3990(1)	1890(1)	60(1)
Br(2)	3753(1)	4108(1)	3387(1)	64(1)
Cl(1)	2397(5)	1433(6)	3935(4)	226(4)
Cl(2)	769(3)	1117(3)	4779(2)	118(1)

X-ray Data of 14a

Table 1. Crystal data and structure refinement for i0569.

Code	i0569	
Empirical formula	$C_{28}H_{24}Br_2CdFeNP$	
Formula weight	733.52	
Temperature	173(2) K	
Wavelength	0.71073 Å	
crystal system	Triclinic	
spacegroup	$P\bar{1}$	
Unit cell dimensions	a = 9.1388(11) Å	α = 84.260(9)°
	b = 9.5318(10) Å	β = 74.946(9)°
	c = 16.6270(17) Å	γ = 77.441(9)°
Volume	1363.7(3) Å^3	
Z	2	
Density (calculated)	1.786 g/cm^3	
Absorption coefficient	4.317 mm^{-1}	
F(000)	716	
Crystal size	0.32 mm × 0.20 mm × 0.05 mm	
θ-range for data collection	2.19 → 25.19°	
Index ranges	-10→ h →10, -11→ k →11, -19→ l →19	
Reflections collected	8927	
Independent reflections	4563 [R_{int} = 0.1210]	
Reflections observed	3667	
Absorption correction	Integration	
Max. and min. transmission	0.6328 and 0.2698	
Refinement method	full-matrix least-squares against F^2	
Data / restraints / parameters	4563 / 0 / 307	
Goodness-of-fit on F^2	1.033	
Final R indices [$I > 2\sigma(I)$]	R_1 = 0.0773, wR_2 = 0.1969	
R indices (all data)	R_1 = 0.0877, wR_2 = 0.2059	
Largest diff. peak and hole	3.222 and -1.885 e/Å^3	

Table 2. Atomic coordinates (· 10^4) and equivalent isotropic displacement parameters (A^2 · 10^3) for i0569. U_{eq} is defined as one third of the trace of the orthogonalized U_{ij}tensor.

	x	y	z	U_{eq}
C(1)	552(10)	5377(8)	6680(5)	31(2)
C(2)	-294(11)	6436(8)	6196(6)	36(2)
C(3)	174(11)	7784(9)	6214(6)	39(2)
C(4)	1288(11)	7563(9)	6693(6)	39(2)
C(5)	1542(10)	6065(8)	6983(5)	33(2)
C(6)	-1487(10)	8447(9)	8331(6)	39(2)
C(7)	-1272(12)	7011(9)	8674(6)	43(2)
C(8)	-2266(12)	6269(10)	8410(6)	45(2)
C(9)	-3089(12)	7256(11)	7913(7)	50(3)
C(10)	-2621(11)	8615(9)	7876(6)	41(2)
C(11)	-629(11)	9593(9)	8436(6)	39(2)
C(12)	-1460(10)	10591(9)	9142(6)	37(2)
C(13)	-2807(12)	10369(10)	9738(6)	44(2)
C(14)	-3502(12)	11367(10)	10349(7)	49(2)
C(15)	-2854(13)	12539(10)	10365(7)	50(2)
C(16)	-1504(11)	12687(10)	9775(6)	41(2)
C(17)	1807(10)	2696(9)	5895(5)	35(2)
C(18)	1790(13)	1278(9)	5712(7)	49(2)
C(19)	2779(14)	629(11)	5005(7)	57(3)
C(20)	3809(14)	1375(14)	4470(8)	63(3)
C(21)	3886(12)	2737(12)	4640(7)	52(2)
C(22)	2885(11)	3435(10)	5357(6)	38(2)
C(23)	-1390(10)	3284(8)	6743(5)	32(2)
C(24)	-1724(12)	3345(10)	5972(6)	42(2)
C(25)	-3190(12)	3176(10)	5926(7)	47(2)
C(26)	-4272(12)	2887(10)	6632(7)	47(2)
C(27)	-3927(12)	2792(12)	7385(7)	52(3)

C(28)	-2516(11)	3017(8)	7457(6)	38(2)
N(1)	-823(9)	11732(7)	9169(5)	35(2)
P(1)	493(2)	3487(2)	6842(1)	30(1)
Fe(1)	-748(1)	7034(1)	7399(1)	31(1)
Br(2)	3375(1)	10052(1)	7602(1)	41(1)
Br(1)	2227(1)	13885(1)	9023(1)	43(1)
Cd(1)	1336(1)	12262(1)	8189(1)	33(1)

X-ray Data of 15

Table 1. Crystal data and structure refinement for i0791.

Code	i0791	
Empirical formula	$C_{28}H_{24}CdFeI_2NP$	
Formula weight	672.47	
Temperature	100(2) K	
Wavelength	0.71073 Å	
crystal system	Monoclinic	
spacegroup	$P2_1/n$	
Unit cell dimensions	a = 9.4757(8) Å	α = 90°
	b = 19.0085(11) Å	β = 94.513(6)°
	c = 15.4717(12) Å	γ = 90°
Volume	2778.1(4) Å^3	
Z	4	
Density (calculated)	1.978 g/cm^3	
Absorption coefficient	3.585 mm^{-1}	
F(000)	1576	
Crystal size	0.27 mm × 0.05 mm × 0.05 mm	
θ-range for data collection	1.70 → 25.00°	
Index ranges	-11→ h →11, -22→ k →22, -18→ l →15	
Reflections collected	14403	
Independent reflections	84897 [R_{int} = 0.1141]	
Reflections observed	3388	
Absorption correction	Integration	
Max. and min. transmission	0.8484 and 0.5150	
Refinement method	full-matrix least-squares against F^2	
Data / restraints / parameters	4897 / 0 / 307	
Goodness-of-fit on F^2	0.893	
Final R indices [$I > 2\sigma(I)$]	R_1 = 0.0460, wR_2 = 0.1027	
R indices (all data)	R_1 = 0.0726, wR_2 = 0.1101	
Largest diff. peak and hole	0.765 and -0.915 e/Å^3	

Table 2. Atomic coordinates (· 10^4) and equivalent isotropic displacement parameters (A^2 · 10^3) for i0791. U_{eq} is defined as one third of the trace of the orthogonalized U_{ij} tensor.

	x	y	z	U_{eq}
C(1)	5051(8)	1319(4)	1422(6)	28(2)
C(2)	5121(8)	903(5)	648(6)	30(2)
C(3)	4181(9)	1229(5)	-28(6)	34(2)
C(4)	3530(9)	1819(5)	345(6)	36(2)
C(5)	4024(9)	1882(4)	1221(6)	31(2)
C(6)	2192(8)	321(4)	1986(6)	26(2)
C(7)	1268(9)	887(4)	1686(6)	31(2)
C(8)	956(8)	801(5)	768(6)	35(2)
C(9)	1668(9)	197(5)	488(6)	34(2)

C(10)	2461(9)	-102(5)	1244(6)	34(2)
C(11)	2745(8)	154(4)	2888(6)	28(2)
C(12)	1920(8)	544(4)	3555(5)	25(2)
C(13)	560(8)	306(4)	3737(6)	30(2)
C(14)	-176(8)	662(5)	4351(6)	33(2)
C(15)	446(9)	1247(5)	4768(6)	37(2)
C(16)	1729(9)	1457(5)	4569(7)	36(2)
C(17)	7568(8)	1845(4)	2346(5)	26(2)
C(18)	8319(9)	2081(4)	3096(6)	32(2)
C(19)	9539(8)	2497(4)	3027(6)	32(2)
C(20)	9975(8)	2685(4)	2210(6)	32(2)
C(21)	9211(9)	2448(5)	1473(7)	39(2)
C(22)	7996(8)	2026(4)	1518(6)	27(2)
C(23)	6874(8)	372(4)	2508(5)	25(2)
C(24)	6542(8)	-120(4)	3145(5)	28(2)
C(25)	7131(9)	-794(4)	3173(7)	36(2)
C(26)	8068(9)	-990(4)	2538(6)	34(2)
C(27)	8415(9)	-505(4)	1910(6)	35(2)
C(28)	7837(8)	171(4)	1882(6)	26(2)
N(1)	2509(7)	1108(3)	3967(5)	28(2)
P(1)	6059(2)	1249(1)	2449(1)	26(1)
Fe(1)	3087(1)	920(1)	1011(1)	26(1)
I(1)	6272(1)	1158(1)	5276(1)	33(1)
I(2)	3938(1)	2994(1)	3703(1)	34(1)
Cd(1)	4701(1)	1593(1)	3788(1)	27(1)

X-ray Data of 16

Table 1. Crystal data and structure refinement for i0776.

Code	i0776	
Empirical formula	$C_{28}H_{24}Br_2FeHgNP$	
Formula weight	821.71	
Temperature	218(2) K	
Wavelength	0.71073 Å	
crystal system	Monoclinic	
spacegroup	$P2_1/n$	
Unit cell dimensions	a = 9.3132(8) Å	α = 90°
	b = 18.5685(17) Å	β = 94.473(7)°
	c = 15.3200(13) Å	γ = 90°
Volume	2641.3(4) Å^3	
Z	4	
Density (calculated)	2.066 g/cm^3	
Absorption coefficient	9.459 mm^{-1}	
F(000)	1560	
Crystal size	0.39 mm × 0.04 mm × 0.04 mm	
θ-range for data collection	1.73 → 25.00°	
Index ranges	-178→ h →11, -18→ k →22, -18→ l →18	
Reflections collected	11523	
Independent reflections	4552 [R_{int} = 0.0746]	
Reflections observed	2932	
Absorption correction	Integration	
Max. and min. transmission	0.7314 and 0.3539	
Refinement method	full-matrix least-squares against F^2	
Data / restraints / parameters	4552 / 0 / 307	
Goodness-of-fit on F^2	0.884	
Final R indices [$I > 2\sigma(I)$]	R_1 = 0.0334, wR_2 = 0.0841	
R indices (all data)	R_1 = 0.0669, wR_2 = 0.0901	
Largest diff. peak and hole	1.067 and -1.043 e/Å^3	

Table 2. Atomic coordinates ($\cdot 10^4$) and equivalent isotropic displacement parameters ($A^2 \cdot 10^3$) for i0776. U_{eq} is defined as one third of the trace of the orthogonalized U_{ij}tensor.

	x	y	z	U_{eq}
C(1)	5091(10)	1355(5)	1457(5)	30(2)
C(2)	5150(10)	942(6)	659(5)	38(2)
C(3)	4132(13)	1266(7)	24(6)	53(3)
C(4)	3431(12)	1846(6)	403(6)	48(3)
C(5)	4024(12)	1908(6)	1288(6)	43(3)
C(6)	2237(10)	298(5)	2056(5)	33(2)
C(7)	2541(12)	-130(6)	1337(6)	44(3)
C(8)	1736(13)	137(7)	576(6)	48(3)
C(9)	956(11)	755(7)	825(6)	45(3)
C(10)	1269(11)	856(6)	1749(5)	39(2)
C(11)	2759(11)	160(6)	3004(5)	36(2)
C(12)	1972(11)	585(5)	3642(5)	34(2)
C(13)	601(11)	384(6)	3854(6)	42(2)
C(14)	-114(11)	782(7)	4444(6)	48(3)
C(15)	554(12)	1384(7)	4821(6)	49(3)
C(16)	1902(10)	1568(6)	4576(5)	39(2)
C(17)	7694(11)	1885(5)	2345(5)	33(2)
C(18)	8464(11)	2168(5)	3087(6)	38(2)
C(19)	9670(12)	2584(6)	3001(6)	42(3)
C(20)	10123(12)	2740(6)	2189(6)	45(3)
C(21)	9367(12)	2483(6)	1443(6)	41(2)
C(22)	8152(11)	2057(5)	1514(5)	35(2)
C(23)	6982(10)	385(5)	2520(5)	30(2)
C(24)	7884(11)	169(6)	1911(5)	36(2)
C(25)	8492(12)	-534(6)	1949(6)	42(3)
C(26)	8156(13)	-998(6)	2600(7)	49(3)
C(27)	7254(14)	-784(6)	3228(7)	53(3)
C(28)	6673(11)	-88(6)	3201(5)	37(2)
N(1)	2585(8)	1190(5)	3996(4)	35(2)
P(1)	6190(3)	1283(1)	2464(1)	28(1)
Fe(1)	3114(2)	913(1)	1080(1)	33(1)
Br(1)	4181(2)	2969(1)	3849(1)	56(1)
Br(2)	6238(1)	1182(1)	5223(1)	53(1)
Hg(1)	4915(1)	1617(1)	3739(1)	36(1)

X-ray Data of 17

Table 1. Crystal data and structure refinement for i0573.

Code	i0573	
Empirical formula	$C_{29.50}H_{24}Br_4FeHg_2NOP$	
Formula weight	1216.14	
Temperature	173(2) K	
Wavelength	0.71073 Å	
crystal system	Orthorhombic	
spacegroup	$Pccn$	
Unit cell dimensions	a = 34.9720(12) Å	α = 90°
	b = 9.9410(5) Å	β = 90°
	c = 18.1638(8) Å	γ = 90°
Volume	6314.8(5) $Å^3$	
Z	8	

Density (calculated)	2.558 g/cm^3
Absorption coefficient	15.292 mm^{-1}
F(000)	4456
Crystal size	0.49 mm $\times$ 0.17 mm $\times$ 0.14 mm
θ-range for data collection	2.13 $\rightarrow$ 25.26°
Index ranges	-41$\rightarrow h \rightarrow$42, -11$\rightarrow k \rightarrow$11, -20$\rightarrow l \rightarrow$20
Reflections collected	37537
Independent reflections	5554 [R_{int} = 0.0991]
Reflections observed	4558
Absorption correction	Integration
Max. and min. transmission	0.1673 and 0.0059
Refinement method	full-matrix least-squares against F^2
Data / restraints / parameters	5554 / 0 / 358
Goodness-of-fit on F^2	1.056
Final R indices [$I > 2\sigma(I)$]	R_1 = 0.0553, wR_2 = 0.1376
R indices (all data)	R_1 = 0.0679, wR_2 = 0.1483
Extinction coefficient	0.00018(4)
Largest diff. peak and hole	4.404 and -2.301 e/Å^3

Table 2. Atomic coordinates ($\cdot$ 10^4) and equivalent isotropic displacement parameters ($A^2 \cdot 10^3$) for i0573. U_{eq} is defined as one third of the trace of the orthogonalized U_{ij}tensor.

	x	y	z	U_{eq}
C(1)	1317(3)	2894(9)	5980(6)	35(2)
C(2)	1317(3)	1436(10)	5953(7)	39(2)
C(3)	1075(4)	954(11)	6517(7)	46(3)
C(4)	926(4)	2122(12)	6902(7)	49(3)
C(5)	1079(3)	3320(11)	6563(7)	43(3)
C(6)	575(3)	1511(9)	4829(6)	35(2)
C(7)	564(3)	2946(10)	4825(7)	40(2)
C(8)	327(3)	3393(10)	5420(6)	39(2)
C(9)	191(3)	2218(10)	5795(7)	42(3)
C(10)	337(3)	1081(10)	5423(6)	38(2)
C(11)	771(3)	591(10)	4281(6)	38(2)
C(12)	548(3)	356(9)	3582(6)	34(2)
C(13)	217(3)	1080(11)	3410(7)	44(3)
C(14)	20(3)	769(11)	2768(7)	46(3)
C(15)	166(3)	-199(11)	2288(7)	44(3)
C(16)	502(3)	-841(10)	2493(6)	39(2)
C(17)	2014(3)	4516(10)	5793(7)	41(3)
C(18)	2138(3)	3898(12)	6449(8)	52(3)
C(19)	2491(4)	4279(15)	6756(8)	60(3)
C(20)	2718(4)	5205(13)	6389(9)	61(4)
C(21)	2593(4)	5788(13)	5745(9)	62(4)
C(22)	2241(4)	5461(12)	5443(8)	52(3)
C(23)	1705(3)	3092(10)	4575(7)	41(2)
C(24)	1543(3)	3352(16)	3894(8)	60(4)
C(25)	1652(5)	2480(20)	3294(8)	77(5)
C(26)	1914(4)	1413(16)	3412(8)	65(4)
C(27)	2072(4)	1268(12)	4077(7)	51(3)
C(28)	1978(4)	2066(11)	4668(7)	46(3)
C(29)	2609(5)	6629(19)	8446(10)	66(5)
C(30)	2500	7500	7810(20)	154(18)
Br(1)	599(1)	7293(1)	5608(1)	48(1)
Br(2)	792(1)	5857(1)	3591(1)	49(1)
Br(3)	1527(1)	8144(1)	2040(1)	56(1)
Br(4)	1576(1)	8137(1)	4562(1)	45(1)
Fe	779(1)	2225(1)	5810(1)	33(1)
Hg(1)	1151(1)	5949(1)	5180(1)	56(1)
Hg(2)	1224(1)	7985(1)	3304(1)	47(1)
O(30)	2806(4)	5968(11)	8285(5)	62(3)
P	1564(1)	4032(3)	5376(2)	37(1)

N	695(2)	-565(8)	3119(5)	33(2)

X-ray Data of 18

Table 1. Crystal data and structure refinement for i0683.

Code	i0683	
Empirical formula	$C_{57}H_{49}Br_2Cl_2Fe_2HgN_2P_2$	
Formula weight	1402.38	
Temperature	173(2) K	
Wavelength	0.71073 Å	
crystal system	Orthorhombic	
spacegroup	$I\ b\ a\ 2$	
Unit cell dimensions	a = 13.7805(6) Å	α = 90°
	b = 40.4138(16) Å	β = 90°
	c = 19.1500(9) Å	γ = 90°
Volume	10665.1(8) Å^3	
Z	8	
Density (calculated)	1.747 g/cm^3	
Absorption coefficient	5.158 mm^{-1}	
F(000)	5504	
Crystal size	0.31 mm × 0.20 mm × 0.15 mm	
θ-range for data collection	1.56 → 25.00°	
Index ranges	-16→ h →16, -48→ k →47, -22→ l →22	
Reflections collected	33209	
Independent reflections	9405 [R_{int} = 0.0449]	
Reflections observed	8569	
Absorption correction	Integration	
Max. and min. transmission	0.5756 and 0.4185	
Refinement method	full-matrix least-squares against F^2	
Data / restraints / parameters	9405 / 1 / 622	
Goodness-of-fit on F^2	1.026	
Final R indices [$I > 2\sigma(I)$]	R_1 = 0.0382, wR_2 = 0.0963	
R indices (all data)	R_1 = 0.0430, wR_2 = 0.1010	
Absolute structure parameter	-0.008(6)	
Largest diff. peak and hole	2.009 and -1.340 e/Å^3	

Table 2. Atomic coordinates (· 10^4) and equivalent isotropic displacement parameters (A^2 · 10^3) for i0683. U_{eq} is defined as one third of the trace of the orthogonalized U_{ij}tensor.

	x	y	z	U_{eq}
C(1)	-5866(6)	-3892(2)	-2097(4)	33(2)
C(2)	-5360(5)	-4009(2)	-1502(4)	37(2)
C(3)	-4698(6)	-4256(2)	-1718(5)	48(2)
C(4)	-4776(6)	-4296(2)	-2463(5)	46(2)
C(5)	-5503(5)	-4070(2)	-2692(4)	36(2)
C(6)	-6938(6)	-4728(2)	-2509(5)	41(2)
C(7)	-7552(5)	-4497(2)	-2168(5)	41(2)
C(8)	-7349(6)	-4506(3)	-1428(5)	52(2)
C(9)	-6615(7)	-4755(2)	-1321(5)	56(2)
C(10)	-6377(6)	-4889(2)	-1968(6)	52(2)
C(11)	-6889(6)	-4795(2)	-3285(6)	57(2)
C(12)	-7612(6)	-5049(2)	-3561(5)	48(2)
C(13)	-8483(8)	-5109(3)	-3272(8)	98(5)
C(14)	-9106(9)	-5341(3)	-3566(8)	92(4)

C(15)	-8868(7)	-5484(3)	-4162(6)	64(3)
C(16)	-7966(9)	-5419(3)	-4428(7)	81(3)
C(17)	-7558(5)	-3610(2)	-1398(5)	36(2)
C(18)	-8509(5)	-3726(2)	-1487(5)	44(2)
C(19)	-9097(6)	-3779(2)	-902(5)	51(2)
C(20)	-8762(7)	-3711(2)	-245(5)	55(2)
C(21)	-7828(9)	-3588(3)	-155(5)	53(2)
C(22)	-7231(8)	-3532(2)	-713(6)	43(2)
C(23)	-6078(5)	-3181(2)	-1991(4)	33(2)
C(24)	-5069(5)	-3170(2)	-2098(4)	41(2)
C(25)	-4609(7)	-2862(3)	-2070(5)	52(2)
C(26)	-5118(7)	-2577(2)	-1919(5)	54(2)
C(27)	-6121(7)	-2593(2)	-1793(5)	49(2)
C(28)	-6585(6)	-2894(2)	-1835(5)	43(2)
C(29)	-5797(5)	-3170(2)	-4484(4)	33(2)
C(30)	-5247(5)	-3062(2)	-5092(4)	37(2)
C(31)	-4551(5)	-2828(2)	-4858(5)	40(2)
C(32)	-4669(5)	-2779(2)	-4124(5)	43(2)
C(33)	-5435(5)	-2985(2)	-3898(4)	39(2)
C(34)	-6711(5)	-2296(2)	-4177(4)	38(2)
C(35)	-7359(5)	-2520(2)	-4511(5)	42(2)
C(36)	-7107(6)	-2529(2)	-5246(4)	44(2)
C(37)	-6311(7)	-2309(2)	-5344(5)	48(2)
C(38)	-6074(6)	-2165(2)	-4687(4)	41(2)
C(39)	-6722(6)	-2199(2)	-3408(5)	48(2)
C(40)	-7003(5)	-1826(2)	-3324(5)	39(1)
C(41)	-6279(4)	-1586(2)	-3298(5)	40(2)
C(42)	-6561(6)	-1256(2)	-3245(5)	47(2)
C(43)	-7534(6)	-1183(2)	-3228(6)	51(2)
C(44)	-8196(5)	-1440(2)	-3261(6)	52(2)
C(45)	-7502(5)	-3434(2)	-5200(5)	33(2)
C(46)	-7180(8)	-3505(2)	-5877(5)	43(2)
C(47)	-7766(7)	-3440(3)	-6461(5)	48(2)
C(48)	-8684(6)	-3299(2)	-6363(4)	44(2)
C(49)	-9004(6)	-3230(2)	-5694(5)	49(2)
C(50)	-8427(5)	-3291(2)	-5117(4)	42(2)
C(51)	-6045(6)	-3869(2)	-4618(4)	36(2)
C(52)	-6538(7)	-4165(2)	-4778(5)	48(2)
C(53)	-6025(9)	-4458(2)	-4831(6)	63(3)
C(54)	-5026(8)	-4464(2)	-4710(5)	63(3)
C(55)	-4527(7)	-4183(2)	-4564(5)	55(2)
C(56)	-5022(6)	-3878(2)	-4522(5)	46(2)
C(57)	-8823(9)	-4640(4)	-6301(9)	94(4)
N(1)	-7329(6)	-5200(3)	-4146(5)	69(2)
N(2)	-7947(4)	-1753(2)	-3303(4)	42(1)
P(1)	-6760(2)	-3565(1)	-2148(1)	29(1)
P(2)	-6706(2)	-3484(1)	-4457(1)	30(1)
Cl(1)	-7981(3)	-4338(1)	-6555(3)	131(2)
Cl(2)	-8894(5)	-4642(3)	-5399(4)	208(4)
Cl(3)	-9962(3)	-4555(1)	-6679(3)	130(2)
Fe(1)	-6107(1)	-4386(1)	-1980(1)	35(1)
Fe(2)	-5943(1)	-2671(1)	-4646(1)	32(1)
Br(1)	-8731(1)	-3006(1)	-3059(1)	44(1)
Br(2)	-8844(1)	-4006(1)	-3595(1)	49(1)
Hg(1)	-7588(1)	-3523(1)	-3312(1)	32(1)

X-ray Data of 19

Table 1. Crystal data and structure refinement for i0812.

Code	i0812	
Empirical formula	$C_{29}H_{24}AgBCl_6F_4FeNP$	
Formula weight	880.69	
Temperature	100(2) K	
Wavelength	0.71073 Å	
crystal system	Monoclinic	
spacegroup	$P2_1/c$	
Unit cell dimensions	a = 10.5259(10) Å	α = 90°
	b = 11.9401(16) Å	β = 93.193(7)°
	c = 26.573(3) Å	γ = 90°
Volume	3334.6(6) $Å^3$	
Z	4	
Density (calculated)	1.754 g/cm^3	
Absorption coefficient	1.596 mm^{-1}	
F(000)	1744	
Crystal size	0.31 mm × 0.10 mm × 0.08 mm	
θ-range for data collection	1.53 → 25.00°	
Index ranges	-12→ h →11, -14→ k →14, -31→ l →30	
Reflections collected	21156	
Independent reflections	5720 [R_{int} = 0.0773]	
Reflections observed	4955	
Absorption correction	Integration	
Max. and min. transmission	0.8971 and 0.7251	
Refinement method	full-matrix least-squares against F^2	
Data / restraints / parameters	5720 / 0 / 397	
Goodness-of-fit on F^2	0.691	
Final R indices [$I > 2\sigma(I)$]	R_1 = 0.0307, wR_2 = 0.0842	
R indices (all data)	R_1 = 0.0377, wR_2 = 0.0903	
Largest diff. peak and hole	0.974 and -0.867 $e/Å^3$	

Table 2. Atomic coordinates (· 10^4) and equivalent isotropic displacement parameters (A^2 · 10^3) for i0812. U_{eq} is defined as one third of the trace of the orthogonalized U_{ij}tensor.

	x	y	z	U_{eq}
C(1)	7802(3)	1202(2)	2107(1)	17(1)
C(2)	8269(3)	705(2)	1656(1)	19(1)
C(3)	9504(3)	255(2)	1783(1)	21(1)
C(4)	9806(3)	481(2)	2308(1)	22(1)
C(5)	8777(3)	1059(2)	2511(1)	20(1)
C(6)	7059(3)	-1746(2)	1936(1)	19(1)
C(7)	8301(3)	-2151(2)	2110(1)	23(1)
C(8)	8477(3)	-1903(2)	2638(1)	25(1)
C(9)	7376(3)	-1345(2)	2793(1)	23(1)
C(10)	6496(3)	-1245(2)	2362(1)	20(1)
C(11)	3485(3)	3147(2)	3594(1)	19(1)
C(12)	2758(3)	3310(2)	4009(1)	23(1)
C(13)	3284(3)	3144(2)	4498(1)	25(1)
C(14)	4558(3)	2823(2)	4562(1)	27(1)
C(15)	5241(3)	2679(2)	4136(1)	25(1)
C(16)	5093(3)	1244(2)	1791(1)	20(1)
C(17)	4077(3)	770(2)	2035(1)	25(1)
C(18)	3129(3)	189(2)	1746(1)	28(1)
C(19)	3176(3)	99(2)	1223(1)	29(1)
C(20)	4177(3)	582(2)	981(1)	27(1)
C(21)	5134(3)	1154(2)	1261(1)	22(1)
C(22)	6589(3)	3259(2)	1835(1)	20(1)
C(23)	5581(3)	3794(2)	1564(1)	25(1)
C(24)	5776(3)	4792(2)	1311(1)	31(1)
C(25)	6983(3)	5265(2)	1325(1)	30(1)
C(26)	7992(3)	4753(2)	1596(1)	29(1)
C(27)	7795(3)	3750(2)	1853(1)	25(1)

C(28)	7974(3)	-490(3)	4704(1)	29(1)
C(29)	11089(3)	-3200(3)	4735(1)	29(1)
N(1)	4725(2)	2821(2)	3657(1)	20(1)
P(1)	6345(1)	1953(1)	2174(1)	17(1)
Fe(1)	8166(1)	-458(1)	2222(1)	16(1)
Ag(1)	5763(1)	2362(1)	3003(1)	21(1)
Cl(1)	12442(1)	-4072(1)	4837(1)	40(1)
Cl(2)	11436(1)	-2096(1)	4323(1)	42(1)
Cl(3)	9783(1)	-3978(1)	4484(1)	39(1)
Cl(4)	8897(1)	-1032(1)	5226(1)	29(1)
Cl(5)	7648(1)	-1550(1)	4243(1)	55(1)
Cl(6)	6524(1)	52(1)	4903(1)	38(1)
B(1)	8933(3)	2377(3)	3873(1)	24(1)
F(1)	8229(2)	1864(2)	4242(1)	34(1)
F(2)	9533(2)	3318(2)	4091(1)	33(1)
F(3)	9830(2)	1632(2)	3710(1)	32(1)
F(4)	8121(2)	2717(2)	3463(1)	36(1)

X-ray Data of 20

Table 1. Crystal data and structure refinement for i0703.

Code	i0703	
Empirical formula	$C_{56}H_{46}Ag_2B_2Cl_6F_8Fe_2N_2P_2$	
Formula weight	1522.65	
Temperature	173(2) K	
Wavelength	0.71073 Å	
crystal system	Monoclinic	
spacegroup	$P2_1/n$	
Unit cell dimensions	a = 9.1606(5) Å	α = 90°
	b = 21.4054(9) Å	β = 93.684(5)°
	c = 15.4766(9) Å	γ = 90°
Volume	3028.5(3) Å^3	
Z	2	
Density (calculated)	1.670 g/cm^3	
Absorption coefficient	1.488 mm^{-1}	
F(000)	1512	
Crystal size	0.50 mm × 0.11 mm × 0.09 mm	
θ-range for data collection	1.63 → 25.16°	
Index ranges	-10→ h →10, -23→ k →25, -18→ l →18	
Reflections collected	19521	
Independent reflections	5387 [R_{int} = 0.0304]	
Reflections observed	4463	
Absorption correction	Integration	
Max. and min. transmission	0.8975 and 0.6853	
Refinement method	full-matrix least-squares against F^2	
Data / restraints / parameters	5387 / 0 / 361	
Goodness-of-fit on F^2	1.070	
Final R indices [$I > 2\sigma(I)$]	R_1 = 0.0409, wR_2 = 0.1115	
R indices (all data)	R_1 = 0.0499, wR_2 = 0.1157	
Largest diff. peak and hole	1.418 and -0.746 e/Å^3	

Table 2. Atomic coordinates (· 10^4) and equivalent isotropic displacement parameters (A^2 · 10^3) for i0703. U_{eq} is defined as one third of the trace of the orthogonalized U_{ij}tensor.

	x	y	z	U_{eq}

C(1)	4127(4)	-96(2)	-2005(2)	40(1)
C(2)	3997(5)	-706(2)	-2379(3)	47(1)
C(3)	5326(4)	-109(2)	-1354(2)	34(1)
C(4)	6849(4)	-596(2)	-3698(2)	40(1)
C(5)	7897(4)	157(2)	-2771(3)	39(1)
C(6)	5918(4)	-729(2)	-1337(2)	36(1)
C(7)	6675(5)	424(2)	-3240(3)	45(1)
C(8)	5096(5)	-1093(2)	-1972(3)	43(1)
C(9)	6028(5)	-32(2)	-3811(3)	46(1)
C(10)	8026(4)	-484(2)	-3044(2)	34(1)
C(11)	6992(4)	364(2)	-193(2)	33(1)
C(12)	5853(4)	431(2)	-832(2)	33(1)
C(13)	5759(6)	1510(2)	-424(3)	54(1)
C(14)	6898(5)	1403(2)	182(3)	47(1)
C(15)	5224(5)	1019(2)	-935(3)	45(1)
C(16)	11534(4)	1762(2)	2475(3)	37(1)
C(17)	9231(4)	706(2)	4115(3)	39(1)
C(18)	8608(5)	1715(2)	3518(3)	43(1)
C(19)	9437(4)	1168(2)	3502(2)	35(1)
C(20)	11731(5)	1980(2)	1638(3)	44(1)
C(21)	12118(5)	2111(2)	3188(3)	48(1)
C(22)	12520(6)	2526(2)	1524(4)	57(1)
C(23)	7334(5)	1316(2)	4719(3)	49(1)
C(24)	7550(5)	1788(2)	4122(3)	50(1)
C(25)	8191(5)	781(2)	4723(3)	48(1)
C(26)	13077(6)	2864(2)	2233(4)	62(1)
C(27)	12882(6)	2654(2)	3065(4)	60(1)
C(28)	17172(6)	3434(2)	1468(3)	55(1)
Ag(1)	9163(1)	729(1)	1365(1)	44(1)
B(1)	15901(6)	3908(3)	3950(3)	48(1)
F(1)	14458(4)	3856(2)	3726(3)	94(1)
F(2)	16659(5)	3491(3)	3461(3)	122(2)
F(3)	16328(7)	3852(3)	4773(3)	148(2)
F(4)	16299(6)	4500(2)	3710(4)	134(2)
Fe(1)	6030(1)	-337(1)	-2552(1)	32(1)
N(1)	7508(4)	840(2)	306(2)	37(1)
P(1)	10616(1)	1024(1)	2612(1)	33(1)
Cl(1)	17364(2)	4210(1)	1134(1)	90(1)
Cl(2)	18890(2)	3065(1)	1573(2)	101(1)
Cl(3)	15983(2)	3043(1)	701(1)	74(1)

X-ray Data of 21

Table 1. Crystal data and structure refinement for i0760a.

Code	i0760a	
Empirical formula	$C_{29}H_{24}AgBCl_3F_4FeNP$	
Formula weight	774.34	
Temperature	298(2) K	
Wavelength	0.71073 Å	
crystal system	Monoclinic	
spacegroup	$P2_1/c$	
Unit cell dimensions	a = 13.2362(14) Å	α = 90°
	b = 11.5572(13) Å	β = 91.336(11)°
	c = 20.694(3) Å	γ = 90°
Volume	3164.7(7) Å^3	
Z	4	
Density (calculated)	1.625 g/cm^3	
Absorption coefficient	1.425 mm^{-1}	

F(000)	1540
θ-range for data collection	1.54 $\rightarrow$ 25.00°
Index ranges	-14$\rightarrow h \rightarrow$15, -5$\rightarrow k \rightarrow$13, -23$\rightarrow l \rightarrow$9
Reflections collected	2375
Independent reflections	2074 [R_{int} = 0.0254]
Reflections observed	None
Absorption correction	Integration
Refinement method	full-matrix least-squares against F^2
Data / restraints / parameters	2074 / 0 / 370
Goodness-of-fit on F^2	0.790
Final R indices [$I > 2\sigma(I)$]	R_1 = 0.0321, wR_2 = 0.0495
R indices (all data)	R_1 = 0.0737, wR_2 = 0.0557
Largest diff. peak and hole	0.175 and -0.150 e/Å^3

Table 2. Atomic coordinates ($\cdot$ 10^4) and equivalent isotropic displacement parameters ($A^2 \cdot 10^3$) for i0760a. U_{eq} is defined as one third of the trace of the orthogonalized U_{ij}tensor.

	x	y	z	U_{eq}
C(1)	1748(4)	5341(7)	3059(6)	53(3)
C(2)	2338(5)	5126(10)	3611(6)	67(3)
C(3)	1699(6)	4764(12)	4128(6)	74(4)
C(4)	686(6)	4878(11)	3871(7)	74(4)
C(5)	726(5)	5159(9)	3223(6)	60(3)
C(6)	1216(5)	2026(9)	3633(6)	55(3)
C(7)	736(6)	2271(10)	3038(7)	70(4)
C(8)	1517(10)	2580(12)	2614(8)	91(4)
C(9)	2445(9)	2506(12)	2930(9)	91(5)
C(10)	2277(5)	2174(9)	3559(7)	68(4)
C(11)	733(4)	1626(9)	4262(6)	55(3)
C(12)	941(4)	360(7)	4391(5)	51(3)
C(13)	1805(4)	11(10)	4746(5)	67(3)
C(14)	2013(5)	-1137(10)	4840(6)	80(4)
C(15)	1353(5)	-1938(9)	4604(6)	68(4)
C(16)	497(4)	-1574(8)	4269(6)	59(3)
C(17)	2113(4)	7262(8)	2223(6)	51(3)
C(18)	1867(4)	7976(9)	2740(6)	57(3)
C(19)	1805(5)	9161(10)	2674(7)	64(4)
C(20)	1999(5)	9659(9)	2086(7)	70(4)
C(21)	2263(7)	9000(11)	1590(8)	90(6)
C(22)	2309(6)	7836(11)	1648(7)	73(4)
C(23)	3446(4)	5330(7)	2203(6)	56(3)
C(24)	3713(5)	4426(9)	1811(6)	64(4)
C(25)	4713(6)	4104(12)	1782(7)	105(5)
C(26)	5413(6)	4650(12)	2112(9)	120(6)
C(27)	5194(5)	5559(13)	2533(7)	96(5)
C(28)	4174(4)	5896(9)	2554(6)	77(4)
C(29)	-5035(6)	6980(13)	5248(7)	97(5)
B(1)	-2360(6)	7053(14)	4256(8)	69(4)
N(1)	296(3)	-444(6)	4154(4)	50(2)
F(1)	-3038(3)	6740(6)	3781(4)	106(3)
F(2)	-2810(3)	7284(7)	4807(4)	121(3)
F(3)	-1859(3)	8044(7)	4053(4)	104(3)
F(4)	-1616(3)	6250(7)	4323(4)	121(3)
P(1)	2121(1)	5721(2)	2259(1)	46(1)
Fe(1)	1532(1)	3688(1)	3359(1)	54(1)
Ag(1)	990(1)	4990(1)	1462(1)	57(1)
Cl(1)	-5964(2)	6616(6)	4794(4)	262(5)
Cl(2)	-4998(2)	6383(7)	6026(4)	251(4)
Cl(3)	-5100(2)	8463(6)	5431(4)	246(4)

X-ray Data of 22

Table 1. Crystal data and structure refinement for i0777.

Code	i0777	
Empirical formula	$C_{27}H_{22}AuClFeNP$	
Formula weight	679.69	
Temperature	218(2) K	
Wavelength	0.71073 Å	
crystal system	Monoclinic	
spacegroup	$P2_1/n$	
Unit cell dimensions	a = 13.8398(9) Å	α = 90°
	b = 10.7636(5) Å	β = 107.505(5)°
	c = 16.6681(12) Å	γ = 90°
Volume	2368.0(3) Å^3	
Z	4	
Density (calculated)	1.907 g/cm^3	
Absorption coefficient	6.997 mm^{-1}	
F(000)	1312	
Crystal size	0.17 mm × 0.15 mm × 0.06 mm	
θ-range for data collection	1.68 → 25.00°	
Index ranges	-16→ h →16, -12→ k →11, -19→ l →16	
Reflections collected	10860	
Independent reflections	4149 [R_{int} = 0.0607]	
Reflections observed	3172	
Absorption correction	Integration	
Max. and min. transmission	0.6590 and 0.3593	
Refinement method	full-matrix least-squares against F^2	
Data / restraints / parameters	4149 / 0 / 289	
Goodness-of-fit on F^2	0.999	
Final R indices [$I > 2\sigma(I)$]	R_1 = 0.0327, wR_2 = 0.0741	
R indices (all data)	R_1 = 0.0461, wR_2 = 0.0766	
Largest diff. peak and hole	1.310 and -2.150 e/Å^3	

Table 2. Atomic coordinates (· 10^4) and equivalent isotropic displacement parameters (A^2 · 10^3) for i0777. U_{eq} is defined as one third of the trace of the orthogonalized U_{ij}tensor.

	x	y	z	U_{eq}
C(1)	5872(4)	44(6)	3688(4)	36(1)
C(2)	4808(4)	217(7)	3564(4)	45(2)
C(3)	4279(5)	-414(8)	2808(5)	54(2)
C(4)	4991(5)	-949(7)	2457(5)	53(2)
C(5)	5978(5)	-679(6)	2986(4)	42(2)
C(6)	5888(5)	1821(7)	1781(4)	45(2)
C(7)	5977(5)	2556(7)	2522(5)	51(2)
C(8)	4979(6)	2831(9)	2556(6)	66(2)
C(9)	4285(5)	2257(9)	1858(6)	69(2)
C(10)	4828(5)	1634(9)	1373(5)	63(2)
C(11)	6722(5)	1316(7)	1490(4)	46(2)
N(13)	6456(5)	829(7)	710(4)	58(2)
C(13)	7210(7)	382(8)	447(5)	65(2)
C(14)	8219(6)	383(8)	904(5)	58(2)
C(15)	8468(6)	885(8)	1691(5)	60(2)
C(16)	7042(5)	-710(7)	5337(4)	41(2)
C(17)	7686(5)	-549(9)	6159(5)	58(2)
C(18)	7778(6)	-1519(11)	6754(5)	72(3)
C(19)	7235(7)	-2587(10)	6536(6)	73(3)
C(20)	6608(7)	-2770(9)	5717(6)	66(2)
C(21)	6519(5)	-1843(7)	5131(5)	50(2)

C(22)	7980(4)	857(6)	4358(4)	39(2)
C(23)	8366(5)	2051(7)	4411(4)	44(2)
C(24)	9285(5)	2289(8)	4247(5)	50(2)
C(25)	9791(5)	1321(8)	4013(4)	51(2)
C(26)	9420(5)	117(7)	3966(4)	47(2)
C(27)	8518(4)	-132(7)	4140(4)	44(2)
C(28)	7724(5)	1348(7)	2000(5)	53(2)
P(1)	6810(1)	591(2)	4616(1)	36(1)
Cl(1)	5923(2)	3887(2)	5937(1)	57(1)
Fe(1)	5214(1)	939(1)	2580(1)	41(1)
Au(1)	6334(1)	2233(1)	5233(1)	39(1)

X-ray Data of 23

Table 1. Crystal data and structure refinement for i0702.

Code	i0702	
Empirical formula	$C_{27}H_{22}AuClFeNP$	
Formula weight	679.69	
Temperature	173(2) K	
Wavelength	0.71073 Å	
crystal system	Triclinic	
spacegroup	$P\bar{1}$	
Unit cell dimensions	a = 8.6932(8) Å	α = 94.337(8)°
	b = 8.9534(9) Å	β = 103.354(8)°
	c = 16.2110(16) Å	γ = 107.402(8)°
Volume	1157.14(19) $Å^3$	
Z	2	
Density (calculated)	1.951 g/cm^3	
Absorption coefficient	7.159 mm^{-1}	
F(000)	656	
Crystal size	0.46 mm × 0.37 mm × 0.18 mm	
θ-range for data collection	1.31 → 25.18°	
Index ranges	-10→ h →10, -9→ k →10, -19→ l →19	
Reflections collected	6997	
Independent reflections	3841 [R_{int} = 0.0361]	
Reflections observed	3716	
Absorption correction	Integration	
Max. and min. transmission	0.3441 and 0.1085	
Refinement method	full-matrix least-squares against F^2	
Data / restraints / parameters	3841 / 0 / 290	
Goodness-of-fit on F^2	1.070	
Final R indices [$I > 2\sigma(I)$]	R_1 = 0.0249, wR_2 = 0.0654	
R indices (all data)	R_1 = 0.0260, wR_2 = 0.0659	
Extinction coefficient	0.0025(4)	
Largest diff. peak and hole	1.321 and -1.531 $e/Å^3$	

Table 2. Atomic coordinates (· 10^4) and equivalent isotropic displacement parameters (A^2 · 10^3) for i0702. U_{eq} is defined as one third of the trace of the orthogonalized U_{ij} tensor.

	x	y	z	U_{eq}
C(1)	5486(5)	2080(4)	2901(3)	29(1)
C(2)	4006(5)	1173(5)	2231(3)	35(1)
C(3)	2672(6)	1698(5)	2328(3)	41(1)
C(4)	3277(6)	2917(5)	3049(3)	41(1)

C(5)	5007(6)	3165(5)	3405(3)	34(1)
C(6)	4063(6)	5420(4)	1635(3)	30(1)
C(7)	3985(6)	4217(5)	969(3)	35(1)
C(8)	5576(7)	4007(6)	1124(3)	42(1)
C(9)	6638(6)	5052(5)	1871(3)	39(1)
C(10)	5713(6)	5919(4)	2195(3)	34(1)
C(11)	2730(6)	6090(4)	1694(3)	30(1)
C(12)	1558(6)	6129(5)	955(3)	38(1)
N(16)	354(5)	6791(5)	945(3)	43(1)
C(13)	315(6)	7463(5)	1697(3)	40(1)
C(14)	1404(7)	7484(5)	2465(3)	40(1)
C(16)	7508(5)	250(4)	3661(2)	28(1)
C(17)	6277(6)	-373(5)	4066(3)	38(1)
C(18)	6345(7)	-1593(6)	4541(3)	45(1)
C(19)	7643(7)	-2218(5)	4600(3)	43(1)
C(20)	8882(7)	-1602(5)	4198(3)	43(1)
C(21)	8836(6)	-368(5)	3730(3)	35(1)
C(22)	7691(5)	1222(4)	2019(2)	30(1)
C(23)	6737(6)	-318(5)	1621(3)	37(1)
C(24)	6832(8)	-851(6)	803(3)	49(1)
C(25)	7857(8)	168(7)	400(3)	55(2)
C(26)	8781(7)	1699(7)	800(3)	48(1)
C(27)	8734(6)	2242(5)	1625(3)	35(1)
C(15)	2623(6)	6777(5)	2462(3)	37(1)
Au(1)	9659(1)	4076(1)	3774(1)	27(1)
Cl(1)	11984(1)	6170(1)	4515(1)	36(1)
Fe(1)	4622(1)	3546(1)	2161(1)	27(1)
P(1)	7534(1)	1917(1)	3074(1)	26(1)

X-ray Data of 24

Table 1. Crystal data and structure refinement for i0763.

Code	i0763	
Empirical formula	$C_{28}H_{24}AuClFeNP$	
Formula weight	693.72	
Temperature	223(2) K	
Wavelength	0.71073 Å	
crystal system	Monoclinic	
spacegroup	$P2_1/c$	
Unit cell dimensions	a = 9.972(4) Å	α = 90°
	b = 22.351(9) Å	β = 105.81(3)°
	c = 11.648(4) Å	γ = 90°
Volume	2497.9(15) $Å^3$	
Z	4	
Density (calculated)	1.845 g/cm^3	
Absorption coefficient	6.635 mm^{-1}	
F(000)	1344	
Crystal size	0.600 mm × 0.553 mm × 0.260 mm	
θ-range for data collection	1.82 → 25.00°	
Index ranges	-11→ h →11, -26→ k →26, -12→ l →13	
Reflections collected	15428	
Independent reflections	4384 [R_{int} = 0.1663]	
Reflections observed	4081	
Absorption correction	Integration	
Max. and min. transmission	0.2415 and 0.0605	
Refinement method	full-matrix least-squares against F^2	
Data / restraints / parameters	4384 / 0 / 299	
Goodness-of-fit on F^2	1.102	

Final R indices [$I > 2\sigma(I)$]	R_1 = 0.0521, wR_2 = 0.1370
R indices (all data)	R_1 = 0.0550, wR_2 = 0.1400
Extinction coefficient	0.0027(5)
Largest diff. peak and hole	2.484 and -3.026 $e/$Å^3

Table 2. Atomic coordinates ($\cdot$ 10^4) and equivalent isotropic displacement parameters ($A^2 \cdot 10^3$) for i0763. U_{eq} is defined as one third of the trace of the orthogonalized U_{ij}tensor.

	x	y	z	U_{eq}
C(1)	8634(6)	1292(3)	3611(5)	38(1)
C(2)	9212(7)	1885(4)	3832(6)	49(2)
C(3)	10655(8)	1812(5)	4410(7)	66(2)
C(4)	10950(7)	1219(5)	4534(6)	60(2)
C(5)	9719(6)	867(4)	4069(5)	51(2)
C(6)	10211(6)	1207(3)	7150(5)	42(1)
C(7)	8944(7)	918(5)	6667(6)	64(2)
C(8)	7939(7)	1377(7)	6211(6)	91(4)
C(9)	8591(11)	1951(7)	6411(6)	83(4)
C(10)	9979(8)	1840(4)	7003(6)	58(2)
C(11)	11543(7)	904(3)	7816(5)	48(2)
C(12)	11761(6)	940(3)	9144(5)	44(1)
N(14)	12020(6)	1488(3)	9632(5)	52(1)
C(37)	12175(9)	1526(5)	10842(7)	72(2)
C(38)	12085(8)	1047(5)	11541(6)	64(2)
C(39)	11821(10)	493(5)	11025(7)	72(2)
C(17)	6902(6)	1055(3)	1280(4)	35(1)
C(18)	8024(6)	1259(3)	886(6)	44(1)
C(19)	7950(8)	1228(4)	-323(6)	52(2)
C(20)	6805(8)	1002(4)	-1117(6)	57(2)
C(21)	5687(7)	794(4)	-728(5)	50(2)
C(22)	5737(6)	825(3)	470(5)	43(1)
C(23)	5823(5)	1731(3)	2927(5)	35(1)
C(24)	5763(6)	2247(3)	2224(6)	47(1)
C(25)	5001(7)	2735(3)	2339(7)	57(2)
C(26)	4259(8)	2733(4)	3209(7)	62(2)
C(27)	4264(7)	2223(4)	3895(6)	56(2)
C(28)	5028(6)	1726(4)	3770(5)	47(2)
C(36)	11665(9)	441(4)	9805(7)	62(2)
P(1)	6892(1)	1088(1)	2837(1)	32(1)
Cl(1)	5528(2)	-681(1)	4062(2)	52(1)
Fe(1)	9462(1)	1418(1)	5381(1)	43(1)
Au(1)	6193(1)	230(1)	3478(1)	37(1)

X-ray Data of 25

Table 1. Crystal data and structure refinement for i0696.

Code	i0696	
Empirical formula	$C_{62}H_{44}B_2F_8Fe_2N_2O_4P_2$	
Formula weight	1622.18	
Temperature	173(2) K	
Wavelength	0.71073 Å	
crystal system	Monoclinic	
spacegroup	$P2_1/c$	
Unit cell dimensions	a = 13.332(2) Å	α = 90°

	b = 27.486(4) Å	β = 107.523(11)°
	c = 8.8823(12) Å	γ = 90°
Volume	3103.7(8) Å^3	
Z	2	
Density (calculated)	1.736 g/cm^3	
Absorption coefficient	5.293 mm^{-1}	
F(000)	1586	
Crystal size	0.35 mm × 0.08 mm × 0.06 mm	
θ-range for data collection	1.48 → 25.00°	
Index ranges	-15→ h →15, -32→ k →32, -9→ l →10	
Reflections collected	17797	
Independent reflections	5467 [R_{int} = 0.1642]	
Reflections observed	2296	
Absorption correction	Integration	
Max. and min. transmission	0.7484 and 0.4200	
Refinement method	full-matrix least-squares against F^2	
Data / restraints / parameters	5467 / 0 / 379	
Goodness-of-fit on F^2	0.973	
Final R indices [$I > 2\sigma(I)$]	R_1 = 0.0924, wR_2 = 0.1934	
R indices (all data)	R_1 = 0.1914, wR_2 = 0.2313	
Largest diff. peak and hole	2.405 and -1.078 e/Å^3	

Table 2. Atomic coordinates (· 10^4) and equivalent isotropic displacement parameters (A^2 · 10^3) for i0696. U_{eq} is defined as one third of the trace of the orthogonalized U_{ij}tensor.

	x	y	z	U_{eq}
C(1)	-2880(16)	27(8)	2450(20)	57(5)
C(2)	-3220(15)	338(7)	1130(20)	61(5)
C(3)	-3048(15)	820(8)	1620(30)	62(5)
C(4)	-2576(16)	823(7)	3270(20)	63(6)
C(5)	-2435(14)	335(8)	3800(20)	63(6)
C(6)	-336(15)	843(8)	2390(30)	61(5)
C(7)	-95(16)	408(8)	3300(20)	64(6)
C(8)	-364(15)	10(9)	2320(30)	74(7)
C(9)	-894(15)	181(8)	730(30)	66(6)
C(10)	-851(17)	692(8)	780(20)	68(6)
C(11)	-223(17)	1353(7)	2860(20)	60(5)
C(12)	-831(19)	1733(8)	1970(30)	75(6)
C(13)	-680(20)	2210(8)	2410(30)	80(7)
C(14)	73(19)	2330(7)	3740(30)	71(6)
C(15)	666(19)	1957(9)	4720(30)	78(7)
C(16)	-3127(17)	-818(7)	420(20)	57(5)
C(17)	-2226(17)	-948(7)	20(30)	64(6)
C(18)	-2310(20)	-1068(9)	-1530(30)	83(7)
C(19)	-3240(20)	-1044(10)	-2670(30)	86(7)
C(20)	-4130(20)	-917(10)	-2280(30)	95(9)
C(21)	-4084(19)	-818(8)	-720(40)	83(8)
C(22)	-4231(18)	-760(8)	2760(30)	67(6)
C(23)	-4865(18)	-398(9)	3030(30)	76(7)
C(24)	-5856(19)	-501(11)	3260(30)	84(7)
C(25)	-6200(20)	-970(13)	3250(30)	97(9)
C(26)	-5580(30)	-1326(12)	2950(40)	119(11)
C(27)	-4600(20)	-1238(10)	2660(30)	90(8)
C(28)	-4230(30)	2028(11)	2890(70)	166(19)
C(29)	-3590(30)	2227(16)	1080(100)	210(40)
C(30)	-6940(30)	2630(14)	1740(40)	133(12)
C(31)	-7020(50)	2227(18)	-160(110)	260(40)
B(1)	-970(20)	1463(11)	7150(30)	69(7)
N(1)	512(14)	1483(6)	4210(20)	67(5)
F(1)	-1183(11)	951(4)	6903(15)	89(4)
F(2)	-1333(11)	1687(4)	5684(15)	87(4)

F(3)	70(11)	1527(5)	7884(16)	99(4)
F(4)	-1563(12)	1638(5)	8123(15)	92(4)
P(1)	-2975(5)	-632(2)	2453(6)	60(1)
Fe(1)	-1667(2)	437(1)	2186(3)	60(1)
Au(1)	-1668(1)	-1032(1)	4207(1)	68(1)
O(1)	-3610(40)	2420(30)	-340(90)	390(60)
O(2)	-6840(50)	2564(17)	-1080(80)	340(30)

X-ray Data of 28

Table 1. Crystal data and structure refinement for tkpd1.

Code	tkpd1	
Empirical formula	$C_{27}H_{22}Cl_2FeNPPd$	
Formula weight	624.58	
Temperature	150(2) K	
Wavelength	0.71073 Å	
crystal system	Monoclinic	
spacegroup	$P2_1/n$	
Unit cell dimensions	a = 15.4619(2) Å	α = 90°
	b = 10.5555(2) Å	β = 114.4480(10)°
	c = 15.9837(3) Å	γ = 90°
Volume	2374.77(7) Å^3	
Z	4	
Density (calculated)	1.747 g/cm^3	
Absorption coefficient	1.678 mm^{-1}	
F(000)	1248	
Crystal size	0.25 mm × 0.23 mm × 0.10 mm	
θ-range for data collection	1.54 → 27.49°	
Index ranges	-19→ h →20, -13→ k →13, -20→ l →20	
Reflections collected	43867	
Independent reflections	5433 [R_{int} = 0.0461]	
Reflections observed	4613	
Absorption correction	Integration	
Max. and min. transmission	0.864 and 0.665	
Refinement method	full-matrix least-squares against F^2	
Data / restraints / parameters	5433 / 0 / 298	
Goodness-of-fit on F^2	1.063	
Final R indices [$I > 2\sigma(I)$]	R_1 = 0.0292, wR_2 = 0.0673	
R indices (all data)	R_1 = 0.0388, wR_2 = 0.0723	
Largest diff. peak and hole	1.130 and -0.687 e/Å^3	

Table 2. Atomic coordinates (($\cdot$ 10^4)) and equivalent isotropic displacement parameters ($A^2 \cdot 10^3$) for tkpd1. U_{eq} is defined as one third of the trace of the orthogonalized U_{ij} tensor.

	x	y	z	U_{eq}
Pd	662(1)	19(1)	3986(1)	15(1)
Fe	1593(1)	1286(1)	2343(1)	20(1)
Cl(1)	-928(1)	-697(1)	3398(1)	24(1)
Cl(2)	1218(1)	-2034(1)	4135(1)	22(1)
P	2156(1)	764(1)	4587(1)	16(1)
N	159(1)	1835(2)	3746(1)	17(1)
C(1)	2521(2)	878(2)	3662(2)	20(1)
C(2)	2417(2)	-178(2)	3067(2)	25(1)
C(3)	2705(2)	208(3)	2373(2)	29(1)

C(4)	2984(2)	1491(3)	2521(2)	26(1)
C(5)	2879(2)	1918(2)	3314(2)	22(1)
C(6)	315(2)	1986(2)	2268(2)	21(1)
C(7)	201(2)	721(3)	1921(2)	25(1)
C(8)	475(2)	704(3)	1171(2)	33(1)
C(9)	753(2)	1944(3)	1049(2)	32(1)
C(10)	655(2)	2737(3)	1719(2)	27(1)
C(12)	58(2)	2519(2)	2991(2)	20(1)
C(13)	-95(2)	2345(2)	4379(2)	23(1)
C(14)	-451(2)	3554(3)	4302(2)	29(1)
C(15)	-550(2)	4277(3)	3548(2)	31(1)
C(16)	-300(2)	3749(3)	2890(2)	26(1)
C(17)	3033(2)	-249(2)	5441(2)	20(1)
C(18)	3927(2)	-401(3)	5441(2)	25(1)
C(19)	4590(2)	-1203(3)	6089(2)	30(1)
C(20)	4358(2)	-1828(3)	6731(2)	31(1)
C(21)	3460(2)	-1667(3)	6728(2)	28(1)
C(22)	2802(2)	-889(2)	6087(2)	23(1)
C(23)	2323(2)	2317(2)	5127(2)	18(1)
C(24)	2671(2)	2412(3)	6080(2)	23(1)
C(25)	2794(2)	3594(3)	6498(2)	28(1)
C(26)	2579(2)	4684(3)	5973(2)	30(1)
C(27)	2204(2)	4600(3)	5021(2)	28(1)
C(28)	2070(2)	3428(2)	4601(2)	22(1)

X-ray Data of 30

Table 1. Crystal data and structure refinement for tkpd2.

Code	tkpd2	
Empirical formula	$C_{55}H_{46}Cl_4Fe_2N_2P_2Zn_{Pd}$	
Formula weight	1156.78	
Temperature	150(2) K	
Wavelength	0.71073 Å	
crystal system	Triclinic	
spacegroup	$P\bar{1}$	
Unit cell dimensions	a = 11.2998(3) Å	α = 85.8700(11)°
	b = 12.3849(2) Å	β = 81.0170(11)°
	c = 18.7197(4) Å	γ = 70.1510(10)°
Volume	2433.39(9) Å^3	
Z	2	
Density (calculated)	1.579 g/cm^3	
Absorption coefficient	1.280 mm^{-1}	
F(000)	1172	
Crystal size	0.35 mm × 0.35 mm × 0.13 mm	
θ-range for data collection	1.75 → 27.53°	
Index ranges	-14→ h →14, -16→ k →16, -23→ l →24	
Reflections collected	44051	
Independent reflections	11175 [R_{int} = 0.0485]	
Reflections observed	8567	
Absorption correction	Integration	
Max. and min. transmission	0.857 and 0.655	
Refinement method	full-matrix least-squares against F^2	
Data / restraints / parameters	11175 / 0 / 598	
Goodness-of-fit on F^2	0.990	
Final R indices [$I > 2\sigma(I)$]	R_1 = 0.0389, wR_2 = 0.0886	
R indices (all data)	R_1 = 0.0620, wR_2 = 0.1006	
Largest diff. peak and hole	1.003 and -0.897 e/Å^3	

Table 2. Atomic coordinates (($\cdot$ 10^4)) and equivalent isotropic displacement parameters ($A^2 \cdot 10^3$) for tkpd2. U_{eq} is defined as one third of the trace of the orthogonalized U_{ij}tensor.

	x	y	z	U_{eq}
Pd(1)	5000	0	5000	19(1)
Pd(2)	0	0	10000	18(1)
Fe(1)	3547(1)	3152(1)	6301(1)	23(1)
Fe(2)	-3007(1)	2667(1)	9033(1)	21(1)
P(1)	2967(1)	1370(1)	5149(1)	20(1)
P(2)	-2111(1)	102(1)	10024(1)	19(1)
Cl(1)	4565(1)	-1129(1)	5966(1)	27(1)
Cl(2)	391(1)	-842(1)	8891(1)	28(1)
C(1)	2915(3)	2748(2)	5426(2)	22(1)
C(2)	3855(3)	3294(3)	5203(2)	27(1)
C(3)	3399(4)	4390(3)	5513(2)	32(1)
C(4)	2194(3)	4545(3)	5928(2)	32(1)
C(5)	1886(3)	3538(3)	5882(2)	27(1)
C(6)	3477(3)	3454(3)	7372(2)	28(1)
C(7)	3398(3)	2343(3)	7289(2)	30(1)
C(8)	4511(3)	1693(3)	6837(2)	32(1)
C(9)	5279(3)	2391(3)	6638(2)	34(1)
C(10)	4650(3)	3473(3)	6968(2)	31(1)
N(1)	1284(3)	4408(3)	7872(2)	38(1)
C(12)	2494(3)	4404(3)	7778(2)	28(1)
C(13)	376(4)	5292(3)	8221(2)	35(1)
C(14)	652(4)	6184(3)	8496(2)	35(1)
C(15)	1896(4)	6139(3)	8402(2)	39(1)
C(16)	2823(3)	5250(3)	8049(2)	32(1)
C(17)	2325(3)	1653(3)	4293(2)	25(1)
C(18)	1590(3)	2728(3)	4084(2)	34(1)
C(19)	1144(4)	2907(4)	3421(2)	44(1)
C(20)	1471(4)	2011(4)	2953(2)	45(1)
C(21)	2221(3)	931(4)	3151(2)	38(1)
C(22)	2644(3)	753(3)	3819(2)	31(1)
C(23)	1729(3)	1055(3)	5793(2)	26(1)
C(24)	1926(3)	796(3)	6512(2)	30(1)
C(25)	1012(4)	561(3)	7015(2)	40(1)
C(26)	-103(4)	575(4)	6810(2)	48(1)
C(27)	-319(4)	819(4)	6103(2)	47(1)
C(28)	596(3)	1067(3)	5589(2)	35(1)
C(31)	-2924(3)	1020(2)	9334(2)	22(1)
C(32)	-2418(3)	1087(3)	8586(2)	25(1)
C(33)	-3396(3)	1862(3)	8228(2)	31(1)
C(34)	-4495(3)	2289(3)	8738(2)	34(1)
C(35)	-4216(3)	1777(3)	9426(2)	27(1)
C(36)	-2546(3)	4027(2)	8518(2)	24(1)
C(37)	-3578(3)	4417(3)	9084(2)	30(1)
C(38)	-3168(4)	3905(3)	9747(2)	33(1)
C(39)	-1885(3)	3194(3)	9599(2)	27(1)
C(40)	-1497(3)	3254(3)	8843(2)	26(1)
N(2)	-3554(3)	5267(2)	7592(2)	38(1)
C(42)	-2585(3)	4338(3)	7749(2)	26(1)
C(43)	-3604(4)	5564(3)	6889(2)	48(1)
C(44)	-2749(4)	4956(4)	6332(2)	47(1)
C(45)	-1762(4)	3995(4)	6495(2)	46(1)
C(46)	-1675(4)	3691(3)	7216(2)	38(1)
C(47)	-3229(3)	592(3)	10846(2)	22(1)
C(48)	-3933(3)	-57(3)	11213(2)	25(1)
C(49)	-4789(3)	370(3)	11824(2)	31(1)
C(50)	-4954(3)	1439(3)	12076(2)	33(1)
C(51)	-4268(3)	2102(3)	11708(2)	34(1)
C(52)	-3408(3)	1675(3)	11099(2)	27(1)
C(53)	-2174(3)	-1317(2)	9881(2)	21(1)
C(54)	-2761(3)	-1535(3)	9337(2)	26(1)

C(55)	-2777(3)	-2642(3)	9257(2)	33(1)
C(56)	-2221(3)	-3519(3)	9719(2)	37(1)
C(57)	-1631(4)	-3307(3)	10255(2)	37(1)
C(58)	-1590(3)	-2214(3)	10338(2)	30(1)
C(90)	1895(4)	-1992(4)	5964(2)	54(1)
Cl(91)	2471(2)	-2936(1)	6663(1)	81(1)
Cl(92)	2413(1)	-2590(1)	5121(1)	65(1)

X-ray Data of 31

Table 1. Crystal data and structure refinement for ps307b.

Code	ps307b	
Empirical formula	$C_{56}H_{48}Cl_2Fe_2N_2P_2Pd$	
Formula weight	1099.90	
Temperature	150(2) K	
Wavelength	0.71073 Å	
crystal system	Triclinic	
spacegroup	$P\bar{1}$	
Unit cell dimensions	a = 9.94370(10) Å	α = 66.8117(7)°
	b = 10.99230(10) Å	β = 72.6510(6)°
	c = 12.0044(2) Å	γ = 77.0771(7)°
Volume	1142.79(2 Å^3	
Z	1	
Density (calculated)	1.598 g/cm^3	
Absorption coefficient	1.245 mm^{-1}	
F(000)	560	
Crystal size	0.43 mm × 0.42 mm × 0.20 mm	
θ-range for data collection	1.90 → 27.57°	
Index ranges	-12→ h →12, -14→ k →14, -15→ l →15	
Reflections collected	41724	
Independent reflections	5249 [R_{int} = 0.0315]	
Reflections observed	4978	
Absorption correction	Integration	
Max. and min. transmission	0.815 and 0.615	
Refinement method	full-matrix least-squares against F^2	
Data / restraints / parameters	5249 / 0 / 295	
Goodness-of-fit on F^2	1.065	
Final R indices [$I > 2\sigma(I)$]	R_1 = 0.0218, wR_2 = 0.0514	
R indices (all data)	R_1 = 0.0235, wR_2 = 0.0524	
Largest diff. peak and hole	0.390 and -0.639 e/Å^3	

Table 2. Atomic coordinates ((· 10^4)) and equivalent isotropic displacement parameters (A^2 · 10^3) for ps307b. U_{eq} is defined as one third of the trace of the orthogonalized U_{ij}tensor.

	x	y	z	U_{eq}
Pd	10000	0	0	13(1)
Fe	5894(1)	2006(1)	1620(1)	15(1)
Cl	8798(1)	-1402(1)	-254(1)	21(1)
P	8502(1)	1801(1)	-1030(1)	13(1)
N	3191(2)	2500(2)	5675(1)	32(1)
C(1)	6706(2)	1970(1)	-142(1)	16(1)
C(2)	5785(2)	3189(2)	-169(1)	18(1)
C(3)	4414(2)	2851(2)	556(2)	22(1)
C(4)	4466(2)	1441(2)	1028(2)	22(1)

C(5)	5873(2)	885(2)	610(1)	19(1)
C(6)	5138(2)	2639(2)	3115(1)	22(1)
C(7)	5338(2)	1224(2)	3531(1)	22(1)
C(8)	6787(2)	801(2)	3090(1)	23(1)
C(9)	7498(2)	1953(2)	2391(2)	24(1)
C(10)	6482(2)	3090(2)	2409(2)	24(1)
C(11)	3747(2)	3467(2)	3408(2)	33(1)
C(12)	3445(2)	3606(2)	4672(2)	25(1)
C(13)	2948(2)	2606(2)	6794(2)	31(1)
C(14)	2931(2)	3768(2)	6977(2)	31(1)
C(15)	3155(2)	4906(2)	5939(2)	35(1)
C(16)	3414(2)	4819(2)	4770(2)	30(1)
C(17)	8310(2)	1591(1)	-2404(1)	17(1)
C(18)	9544(2)	1323(2)	-3244(2)	22(1)
C(19)	9460(2)	1214(2)	-4333(2)	29(1)
C(20)	8147(2)	1339(2)	-4574(2)	32(1)
C(21)	6919(2)	1581(2)	-3737(2)	30(1)
C(22)	6994(2)	1720(2)	-2651(2)	21(1)
C(23)	8982(2)	3499(1)	-1644(1)	16(1)
C(24)	8952(2)	4121(2)	-816(1)	20(1)
C(25)	9255(2)	5427(2)	-1261(2)	23(1)
C(26)	9623(2)	6120(2)	-2531(2)	26(1)
C(27)	9673(2)	5509(2)	-3357(2)	27(1)
C(28)	9348(2)	4212(2)	-2921(2)	21(1)

X-ray Data of 32

Table 1. Crystal data and structure refinement for tkpd3.

Code	tkpd3	
Empirical formula	$C_{36}H_{34}ClFeN_2O_4PPd$	
Formula weight	787.32	
Temperature	150(2) K	
Wavelength	0.71073 Å	
crystal system	Monoclinic	
spacegroup	$P2_1/c$	
Unit cell dimensions	a = 17.2610(6) Å	α = 90°
	b = 10.9697(2) Å	β = 92.5390(14)°
	c = 16.9970(5) Å	γ = 90°
Volume	3215.19(16) Å^3	
Z	4	
Density (calculated)	1.627 g/cm^3	
Absorption coefficient	1.187 mm^{-1}	
F(000)	1600	
Crystal size	0.13 mm × 0.10 mm × 0.03 mm	
θ-range for data collection	2.20 → 26.07°	
Index ranges	-21→ h →21, -13→ k →12, -19→ l →20	
Reflections collected	42208	
Independent reflections	6352 [R_{int} = 0.0876]	
Reflections observed	4458	
Absorption correction	Integration	
Max. and min. transmission	0.956 and 0.865	
Refinement method	full-matrix least-squares against F^2	
Data / restraints / parameters	6352 / 0 / 417	
Goodness-of-fit on F^2	1.023	
Final R indices [$I > 2\sigma(I)$]	R_1 = 0.0393, wR_2 = 0.0677	
R indices (all data)	R_1 = 0.0763, wR_2 = 0.0782	
Largest diff. peak and hole	0.570 and -0.561 e/Å^3	

Table 2. Atomic coordinates ((· 10^4)) and equivalent isotropic displacement parameters ($A^2 \cdot 10^3$) for tkpd3. U_{eq} is defined as one third of the trace of the orthogonalized U_{ij}tensor.

	x	y	z	U_{eq}
Pd	2920(1)	3960(1)	1725(1)	21(1)
Fe	2578(1)	5689(1)	-374(1)	24(1)
P	1742(1)	4196(1)	1113(1)	21(1)
N(1)	3567(2)	3358(3)	727(2)	23(1)
N(2)	4000(2)	4088(3)	2419(2)	25(1)
C(1)	1726(2)	4707(3)	105(2)	25(1)
C(2)	2024(2)	4071(3)	-555(2)	28(1)
C(3)	1914(2)	4821(4)	-1229(2)	34(1)
C(4)	1548(2)	5912(4)	-1002(2)	35(1)
C(5)	1428(2)	5856(3)	-186(2)	29(1)
C(6)	3673(2)	5267(3)	-13(2)	23(1)
C(7)	3661(2)	5781(3)	-788(2)	28(1)
C(8)	3341(2)	6972(3)	-745(2)	30(1)
C(9)	3165(2)	7203(3)	41(2)	30(1)
C(10)	3367(2)	6160(3)	497(2)	25(1)
C(12)	3918(2)	3999(3)	164(2)	22(1)
C(13)	3773(2)	2179(3)	831(2)	27(1)
C(14)	4354(2)	1622(3)	422(2)	31(1)
C(15)	4737(2)	2294(3)	-117(2)	31(1)
C(16)	4509(2)	3487(3)	-259(2)	27(1)
C(17)	1168(2)	2818(3)	1056(2)	24(1)
C(18)	485(2)	2739(3)	578(2)	31(1)
C(19)	56(2)	1674(4)	551(3)	41(1)
C(20)	317(2)	666(4)	972(3)	43(1)
C(21)	998(2)	715(3)	1421(3)	39(1)
C(22)	1421(2)	1785(3)	1465(2)	29(1)
C(23)	1169(2)	5404(3)	1551(2)	22(1)
C(24)	366(2)	5406(3)	1548(2)	28(1)
C(25)	-27(2)	6409(3)	1820(2)	36(1)
C(26)	382(2)	7426(3)	2098(2)	35(1)
C(27)	1179(2)	7429(3)	2096(2)	31(1)
C(28)	1573(2)	6429(3)	1827(2)	27(1)
C(29)	2479(2)	4199(3)	2791(2)	22(1)
C(30)	3029(2)	4668(3)	3346(2)	26(1)
C(31)	2855(2)	4788(3)	4132(2)	32(1)
C(32)	2134(2)	4445(3)	4387(2)	35(1)
C(33)	1597(2)	3958(3)	3849(2)	33(1)
C(34)	1768(2)	3839(3)	3064(2)	27(1)
C(35)	3808(2)	4984(3)	3045(2)	29(1)
C(36)	4217(2)	2897(3)	2790(2)	32(1)
C(37)	4663(2)	4555(4)	1993(2)	37(1)
Cl	3328(1)	9133(1)	1838(1)	29(1)
O(1)	3978(2)	9120(2)	1344(2)	45(1)
O(2)	3326(2)	8048(3)	2294(2)	67(1)
O(3)	3384(2)	10178(2)	2348(2)	40(1)
O(4)	2631(2)	9220(3)	1357(2)	64(1)

X-ray Data of 33

Table 1. Crystal data and structure refinement for ps304b.

Code	ps304b
Empirical formula	$C_{37}H_{36}ClFeN_2O_4PPd$
Formula weight	801.35

Temperature	120(2) K	
Wavelength	0.71073 Å	
crystal system	Monoclinic	
spacegroup	$C2/c$	
Unit cell dimensions	a = 22.9503(3) Å	α = 90°
	b = 18.1430(2) Å	β = 125.6086(5)°
	c = 19.2860(2) Å	γ = 90°
Volume	6528.85(13) Å^3	
Z	8	
Density (calculated)	1.631 g/cm^3	
Absorption coefficient	1.171 mm^{-1}	
F(000)	3264	
Crystal size	0.37 mm × 0.25 mm × 0.23 mm	
θ-range for data collection	1.57 → 27.51°	
Index ranges	-29→ h →29, -23→ k →23, -25→ l →25	
Reflections collected	70441	
Independent reflections	7503 [R_{int} = 0.0390]	
Reflections observed	6652	
Absorption correction	Gaussian integration	
Max. and min. transmission	0.853 and 0.707	
Refinement method	full-matrix least-squares against F^2	
Data / restraints / parameters	7503 / 0 / 429	
Goodness-of-fit on F^2	1.039	
Final R indices [$I > 2\sigma(I)$]	R_1 = 0.0281, wR_2 = 0.0662	
R indices (all data)	R_1 = 0.0341, wR_2 = 0.0700	
Largest diff. peak and hole	1.048 and -0.848 e/Å^3	

Table 2. Atomic coordinates ((· 10^4)) and equivalent isotropic displacement parameters (A^2 · 10^3) for ps304b. U_{eq} is defined as one third of the trace of the orthogonalized U_{ij}tensor.

	x	y	z	U_{eq}
Pd	3311(1)	2649(1)	2945(1)	15(1)
Fe	3372(1)	698(1)	4447(1)	19(1)
P	2414(1)	2002(1)	2809(1)	16(1)
N(1)	3882(1)	2704(1)	4303(1)	17(1)
N(2)	4094(1)	3332(1)	2995(1)	19(1)
C(1)	2568(1)	1417(1)	3657(1)	19(1)
C(2)	2291(1)	682(1)	3537(1)	24(1)
C(3)	2442(1)	431(1)	4322(2)	28(1)
C(4)	2808(1)	1001(1)	4933(1)	25(1)
C(5)	2893(1)	1612(1)	4536(1)	20(1)
C(6)	4346(1)	917(1)	4661(1)	22(1)
C(7)	3956(1)	383(1)	4002(2)	26(1)
C(8)	3821(1)	-235(1)	4342(2)	31(1)
C(9)	4124(1)	-89(1)	5214(2)	29(1)
C(10)	4449(1)	620(1)	5410(1)	24(1)
C(11)	4625(1)	1630(1)	4559(1)	23(1)
C(12)	4445(1)	2284(1)	4878(1)	18(1)
C(13)	3685(1)	3271(1)	4581(1)	20(1)
C(14)	4040(1)	3443(1)	5434(2)	25(1)
C(15)	4633(1)	3026(1)	6026(1)	26(1)
C(16)	4835(1)	2445(1)	5746(1)	23(1)
C(17)	1946(1)	1373(1)	1902(1)	19(1)
C(18)	1224(1)	1204(1)	1489(1)	24(1)
C(19)	881(1)	729(1)	792(2)	31(1)
C(20)	1265(2)	413(1)	520(2)	36(1)
C(21)	1990(2)	557(1)	948(2)	33(1)
C(22)	2331(1)	1042(1)	1635(2)	26(1)
C(23)	1786(1)	2677(1)	2735(1)	17(1)
C(24)	1802(1)	3404(1)	2505(1)	22(1)
C(25)	1390(1)	3948(1)	2528(1)	26(1)

C(26)	951(1)	3778(1)	2783(1)	25(1)
C(27)	934(1)	3065(1)	3015(1)	25(1)
C(28)	1345(1)	2513(1)	2998(1)	21(1)
C(29)	2776(1)	2837(1)	1674(1)	19(1)
C(30)	3222(1)	3149(1)	1471(1)	20(1)
C(31)	2941(1)	3411(1)	653(2)	25(1)
C(32)	2214(1)	3371(1)	18(1)	26(1)
C(33)	1763(1)	3070(1)	203(1)	24(1)
C(34)	2043(1)	2807(1)	1024(1)	22(1)
C(35)	4007(1)	3200(1)	2173(1)	22(1)
C(36)	4856(1)	3222(1)	3712(2)	27(1)
C(37)	3888(1)	4105(1)	3022(2)	28(1)
Cl(1)	5000	5370(1)	2500	21(1)
O(11)	4668(1)	4917(1)	1758(1)	53(1)
O(12)	5543(1)	5822(1)	2578(2)	50(1)
Cl(2)	4828(1)	1062(1)	2470(1)	31(1)
O(21)	5197(2)	382(3)	2589(4)	60(1)
O(22)	4153(4)	828(4)	2230(5)	102(2)
O(23)	4657(2)	1490(2)	1759(3)	34(1)
O(24)	5106(3)	1478(2)	3193(3)	36(1)